Development and Analysis of Adaptive Interference Rejection Techniques for Direct Sequence Code Division Multiple Access Systems

Nitin R. Mangalvedhe

Dissertation submitted to the Faculty of the
Virginia Polytechnic Institute and State University
in partial fulfillment of the requirements for the degree of

Doctor of Philosophy
in
Electrical Engineering

Jeffrey H. Reed, Chair
A. A. (Louis) Beex
John E. Kobza
William H. Tranter
Brian D. Woerner

July, 1999
Blacksburg, Virginia

Keywords: CDMA Systems, Interference Rejection, Multiple Access Interference, Adaptive Receivers, Adaptation Algorithms, MMSE Analysis, Multi-Rate Systems

Development and Analysis of Adaptive Interference Rejection Techniques for Direct Sequence Code Division Multiple Access Systems

Nitin R. Mangalvedhe

(ABSTRACT)

The inadequacy of conventional CDMA receivers in a multiple access interference-limited mobile radio environment has spurred research on advanced receiver technologies. This research investigates the use of adaptive receivers for single user demodulation to overcome some of the deficiencies of a conventional receiver and, hence, enhance the system capacity. Several new adaptive techniques are proposed. The new techniques and some existing schemes are analyzed. The limitation of existing blind algorithms in multipath channels is analyzed and a new blind algorithm is proposed that overcomes this limitation. The optimal receiver structure for multi-rate spread spectrum systems is derived and the performance of this receiver in various propagation channels is investigated. The application of coherent and differentially coherent implementations of the adaptive receiver in the presence of carrier frequency offsets is analyzed. The performance of several new adaptive receiver structures for frequency offset compensation is also studied in this research. Analysis of the minimum mean-squared error receiver is carried out to provide a better understanding of the dependence of its performance on channel parameters and to explain the near-far resilience of the receiver. Complex differentially coherent versions of the sign algorithm and the signed regressor algorithm, algorithms that have a much lower computational complexity than the least-means square algorithm, are proposed and applied for CDMA interference rejection.

Funded by the Defense Advanced Research Projects Agency (DARPA).

Acknowledgments

This research was possible because of the help and support of numerous individuals. I wish to express my profound gratitude to all of them. From the time Dr. Jeff Reed started advising me as a Master's student, he has always motivated me to excel in research. I am greatly thankful to Dr. Reed for his continuous support and guidance throughout my time as his graduate student. I also thank the other members of my committee for their valuable comments and feedback.

I shall always be grateful to my parents for providing me with the best educational opportunities. They have been a source of incessant support and encouragement, which have been vital to all of my accomplishments. I am thankful to my wife, Anupama, for her constant understanding during the most important time of my Ph.D. and for the love and encouragement she has given me.

I have had the opportunity to interact with many wonderful researchers at the MPRG. I have been influenced directly or indirectly by several colleagues. I was fortunate to have been able to mentor Steve Nicoloso during the GloMo project and Steve's MS thesis research. A lot of the work reported in Chapter 8 was possible because of him. Many a fruitful discussion with Milap Majmundar, Steve Nicoloso, and Paul Petrus have helped me expand my knowledge. Initial ideas for my research were inspired by the work of Nena Zečević. The GloMo project gave me the opportunity to learn about new areas that are not directly related to my research. Specifically, I have benefited from my interactions with Don Breslin, Mike Buehrer, Rick Cameron, Neiyer Correal, Francis Dominique, Rich Ertel, Kim Phillips, Pascal Renucci, Zhigang Rong, Steve Swanchara, and Matt Valenti, besides others previously mentioned. Others who have influenced my research experience include Zhong Hu, Monika Maheshwari, and Raqibul Mostafa. I have also enjoyed working alongside numerous other students at the MPRG.

I am obliged to the supporting staff at the MPRG for helping me in many different ways. I owe many thanks to Prabhakar Koushik for the support he provided with computing resources during much of my tenure at the MPRG. I am also thankful to Anjala Krishen and Dan Davis for their computing support. I am highly appreciative of Jenny Frank, Christine Holmfelt, Lori Hughes, Hilda Reynolds, Annie Wade, and Kathy Wolfe for taking care of all the administrative details so I could focus on research. I particularly

thank Hilda Reynolds for the numerous ways that she has assisted me in. I am greatly indebted to Lori Hughes and Christine Holmfelt for editing my reports to insure good quality.

This research was enabled by the sponsorship of DARPA through the GloMo project. I wish to express my sincere thanks to DARPA not only for the financial assistance but also the innumerable learning opportunities that the GloMo project presented.

Contents

List of Figures

List of Tables

Chapter 1

Introduction

The tremendous strides achieved in wireless communications over the past decade have been spurred by the equally huge increase in the demand for wireless connectivity. The path from wireless telegraphy to third-generation personal communications has been a long one, and the stretch spanning the last decade has seen the most rapid progress with no indications of the pace reducing in the near future. The rapid developments are primarily due to growth in very large scale integration (VLSI), which has led to the availability of greater computational capabilities for lower costs, thus making the implementation of novel technologies feasible.

The industry has increasingly supported the development of new technologies that improve the quality of wireless communications. Due to the finite amount of allocated radio spectrum and the evolution of several wireless communication applications in recent years, the wireless industry is seeking new ways to meet the demands of mobile radio subscribers. Since the ultimate objective of the industry is to establish ubiquitous wireless mobility , there is greater cooperation between industries and research institutions to achieve this goal. The competition between industries has further spurred this progress. Thus, it has been possible for novel and ingenious technologies to be realized commercially. The research presented here was motivated by this perspective of the industry and is a contribution to the cycle of supply and demand in mobile wireless communications. The objective of this research is to propose new techniques for interference mitigation in direct sequence code division multiple access communications systems and to analyze these and existing techniques. Evaluation of techniques is achieved through both mathematical analysis and computer simulation.

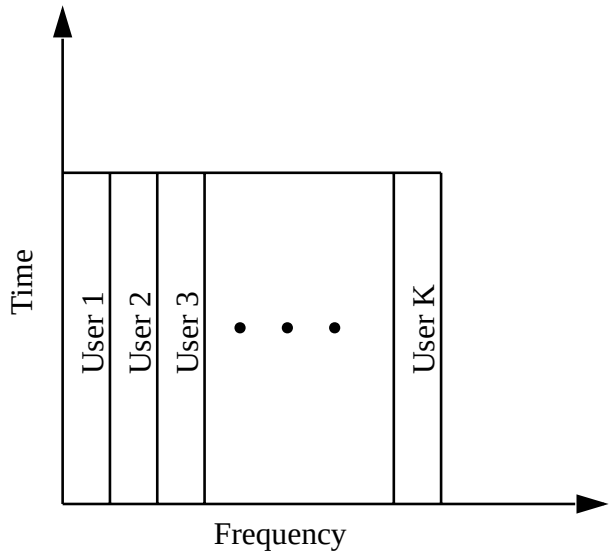

Figure 1.1: Frequency Division Multiple Access.

1.1 Multiple Access Techniques

In any wireless communication system, there are many users who need to communicate simultaneously. Therefore, the available radio frequency (RF) resources must be distributed among these users in a way that allows them to access the communication system. In a coordinated system, such as a cellular network, the allocation of these resources requires extensive planning.

Perhaps the most natural and fundamental way for multiple users to communicate simultaneously is to allocate a different subband of the RF spectrum to each user. A simple bandpass filter at the receiver would then select the bandwidth of interest. This method, *frequency division multiple access* (FDMA), is the oldest method for multiple access, dating back to the invention of broadcast radio. Different *channels* in a FDMA system are simply assigned different frequency bands that do not overlap, as illustrated in Figure 1.1. One of the main features of FDMA is that each channel is narrowband, allowing either an analog or digital modulation scheme.

Instead of splitting the RF spectrum into subbands for each user, multiple non-overlapping time slots can be created and assigned to each user. The receiver synchronizes to the correct time slot to recover the user's information. Figure 1.2 shows resource allocation in a *time division multiple access* (TDMA) system, which is somewhat more complex technology. Since all users occupy the entire RF bandwidth, TDMA channels have much wider bandwidths compared with FDMA channels, usually necessitating equalization to overcome degradation due to multipath. One key source of complexity is the multiple lev-

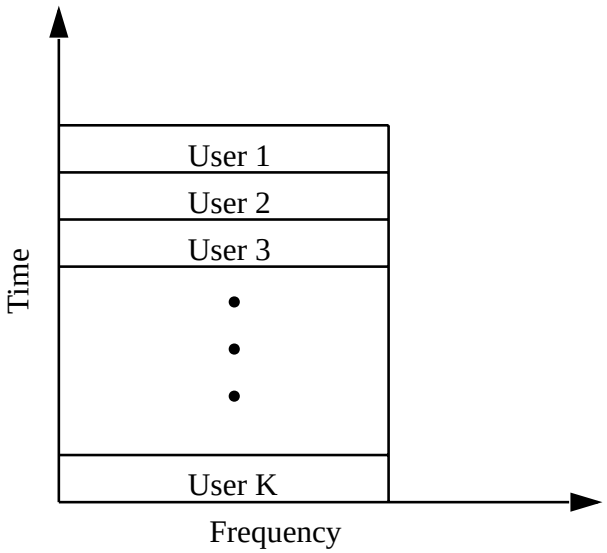

Figure 1.2: Time Division Multiple Access.

els of synchronization necessary to recover information for each user. Due to the nature of TDMA, digital modulation schemes must be used.

The most recent multiple access technology is *code division multiple access* (CDMA), based on *direct sequence spread spectrum* (DS/SS) communications. Unlike TDMA and FDMA, CDMA users occupy the entire bandwidth all the time. Users are distinguished from each other through the *spreading codes* assigned to them (Figure 1.3). The spreading code acts as a signature for the user and allows the user's receiver to extract the desired signal from all of the *multiple access interference* (MAI). Thus, the codes must be sufficiently different, i.e., they must have good crosscorrelation properties, to reduce interference. Section 2.2 explains the impact of MAI.

Wideband CDMA technology is being proposed for third-generation wireless personal communications [1, 2, 3, 4]. A wide range of services will be provided by these systems, with the key being a unified radio infrastructure. Third-generation systems will improve the technology and services provided by second generation systems. Furthermore, a lot of flexibility is being provided to allow for the evolution of technology. One of the special attributes of the proposals for wideband CDMA is the provision for advanced receivers. The novel aspects of wideband CDMA allow for the implementation of interference suppression and cancellation schemes. As Chapter 7 will show, adaptive receivers may be employed in multi-rate third-generation systems to perform interference rejection and improve system performance. More extensive discussions of multiple access technologies can be found in [5, 6]. Some recent developments in multiple access technologies are presented in [7].

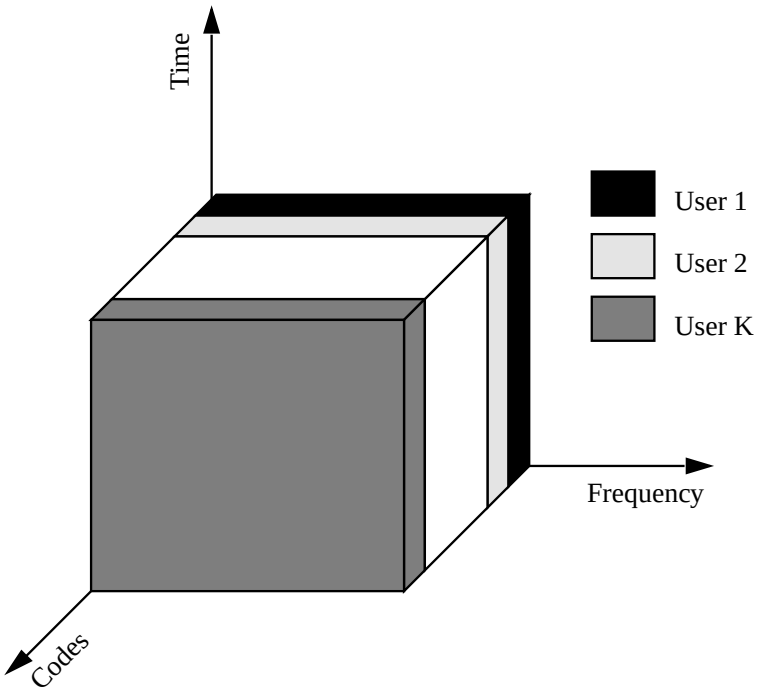

Figure 1.3: Code Division Multiple Access.

1.2 Advantages of Cellular CDMA over FDMA and TDMA

In a single cell scenario in an additive white Gaussian noise (AWGN) channel, the capacities of FDMA, TDMA, and deterministic CDMA, where the spreading waveforms are assumed orthogonal [8], are equal [8, 9, 10]. However, the potential advantages of CDMA are fully realized in a multi-cell system in the presence of fading multipath radio propagation channels.

The advantages of CDMA are primarily a result of spread spectrum technology [8, 9, 10, 11]. Spread spectrum provides resistance to frequency selective fading due to multipath through spectral diversity, and robustness to MAI. The variance of the signal-to-noise ratio (SNR) at the receiver is lower for CDMA than for narrowband FDMA when operating in frequency-selective fading channels [9]. This applies to most practical CDMA systems where the signal bandwidth is significantly larger than the channel coherence bandwidth. CDMA is less susceptible to degradation due to inter-symbol interference than is TDMA [9].

One of the principal factors that influence the increase in the system capacity in CDMA

systems is *universal frequency reuse* [12, 13], which means that the same spectrum can be used in all cells, i.e., the reuse factor is 1. This also eliminates the need for frequency planning. The higher the reuse factor, the lower the system capacity. A typical reuse factor used in TDMA and FDMA cellular systems is 7. Furthermore, the impact of cochannel interference, which results from other cells using the same frequency, is greater for TDMA and FDMA systems than for CDMA systems with accurate power control. Power control in TDMA and FDMA systems helps reduce interference. However, power control is a more serious problem in CDMA systems. In the absence of fast and accurate power control, the *near-far* problem can cause much stronger signals received from users closer to the basestation to jam weaker signals received from mobiles at the edge of the cell. The processing gain of the spread spectrum signal slightly mitigates the impact of interference.

CDMA allows for the exploitation of multipath energy with a Rake receiver [14]. The Rake receiver provides a means of constructive combining of multipath. Distinguishing multipath components is possible because the coherence bandwidth of the channel is much lower than the signal bandwidth or, equivalently, the delays of the components are much larger than a chip duration.

To improve capacity, CDMA may take advantage of the low voice-activity of normal speech. Humans speak only about 35–40% of the time during a conversation and listen for the rest of the time. If transmission is blocked during periods of silence, then interference can be reduced, thus increasing capacity [13].

When a user moves from one cell to a neighboring cell, the signal must also move from one base station to another via handoff. The Rake receiver can be used to monitor the signal powers from two (or more) base stations carrying the same user's information. The gradual transition to another serving basestation is carried out through a process known as *soft handoff* [5, 15]. Soft handoff usually allows for fewer dropped calls and a more consistent coverage area [16].

Another attribute of CDMA is its soft capacity limit, which results in "soft blocking" of calls and a graceful degradation in performance. TDMA and FDMA place a hard limit on the number of users in a cell, resulting in "hard blocking". With CDMA, however, there is a graceful degradation in voice quality when the number of users exceeds a certain limit.

1.3 A Cellular CDMA System

In the *forward link* of a cellular CDMA system, the signals intended for all mobile users are chip, bit, and carrier synchronous, which is possible due to their common source, i.e., the basestation. The signal transmitted at the basestation is actually the sum of these signals. The powers of these individual component signals are equal. Since the

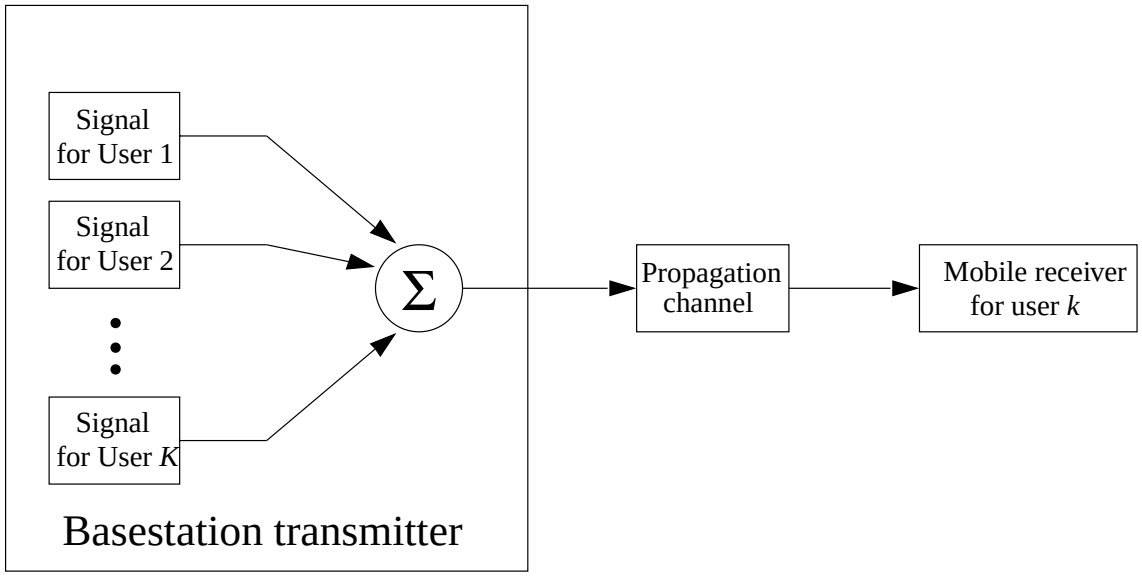

Figure 1.4: Forward Link of a CDMA System.

component signals propagate through a common radio propagation channel, the powers of the received signals at a particular receiver are also equal. A conceptual representation of the forward link is shown in Figure 1.4.

In contrast, the *reverse link* of the CDMA system is uncoordinated. Signals originate from the various mobile sources at different times and, therefore, the signals reaching the basestation are completely asynchronous. Furthermore, the average powers can vary widely without feedback from the base station to control the mobile transmitter power. The instantaneous powers can also vary since the signals propagate through different radio channels. These effects can give rise to the near-far problem, explained in Section 2.2. The reverse link is illustrated in Figure 1.5.

1.4 Outline of Report and Personal Contributions

With CDMA rapidly establishing itself as the multiple-access technology of choice, the need for improving the technology has arisen. This is especially important given the strong backing for CDMA in third generation personal communications systems (PCS). Chapter 2 clearly explains the limitations of a conventional CDMA receiver employed in deterministic CDMA communications. The primary deficiency of CDMA is MAI and can be effectively addressed by adaptive receivers. The objective of this research work is to develop new adaptive receiver techniques and provide a thorough analysis of these new

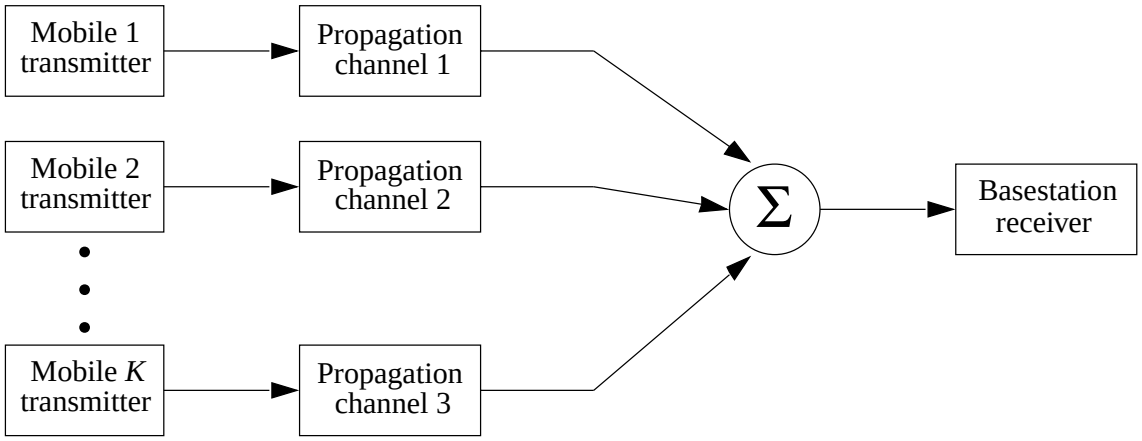

Figure 1.5: Reverse Link of a CDMA System.

and existing interference rejection techniques under the conditions of a practical radio environment.

Chapter 2 provides a motivation for research into adaptive receivers. The limitations of a conventional receiver are explained and new receivers are introduced for overcoming the limitations. The relative merits of multiuser and single user receivers are discussed, motivating the investigation of the minimum mean-squared error receiver. A classification of adaptive receivers is provided with a brief overview of proposed structures.

The common adaptive receiver structure exploits the cyclostationary property of DS/SS signals. Chapter 3 provides an introduction to cyclostationarity as background for understanding the spectral correlation property of DS/SS signals. This theory is used to show that the optimal receiver for demodulating a spread spectrum signal amidst MAI reduces to a single transversal filter.

Minimum mean-squared error receivers are implemented in practice by allowing an adaptive filter to learn the characteristics of the radio environment and converge to the optimal solution. Adaptation algorithms that perform this optimization are briefly discussed in Chapter 4. Relationship between these adaptation algorithms is analyzed. This chapter also presents an analogy between adaptive antenna array systems and CDMA systems that enables the direct use of antenna array algorithms for CDMA interference rejection. *The extensive discussion on the similarities and differences between adaptive antenna array systems and CDMA systems is original to this work.*

Chapter 5 introduces a new blind algorithm for adaptive receivers. Unlike previous algorithms, this new algorithm is able to exploit multipath. This algorithm is motivated by the linearly constrained constant modulus algorithm. The stationary points of the linearly constrained constant modulus cost function are analyzed to investigate the con-

vergence behavior of the algorithm. *The analysis of the stationary points of the existing cost function and the newly proposed algorithm and its analysis are original contributions.*

Minimum mean-squared error receivers have been widely discussed in the literature. Chapter 6 provides a discussion of the minimum mean-squared error achieved by the receiver in additive white Gaussian noise channels and static multipath channels. An expression for the minimum mean-squared error for additive white Gaussian noise channels is derived in terms of cross-correlations between spreading codes of the users, the interference-to-signal power ratios, and the signal-to-noise ratio of the desired signal. This expression is further simplified based on simple assumptions that help demonstrate that the receiver is near-far resistant. A similar analysis is performed on the matched filter receiver to provide a comparison. The minimum mean-squared error analysis is extended to static multipath channels. The gain derived by the optimum receiver from correlated multipath is investigated. *Although related expressions exist in the literature, a unique approach is used to derive the expression for the minimum mean-squared error. The final expression provides new insight into the dependence of the minimum mean-squared error on channel parameters and the approach can be used to extend the analysis to other channels. The minimum mean-squared error analysis for static multipath channels, including the analysis of "multipath gain" and the loss due to uncorrelated multipath, is an original contribution. The new method of demonstrating the near-far resilience of the minimum mean-squared error receiver and an equivalent analysis for the matched filter receiver are also personal contributions.*

A single transversal filter is the optimal receiver only when all of the MAI signals possess commensurate statistical periodicities. This is violated in multi-rate spread spectrum systems where signals have different code lengths and/or bandwidths. Chapter 7 derives the optimal receiver structure for a multi-rate spread spectrum system and shows it to be a bank of transversal filters. The minimum mean-squared errors of a filter bank receiver and a single filter receiver for a multi-rate system are compared. Simulation results are provided to demonstrate the bit error rate performance gains obtained with an adaptive filter bank receiver over an adaptive single filter receiver in both additive white Gaussian noise and multipath fading channels. The strengths and weaknesses of the adaptive filter bank receiver are explored. *The derivation and extensive performance investigation of the optimum structure for a multi-rate system constitute original contributions.*

Chapter 8 investigates the performance of adaptive receiver structures in the presence of a frequency offset on the received signal. The absence of a coherent carrier reference almost always leads to a residual frequency offset on the received signal. Use of the coherent minimum mean-square error receiver in the presence of carrier offsets is discussed. The mean-square error of the coherent adaptive receiver using the least-mean square algorithm is derived. Some conventional techniques for offset compensation are briefly outlined. The differentially coherent adaptive receiver is proposed for offset compensation. The modified cost function for this new structure is presented and its stationary points are analyzed. Simulation results are provided to compare the performances of

various schemes for offset compensation when used with an adaptive receiver. *The proposal of various receiver structures for offset compensation in CDMA systems and their performance investigation were jointly performed with Nicoloso [17]. The investigation of the optimum coherent receiver in the presence of frequency offsets, the mean-square error analysis of the coherent adaptive receiver, and the analysis of the differentially coherent adaptive receiver are original contributions of this research.*

Although the least-mean square algorithm is a simple and effective stochastic gradient descent algorithm for implementing the minimum mean-squared error receiver, nearly half of its multiplication operations are due to the complex weight update. Simple algorithms that almost completely eliminate multiplication operations have been used in echo cancellation applications. Chapter 9 discusses the application of the sign algorithm and the signed regressor algorithm in adaptive receivers. Complex versions of the reduced complexity algorithms for a differentially coherent adaptive receiver are proposed. The bit-error rate performances of the three algorithms for additive white Gaussian noise and multipath fading channels are compared through simulation. Convergence analyses of the two reduced complexity algorithms are provided for reference in Appendix A. *The application of the sign algorithm and the signed regressor algorithm for CDMA interference rejection is a personal contribution. The proposal of complex versions of the algorithms for a differentially coherent receiver and the performance investigation of the algorithms are original contributions.*

Chapter 10 provides a summary of the report and offers important conclusions of this research. Some recommendations are provided for future research in this area.

Chapter 2

Adaptive Receivers for CDMA Systems

Since the origin of DS/SS technology, the classical technique of matched filtering has been used for the detection of DS/SS signals. The principal assumption that the background noise is white makes the matched filter the optimum receiver in the sense that is maximizes the SNR assuming perfect synchronization. Furthermore, when the noise is Gaussian, the matched filter is also the *maximum a posteriori* (MAP) detector. Thus, no receiver can provide a lower probability of bit error, or bit error rate (BER), than a matched filter based receiver when detecting a DS/SS signal in AWGN [14, 18]. The correlation receiver is merely a realization of the matched filter. In practical DS/SS CDMA systems, the assumption that the desired signal is received with only AWGN is not true and thus there exist better receivers than the matched filter. Understanding the operation of the conventional receiver is helpful in explaining the need for adaptive receivers.

2.1 The Conventional Receiver

The motivation behind the development of the correlation receiver is quite simple. A binary baseband DS/SS signal is derived by multiplying a binary level (± 1) information signal with a binary level spreading sequence. The spreading signal $c(t)$ exhibits the constant modulus property:

$$|c(t)| = 1 \tag{2.1}$$

where $|\cdot|$ denotes absolute value. The spread signal $s(t)$ is given by

$$s(t) = d(t)\, c(t) \tag{2.2}$$

where $d(t)$ is the information bearing data signal. The signal at the receiver is a delayed version of $s(t)$. Assuming that there is no background noise, multiplication of $s(t)$ with an exact local replica of $c(t)$ (with the appropriate delay) results in the recovery of $d(t)$:

$$s(t)\,c(t) = d(t), \tag{2.3}$$

where Equation (2.1) has been used. Assuming the presence of background noise, the signal at the receiver may be expressed as

$$s(t) = d(t)\,c(t) + n(t) \tag{2.4}$$

where $n(t)$ is the additive noise. Multiplication of the signal with a local replica of the spreading code now yields

$$s(t)\,c(t) = d(t) + n(t)\,c(t). \tag{2.5}$$

Filtering the recovered signal with a filter of bandwidth equal to the data bandwidth reduces out of band noise, including background noise and self-noise from imperfect synchronization. The recovered signal is of the form

$$\hat{d}(t) = \mathcal{F}_d\{d(t)\} + \mathcal{F}_d\{n(t)\,c(t)\} \tag{2.6}$$

where $\mathcal{F}_d\{\cdot\}$ represents data-bandwidth filtering.

The optimum MAP detector for the DS/SS signal in AWGN is the matched filter [14], whose impulse response is the spreading sequence reversed in time. A "peak" appears periodically at its output, and the synchronization system enables sampling this signal at the peak to extract optimum performance. The equivalent correlation receiver realization consists of multiplying the received signal with the synchronized spreading code, followed by integration and a sample-and-dump operation [14, 18] and may be expressed as

$$\hat{d}(nT_b) = \frac{1}{T_b}\int_{(n-1)T_b}^{nT_b} d(t) + \frac{1}{T_b}\int_{(n-1)T_b}^{nT_b} n(t)\,c(t) \tag{2.7}$$

where T_b is the symbol period of $d(t)$. However, in practice, a spread spectrum system may need to contend with other interference and the matched filter is no longer optimum.

Optimum performance of the correlation or matched filter receiver requires perfect *synchronization* of the spreading or pseudonoise (PN) code at the receiver. Synchronization includes both initial *code acquisition* as well as *code tracking*. This alone is a vast and important research area. To limit this research to reasonable scope, it is assumed in most instances that perfect synchronization is achievable. References [10, 19, 20] provide excellent overviews of techniques for code acquisition and tracking.

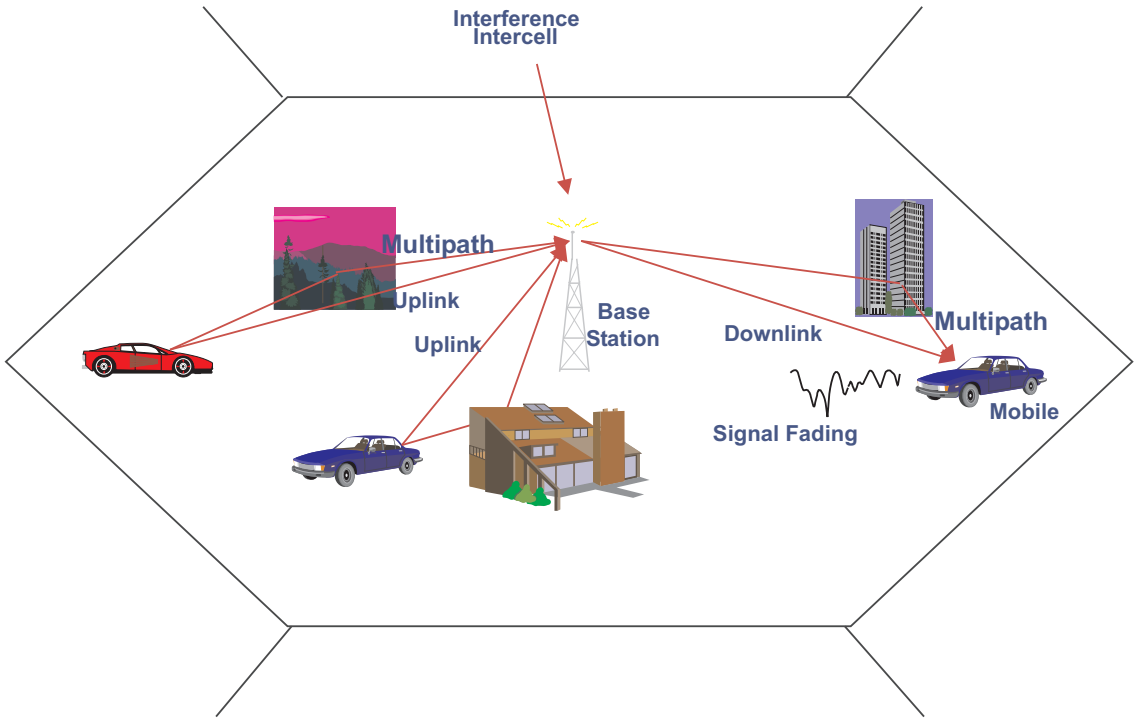

Figure 2.1: A Cellular CDMA System.

2.2 The Need for Adaptive Receivers

2.2.1 Why is the Conventional Receiver Not Optimal?

The matched filter receiver based on AWGN is non-optimal due to numerous factors of real channels. Figure 2.1 shows a practical scenario. For example, multipath propagation is a major source of distortion. Multipath components arrive simultaneously at the receiver with time varying phase shifts due to the motion of the mobile user, causing the amplitude of the combined signal to fluctuate. Motion also causes a Doppler shift in the frequency of the received signal. The overall result is *fading* [5, 15, 21], and destructive combining of multipath can cause fades as deep as 20–30 dB. The received signal $r(t)$ may be modeled as

$$r(t) = \sum_{i=0}^{L} a_i(t)\, s(t - \tau_i) + n(t) \tag{2.8}$$

where L is the number of distinguishable paths, $a_i(t)$ represents the time-varying amplitude of the ith path for the signal $s(t)$, τ_i is the delay of the ith path, and $n(t)$ is the

AWGN. Another phenomenon known as *shadowing* [5, 21] results from the mobile being blocked by large obstacles such as buildings and hills and results in long-term fading. Thus, practical channels are not merely AWGN for mobile systems and the matched filter is not optimal in these situations.

Yet another important factor, often the *most* important factor, is the presence of MAI. This is especially true in the reverse link of a cellular CDMA system. Ignoring propagation effects, the received signal $r_{RF}(t)$ for BPSK modulation is represented by

$$r_{RF}(t) = \sum_{k=0}^{K} \sqrt{\frac{P_k}{2}}\, c_k(t-\tau_k)\, d_k(t-\tau_k)\, \cos(\omega_{ck}(t-\tau_k)+\phi_k) + n_{RF}(t) \tag{2.9}$$

where P_k is the received power of the kth user, K is the number of active users, $c_k(t)$ is the kth user's spreading signal, $d_k(t)$ is the kth user's data signal, τ_k is the kth user's delay, ω_{ck} is the frequency of the kth user's local oscillator, ϕ_k is the phase of the kth user's carrier signal, and $n_{RF}(t)$ is the AWGN resulting from the RF front end. Assuming that the first user is the user of interest, and assuming perfect carrier recovery, the baseband signal $r(t)$ at the mobile unit is given by

$$\begin{aligned} r(t) &= \sqrt{\frac{P_1}{2}}\, c_1(t-\tau_1)\, d_1(t-\tau_1) \\ &\quad + \sum_{k=2}^{K} \sqrt{\frac{P_k}{2}}\, \cos(\omega_{ck}\tau_k+\phi_k)\, c_k(t-\tau_k)\, d_k(t-\tau_k) + n(t) \end{aligned} \tag{2.10}$$

where $n(t)$ is the equivalent AWGN at baseband. Assuming perfect code synchronization, the decision statistic Z_{1i} for the ith bit estimate (at the output of the correlator) is obtained as

$$Z_{1i} = \frac{1}{T}\int_0^T r(t)\, c_1(t-\tau_1)\, dt \tag{2.11}$$

where T is the bit period. Letting $\tau_1 = 0$, i.e., shifting the time reference to the delay of the first user, we get

$$\begin{aligned} Z_{1i} &= \frac{\sqrt{\frac{P_1}{2}}}{T}\int_0^T d_1(t)\, c_1(t)\, c_1(t)\, dt \\ &\quad + \sum_{k=2}^{K} \frac{\sqrt{\frac{P_k}{2}}\, \cos(\omega_{ck}\tau_k+\phi_k)}{T}\int_0^T d_k(t-\tau_k)\, c_k(t-\tau_k)\, c_1(t)\, dt \\ &\quad + \frac{1}{T}\int_0^T n(t)\, c_1(t)\, dt. \end{aligned} \tag{2.12}$$

If the transmission of the signals is synchronous, as is the case on the forward link, $\tau_k = 0$, $\phi_k = 0$, and $P_k = P_1$ for all k. If b_{ki} is the kth user's ith bit, then

$$\begin{aligned} Z_{1i} &= \sqrt{\frac{P_1}{2}}\, b_{1i} \cdot \left[\frac{1}{T}\int_0^T c_1(t)\, c_1(t)\, dt\right] \\ &\quad + \sum_{k=2}^{K} \sqrt{\frac{P_1}{2}}\, b_{ki} \cdot \left[\frac{1}{T}\int_0^T c_k(t)\, c_1(t)\, dt\right] + \frac{1}{T}\int_0^T n(t)\, c_1(t)\, dt. \end{aligned} \tag{2.13}$$

The term within the first pair of brackets is unity as a result of Equation (2.1). If a set of orthogonal spreading codes is chosen, the term in the second pair of brackets is zero.

However, for the asynchronous reverse link, Equation (2.12) may be rewritten as

$$Z_{1i} = \sqrt{\frac{P_1}{2}}\, b_{1i} + \sum_{k=2}^{K} I_{ki} + n_i, \tag{2.14}$$

$$I_{ki} = \frac{\sqrt{\frac{P_k}{2}}\, \cos(\omega_{ck}\tau_k + \phi_k)}{T} \int_0^T d_k(t-\tau_k)\, c_k(t-\tau_k)\, c_1(t)\, dt, \tag{2.15}$$

$$n_i = \frac{1}{T}\int_0^T n(t)\, c_1(t)\, dt. \tag{2.16}$$

The first term in Equation (2.14) is the desired signal component, the second term is due to MAI, and the third term is AWGN. Orthogonality of the codes holds only for zero relative delay between them. When the signals are received with random delays, the crosscorrelation between the codes is no longer zero and the signals not of interest contribute to the MAI. Since the second term arises from the non-orthogonal MAI, again the condition for optimality of the correlator/matched filter is violated. When a large number of interference signals are received with almost identical powers, the MAI appears Gaussian according to the Central Limit Theorem and almost white within the band of interest. Thus, the conventional receiver approaches optimality. In practice, only a moderate number of users can occupy the band for reasonable bit error rate (BER) performance and thus the Gaussian assumption is not realistic.

2.2.2 The Near Far Problem

Another phenomenon that seriously affects the performance of the conventional receiver is the *near-far* effect. It occurs when the signal of interest is much weaker than that received from an interfering user. This can happen, for example, when one mobile user is at the edge of the cell while another mobile user is close to the basestation. Without

power control, the signal from the "near" user can be so overpowering that the signal from the "far" user is completely jammed. This results in the power of the first term in Equation (2.14), the desired signal, being much smaller than that of the second term. Consequently, the signal-to-interference-plus-noise (SINR) is too low—it can even be negative on a dB scale—for acceptable BERs.

A closer examination of Equation (2.14) shows that the near-far effect is not inherent to CDMA but is a consequence of the receiver implementation. The I_k terms arise due to the use of the conventional correlator/matched filter receiver, i.e., due to the non-zero *crosscorrelation* between the kth user's code and the desired user's code. Therefore, to ensure that the received powers from all of the mobile users are almost equal with very little variance, rapid and tight power control is essential. Without power control, the performance degradation can be serious and even in the presence of tight power control, the system performance is still interference limited.

Thus, there is a need for a receiver implementation that suppresses the I_k terms. Methods for performing this task lead to alternative CDMA receivers capable of supporting more users.

2.2.3 Multiuser Receivers

Since the conventional receiver is far from optimum, a question naturally arises: "what is the optimum receiver?" One approach to creating the optimal or near optimal receiver is to demodulate the signals of all of the users in the system. The receivers belonging to this class are known as *multiuser receivers*. A vast amount of research work exists in this area. Verdu has shown that a maximum likelihood sequence detection approach minimizing the probability of sequence error can provide a solution to this problem [22]. Minimum probability of bit error can be achieved by implementing the optimum receiver as a backward-forward dynamic programming algorithm [23]. It turns out that the structure of the multiuser receiver consists of a bank of matched filters followed by the Viterbi algorithm [14, 24]. The computational complexity of the optimum receiver is exponential in the number of users and is prohibitive for practical implementation.

From a practical standpoint, a sub-optimum receiver with a much lower complexity is desirable. The decorrelating detector [25] is a relatively low complexity linear receiver. The decision statistics are obtained by a linear transformation of the vector formed by the outputs of the bank of matched filters. The transformation matrix is the inverse of the crosscorrelation matrix. The complexity of this receiver is linear in the number of users. The decorrelating detector far outperforms the conventional receiver in most cases of interest and is near-far resistant [26]. The detector has a higher complexity for an asynchronous channel than for a synchronous channel and accurate knowledge of the signal delays is essential. Furthermore, recomputation of the crosscorrelation matrix and its inverse is required whenever a user leaves or enters the system. Finally, there can be

problems with matrix inversion with fixed point arithmetic.

There are also nonlinear sub-optimum multiuser receivers. One such receiver performs successive interference cancellation and uses decision feedback [27]. In this receiver, the signals from all of the users are ranked according to their powers (based on their detected amplitudes). The strongest user is detected by a conventional receiver and the corresponding spread signal regenerated; the strongest interference signal is subtracted out of the received signal; the process is repeated for progressively weaker signals for all of the signals. Multistage receivers differ from this receiver in that the decisions made at the outputs of the initial matched filters are tentative, and the users' signal estimates are made in parallel rather than in succession [28, 29, 30]. A multistage Rake receiver [31] can cancel interference as well as combine multipath. These schemes also exhibit near-far resistance [32, 33] and their complexities are linear in the number of users, but they again require accurate knowledge of the spreading codes of all of the users, their phases, and their delays. A detailed discussion of multiuser receivers can be found in [33, 34], and the performance comparison of various multiuser receivers is addressed in [32, 33].

2.2.4 Why Use Adaptive Minimum Mean Squared Error Receivers?

It was noted in Section 2.2.3 that the optimum receiver for a spread spectrum signal has a very high computational complexity for practical implementation. The sub-optimum receivers, while less complex, are still multiuser receivers and require not only the knowledge of the spreading codes of all of the users, but also accurate estimates of the phase, timing, and, in some cases, the amplitudes. Accurate estimation of all of these parameters is almost impossible to achieve, and often, a slight loss in accuracy can result in a large degradation of the performance of the receiver [35, 36]. When the receiver is intended for a mobile unit, not only the computational complexity of multiuser receivers, but also the lack of knowledge of the spreading codes of all of the users precludes their use. A conventional receiver may be inadequate for spreading codes that are non-orthogonal on the forward link or for an ad hoc peer-to-peer communication network with little coordination between the mobiles.

The adaptive minimum mean squared error (MMSE) receiver is basically a single user receiver in that it requires knowledge of only the desired user's spreading code. Essentially, it is a complex adaptive filter that exploits the *cyclostationary* property exhibited by DS/SS signals. Although initial code synchronization is necessary, the timing accuracy requirement is not stringent. Furthermore, phase and amplitude estimates are not required.

2.3 Classification of Adaptive Receivers for CDMA Systems

CDMA receivers may be categorized broadly into *multiuser* receivers and *single user* receivers. This classification is based on the receiver structure, i.e., based on whether the receiver demodulates a single user or *jointly* demodulates some or all of the active users in the system. In the literature, receivers which we call "single user" receivers are often classified under multiuser receivers when a number of them are used in parallel to *separately* demodulate multiple users. But here the term "multiuser receivers" is used to describe strictly those receivers that *need* to demodulate multiple users even if only one user is of interest. Buehrer [33] and Duel-Hallen et al. [34] discuss the classification of multiuser receivers in detail.

Figure 2.2 shows the classification of single user receivers into two main categories: *fixed* receivers and *adaptive* receivers [37]. As the name indicates, fixed receivers are those that do not change with time. In contrast, adaptive receivers make use of *adaptive filters* whose coefficients, also known as weights, are adapted to minimize a certain error criterion [38, 39]. There are basically two types of fixed receivers, the correlator and the matched filter, which differ in their implementation but are functionally equivalent.

Adaptive receivers may be further classified into *linear* and *nonlinear* receivers. In a linear receiver, the output may be obtained as a linear transformation of the input. If $\mathbf{x}$ is a vector of input samples and $\mathbf{w}$ is the vector of filter weights, then the output y of the linear receiver is given by $y = \mathbf{w}^H\mathbf{x}$ where $(\cdot)^H$ denotes a Hermitian transpose, also known as conjugate transpose. A decision feedback receiver [40] is an example of a nonlinear receiver because it incorporates past symbol decisions, which involve nonlinear operations, in performing the current symbol estimates. Neural network based receivers also compute the output as a nonlinear function of the input [41, 42]. Linear receivers are classified into high complexity and reduced complexity receivers. High complexity receivers include the fractionally spaced receiver and the chip rate receiver. The tap spacing in the adaptive filter is equal to the chip period in the chip rate receiver, whereas it is a fraction of the chip period in the fractionally spaced receiver. Fractionally spaced receivers are further divided into the optimum linear-conjugate-linear (LCL) filter [43] and the complex time dependent adaptive filter (TDAF) [44]. The TDAF may be either a waveform estimating filter or a symbol estimating filter. In the latter case, it reduces to a fractionally spaced equalizer or a bank of equalizers. Reduced complexity receivers are categorized based on whether the complexity reduction is optimal or suboptimal. Two examples of suboptimal complexity reduction are the cyclically shifted filter bank and the data symbol oversampling receiver [45, 46]. The structures of some of the above receivers are discussed in further detail in Section 2.4.

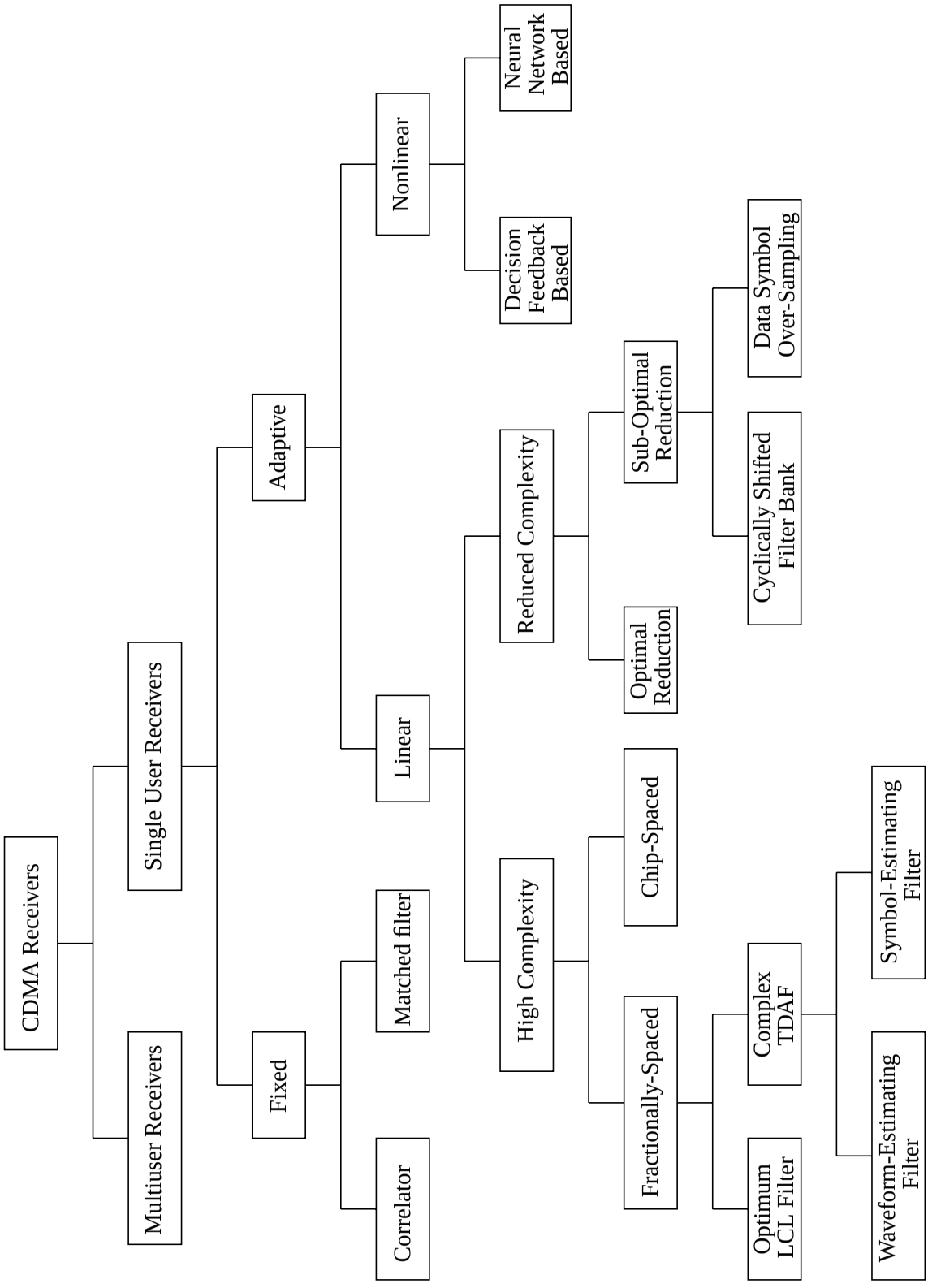

Figure 2.2: Classification of Single User Receivers for CDMA Systems.

2.4 Adaptive Receiver Structures

The adaptive receivers discussed above differ in the extent to which they exploit the cyclostationary property of the CDMA signals and, hence, their performances differ. There is a tradeoff between computational complexity and receiver performance.

2.4.1 The Linear Fractionally-Spaced Receiver and the Chip-Rate Receiver

The linear fractionally-spaced receiver (LFSR) and the chip-rate receiver (CRR) are perhaps the most widely investigated receivers. The earliest work on CDMA interference suppression using LFSRs and CRRs can be found in [45, 47, 48]. Abdulrahman [49] used similar techniques with DFEs. Madhow and Honig [45, 47] and Monogioudis et al. [50] showed that MMSE receivers are near-far resistant. More analysis on MMSE receivers was carried out in [37, 46, 51, 52, 53]. Cheng [54] compared the performance of MMSE receivers with and without error correction coding. As shown in Section 3.5, the optimum filter for extracting a cyclostationary signal (cf. Chapter 3), which a DS/SS signal is, reduces to an equalizer when

- the spreading code repeats every symbol,
- the estimated signal is sampled once every symbol, and
- the symbol rate is harmonically related to the sample rate.

Figures 2.3 and 2.4 show the adaptive LFSR and CRR, respectively.

Both of them make use of an adaptive finite impulse response (FIR) filter for interference rejection. The adaptive filter, while performing despreading, rejects MAI and combines multipath energy within the current received symbol interval. The difference between the structures of the two receivers is, the CRR has a chip-matched filter (whose output is sampled at the chip rate) followed by an adaptive equalizer, whereas the LFSR has a fractionally spaced adaptive equalizer directly operating on the sampled data. Consequently, tap spacing of the FIR filter and, hence, the number of adaptive tap weights, is different in the two cases. The performance of the two receivers is very similar and the LFSR proves advantageous in multipath channels and for asynchronous transmission [55]. The optimum receiver for a multipath channel is a filter matched to the channel impulse response followed by an equalizer and an LFSR, which, with its fractional tap-spacing, can synthesize this receiver better than a CRR can [14, 56]. In an asynchronous channel, the interference subspace has a larger dimension. Therefore, the fractionally spaced receiver, with its higher dimensionality, is able to perform better [55]. Finally, the LFSR is less sensitive to the sampling time [14, 56].

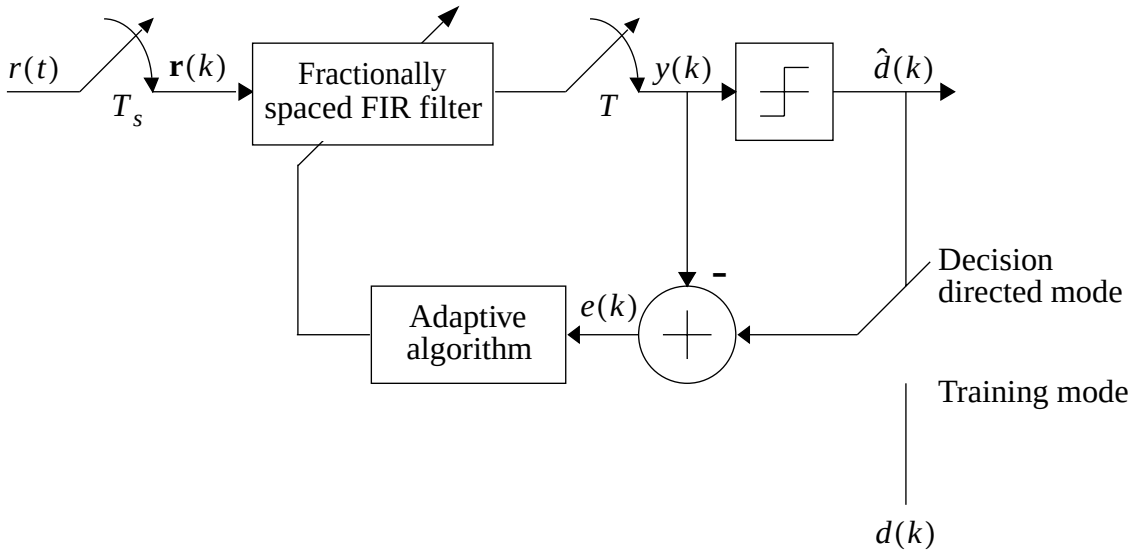

Figure 2.3: The Linear Fractionally-Spaced Receiver.

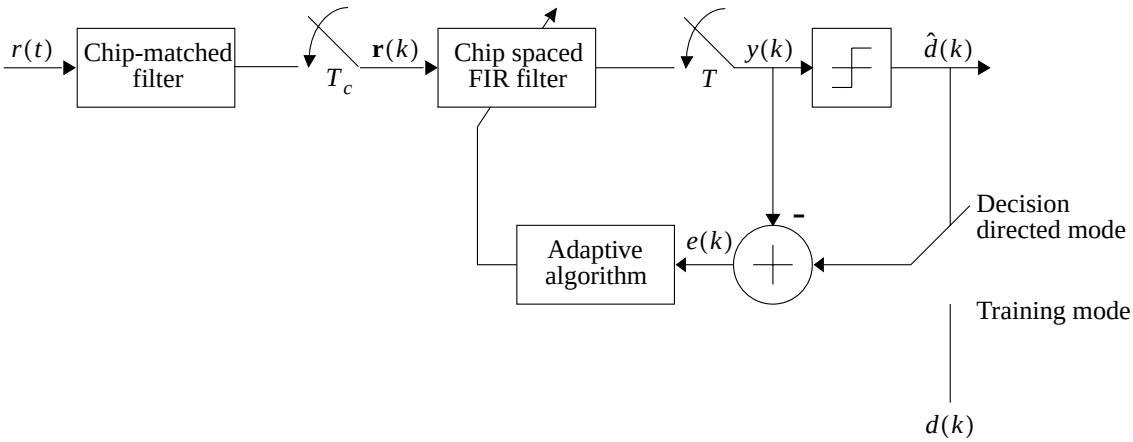

Figure 2.4: The Chip-Rate Receiver.

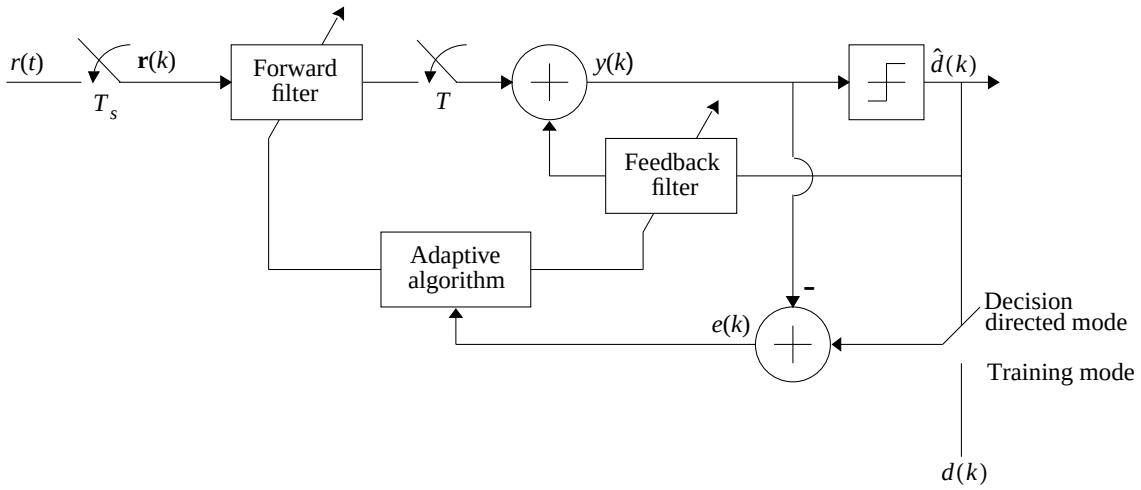

Figure 2.5: The Decision Feedback Receiver.

2.4.2 The Decision Feedback Receiver

The decision feedback receiver (DFR) is an extension of the linear receivers discussed in the previous section. The DFR is illustrated in Figure 2.5. It consists of a forward adaptive FIR filter and a feedback adaptive FIR filter. The function of the feedback filter is to cancel inter-symbol interference from previously detected symbols arising from multipath [56]. The forward filter, while performing despreading, rejects MAI and combines multipath energy within the current received symbol. If previous symbols have been correctly detected, then the interference they cause can be effectively canceled. When incorrect decisions are fedback, error propagation can result. The performance loss due to error propagation is not substantial in many instances [14]. Abdulrahman et al. [40, 49, 57] extensively studied the performance of both the fractionally-spaced as well as the chip-rate DFR in CDMA systems. Majmundar's results [55] showed that there are no gains to be achieved from a fractionally-spaced DFR over a LFSR for multipath delays less than a symbol period. Monogioudis et al. [50] demonstrated gains in AWGN with static multipath with unreported delays of the multipath components. However, it is widely agreed that a fractionally-spaced DFR is superior to a chip-rate DFR in multipath channels.

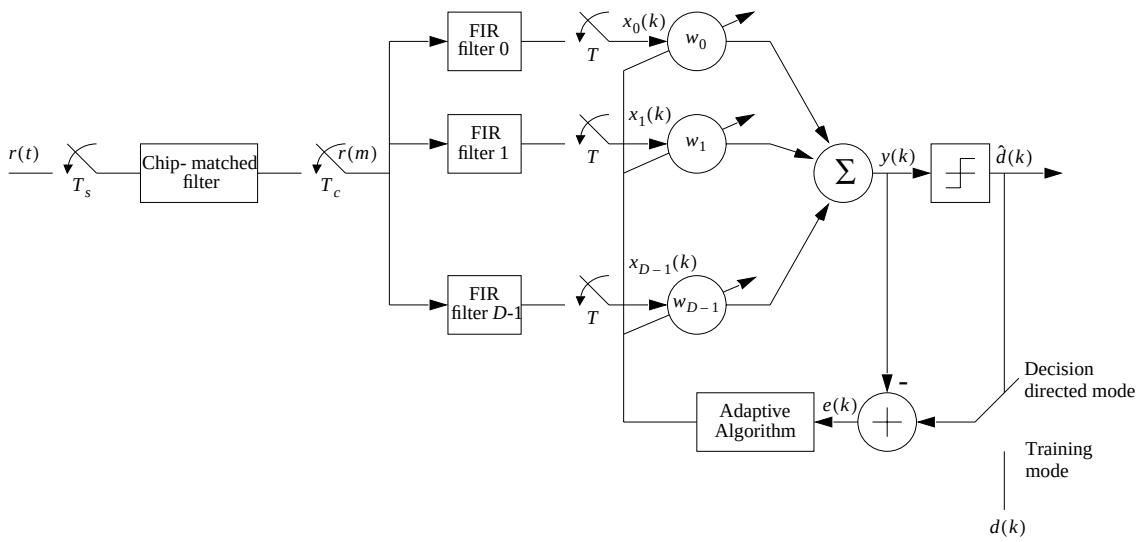

Figure 2.6: The Cyclically Shifted Filter Bank.

2.4.3 Linear Receivers with Sub-Optimum Complexity Reduction

In the CRR, the number of adaptive weights is typically equal to the spreading gain. This can be a large number and may prove costly for implementation. Ström and Miller [58] proposed an optimum complexity reduction for these receivers. The method involves the transformation of the received signal vector and requires the knowledge of the signal subspace. More specifically, the spreading codes of all of the users as well as their delays must be known, and hence the technique is not practical. Furthermore, it is not adaptive since it requires the recomputation of the transform whenever a user enters or leaves the system. Two receivers with sub-optimum complexity reduction were proposed by Madhow and Honig [45, 46]. They are briefly discussed here.

The Cyclically Shifted Filter Bank

The first receiver with sub-optimum complexity reduction is the cyclically shifted filter bank (CSFB) depicted in Figure 2.6. As the name suggests, it consists of a bank of D chip-rate FIR filters, which are cyclically shifted versions of the matched filter for the desired user. The successive shifts are equi-spaced, and the spacing is given by $\Delta = \lfloor N_B/D \rfloor$ where N_B is the number of samples per bit and $\lfloor(\cdot)\rfloor$ denotes the largest integer less than $(\cdot)$. The received signal is passed through each of these filters, whose outputs are sampled once every symbol. The D sampled outputs are weighted and

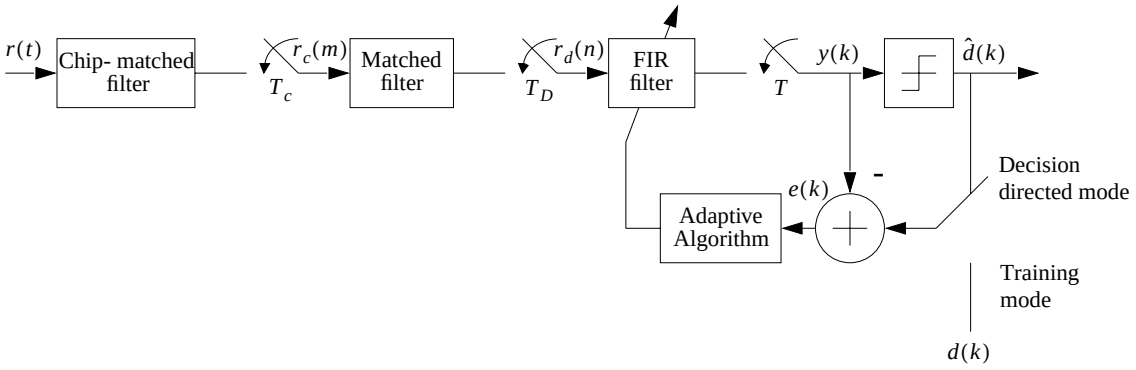

Figure 2.7: The Data Oversampling Receiver.

combined to satisfy the MMSE criterion. The receiver projects the N-dimensional signal vectors onto a D-dimensional subspace. The near-far resistance of the CSFB is equal to that of the CRR if the projection of the desired user's signal onto the subspace orthogonal to the subspace spanned by the interference vectors is contained in the D-dimensional subspace spanned by filters [46]. Furthermore, the CSFB has enough degrees of freedom to suppress up to $(D-1)/2$ strong asynchronous interferers or up to $D-1$ synchronous interferers. It exploits the linear independence of the cyclically shifted versions of the matched filter vector.

Data Over-Sampling Receiver

The second reduced complexity receiver proposed by Madhow and Honig is the data oversampling receiver (DOSR) shown in Figure 2.7. In this receiver, the output of the matched filter for the desired user is sampled D times per symbol period. The sampling interval is $\Delta = \lfloor N_B/D \rfloor$. The over-sampled matched filter outputs are combined by a T_D-spaced FIR filter whose weights are adapted to minimize the MMSE criterion where $T_D = \lfloor T/D \rfloor$, T being the symbol period. The length of the adaptive filter is chosen to be $2\lfloor (D-1)/2 \rfloor$, and the decision statistic is obtained by placing the outputs of the matched filter such that the decision statistic for the conventional detector is at the center of the adaptive filter. Due to the increased interference from adjacent bits, the DOSR can suppress only up to $(D-1)/3$ strong asynchronous interferers. Over all, the CSFB has a slightly higher complexity, but outperforms the DOSR [46]. While neither receiver matches the performance of the CRR, their obvious advantage is reduced complexity.

2.5 Summary

This chapter provided a motivation and an overview of adaptive receivers. It was shown that the conventional matched filter receiver is not optimal when a signal is received in multiple access interference. The near far problem in cellular CDMA systems occurs when strong multiple access interference completely jams a weak desired signal. Multiuser receivers, which simultaneously demodulate signals from multiple users, are able to alleviate the problems arising from multiple access interference and are near-far resistant. When only a single user's signal is of interest, such a receiver can be not only expensive, but also impractical. Adaptive receivers, which are single user receivers, can perform interference rejection with reasonable complexity. A classification of adaptive receivers was provided and details of commonly used adaptive receiver structures were presented.

Chapter 3

Cyclostationary Property of DS/SS Signals

3.1 The Basics of Cyclostationarity

Physical phenomena encountered in a communications system are random in nature. Examples include the information signal that is communicated over a wireless medium from one location to another, the effects of the propagation channel that influence the distortion of this signal, the noise that is introduced at the receiver by its electronic components, and the radio signals emitted from other sources that serve as interference to the signal of interest. These phenomena are modeled by probabilistic methods for the purposes of mathematical analysis. Statistics of these processes are used in the performance evaluation of a communications system, the idea being that these statistics, expected values such as the *mean* and *variance*, account for the ensemble behavior of the random process [59].

There is a sub-class of random processes, *cyclostationary processes*, which is characterized by periodically time-variant parameters [59, 60]. Gardner defines cyclostationarity as follows [61]: "A signal is said to be cyclostationary of order n (in the wide sense) if and only if we can find some nth-order nonlinear transformation of the signal that will generate finite-strength additive sine-wave components, which will result in spectral lines." Thus, a random process $X(t)$ whose mean $m_X(t)$ and autocorrelation function $R_X(t,\tau)$ are periodic is said to be (second order) cyclostationary in the wide sense. For example, the process $X(t)$ is cyclostationary if

$$m_X(t+T) = m_X(t) \triangleq E\{X(t)\} \tag{3.1}$$

$$R_X(t+T,\tau) = R_X(t,\tau) \triangleq E\left\{X\left(t+\frac{\tau}{2}\right) X^*\left(t-\frac{\tau}{2}\right)\right\} \tag{3.2}$$

for all t and τ where T is the period. Since $R_X(t,\tau)$ is periodic, it can be represented by a Fourier series as

$$R_X(t,\tau) = \sum_{\alpha} R_X^{\alpha}(\tau) e^{j2\pi\alpha t} \tag{3.3}$$

where the Fourier coefficients $\{R_X^{\alpha}(\tau)\}$ are given by

$$R_X^{\alpha}(\tau) \triangleq \frac{1}{T} \int_{-T/2}^{T/2} R_X(t,\tau)\ e^{-j2\pi\alpha t}\, dt. \tag{3.4}$$

α ranges over all integer multiples of the fundamental frequency $1/T$. $R_X^{\alpha}(\tau)$ is known as the *cyclic autocorrelation function* and α as the *cycle frequency*. When there is more than one fundamental frequency of interest, the *cycle spectrum* $\{\alpha\}$ includes all integer multiples of all of these fundamental frequencies. In such a case, $R_X^{\alpha}(\tau)$ is more generally redefined as [59]

$$R_X^{\alpha}(\tau) \triangleq \lim_{Z\to\infty} \frac{1}{Z} \int_{-Z/2}^{Z/2} R_X(t,\tau)\, e^{-j2\pi\alpha t}\, dt \tag{3.5}$$

and the process $X(t)$ itself is said to be *polycyclostationary* due to the presence of more than one periodicity. The definition of cyclostationarity noted above then implies that a signal $X(t)$ exhibits cyclostationarity if there exists a cycle frequency α for which the Fourier coefficient defined in Equation(3.5) is not identically zero as a function of τ.

The *spectral density* $S_X(t,f)$ of the process $X(t)$ is the Fourier transform of the autocorrelation function:

$$S_X(t,f) \triangleq \mathcal{F}\{R_X(t,\tau)\} = \int_{-\infty}^{\infty} R_X(t,\tau)\ e^{-j2\pi f\tau}\, d\tau. \tag{3.6}$$

From Equation (3.3) it follows that

$$S_X(t,f) = \sum_{\alpha} S_X^{\alpha}(f) e^{j2\pi\alpha t} \tag{3.7}$$

where the *cyclic spectrum* or *cyclic spectral density*

$$S_X^{\alpha}(f) \triangleq \mathcal{F}\{R_X^{\alpha}(\tau)\}. \tag{3.8}$$

The cyclostationary property of a signal translates to spectral correlation. To see this, let

$$Y(t) \triangleq X(t)e^{-j2\pi\frac{\alpha}{2}t} \tag{3.9a}$$

$$Z(t) \triangleq X(t)e^{+j2\pi\frac{\alpha}{2}t}. \tag{3.9b}$$

The time-averaged crosscorrelation between $Y(t)$ and $Z(t)$ is

$$\bar{R}_{YZ}(\tau) \triangleq \lim_{Z\to\infty}\frac{1}{Z}\int_{-Z/2}^{Z/2} R_{YZ}(t,\tau)\,dt \tag{3.10}$$

$$R_{YZ}(t,\tau) \triangleq E\left\{Y\left(t+\frac{\tau}{2}\right)\,Z^*\left(t-\frac{\tau}{2}\right)\right\} \tag{3.11}$$

so that

$$\begin{aligned}
\bar{R}_{YZ}(\tau) &= \lim_{Z\to\infty}\frac{1}{Z}\int_{-Z/2}^{Z/2} E\left\{X\left(t+\frac{\tau}{2}\right)e^{-j\pi\alpha\left(t+\frac{\tau}{2}\right)}\,X^*\left(t-\frac{\tau}{2}\right)e^{-j\pi\alpha\left(t-\frac{\tau}{2}\right)}\right\}dt \\
&= \lim_{Z\to\infty}\frac{1}{Z}\int_{-Z/2}^{Z/2} E\left\{X\left(t+\frac{\tau}{2}\right)\,X^*\left(t-\frac{\tau}{2}\right)\right\}e^{-j2\pi\alpha t}\,dt \\
&= \lim_{Z\to\infty}\frac{1}{Z}\int_{-Z/2}^{Z/2} R_X(t,\tau)\,e^{-j2\pi\alpha t}\,dt \\
&\equiv R_X^\alpha(\tau).
\end{aligned} \tag{3.12}$$

Equation (3.12) shows that the cyclic autocorrelation of the process $X(t)$ is the time-averaged crosscorrelation between frequency translates of $X(t)$. Since $X(t)$ is cyclostationary if $R_X^\alpha(\tau)$ is not identically zero as a function of τ for some $\alpha \neq 0$, there is a correlation between some frequency shifted versions of a cyclostationary signal. Thus spectral correlation exists for a cyclostationary signal. Spectral correlation results in *spectral redundancy*, which is exploited by signal processing techniques for signal enhancement.

Using the definition of Equation (3.2), the autocorrelation of $Y(t)$ is

$$\begin{aligned}
R_Y(t,\tau) &= E\left\{X\left(t+\frac{\tau}{2}\right)e^{-j\pi\alpha\left(t+\frac{\tau}{2}\right)}\,X^*\left(t-\frac{\tau}{2}\right)e^{j\pi\alpha\left(t-\frac{\tau}{2}\right)}\right\} \\
&= E\left\{X\left(t+\frac{\tau}{2}\right)X^*\left(t-\frac{\tau}{2}\right)\right\}e^{-j\pi\alpha\tau} \\
&\equiv R_X(t,\tau)\,e^{-j\pi\alpha\tau}.
\end{aligned} \tag{3.13}$$

Similarly,

$$R_Z(t,\tau) \equiv R_X(t,\tau)\, e^{+j\pi\alpha\tau}. \tag{3.14}$$

The time-averaged spectral density for $Y(t)$ is given by

$$\bar{S}_Y(f) \triangleq \lim_{Z\to\infty} \frac{1}{Z} \int_{-Z/2}^{Z/2} \int_{-\infty}^{\infty} R_Y(t,\tau)\, e^{-j\pi f\tau}\, d\tau\, dt \tag{3.15}$$

$$= \lim_{Z\to\infty} \frac{1}{Z} \int_{-Z/2}^{Z/2} \int_{-\infty}^{\infty} R_X(t,\tau)\, e^{-j\pi\alpha\tau}\, e^{-j\pi f\tau}\, d\tau\, dt \tag{3.16}$$

using Equation (3.13). It follows from Equation (3.6) that

$$\bar{S}_Y(f) = \lim_{Z\to\infty} \frac{1}{Z} \int_{-Z/2}^{Z/2} S_X(f+\alpha/2)\, dt$$

$$= \bar{S}_X(f+\alpha/2) \tag{3.17}$$

and

$$\bar{S}_Z(f) = \bar{S}_X(f-\alpha/2). \tag{3.18}$$

The time-averaged cross spectral density is given by

$$\bar{S}_{YZ}(f) \triangleq \lim_{Z\to\infty} \frac{1}{Z} \int_{-Z/2}^{Z/2} \int_{-\infty}^{\infty} R_{YZ}(t,\tau)\, e^{-j\pi f\tau}\, d\tau\, dt \tag{3.19}$$

$$= \int_{-\infty}^{\infty} \lim_{Z\to\infty} \frac{1}{Z} \int_{-Z/2}^{Z/2} R_{YZ}(t,\tau)\, dt\, e^{-j\pi f\tau}\, d\tau$$

$$= \int_{-\infty}^{\infty} \bar{R}_{YZ}(\tau)\, e^{-j\pi f\tau}\, d\tau$$

$$= \int_{-\infty}^{\infty} R_X^{\alpha}(\tau)\, e^{-j\pi f\tau}\, d\tau \tag{3.20}$$

$$\equiv S_X^{\alpha}(f). \tag{3.21}$$

Equation (3.12) was used to obtain Equation (3.20), and Equation (3.21) follows from Equation (3.8).

The time-averaged *cross coherence function* [59, 60, 61] provides a measure of the degree of similarity between two processes and is defined by

$$\rho_{YZ}(f) \triangleq \frac{\bar{S}_{YZ}(f)}{[\bar{S}_Y(f)\,\bar{S}_Z(f)]^{1/2}} \tag{3.22}$$

$$= \frac{S_X^\alpha(f)}{[\bar{S}_X(f-\alpha/2)\,\bar{S}_X(f+\alpha/2)]^{1/2}} \triangleq \rho_X^\alpha(f). \tag{3.23}$$

$\rho_X^\alpha(f)$ is termed the *autocoherence* of $X(t)$ at cycle frequency α and spectral frequency f. $|\rho_X^\alpha(f)|$ is bounded to the interval $[0,1]$ and is, in fact, the time-averaged correlation coefficient for the corresponding frequency components of $X(t)$ (separated by the cycle frequency α) [59, 60]. Therefore, it can be used as a measure of the extent of spectral redundancy resulting from spectral correlation.

Thus, it is seen that a signal is cyclostationary only if the spectral components at two frequencies, $f-\alpha/2$ and $f+\alpha/2$, separated by some α are correlated. If $|\rho_X^\alpha(f)|=1$, the process $X(t)$ is said to be completely coherent at spectral frequency f and cycle frequency α and there is complete spectral redundancy at $f-\alpha/2$ and $f+\alpha/2$. If $|\rho_X^\alpha(f)|=0$, the process $X(t)$ is said to be completely incoherent at spectral frequency f and cycle frequency α. There is no spectral redundancy in this case.

3.2 Applications of Cyclostationarity

The spectral redundancy associated with the spectral correlation property of cyclostationary signals has many useful applications in communications as well as other areas that employ signal processing of data sampled from random processes. Signal processing techniques that exploit spectral redundancy yield results that are superior to those that don't. Some of the common applications of cyclostationarity in signal processing of communications signals are listed here, they are discussed in greater detail in [60, 61].

1. *Signal selective measurements.* When a signal of interest is received along with noise and other cochannel interference signals, their cyclic spectra may be non-overlapping (due to their different cycle spectra, i.e., sets of cycle frequencies). If so, this property can be exploited. There may be a cycle frequency that is unique to the signal of interest, in which case a cyclic spectrum (at this cycle frequency) exists only for this signal and not for any of the others received with it. Thus, a measurement of the cyclic spectrum (or a parameter associated with it) of the signal may be made with little impact from interference and noise.

2. *Signal detection.* A weak signal received with high levels of background noise can be detected by generating a spectral line at a known cycle frequency of the signal

and ensuring the existence of this line at the cycle frequency. When multiple signals are received, a cycle frequency that is unique to each signal may be used to detect its presence. This method can be used to classify signals of different modulation types.

3. *Parameter estimation.* Signal parameters, such as carrier frequency and phase, and symbol rates can be estimated from estimates of cyclic spectra. Thus applications include, in addition to carrier and symbol synchronization, spreading code synchronization in DS/SS systems [62, 63].

4. *Time-difference-of-arrival estimation.* The time-difference-of-arrival (TDOA) of a signal at two receivers can be estimated from the *cyclic cross spectrum* [60] of the signals received at the two receivers. In particular, the phase of the cyclic cross spectrum is proportional to the TDOA of the signal at the two receivers. This also has applications in multipath channel identification.

5. *Spatial filtering.* A signal with a unique cycle frequency can be enhanced when there are other signals from spatially separated sources. This is achieved through the exploitation of spectral redundancy for blind adaptation of the weights of an adaptive array used at the front end. The weights of the spatial filter are adapted to restore the spectral correlation property of the signal of interest. In the process, the array forms a beam in the direction of the signal of interest or nulls in the directions of the interference sources.

6. *Direction finding.* If the antenna array is calibrated, beamforming can be extended to high-resolution direction finding (DF). There are several advantages over conventional high resolution DF techniques: knowledge of the correlation properties of the noise is not essential, the number of antenna elements does not have to be more than the number of signals, and spatial resolution can be improved.

7. *Signal extraction.* Linear periodically time-variant (LPTV) filters can be used to extract a signal from underlying noise and interference by taking advantage of the spectral redundancy characteristic of the signals. LPTV filters can restore portions of the signal spectrum that are corrupted by interference by exploiting the inherent correlation of these portions with other portions of the spectrum. This topic will be addressed further in Section 3.3.

3.3 Cyclic Filtering

Of particular relevance to this work is the application of cyclostationarity for optimum cyclic filtering [59, 60, 64]. We consider the scenario where a signal $x(t)$ is received over a radio propagation channel. The signal of interest, $s(t)$, is embedded within this received

signal. We seek to estimate the desired signal by optimally filtering $x(t)$. Since $s(t)$ is nonstationary, the linear filter used, $h(t,\cdot)$, is time varying:

$$\hat{s}(t) = \int_{-\infty}^{\infty} h(t,u)x(u)\,du \tag{3.24}$$

where $\hat{s}(t)$ is the best estimate of $s(t)$. The filter is optimal based on some criterion satisfied by the estimated signal. For example, if the mean-squared error (MSE) is being minimized, then $h(t,\cdot)$ minimizes the following error, also known as the *cost function*:

$$J \stackrel{\triangle}{=} E\{|s(t) - \hat{s}(t)|^2\}. \tag{3.25}$$

The design equation for $h(t,\cdot)$ in this case is [59]

$$\int_{-\infty}^{\infty} h(t,u)R_x(v,u)\,du = R_{xs}(t,v), \qquad -\infty < t,v < \infty. \tag{3.26}$$

It can be shown that $h(t,\cdot)$ is periodic and can be represented by a Fourier series as

$$h(t,u) = \sum_{\nu} h_\nu(t-u)e^{j2\pi\nu u} \tag{3.27}$$

$$h_\nu(\tau) \stackrel{\triangle}{=} \lim_{Z\to\infty} \frac{1}{Z} \int_{-Z/2}^{Z/2} h(t+\tau,t)\; e^{-j2\pi\nu t}\,dt. \tag{3.28}$$

$\{\nu\}$ includes all fundamental frequencies of $h(t,\cdot)$ and all integer multiples of each of them. Substitution of Equation (3.27) in Equation (3.24) results in

$$\begin{aligned}\hat{s}(t) &= \sum_{\nu} \int_{-\infty}^{\infty} h_\nu(t-u)\left[x(u)e^{j2\pi\nu u}\right] du \\ &= \sum_{\nu} \int_{-\infty}^{\infty} h_\nu(t-u)x_\nu(u)\,du\end{aligned}$$

where

$$x_\nu(t) \stackrel{\triangle}{=} x(t)e^{j2\pi\nu t} \tag{3.29}$$

so that

$$\hat{s}(t) = \sum_{\nu} h_\nu(t) \otimes x_\nu(t) \tag{3.30}$$

where $\otimes$ represents convolution. Fourier transformation of Equation (3.30) yields

$$\hat{S}(f) = \sum_{\nu} H_\nu(f) X_\nu(f) = \sum_{\nu} H_\nu(f) X(f-\nu). \tag{3.31}$$

According to the above equation, the optimum time-variant filtering amounts to frequency-shifting the signal by the *filter's* periodicities, i.e., $\{\nu\}$, passing these frequency shifted versions through *time-invariant* filters $H_\nu(f)$ $(= \mathcal{F}\{h_\nu(\tau)\})$, and adding their outputs. The frequency-shift operations result in the name of this process, FRESH (FREquency-SHift) filtering. To determine $\{\nu\}$, we consider the orthogonality condition [59, 60]

$$E\{[s(t) - \hat{s}(t)] x^*(t-u) e^{-j2\pi\alpha(t-u)}\} = 0, \tag{3.32}$$

for all u and α of interest. Equation (3.32) specifies the orthogonality of the error $s(t) - \hat{s}(t)$ with all the pre-filtered frequency shifted signals $x(t-u)e^{j2\pi\alpha(t-u)}$. This condition is necessary and sufficient for the minimization of the MSE cost function of Equation (3.25). Using Equations (3.30) and (3.29) in Equation (3.32) and averaging over time, the result is

$$R_{sx}^{\alpha}(u) e^{j2\pi\alpha u} - \sum_{\nu} h_\nu(u) \otimes R_x^{\alpha-\nu}(u) e^{j2\pi(\alpha+\nu)u} = 0 \tag{3.33}$$

for all u and α of interest [1]. Fourier transformation of this equation yields

$$S_{sx}^{\alpha}\left(f - \frac{\alpha}{2}\right) - \sum_{\nu} H_\nu(f)\, S_x^{\alpha-\nu}\left(f - \frac{\alpha+\nu}{2}\right) = 0 \tag{3.34}$$

and therefore

$$\sum_{\nu} H_\nu(f)\, S_x^{\alpha-\nu}\left(f - \frac{\alpha+\nu}{2}\right) = S_{sx}^{\alpha}\left(f - \frac{\alpha}{2}\right) \tag{3.35}$$

for all f and α of interest. Thus the set of all ν that determine the time-invariant filters to be used for estimating the signal of interest as in Equation (3.31) is dependent on the set of all α and these sets are such that the cyclic spectra in Equation (3.35) are not identically zero. It is readily seen from the above discussion that FRESH filtering exploits the cyclostationary property of signals. It may be noted that in the trivial case where neither $x(t)$ is cyclostationary nor $s(t)$ and $x(t)$ are jointly cyclostationary, the

[1] The *cyclic crosscorrelation* $R_{sx}^{(\cdot)}(u)$ is defined as the Fourier coefficient of the polyperiodic crosscorrelation function $R_{sx}(t,u)$ (when $s(t)$ and $x(t)$ are jointly cyclostationary), similar to the definition of the cyclic autocorrelation. Also, the cyclic cross spectrum $S_{sx}^{(\cdot)}(f) \stackrel{\triangle}{=} \mathcal{F}\{R_{sx}^{(\cdot)}(u)\}$.

only values that apply are $\alpha = \nu = 0$ and the optimum solution for the filtering problem reduces to the linear *time-invariant* (LTI) Wiener filter [59]

$$H_0(f) = \frac{S_{sx}(f)}{S_x(f)}. \tag{3.36}$$

Using the orthogonality condition of Equation (3.32), it can be shown that the minimum MSE (MMSE) is given by

$$\begin{aligned} J_{min} &= E\{[s(t) - \hat{s}(t)]s^*(t)\} \\ &= E\{|s(t)|^2\} - E\{s^*(t)\hat{s}(t)\}. \end{aligned} \tag{3.37}$$

The time-averaged MMSE is obtained by substituting Equation (3.30) into Equation (3.37) and averaging over all time:

$$\begin{aligned} \bar{J}_{min} &\triangleq \lim_{Z\to\infty} \int_{-Z/2}^{Z/2} J_{min}\, dt \\ &= \lim_{Z\to\infty} \frac{1}{Z} \int_{-Z/2}^{Z/2} E\{|s(t)|^2\}\, dt \\ &\quad - \lim_{Z\to\infty} \frac{1}{Z} \int_{-Z/2}^{Z/2} E\left\{ s^*(t) \sum_\nu \int_{-\infty}^{\infty} h_\nu(t-\tau)[x(\tau)e^{j2\pi\nu\tau}]\, d\tau \right\} dt \\ &= \lim_{Z\to\infty} \frac{1}{Z} \int_{-Z/2}^{Z/2} R_x(t,0)\, dt \\ &\quad - \sum_\nu \lim_{Z\to\infty} \frac{1}{Z} \int_{-Z/2}^{Z/2} \int_{-\infty}^{\infty} h_\nu(u) E\{s^*(t)x(t-u)e^{j2\pi\nu(t-u)}\}\, du\, dt \\ &= R_x^\alpha(0) \\ &\quad - \sum_\nu \int_{-\infty}^{\infty} h_\nu(u) \lim_{Z\to\infty} \frac{1}{Z} \int_{-Z/2}^{Z/2} E\{s^*(t)x(t-u)\} e^{j2\pi\nu t}\, dt\, e^{-j2\pi\nu u}\, du \\ &= R_x^\alpha(0) - \sum_\nu \int_{-\infty}^{\infty} h_\nu(v) \left[\lim_{Z\to\infty} \frac{1}{Z} \int_{-Z/2}^{Z/2} R_{sx}(t,u) e^{-j2\pi\nu t}\, dt\, e^{j2\pi\nu u} \right]^* du \\ &= R_x^\alpha(0) - \sum_\nu \int_{-\infty}^{\infty} h_\nu(u) [R_{sx}^\nu(u) e^{j2\pi\nu u}]^*\, du. \end{aligned} \tag{3.38}$$

Parseval's relation may be used to rewrite the MMSE equation:

$$\begin{aligned}
\bar{J}_{min} &= \int_{-\infty}^{\infty} S_x^0(f) - \sum_{\nu} \int_{-\infty}^{\infty} h_\nu(u) \left[\int_{-\infty}^{\infty} S_{sx}^{\nu}(f-\nu) e^{j2\pi f u}\, df \right]^* du \\
&= \int_{-\infty}^{\infty} S_x^0(f) - \sum_{\nu} \int_{-\infty}^{\infty} \int_{-\infty}^{\infty} h_\nu(u) e^{-j2\pi f u}\, du\, [S_{sx}^{\nu}(f-\nu)]^*\, df \\
&= \int_{-\infty}^{\infty} S_x^0(f) - \sum_{\nu} \int_{-\infty}^{\infty} H_\nu(f)\, [S_{sx}^{\nu}(f-\nu)]^*\, df. \qquad (3.39)
\end{aligned}$$

Equation (3.39) reveals how spectral redundancy reduces the MSE. Spectral correlation adds more terms to the summation in the equation, which results in a lower MSE. For the previously discussed noncyclostationary case, $\alpha = \nu = 0$ and the optimum filter is time-invariant, and we have

$$\bar{J}_{min} = J_{min} = \int_{-\infty}^{\infty} S_x(f) - \int_{-\infty}^{\infty} H_0(f)\, S_{sx}^*(f)\, df. \qquad (3.40)$$

The term *linear-conjugate-linear (LCL) filtering* refers to separately filtering a signal and its complex conjugate and adding them [65]. This more general filtering operation is optimum in many situations when a complex envelope is processed [64, 65]. The joint-optimization problem then involves deriving both the filter for linear processing as well as the filter for conjugate processing. Conjugate processing is superior to ordinary complex linear processing when the real and the imaginary parts of the signal to be extracted are linearly dependent [65]. Then Equation (3.24) for the estimation of the desired signal is modified for LCL-FRESH filtering as

$$\begin{aligned}
\hat{s}(t) &= \int_{-\infty}^{\infty} [h(t,u)x(t) + g(t,u)x^*(t)]\, du \qquad (3.41) \\
&= \sum_{\nu} h_\nu(t) \otimes x_\nu(t) + \sum_{\eta} g_\eta(t) \otimes x_\eta^*(t) \qquad (3.42)
\end{aligned}$$

where $x_{(\cdot)}(t)$ is as defined in Equation (3.29) and

$$g(t,u) \triangleq \sum_{\eta} g_\eta(t)\, e^{j2\pi\eta t}. \qquad (3.43)$$

It can be shown that the FRESH filter equation of Equation (3.35) is correspondingly modified to the pair of LCL-FRESH filter equations

$$\sum_{\nu} H_\nu(f)\, S_x^{\alpha-\nu}\left(f - \frac{\alpha+\nu}{2}\right) + \sum_{\eta} G_\eta(f) \left[S_{xx^*}^{\eta-\alpha}\left(f - \frac{\alpha+\eta}{2}\right) \right]^*$$

$$= S_{sx}^{\alpha}\left(f - \frac{\alpha}{2}\right) \tag{3.44a}$$

$$\sum_{\nu} H_{\nu}(f)\, S_{xx^*}^{\beta-\nu}\left(f - \frac{\beta+\nu}{2}\right) + \sum_{\eta} G_{\eta}(f)\, S_{x}^{\beta-\eta}\left(f - \frac{\beta+\eta}{2}\right)$$

$$= S_{sx^*}^{\beta}\left(f - \frac{\beta}{2}\right) \tag{3.44b}$$

for all f, α, and β of interest. Again, the sets of frequencies $\{\alpha\}$, $\{\nu\}$, $\{\beta\}$, and $\{\eta\}$ are determined by the existence of the cyclic spectra $S_x^{(\cdot)}(f)$, $S_{xx^*}^{(\cdot)}(f)$, $S_{sx}^{(\cdot)}(f)$, and $S_{sx^*}^{(\cdot)}(f)$ in Equations (3.44a) and (3.44b).

3.4 Spectral Correlation for DS/SS Signals

A DS/SS signal exhibits cyclostationarity. This property stems from the periodic nature of the signal. Equation (2.2) provided a mathematical model for a baseband DS/SS signal. In this case, a conventional BPSK signal is multiplied by a binary signal constituting the spreading signal, whose chip rate is a large multiple of the data rate. The spreading signal is formed by a repetitive PN code. The ratio of the chip rate, f_c, to the data rate, f_d, or equivalently, the ratio of the data period, T_d, to the chip period, T_c, is known as the processing gain, S:

$$S = \frac{f_c}{f_d} = \frac{T_d}{T_c} \gg 1. \tag{3.45}$$

It was shown by Chen [66] that three fundamental periodicities exist in a DS/SS signal:

1. the chip period, T_c
2. the data period, T_d
3. the code repetition period, T_r.

Chen obtained expressions for the cyclic autocorrelation and cyclic spectrum for a DS/SS signal modeled by Equation (2.2) in which $d(t) \in \{-1, 1\}$ and

$$c(t) = \sum_{m=-\infty}^{\infty} c_m q\left(t - mT_c\right) \tag{3.46}$$

where $c_m \in \{-1, 1\}$ are the chips and $q(t)$ is the basic pulse shape. For a rectangular pulse shape,

$$q(t) = \begin{cases} 1, & |t| \leq \frac{T_c}{2} \\ 0, & \text{otherwise.} \end{cases} \tag{3.47}$$

If N is the code length,

$$\begin{aligned} c_{m+N} &= c_m \quad (3.48) \\ T_r &= NT_c. \quad (3.49) \end{aligned}$$

From Equations (3.2) and (3.5), the cyclic autocorrelation is given by

$$\begin{aligned} R_x^\alpha(\tau) &= \lim_{Z\to\infty} \frac{1}{Z} \int_{-Z/2}^{Z/2} E\left\{ c\left(t+\frac{\tau}{2}\right) d\left(t+\frac{\tau}{2}\right) \right. \\ &\quad \left. \cdot\, c^*\left(t-\frac{\tau}{2}\right) d^*\left(t-\frac{\tau}{2}\right) \right\} e^{-j2\pi\alpha t}\, dt \\ &= \lim_{Z\to\infty} \frac{1}{Z} \int_{-Z/2}^{Z/2} E\left\{ \sum_{m=-\infty}^{\infty} C_m e^{j2\pi\frac{m}{T_r}(t+\frac{\tau}{2})}\, d\left(t+\frac{\tau}{2}\right) \right. \\ &\quad \left. \cdot \sum_{n=-\infty}^{\infty} C_n^* e^{-j2\pi\frac{n}{T_r}(t-\frac{\tau}{2})}\, d^*\left(t-\frac{\tau}{2}\right) \right\} e^{-j2\pi\alpha t}\, dt \quad (3.50) \end{aligned}$$

where the following Fourier series expansion for $c(t)$ has been used:

$$\begin{aligned} c(t) &= \sum_{n=-\infty}^{\infty} C_n e^{j2\pi\frac{n}{T_r}t}, \quad (3.51) \\ C_n &= \frac{1}{T_r} \int_{-T_r/2}^{T_r/2} c(t)\, e^{-j2\pi\frac{n}{T_r}t}\, dt \quad (3.52) \\ &= \frac{1}{NT_c} \int_{-NT_c/2}^{NT_c/2} \sum_{m=-\infty}^{\infty} c_m q\left(t-mT_c\right)\, e^{-j2\pi\frac{n}{NT_c}t}\, dt \\ &= \sum_{m=-\infty}^{\infty} c_m \frac{1}{NT_c} \int_{-NT_c/2}^{NT_c/2} q\left(t-mT_c\right)\, e^{-j2\pi\frac{n}{NT_c}t}\, dt \\ &= \sum_{m=0}^{N-1} c_m \frac{1}{NT_c} \int_{-T_c/2-mT_c}^{T_c/2-mT_c} e^{-j2\pi\frac{n}{NT_c}t}\, dt \\ &= \sum_{m=0}^{N-1} c_m \frac{\sin(\pi n/N)}{\pi n}\, e^{-j2\pi\frac{mn}{N}} \\ &= B_n \frac{\sin(\pi n/N)}{\pi n} \quad (3.53) \end{aligned}$$

where

$$B_n = \sum_{m=0}^{N-1} c_m \, e^{-j2\pi \frac{mn}{N}}. \tag{3.54}$$

Equation (3.50) can be written as

$$\begin{aligned} R_x^\alpha(\tau) &= \sum_{m=-\infty}^{\infty} \sum_{n=-\infty}^{\infty} C_m C_n^* \cdot \\ &\quad \lim_{Z\to\infty} \frac{1}{Z} \int_{-Z/2}^{Z/2} E\left\{ d\left(t+\frac{\tau}{2}\right) d^*\left(t-\frac{\tau}{2}\right)\right\} e^{-j2\pi(\alpha-\frac{m-n}{T_r})t}\, dt\, e^{j2\pi(\frac{m+n}{2T_r})\tau} \\ &= \sum_{m=-\infty}^{\infty} \sum_{n=-\infty}^{\infty} C_m C_n^* R_d^{\alpha-\frac{m-n}{T_r}}(\tau)\, e^{j2\pi(\frac{m+n}{2T_r})\tau} \end{aligned} \tag{3.55}$$

where $R_d^\beta(\tau)$ is the cyclic autocorrelation of $d(t)$. Using Equation (3.49), Equation (3.55) becomes

$$R_x^\alpha(\tau) = \sum_{m=-\infty}^{\infty} \sum_{n=-\infty}^{\infty} C_m C_n^* R_d^{\alpha-\frac{m-n}{NT_c}}(\tau)\, e^{j2\pi(\frac{m+n}{2NT_c})\tau}. \tag{3.56}$$

The cyclic spectrum of the DS/SS signal may then be obtained from Equation (3.8):

$$S_x^\alpha = \int_{-\infty}^{\infty} R_x^\alpha(\tau)\, e^{-j2\pi f\tau}\, d\tau. \tag{3.57}$$

Substituting Equation (3.56) into Equation (3.57) and rearranging,

$$\begin{aligned} S_x^\alpha(f) &= \sum_{m=-\infty}^{\infty} \sum_{n=-\infty}^{\infty} C_m C_n^* \int_{-\infty}^{\infty} R_d^{\alpha-\frac{m-n}{NT_c}}(\tau)\, e^{j2\pi(\frac{m+n}{2NT_c})\tau}\, e^{-j2\pi f\tau}\, d\tau \\ &= \sum_{m=-\infty}^{\infty} \sum_{n=-\infty}^{\infty} C_m C_n^* S_d^{\alpha-\frac{m-n}{NT_c}}\left(f-\frac{m+n}{2NT_c}\right) \end{aligned} \tag{3.58}$$

where $S_d^\beta(f)$ is the cyclic spectrum of the data signal $d(t)$. Letting $m-n=l$, we get

$$S_x^\alpha(f) = \sum_{l=-\infty}^{\infty} \sum_{n=-\infty}^{\infty} C_{n+l} C_n^* S_d^{\alpha-\frac{l}{NT_c}}\left(f-\frac{n}{NT_c}-\frac{l}{2NT_c}\right). \tag{3.59}$$

If the data sequence is white, then $S_d^\beta(f)$ is nonzero only when

$$\beta = \frac{k}{T_d} \tag{3.60}$$

for all integers k [59, 60]. That is, the cycle frequencies β_k are harmonics of the fundamental cycle frequency $1/T_d$, the data rate. Thus $S_d^\beta(f)$ is nonzero only when

$$\beta_k = \frac{k}{T_d} = \alpha - \frac{l}{NT_c}. \tag{3.61}$$

Combining Equations (3.61) and (3.45),

$$\alpha = \frac{k}{ST_c} + \frac{l}{NT_c}$$

or

$$\alpha = \frac{kN + lS}{NST_c} \tag{3.62}$$

for all integer values of k and l. When the modulation is code-on-pulse (the code repeats every data symbol), $N = S$ and Equation (3.62) simplifies to

$$\alpha = \frac{k+l}{ST_c} = \frac{p}{T_r} = \frac{p}{T_d} \tag{3.63}$$

for all integer values of p. Thus, in this case, the cycle frequencies of the DS/SS signal are equal to all the integer multiples of the code repetition frequency (which is equal to the symbol rate).

3.5 The Optimal Time-Variant Filter for DS/SS Signals

As discussed in Sections 2.1 and 2.2, the matched filter is optimal in the MAP sense only when the background noise is Gaussian. It is, in fact, a trivial solution for the optimal cyclic filter. In the more general case, it forms one of the arms of the FRESH filter. Since the FRESH filter is based on the Fourier series representation (FSR) of the time-variant filter, it is also known as the FSR time-dependent filter and its implementation is derived from Equation (3.30). The application of the optimal time-dependent filter

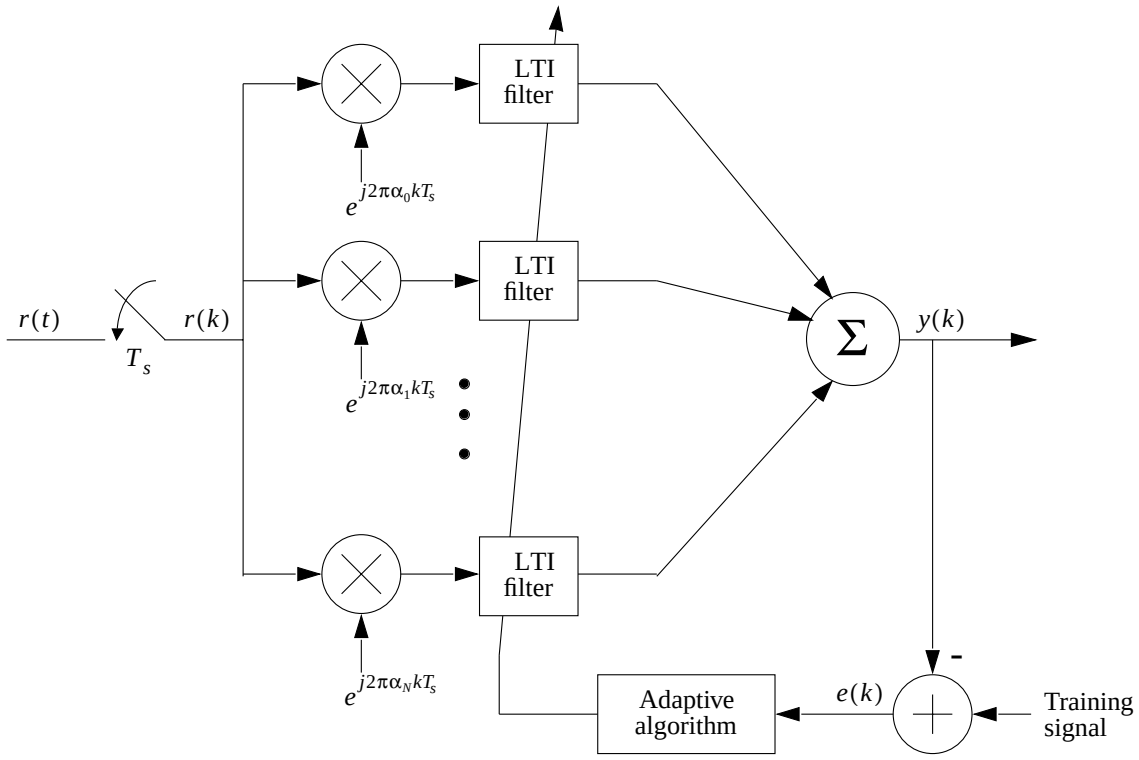

Figure 3.1: The FSR TDAF.

(TDF) for the demodulation of a DS/SS signal and its use for interference rejection have been investigated in [67, 68] where FFT-based implementations of the TDF have been employed.

A discrete-time adaptive implementation of the FRESH filter, known as the FSR time-dependent adaptive filter (TDAF), is shown in Figure 3.1. The frequency shifts in the figure, $\{\alpha_i\}$, $i = 1, 2, \ldots, N$, are the cycle frequencies that can be exploited in the discrete-time case. Code-on-pulse modulation and equal data rates for all signals are assumed. The set $\bar{\alpha}$ of cycle frequencies is given by

$$\bar{\alpha} = \left\{0, \frac{1}{T_d}, \frac{2}{T_d}, \ldots, \frac{N-1}{T_d}\right\}. \tag{3.64}$$

The estimated signal $z(k)$ at the output of the FSR TDAF is given by the following discrete-time equivalent of Equation (3.30):

$$z(k) = \sum_{m=0}^{N_b-1} w_m(k) \otimes [r(k)e^{j2\pi\frac{m}{T_d}kT_s}] \tag{3.65}$$

where $w_m(k)$ is the mth FIR filter's impulse response, $r(k)$ is the sampled received baseband signal at time instant k, and T_s is the sampling period. Following the treatment in [43, 69], we consider the case when $z(k)$ is sampled once every symbol, and the symbol period is an integer multiple of the sampling period of the input signal:

$$T_d = N_b T_s \tag{3.66}$$

where N_b is the number of samples per symbol. For $k = nN_b$ where n is an integer, the estimated signal $y(n) = z(nN_b)$ is rewritten as

$$y(n) = \sum_{m=0}^{N_b-1} \sum_{l=0}^{N_F-1} w_m(l) x(nN_b - l) e^{j2\pi \frac{m}{N_b}(nN_b - l)},$$

where N_F is the length of each of the FIR filters $w_m(k)$. Note that the filter $w_m(l)$ is optimal only at these sampling instants. Since $e^{j2\pi \frac{m}{N_b}(nN_b-l)} = e^{-j2\pi \frac{l}{N_b}m}$,

$$\begin{aligned} y(n) &= \sum_{l=0}^{N_F-1} x(nN_b - l) \sum_{m=0}^{N_b-1} w_m(l) e^{-j2\pi \frac{l}{N_b}m} \\ &= \sum_{l=0}^{N_F-1} \tilde{w}(l) x(nN_b - l) \end{aligned} \tag{3.67}$$

where

$$\tilde{w}(l) = \sum_{m=0}^{N_b-1} w_m(l) e^{-j2\pi \frac{l}{N_b}m} \tag{3.68}$$

and $\tilde{w}(k)$ is another FIR filter. Equation (3.68) is observed to be a discrete-time Fourier transform expression. Equation (3.67) shows that the optimal FSR TDAF is reduced to a single complex FIR filter of length N_F when the estimated signal is sampled once every symbol and the sampling rate is an integer multiple of the symbol rate. Thus, an equalizer, which may be fractionally spaced, can exploit the cyclostationary property of a DS/SS signal to extract the signal received in non-white background noise. The weights of the equalizer are adapted to minimize an error criterion by means of an *adaptation algorithm*. A LCL-FSR TDAF implementation reduces to two complex equalizers (a linear part and a conjugate-linear part) whose outputs are combined.

For BPSK modulation, only the real part of the estimated signal contains the desired information and its imaginary part is of no interest. Taking advantage of this fact, it can be shown [43, 69] that the optimum filter reduces to two *real* FIR filters—one for the real part of the signal and the other for the imaginary part of the signal—whose outputs are combined to obtain the estimate of the real part of the data signal. Such a filter minimizes the estimation error only along the real axis. This implementation results in a reduction of the computational complexity of the receiver.

3.6 Summary

The basic principles of cyclostationarity were discussed. It was shown that spectral correlation results when a signal exhibits cyclostationarity. Spectral correlation implies spectral redundancy, which can be exploited in a number of applications. The method of cyclic filtering can be used for estimating cyclostationary signals corrupted by noise and interference. Direct-sequence spread- spectrum signals are spectrally redundant due to three fundamental periodicities, chip rate, data rate, and code repeat rate periodicities. The discrete-time implementation of the optimum time-dependent adaptive filter reduces to an adaptive linear equalizer when the modulation is code-on-pulse, the estimated signal is sampled only once every symbol, and the sampling rate is harmonically related to the symbol rate.

Chapter 4

Adaptation Algorithms for CDMA Interference Rejection

4.1 Introduction

Various adaptive receiver structures were introduced in Chapter 2. The common denominator among all these structures is filter *weights* that are *adapted* according to some *error criterion* or *cost function*. During the course of the convergence process, the signal is steadily enhanced. The algorithm used to determine the filter weights is known as the *adaptation algorithm*.

Various adaptation algorithms have been used in adaptive CDMA receivers. While some of them are classic algorithms used in adaptive equalization and interference rejection, others are new and have been specially developed for CDMA receivers. This chapter overviews some commonly used error criteria and the adaptation algorithms that minimize them. A comparative study between CDMA and adaptive array algorithms, which is novel to this research, is also presented.

If the statistics of the received signal are known *a priori*, then the optimal filter weights can be computed (since the solution to the problem can usually be expressed in terms of the signal statistics). But often this information is not available *a priori*. An alternative is to estimate these statistics and use them in the solution. This option is expensive and is useful only if the signal is received in a static environment (stationary channel); the solution needs to be recomputed every time the channel changes. A less costly alternative is to use a *recursive* adaptation algorithm to compute the optimal filter weights. If this is done for a stationary channel, the filter weights can be allowed to converge and then the adaptation can be stopped. In wireless communications, however, the radio propagation channel is invariably dynamic and hence the adaptation process must be continuous to allow the receiver to constantly optimize the filter weights. The algorithm must adapt

the weights quickly to keep up with the changing environment. Since the adaptation algorithm is used continuously, its *computational complexity* is often an important issue to be considered, especially when used in single user receivers, where power and physical space may be at a premium. The tradeoff between convergence speed and complexity should be given consideration. Other factors include tracking ability in a nonstationary channel, misadjustment or deviation from the error with the optimal solution, and numerical properties. More details on these and other factors that influence the choice of an adaptation algorithm can be found in [38].

4.2 Types of Adaptation Algorithms

The adaptation algorithm for minimizing any specified cost function is not unique. The choice is made based on the factors mentioned in Section 4.1. However, analysis of the performance of an adaptive algorithm for a particular channel is often considered only for the stationary case due to the difficulty of analysis for nonstationary channels.

Adaptation algorithms may be most generally classified as *block* or *recursive* [70]. In block algorithms, the input signal is divided into blocks and the optimum filter weights are determined for each block independently. Thus the blocks are also filtered independently. In some instances, partial overlap between blocks may be used. In recursive algorithms, the adaptation of weights is carried out through a recursive equation, with the recursion being a continuous operation, i.e., the weights are updated for every output sample produced.

One of the main differences between the two types of algorithms is, block algorithms have finite memory whereas recursive algorithms have infinite memory. The length of the memory in the recursive algorithm is determined by certain *adaptation parameters*. A block algorithm is more desirable in a rapidly changing channel where a long memory can do more harm than good. It is useful to note that, for stationary channels, longer memory results in more accurate estimates of the optimal weights since a larger input data set is used to compute the weights. However, a disadvantage of the block algorithm is, the computational complexity increases linearly with the block size for increasing memory. The complexity is independent of the memory length for the recursive case. Both types of algorithms yield similar results when the channel is stationary or slowly varying [70].

Algorithms may also be categorized based on the adaptive filtering approach [38]. In the approach based on *Wiener filter theory*, a tapped delay line is used as the adaptive filter. First the matrix form of the *Wiener-Hopf equations*, which define the Wiener solution for minimizing the MSE [38], is used to derive the *method of steepest descent*. In this method, the weight vector is altered from its initial (arbitrary) state in a direction opposite to that of the *gradient* of the error criterion. This procedure is continued until the minimum

of the error function is reached. The gradient vector depends on the correlation matrix of the input signal vector, and the crosscorrelation vector between the desired signal and the input signal vector. Next, in the *stochastic gradient descent (SGD) method*, an *estimate* of the gradient vector, consisting of instantaneous estimates of the correlation matrix and the crosscorrelation vector, is used instead. This is the *least-mean-square (LMS) algorithm* [38, 39, 71].

The *Kalman filter approach* is based on state-space concepts. In this approach, a *process equation* models the dynamics of the linear system as a state equation and the *measurement equation* models the observed noisy signal [38, 72]. The Kalman filter tracks the optimum operating conditions, which are expressed as a model. The solution is then comprised of a set of recursive matrix equations. The weight vector is used as the state vector. In a stationary channel, a *fixed-state* model is used where the state vector remains constant; in a nonstationary channel, a *noisy-state* model is used where the state vector of the model takes on a random value around a mean. Different adaptation algorithms may be derived from the recursive solution to the Kalman filtering problem.

In contrast with the previous two approaches, the method of least squares employs time averages. The error criterion is the sum of weighted squares of the "error," the difference between a reference signal and the filter output. The solution may be expressed in terms of either a block algorithm or a recursive algorithm. The well known *recursive least-squares (RLS) algorithm* falls under this category. The Kalman algorithm is closely tied with the RLS algorithm [38].

4.3 Adaptation Algorithms Used for CDMA Interference Rejection

In wireless communications systems, simplicity of algorithms is preferred since power consumption is an important consideration, especially for mobile handsets where long battery life is desirable. For this reason researchers have emphasized SGD algorithms. The most common of the SGD algorithms is the LMS algorithm due to its inherent simplicity, and it is widely used in much of this research work.

It is important to study some of the basic elements of SGD algorithms. Figure 4.1 shows the tapped delay line filter used for adaptive FIR filtering. The adaptive filtering process may be divided into two steps.

1. The first step is a filtering operation represented by the following mathematical equation:

$$y(n) = \mathbf{w}^H(k)\,\mathbf{r}(k) \tag{4.1}$$

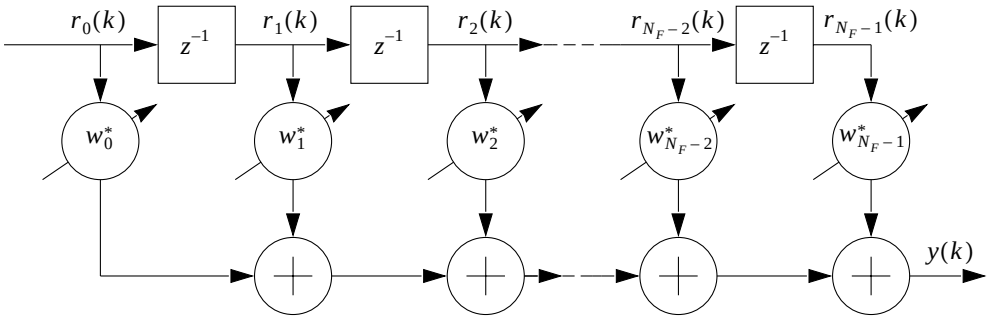

Figure 4.1: The Adaptive Filter.

where $y(k)$ is the filter output at time instant k,

$$\mathbf{w}(k) = \begin{bmatrix} w_0(k) \\ w_1(k) \\ \vdots \\ w_{N_F-2}(k) \\ w_{N_F-1}(k) \end{bmatrix} \tag{4.2}$$

is the weight vector (with N_F elements) at time instant k,

$$\mathbf{r}(k) = \begin{bmatrix} r_0(k) \\ r_1(k) \\ \vdots \\ r_{N_F-2}(k) \\ r_{N_F-1}(k) \end{bmatrix} \tag{4.3}$$

is the input vector composed of N_F received signal samples, $(\cdot)^H$ denotes Hermitian transposition, and $(\cdot)^*$ in Figure 4.1 represents complex conjugation. The output is computed at time kT_d, i.e., at integer multiples of the symbol period T_d.

2. The second step is the weight update according to the following equation:

$$\mathbf{w}(k+1) = \mathbf{w}(k) - \mu\hat{\boldsymbol{\nabla}}(J(k)) \tag{4.4}$$

where μ is a small constant known as the *step-size* and $\hat{\boldsymbol{\nabla}}(J(k))$ is the instantaneous estimate of the gradient vector $\boldsymbol{\nabla}(J(k))$.

In the steepest descent method the weight vector follows a deterministic path along the steepest slope on the error surface, whereas in the SGD method, it follows a random path

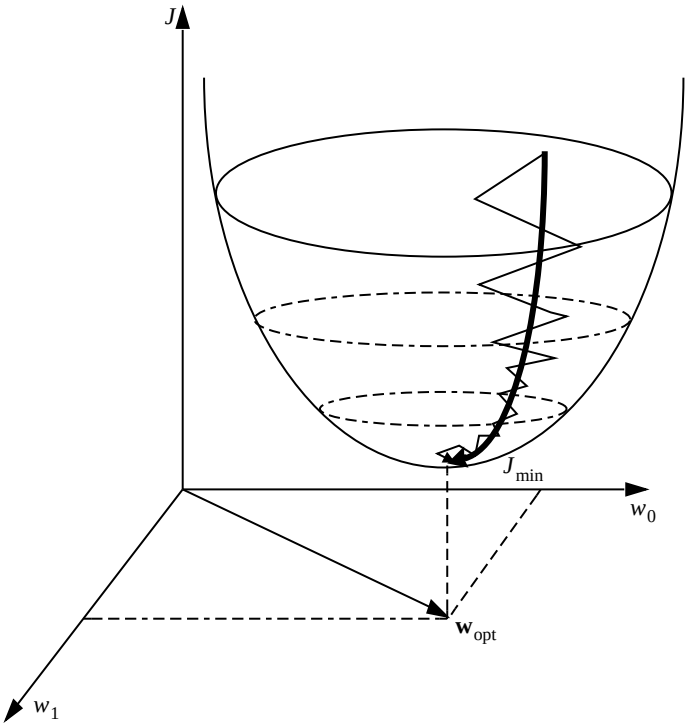

Figure 4.2: The Error Surface for the MSE Cost Function with Two Filter Weights w_0 and w_1, and the Convergence Paths for the Steepest Descent Method (Bold Line) and the Stochastic-Gradient Descent Method (Zig-Zag Line).

using instantaneous estimates of the steepest slope. Random motion is due to *gradient noise*. The convergence of the weights is illustrated in Figure 4.2 for a two-dimensional filter. The step-size parameter determines the rate of convergence and also the effect of gradient noise. For example, a small step-size implies slow convergence of the weights but also reduced gradient noise effects, which influence the *misadjustment*, a measure of the deviation from the MMSE solution in the case of the LMS algorithm.

4.3.1 The Wiener Filter

It may be recalled the Wiener solution is based on the MSE cost function:

$$\begin{aligned} J &= E[|e(k)|^2] \\ &= E[|d(k) - \mathbf{w}^H \mathbf{r}(k)|^2]. \end{aligned} \tag{4.5}$$

In the following derivation, it is assumed that the received signal at the input of the filter and desired signal are zero mean, jointly wide-sense stationary (WSS) processes.

Equation (4.5) may be expanded as

$$\begin{aligned} J &= E[(d(k) - \mathbf{w}^H \mathbf{r}(k))^*(d(k) - \mathbf{w}^H \mathbf{r}(k))] \\ &= E[|d(k)|^2] - \mathbf{w}^H E[d(k)\,\mathbf{r}(k)] - E[d(k)\,\mathbf{r}^H(k)]\mathbf{w} + \mathbf{w}^H E[\mathbf{r}(k)\,\mathbf{r}^H(k))]\mathbf{w} \\ &= \sigma_d^2 - \mathbf{w}^H\mathbf{p} - \mathbf{p}^H\mathbf{w} + \mathbf{w}^H\mathbf{R}\mathbf{w} \end{aligned} \tag{4.6}$$

where $\mathbf{p}$ is the crosscorrelation vector and $\mathbf{R}$ is the correlation matrix:

$$\mathbf{p} \triangleq E[d(k)\,\mathbf{r}(k)] \tag{4.7}$$

$$\mathbf{R} \triangleq E[\mathbf{r}(k)\,\mathbf{r}^H(k))] \tag{4.8}$$

$$\sigma_d^2 \triangleq E[|d(k)|^2]. \tag{4.9}$$

The cost function J is minimized if its gradient (defined below) is minimized as well. The gradient operator $\boldsymbol{\nabla}$ is defined by

$$\boldsymbol{\nabla} \triangleq \begin{bmatrix} \dfrac{\partial}{\partial w_0^r} + j\,\dfrac{\partial}{\partial w_0^i} \\ \dfrac{\partial}{\partial w_1^r} + j\,\dfrac{\partial}{\partial w_1^i} \\ \vdots \\ \dfrac{\partial}{\partial w_{N_F}^r} + j\,\dfrac{\partial}{\partial w_{N_F}^i} \end{bmatrix} \tag{4.10}$$

$$w_l = w_l^r + j\,w_l^i. \tag{4.11}$$

The gradient is also related to the *conjugate derivative* of J with respect to $\mathbf{w}$, $\partial J/\partial \mathbf{w}^*$, through the following equation [38, Appendix B]:

$$\boldsymbol{\nabla}(J) = 2\frac{\partial J}{\partial \mathbf{w}^*}. \tag{4.12}$$

The cost function assumes a minimum value if each of the elements in its gradient is simultaneously zero. Thus, the filter is optimum in the MMSE sense if

$$\boldsymbol{\nabla}(J) = \mathbf{0} \tag{4.13}$$

where $\mathbf{0}$ is the null vector. Using Equations (4.6) and (4.12) and applying the rules for differentiation with respect to a vector,

$$\boldsymbol{\nabla}(J) = 2(-\mathbf{p} + \mathbf{R}\mathbf{w}_{\text{opt}}) \tag{4.14}$$

and the condition for optimality becomes

$$-\mathbf{p} + \mathbf{R}\mathbf{w}_{\text{opt}} = \mathbf{0} \tag{4.15}$$

where $\mathbf{w}_{\text{opt}}$ is the optimum weight vector. Equation (4.15) may be rewritten as

$$\mathbf{R}\mathbf{w}_{\text{opt}} = \mathbf{p}. \tag{4.16}$$

Equation (4.16) is the matrix formulation of the *Wiener-Hopf equations* for a transversal filter[1] [38]. Assuming that the correlation matrix $\mathbf{R}$ is nonsingular, both sides of Equation (4.16) are premultiplied by $\mathbf{R}^{-1}$, the inverse of the correlation matrix, to obtain the Wiener solution for the optimum weight vector:

$$\mathbf{w}_{\text{opt}} = \mathbf{R}^{-1}\mathbf{p}. \tag{4.17}$$

Noting that $J = J_{\min}$ when $\mathbf{w} = \mathbf{w}_{\text{opt}}$, Equation (4.17) may be rewritten as

$$J_{\min} = \sigma_d^2 - \mathbf{w}_{\text{opt}}^H(\mathbf{p} - \mathbf{R}\mathbf{w}_{\text{opt}}) - \mathbf{p}^H\mathbf{w}_{\text{opt}}. \tag{4.18}$$

The MMSE may be obtained by using Equations (4.15) and (4.17) in Equation (4.18):

$$J_{\min} = \sigma_d^2 - \mathbf{p}^H\mathbf{R}^{-1}\mathbf{p}. \tag{4.19}$$

Equation (4.19) shows that the MMSE depends on the power (variance) of the signal of interest, the correlation matrix of the received signal at the input of the filter, and the crosscorrelation vector between the input signal and the signal of interest.

4.3.2 The Least-Mean Square Algorithm

It was noted earlier that the steepest descent algorithm changes the weight vector from its initial state in a direction opposite to the gradient vector. That is, the weight update algorithm is

$$\mathbf{w}(k+1) = \mathbf{w}(k) + \frac{\mu}{2}[-\boldsymbol{\nabla}(J(k))] \tag{4.20}$$

[1]The discrete-time versions of the Wiener-Hopf equations are of the form

$$\sum_{i=0}^{\infty} w_{oi}\gamma(i-n) = p(-n), \qquad n = 0, 1, 2, \ldots,$$

where w_{oi} is the ith element of the optimum filter, $\gamma(i-n)$ is the autocorrelation function of the input signal for a lag $i-n$, and $p(-n)$ is the crosscorrelation between the input and the desired signals for a lag $-k$.

where $\mu/2$ is the real-valued step-size (the division by 2 is for convenience). Using Equation (4.14), this becomes

$$\mathbf{w}(k+1) = \mathbf{w}(k) + \mu[\mathbf{p} - \mathbf{R}\mathbf{w}(k)]. \tag{4.21}$$

It is thus necessary to accurately know $\mathbf{p}$ and $\mathbf{R}$ for weight vector adaptation.

The knowledge of $\mathbf{p}$ and $\mathbf{R}$ is impossible in most cases, and if they were known and the complexity could be afforded, $\mathbf{w}_{\text{opt}}$ could be computed directly. Therefore, the SGD algorithm uses *instantaneous estimates* $\hat{\mathbf{p}}$ and $\hat{\mathbf{R}}$ of $\mathbf{p}$ and $\mathbf{R}$ (by removing the expectation operators in Equations (4.7) and (4.8)), respectively:

$$\hat{\mathbf{p}} = \mathbf{r}(k)d^*(k) \tag{4.22}$$
$$\hat{\mathbf{R}} = \mathbf{r}(k)\mathbf{r}^H(k). \tag{4.23}$$

Using these estimates in Equation (4.21), we get the SGD update equation of Equation (4.4)

$$\mathbf{w}(k+1) = \mathbf{w}(k) + \mu\mathbf{r}(k)[d^*(k) - \mathbf{r}^H(k)\mathbf{w}(k)]. \tag{4.24}$$

At this stage, we realize that the adaptive filtering process may be broken down into three steps:

1. Computation of filter output,
$$y(k) = \mathbf{w}^H(k)\mathbf{r}(k); \tag{4.25}$$
2. Computation of estimation error,
$$e(k) = d(k) - y(k); \tag{4.26}$$
3. Update of filter weight vector,
$$\mathbf{w}(k+1) = \mathbf{w}(k) + \mu e^*(k)\mathbf{r}(k). \tag{4.27}$$

The weight update algorithm of Equation (4.27) is the general complex form of the LMS algorithm.

Convergence (Stability) of the LMS Algorithm

The stability of the LMS algorithm is generally analyzed in terms of its convergence behavior. The MMSE cost function is *unimodal*, i.e., it has a unique minimum, and hence the initial value of the filter weight vector has no bearing on the eventual convergence

to the optimum solution. However, the speed of convergence is influenced by the initial weight vector. Choosing a "good" initial weight vector in the presence of some *a priori* knowledge can help. In the absence of such information, however, it is common practice to initialize to the null weight vector, $\mathbf{0}$.

The convergence behavior is dictated by the step-size to a large extent. While a larger step-size speeds up convergence, it also increases the steady state MSE by amplifying the effects of gradient noise. Thus, even after the filter has converged to the optimal solution, the weights tend to fluctuate around this, leading to increased steady state MSE. The difference between the actual MSE obtained with the LMS algorithm and the MMSE obtained with the optimum solution is termed the *excess MSE*. Furthermore, there is a limit to the value of the step-size that can be used. Use of a step-size larger than this value leads to algorithm instability.

Convergence of the weight vector in the LMS algorithm is usually studied in the mean and mean-square forms. Convergence in the mean implies that

$$\lim_{k\to\infty} E[\mathbf{w}(k)] = \mathbf{w}_{\text{opt}}. \tag{4.28}$$

To prove this, the weight-error vector, defined below, is considered:

$$\mathbf{v}(k) \triangleq \mathbf{w}(k) - \mathbf{w}_{\text{opt}}. \tag{4.29}$$

Subtracting $\mathbf{w}_{\text{opt}}$ from both sides of Equation (4.27) and taking expectations, we get

$$E[\mathbf{v}(k+1)] = E[\mathbf{v}(k)] - \mu E[\mathbf{r}(k)\mathbf{r}^H(k)\mathbf{v}(k)] + E[\mathbf{r}(k)e^*_{\text{opt}}(k)] \tag{4.30}$$

where $e_{\text{opt}}(k)$ is the error obtained with $\mathbf{w}_{\text{opt}}$. Using the *principle of orthogonality* [38],

$$E[\mathbf{r}(k)e^*_{\text{opt}}(k)] = \mathbf{0} \tag{4.31}$$

and the *independence assumption*, which specifies that the weight vector $\mathbf{w}(k)$ is statistically independent of the input vector $\mathbf{r}(k)$, it follows that

$$E[\mathbf{v}(k+1)] = (\mathbf{I} - \mu\mathbf{R})E[\mathbf{v}(k)] \tag{4.32}$$

where $\mathbf{I}$ is the identity matrix. If

$$\mathbf{R} = \mathbf{Q}\mathbf{\Lambda}\mathbf{Q}^H \tag{4.33}$$

where $\mathbf{\Lambda}$ is a diagonal matrix whose diagonal elements are the eigenvalues of the correlation matrix $\mathbf{R}$ and $\mathbf{Q}$ is the unitary *modal matrix* whose columns are the eigenvectors of $\mathbf{R}$, then it can be shown [38, 71] that

$$\tilde{\mathbf{v}}(k+1) = (\mathbf{I} - \mu\mathbf{\Lambda})\tilde{\mathbf{v}}(k) \tag{4.34}$$

$$\tilde{\mathbf{v}}(k) = \mathbf{Q}^H E[\mathbf{v}(k)]. \tag{4.35}$$

It follows that

$$\tilde{v}_i(k+1) = (1 - \mu\lambda_i)^k \tilde{v}_i(0) \tag{4.36}$$

where $\tilde{v}_i(k)$ is the ith element of $\tilde{\mathbf{v}}(k)$ and λ_i is the ith diagonal element of $\mathbf{\Lambda}$. Then it can be shown that for

$$\lim_{k\to\infty} \tilde{v}_i(k) = 0 \qquad \forall\, i, \tag{4.37}$$

and, hence, for Equation (4.28) to hold, the condition for convergence of the LMS algorithm is

$$0 < \mu < \frac{2}{\lambda_{\max}} \tag{4.38}$$

where $\lambda_{\max}$ is the largest eigenvalue of the correlation matrix $\mathbf{R}$.

The convergence of each tap weight to its optimum value depends on the eigenvalue associated with that mode. More specifically, the rate of convergence is a function of the term $(1 - \mu\lambda_i)$, the ith time constant $\tau_i = -1/\ln(1 - \mu\lambda_i)$. Therefore, in general, each mode converges at a different rate. When the *eigenvalue spread* is large, the convergence rate of the average weight vector is limited by the smallest eigenvalue $\lambda_{\min}$.

4.3.3 The Normalized LMS Algorithm

During the course of adaptation using the LMS algorithm, a large input vector, when used in the weight update equation of (4.27), can cause *gradient noise amplification* if the step-size is not chosen properly. This can result in a high steady-state MSE and, in extreme cases, even instability of the algorithm. While the analysis thus far has been for stationary channels, a similar situation can occur in nonstationary channels where the signal undergoes fading causing the signal power to fluctuate. This problem may be overcome by using the *normalized LMS (NLMS) algorithm*. In this algorithm, the weight update factor in Equation (4.27) is normalized with respect to the squared Euclidean norm of the input vector $\mathbf{r}(k)$, thus neutralizing the deleterious effects of large input

vectors. The NLMS algorithm may also be derived as the solution to a constrained optimization problem [38]. Given the input signal vector $\mathbf{r}(k)$ and the desired signal $d(k)$, the problem is to determine the weight vector $\mathbf{w}(k+1)$ that minimizes the squared Euclidean norm of the change in the weight vector in the next iteration,

$$\delta\mathbf{w}(k+1) \stackrel{\triangle}{=} \mathbf{w}(k+1) - \mathbf{w}(k) \tag{4.39}$$

subject to the constraint

$$\mathbf{w}^H(k+1)\mathbf{r}(k) = d(k). \tag{4.40}$$

Thus, the problem is to minimize the following cost function:

$$\tilde{J}(k) = ||\delta\mathbf{w}(k+1)||^2 + \lambda[d(k) - \mathbf{w}^H(k+1)\mathbf{r}(k)] \tag{4.41}$$

where λ is a complex Lagrange multiplier [73]. Expanding the first term, we get

$$\begin{aligned}\tilde{J}(k) &= [\mathbf{w}(k+1) - \mathbf{w}(k)]^H[\mathbf{w}(k+1) - \mathbf{w}(k)] + \lambda[d(k) - \mathbf{w}^H(k+1)\mathbf{r}(k)] \\ &= \mathbf{w}^H(k+1)\mathbf{w}(k+1) - \mathbf{w}^H(k+1)\mathbf{w}(k) - \mathbf{w}^H(k)\mathbf{w}(k+1) \\ &\quad + \mathbf{w}^H(k)\mathbf{w}(k) + \lambda[d(k) - \mathbf{w}^H(k+1)\mathbf{r}(k)].\end{aligned} \tag{4.42}$$

To find the value of $\mathbf{w}(k+1)$ that minimizes this cost function, we need to use the condition

$$\boldsymbol{\nabla}\tilde{J}(k) = \mathbf{0} \tag{4.43}$$

or equivalently,

$$\frac{\partial\tilde{J}(k)}{\partial\mathbf{w}^*(k+1)} = \mathbf{0}. \tag{4.44}$$

Evaluating the derivative, we get

$$\mathbf{w}(k+1) - \mathbf{w}(k) - \lambda\mathbf{r}(k) = \mathbf{0} \tag{4.45}$$

or

$$\mathbf{w}(k+1) - \mathbf{w}(k) = \lambda\mathbf{r}(k). \tag{4.46}$$

Premultiplying both sides of Equation (4.46) with $\mathbf{r}^H(k)$, we get

$$\mathbf{r}^H(k)[\mathbf{w}(k+1) - \mathbf{w}(k)] = \lambda \mathbf{r}^H(k)\mathbf{r}(k). \tag{4.47}$$

Using Equation (4.40) and solving for λ yields

$$\begin{aligned} \lambda &= \frac{d^*(k) - \mathbf{r}^H(k)\mathbf{w}(k)}{||\mathbf{r}(k)||^2} \\ &= \frac{e^*(k)}{||\mathbf{r}(k)||^2}, \end{aligned} \tag{4.48}$$

where $e(k)$ is the estimation error defined in Equation (4.26). Using Equation (4.48) in Equation (4.45) and rearranging results in

$$\mathbf{w}(k+1) = \mathbf{w}(k) + \frac{1}{||\mathbf{r}(k)||^2} e^*(k)\mathbf{r}(k). \tag{4.49}$$

This may be recognized as a weight vector update equation similar to Equation (4.27). Multiplying the second term in Equation (4.49) with a positive real constant μ_0 to control the weight update yields the NLMS update equation

$$\mathbf{w}(k+1) = \mathbf{w}(k) + \frac{\mu_0}{||\mathbf{r}(k)||^2} e^*(k)\mathbf{r}(k). \tag{4.50}$$

Convergence of the NLMS Algorithm

Comparing the NLMS weight update equation with the LMS weight update equation, we can define

$$\mu(k) = \frac{\mu_0}{||\mathbf{r}(k)||^2} \tag{4.51}$$

as a time-varying step-size. Furthermore, the NLMS algorithm is convergent in the mean-square sense if [38]

$$0 < \mu_0 < 2. \tag{4.52}$$

The NLMS algorithm may also be viewed as a way of ensuring that the step-size in the LMS algorithm satisfies the condition of Equation (4.38) for convergence in the mean, especially when $\lambda_{\max}$ is unknown or hard to estimate, and a step-size that is too small is undesirable. This may be seen as follows.

The condition

$$0 < \mu < \frac{2}{\sum_{i=1}^{N_F} \lambda_i} \tag{4.53}$$

is more stringent than the condition of Equation (4.38) since

$$\sum_{i=1}^{N_F} \lambda_i \geq \lambda_{\max}. \tag{4.54}$$

Therefore, if a step-size $\mu_0 / \sum_{i=1}^{N_F} \lambda_i$ is used, then for convergence, it is sufficient for the step-size to satisfy

$$0 < \frac{\mu_0}{\sum_{i=1}^{N_F} \lambda_i} < \frac{2}{\sum_{i=1}^{N_F} \lambda_i} \tag{4.55}$$

which is equivalent to condition (4.52). It is easy to pick a μ_0 that satisfies this condition. Since $\sum_{i=1}^{N_F} \lambda_i$ is unknown, an estimate may be used instead. We note that

$$\begin{aligned} \sum_{i=1}^{N_F} \lambda_i &= \text{tr}\{\mathbf{R}\} \\ &= \text{tr}\{E[\mathbf{r}(k)\mathbf{r}^H(k)]\} \\ &= E[\mathbf{r}^H(k)\mathbf{r}(k)] \\ &\approx ||\mathbf{r}(k)||^2. \end{aligned} \tag{4.56}$$

Thus, the need for knowledge of $\lambda_{\max}$ is eliminated by using the step-size defined in Equation (4.51), where μ_0 satisfies condition (4.52), while ensuring that the step-size satisfies condition (4.38) for convergence of the weight vector in the mean in the LMS algorithm.

To overcome numerical problems during weight update when the input vector $\mathbf{r}(k)$ is small, due to the division by the small number $||\mathbf{r}(k)||^2$, the following modified weight update equation is used:

$$\mathbf{w}(k+1) = \mathbf{w}(k) + \frac{\mu_0}{\alpha + ||\mathbf{r}(k)||^2} e^*(k)\mathbf{r}(k) \tag{4.57}$$

where α is small positive constant.

4.3.4 The Decision-Directed Algorithm

The LMS algorithm requires the knowledge of the desired signal $d(k)$ during its adaptation. This signal acts as a training or reference signal for updating the weight vector. Obviously, it is not practical to assume the knowledge of the desired signal throughout the transmission because if the signal were known, then its transmission wouldn't be necessary in the first place.

The decision-directed algorithm makes a decision on the adaptive filter output and uses the resulting signal as the reference signal, assuming that the decisions made were good enough for the estimation error to be accurate "most of the time." Thus the algorithm consists of the following steps:

1. Computation of filter Output,
$$y(k) = \mathbf{w}^H(k)\mathbf{r}(k); \tag{4.58}$$
2. Making a decision,
$$\hat{d}(k) = \text{dec}[y(k)]; \tag{4.59}$$
3. Computation of estimation error,
$$\tilde{e}(k) = \hat{d}(k) - y(k); \tag{4.60}$$
4. Update of filter weight vector,
$$\mathbf{w}(k+1) = \mathbf{w}(k) + \mu\tilde{e}^*(k)\mathbf{r}(k). \tag{4.61}$$

With this method, the error surface is changed from a unimodal surface to a multi-modal one consisting of global and local minima, and the behavior of the algorithm becomes complicated. If the filter is allowed to adapt using this method from startup, then a bad choice of the initial weight vector can result in the algorithm converging to an undesirable local minimum [74]. The extraneous minima are not stable, however, and for finite step-sizes, the algorithm will eventually reach a global minimum.

A practical solution to the above problem is to let the adaptive filter train first (with a training sequence) and then switch to the decision-directed mode. At the end of the training period, the weight vector $\mathbf{w}(k)$ is close to the Wiener filter $\mathbf{w}_{\text{opt}}$ and the estimated signal $\hat{d}(k)$ is equal to the desired signal $d(k)$ with a high probability. Macchi and Eweda [75] have proved that the algorithm is bounded, stable, and convergent to the optimal solution $\mathbf{w}_{\text{opt}}$. Nowlan and Hinton [76] have proposed a soft decision-directed algorithm for use on binary signals in channels for which the decision-directed algorithm does not converge. This algorithm is based on the maximization of the likelihood that the filter outputs come from an independent identically distributed (i.i.d.) source that is a mixture of two Gaussians with known means.

4.3.5 The Minimum Output-Energy Algorithm

The principal disadvantage of using the LMS algorithm is that it requires a training sequence at startup. Even if the adaptive filter is operated in the decision-directed mode, a drastic change in the propagation channel will necessitate retraining of the adaptive filter. This implies not only that the request for a training signal be conveyed to the transmitter, but also that the transmission of useful information be temporarily suspended while the filter trains. One alternative is to build a training sequence periodically into the transmitted signal. Either way, the overhead is significant may not be feasible. It is desirable, therefore, to have a *blind* algorithm that does not need a training signal. The decision-directed algorithm discussed in Section 4.3.4 is blind but is not suitable for startup in "closed-eye" situations, those in which the *eye-pattern* of the filter output signal is "closed."

The *minimum output-energy (MOE) algorithm* proposed by Honig et al. [77, 78] is a blind algorithm that is based on decomposing the adaptive filter into two orthogonal components, a fixed filter with tap weights equal to the spreading sequence of the desired signal, and an adaptive filter. The receiver $\mathbf{w}$ is represented by

$$\mathbf{w} = \mathbf{c}_1 + \mathbf{u} \tag{4.62a}$$

$$\mathbf{u}^H \mathbf{c}_1 = 0 \tag{4.62b}$$

where $\mathbf{c}_1$ is the fixed filter whose coefficients are equal to the spreading code of the desired user and $\mathbf{u}$ is the adaptive filter. Also, $\mathbf{c}_1$ is assumed to have unit norm, i.e.,

$$||\mathbf{c}_1||^2 = 1. \tag{4.63}$$

From Equations (4.62a), (4.62b), and (4.63), it follows that

$$\mathbf{w}^H \mathbf{c}_1 = 1. \tag{4.64}$$

That is, the inner product of the filter weight vector with the desired user's spreading code is unity. There is no loss of generality in imposing the above conditions since any signal orthogonal to the desired signal's spreading code is not of interest. Furthermore, the bit decision, given by

$$\hat{d} = \text{sgn}(\mathbf{w}^H \mathbf{r}) \tag{4.65}$$

where $\text{sgn}(\cdot)$ denotes the sign, is invariant to positive scaling of the signal.

The MOE problem is to find a $\mathbf{w}$ that minimizes the mean output energy (ME) of the adaptive receiver given by

$$\text{ME} = E[|\mathbf{w}^H \mathbf{r}|^2] \tag{4.66}$$

subject to the constraint of Equation (4.62b). It may be noted here that without this constraint, $\mathbf{w} = \mathbf{0}$ would be a trivial solution to the minimization problem. Honig et al. [78] show that the solution that minimizes the ME is the same as the one that minimizes the MMSE. Hence, the optimum solution for the MMSE problem is the Wiener solution of Equation (4.17).

To derive the SGD algorithm for updating the weight vector, we consider the following cost function for the constrained optimization problem:

$$J = E[|\mathbf{w}^H\mathbf{r}|^2] + \lambda\mathbf{u}^H\mathbf{c}_1 \tag{4.67}$$

where λ is a Lagrange multiplier. The gradient of the cost function is given by

$$\boldsymbol{\nabla}(J) = 2[\mathbf{R}\mathbf{w} + \lambda\mathbf{c}_1]. \tag{4.68}$$

The gradient is equated to the null vector for minimization, yielding

$$\lambda\mathbf{c}_1 = -\mathbf{R}\mathbf{w}. \tag{4.69}$$

Premultiplying for $\mathbf{c}_1^H$ and solving for λ, we get

$$\lambda = -\mathbf{c}_1^H\mathbf{R}\mathbf{w}. \tag{4.70}$$

Thus, the gradient gradient is given by

$$\boldsymbol{\nabla}(J) = 2[\mathbf{R}\mathbf{w} - \mathbf{c}_1^H\mathbf{R}\mathbf{w}\mathbf{c}_1]. \tag{4.71}$$

To formulate the SGD algorithm, an instantaneous estimate of the correlation matrix $\mathbf{R}$ is used to obtain the gradient estimate,

$$\hat{\boldsymbol{\nabla}}(J(k)) = 2[\mathbf{r}\mathbf{r}^H\mathbf{w} - \mathbf{c}_1^H\mathbf{r}\mathbf{r}^H\mathbf{w}\mathbf{c}_1]. \tag{4.72}$$

The MOE algorithm consists of the following steps:

1. Computation of the output of the fixed matched filter $\mathbf{c}_1$,
$$y_{MF}(k) = \mathbf{c}_1^H\mathbf{r}(k); \tag{4.73}$$
2. Computation of the output of the overall filter $\mathbf{w}(k)$,
$$y(k) = \mathbf{w}^H\mathbf{r}(k) = y_{MF}(k) + \mathbf{u}^H(k)\mathbf{r}(k); \tag{4.74}$$
3. Update of the adaptive filter weight vector $\mathbf{u}(k)$,
$$\mathbf{u}(k+1) = \mathbf{u}(k) - \mu y^*(k)[\mathbf{r}(k) - y_{MF}(k)\mathbf{c}_1]. \tag{4.75}$$

Convergence of the MOE Algorithm

For analyzing convergence of the MOE algorithm, we follow the same approach as for the LMS algorithm. Adding $\mathbf{c}_1$ to both sides of Equation (4.75) results in

$$\begin{aligned} \mathbf{w}(k+1) &= \mathbf{w}(k) - \mu y^*(k)[\mathbf{r}(k) - y_{MF}(k)\mathbf{c}_1] && (4.76) \\ &= \mathbf{w}(k) - \mu \mathbf{r}^H(k)\mathbf{w}(k)[\mathbf{r}(k) - \mathbf{c}_1^H\mathbf{r}(k)\mathbf{c}_1] \\ &= [\mathbf{I} - \mu(\mathbf{I} - \mathbf{c}_1\mathbf{c}_1^H)\mathbf{r}(k)\mathbf{r}^H(k)]\mathbf{w}(k). && (4.77) \end{aligned}$$

Subtracting the optimum weight vector $\mathbf{w}_{\text{opt}}$ from both sides of Equation (4.75) and using the error vector $\mathbf{v}(k)$ defined in Equation (4.29), we get

$$\begin{aligned} \mathbf{v}(k+1) &= [\mathbf{I} - \mu(\mathbf{I} - \mathbf{c}_1\mathbf{c}_1^H)\mathbf{r}(k)\mathbf{r}^H(k)]\mathbf{v}(k) \\ &\quad - \mu(\mathbf{I} - \mathbf{c}_1\mathbf{c}_1^H)\mathbf{r}(k)\mathbf{r}^H(k)]\mathbf{w}_{\text{opt}}. && (4.78) \end{aligned}$$

Taking expectations on both sides,

$$E[\mathbf{v}(k+1)] = [\mathbf{I} - \mu(\mathbf{I} - \mathbf{c}_1\mathbf{c}_1^H)\mathbf{R}]E[\mathbf{v}(k)] - \mu(\mathbf{I} - \mathbf{c}_1\mathbf{c}_1^H)\mathbf{R}\mathbf{w}_{\text{opt}} \quad (4.79)$$

Since[2]

$$(\mathbf{I} - \mathbf{c}_1\mathbf{c}_1^H)\mathbf{R}\mathbf{w}_{\text{opt}} = \nu\mathbf{c}_1 - \nu\mathbf{c}_1\mathbf{c}_1^H\mathbf{c}_1 = \mathbf{0}, \quad (4.80)$$

we get

$$\begin{aligned} E[\mathbf{v}(k+1)] &= (\mathbf{I} - \mu\tilde{\mathbf{R}})E[\mathbf{v}(k)] && (4.81) \\ \tilde{\mathbf{R}} &\triangleq (\mathbf{I} - \mathbf{c}_1\mathbf{c}_1^H)\mathbf{R}. && (4.82) \end{aligned}$$

Equation (4.82) is similar to Equation (4.32) for the LMS algorithm, and following a similar procedure, it can be shown [78] that the condition for convergence is

$$0 < \mu < \min_i \frac{2}{|\tilde{\lambda}_i|}, \qquad \forall\, i, \quad (4.83)$$

where $\tilde{\lambda}_i$ are the complex (in general) eigenvalues of $\tilde{\mathbf{R}}$.

[2]It can be shown that $\mathbf{R}\mathbf{w}_{\text{opt}} = \mathbf{p} = \nu\mathbf{c}_1$ where ν is a constant dependent on the desired signal power.

4.3.6 Griffiths' Algorithm

Griffiths' algorithm [79] for CDMA interference rejection was inspired by the analogy of the DS/SS signal detection problem to beamforming with linear antenna arrays [55, 80]. The spatial filter used in beamforming has taps separated by linear phase shifts, much in the way the filter taps of the transversal filter used for DS/SS signal detection are separated by linear time shifts.

The cost function for Griffiths' algorithm is the MSE. However, it differs from the LMS algorithm in that the SGD algorithm exploits the *a priori* knowledge of the crosscorrelation vector $\mathbf{p}$. It may be noted [80, 81] that

$$\mathbf{p} = \beta \mathbf{s}_1 \tag{4.84}$$

where β is the amplitude of the desired signal component in the received signal and $\mathbf{s}_1$ is the spreading code (of unit amplitude) of the desired user. Using an instantaneous estimate for only the correlation matrix, the SGD algorithm of Equation (4.21) now becomes

$$\begin{aligned} \mathbf{w}(k+1) &= \mathbf{w}(k) + \mu[\beta \mathbf{s}_1 - \mathbf{r}(k)\mathbf{r}^H(k)\mathbf{w}(k)] \\ &= \mathbf{w}(k) - \mu[y^*(k)\mathbf{r}(k) - \beta \mathbf{s}_1]. \end{aligned} \tag{4.85}$$

Zečević [80] notes that this is identical to the adaptation algorithm obtained by applying the array analogy to the algorithm used for Applebaum's array, which maximizes the signal-to-interference-plus-noise ratio. If the value of β is unknown, as is usually the case, then it may be picked arbitrarily. If $\beta = \beta_0$ for example, then the filter output converges to a scaled version of the desired signal, the scaling factor being proportional to (β_0/β). But this is not a problem since the decision made on this signal is invariant to scaling.

It is interesting to note the similarity between the update equations of Griffiths' algorithm of Equation (4.85) and of the MOE algorithm in Equation (4.76). This is not completely surprising because the optimal solution in both cases is the Wiener filter. The difference in the update equations is that there is a signal dependent factor $(y^*(k)\, y_{MF}(k))$ in Equation (4.76) instead of the fixed factor β in Equation (4.85). The MOE algorithm imposes the constraint of Equation (4.64), which ensures that a constant correlation of unity is maintained between the weight vector and the spreading code of desired user, whereas there is no such constraint in Griffiths' algorithm, and this is their essential difference. In fact, if a constrained MSE cost function is used, the MOE algorithm results.

Convergence of Griffiths' Algorithm

Equation (4.85) may be rewritten as

$$\mathbf{w}(k+1) = [\mathbf{I} - \mu\mathbf{r}(k)\mathbf{r}^H(k)]\mathbf{w}(k) - \mu\beta_0\mathbf{s}_1. \tag{4.86}$$

Subtracting the optimum weight vector[3] $\mathbf{w}_{\text{opt}}$ from both sides of Equation (4.86) and rewriting in terms of the error vector $\mathbf{v}(k)$, we get

$$\mathbf{v}(k+1) = [\mathbf{I} - \mu\mathbf{r}(k)\mathbf{r}^H(k)]\mathbf{v}(k) + \mu\mathbf{r}(k)\mathbf{r}^H(k) - \mu\beta_0\mathbf{s}_1. \tag{4.87}$$

Taking expectations on both sides results in

$$\begin{aligned} E[\mathbf{v}(k+1)] &= [\mathbf{I} - \mu\mathbf{R}]E[\mathbf{v}(k)] + \mu\mathbf{R}\mathbf{w}_{\text{opt}} - \mu\beta_0\mathbf{s}_1 \\ &= [\mathbf{I} - \mu\mathbf{R}]E[\mathbf{v}(k)] + \mu\beta_0\mathbf{s}_1 - \mu\beta_0\mathbf{s}_1 \\ &= [\mathbf{I} - \mu\mathbf{R}]E[\mathbf{v}(k)]. \end{aligned} \tag{4.88}$$

This Equation is identical to Equation (4.32) for the LMS algorithm, and therefore, it can be concluded that Griffiths' algorithm is convergent in the mean if

$$0 < \mu < \frac{2}{\lambda_{\max}}. \tag{4.89}$$

4.3.7 The Linearly Constrained Constant Modulus Algorithm

The constant modulus algorithm (CMA) [82], which is related to the Godard algorithm [83], has been used for the extraction of constant modulus waveforms in blind equalization, beamforming, and interference rejection [82, 84, 85]. Lee et al. [86] and Zečević [80] independently investigated the use of the CMA for CDMA interference rejection. Since the algorithm extracts a constant modulus signal and the signals of all the users in a CDMA system have a constant modulus, there is no certainty that the desired signal will be extracted. Lee et al. [86] have investigated the convergence behavior for arbitrary initial filter coefficients and have found that that it is generally difficult to predict which signal will be captured. When the filter is initialized to the spreading code of the desired user, capture of the desired signal can be guaranteed only when it is the strongest. Even then, it is not guaranteed to remain locked onto same signal [80].

[3]We define the optimum weight vector $\mathbf{w}_{\text{opt}} \triangleq (\beta_0/\beta)\mathbf{R}^{-1}\mathbf{p} = \beta_0\mathbf{R}^{-1}\mathbf{s}_1$. This doesn't affect the DS/SS detector since the detected signal is invariant to scaling. In other words, any scaled version of the optimum filter is still optimum.

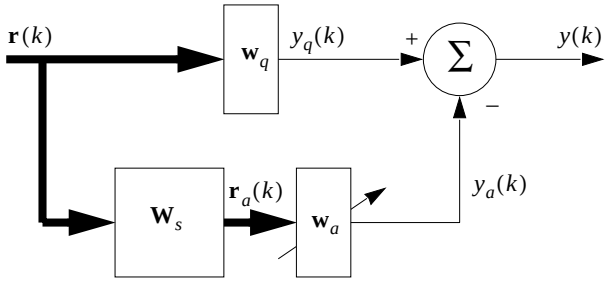

Figure 4.3: The Generalized Sidelobe Canceler.

To overcome the above problem, linear constraints may be used. The linearly constrained constant modulus algorithm (LCCMA) is yet another algorithm inspired by adaptive arrays [87, 88]. It is based on the generalized side-lobe canceler (GSC) used in adaptive array systems for incorporating *a priori* information about the signal into the algorithm [89]. The linear constraint helps to capture the signal of interest as opposed to one of the interference signals.

The constant modulus (CM) error criterion is given by

$$J = \frac{1}{4}E[(|y(k)|^2 - \delta)^2] \tag{4.90}$$

where δ is the actual or estimated output power with the optimum filter[4]. The following linear constraint is used:

$$\mathbf{w}^H \mathbf{s}_1 = 1 \tag{4.91}$$

where $\mathbf{w}$ is the weight vector and $\mathbf{s}_1$ is the constraint vector with elements equal to the spreading code coefficients of the desired user. This constraint ensures that the weight vector $\mathbf{w}$ maintains a unity correlation with the desired user's spreading code while adapting to minimize the error criterion. As shown in Figure 4.3, the overall weight vector is decomposed into

$$\mathbf{w} = \mathbf{w}_q - \mathbf{W}_s\, \mathbf{w}_a \tag{4.92}$$

where $\mathbf{w}_q$ is the constrained weight vector obtained by

$$\mathbf{w}_q = \mathbf{s}_1\, (\mathbf{s}_1^H \mathbf{s}_1)^{-1}, \tag{4.93}$$

[4]Unlike the CMA where the free scaling possible on the unconstrained weight vector allows for the arbitrary choice of δ, in the LCCMA this freedom is not available [88].

$\mathbf{W}_s$ is the *blocking matrix* whose columns span the left null space of $\mathbf{s}_1$, i.e.,

$$\mathbf{W}_s^H \mathbf{s}_1 = \mathbf{0} \tag{4.94}$$

and $\mathbf{w}_a$ is the unconstrained weight vector which is adapted to minimize the CM error criterion. The fact that $\mathbf{w}_a$ is unconstrained is seen from

$$\mathbf{w}^H \mathbf{s}_1 = \mathbf{w}_q^H \mathbf{s}_1 - \mathbf{w}_a^H \mathbf{W}_s^H \mathbf{s}_1 = \mathbf{w}_q^H \mathbf{s}_1 = 1, \tag{4.95}$$

where the constraint is satisfied regardless of the value of $\mathbf{w}_a$. The instantaneous estimate of the gradient of the CM cost function with respect to $\mathbf{w}_a$ is

$$\hat{\boldsymbol{\nabla}}_{\mathbf{w}_a}(J(k)) = -2(|y(k)|^2 - \delta)\, y^*(k) \mathbf{W}_s^H \mathbf{r}(k). \tag{4.96}$$

Thus, the signal component is extracted by the constrained weight vector $\mathbf{w}_q$ in the upper path of the GSC structure of Figure 4.3. The lower path completely blocks the signal component and operates on only noise and interference. The unconstrained weight vector $\mathbf{w}_a$ is adapted to suppress the noise and interference components in the symbol estimate that are allowed by $\mathbf{w}_q$. In adaptive array terms, the function of the lower path is to suppress the noise and interference that the upper path, the conventional beamformer, allows through its sidelobes. Thus, the lower path is the sidelobe canceler.

Thus the LCCMA consists of the following steps:

1. Computation of the "blocked" signal,
$$\mathbf{r}_a(k) = \mathbf{W}_s^H \mathbf{r}(k); \tag{4.97}$$
2. Computation of the output of the fixed filter,
$$y_F(k) = \mathbf{w}_q^H \mathbf{r}(k); \tag{4.98}$$
3. Computation of the output of the overall filter,
$$y(k) = y_F(k) - \mathbf{w}_a^H(k) \mathbf{r}_a(k); \tag{4.99}$$
4. Update of the adaptive filter weight vector,
$$\mathbf{w}_a(k+1) = \mathbf{w}_a(k) + \mu(|y(k)|^2 - \delta)\, y^*(k) \mathbf{r}_a(k). \tag{4.100}$$

Despite the matrix-vector multiplication in Equation (4.97), the LCCMA is not much more computationally complex than the MOE algorithm. Letting

$$\mathbf{u}(k) = \mathbf{W}_s \mathbf{w}_a(k) \tag{4.101}$$

we get

$$\mathbf{u}(k+1) = \mathbf{u}(k) + \mu(|y(k)|^2 - \delta)\, y^*(k)\mathbf{W}_s\mathbf{W}_s^H\mathbf{r}(k) \tag{4.102}$$

from Equation (4.100). Noting that[5]

$$\mathbf{W}_s\mathbf{W}_s^H = \mathbf{I} - \frac{\mathbf{s}_1\mathbf{s}_1^H}{\mathbf{s}_1^H\mathbf{s}_1} = \mathbf{s}_1\mathbf{w}_q^H \tag{4.103}$$

we get

$$\begin{aligned}\mathbf{u}(k+1) &= \mathbf{u}(k) + \mu(|y(k)|^2 - \delta)\, y^*(k)(\mathbf{I} - \mathbf{s}_1\mathbf{w}_q^H)\mathbf{r}(k) \\ &= \mathbf{u}(k) + \mu(|y(k)|^2 - \delta)\, y^*(k)[\mathbf{r}(k) - y_{MF}(k)\mathbf{s}_1].\end{aligned} \tag{4.104}$$

Equation (4.104) is very similar to Equation (4.75) of the MOE algorithm but has an additional factor $(|y(k)|^2-\delta)$, the CM error, in the update term of the LCCMA equation. The difference in the sign of the update term arises from the way $\mathbf{u}(k)$ is defined for the two algorithms.

Convergence of the LCCMA

The weight update factor in the LCCMA is a nonlinear function of the current weight vector, making the algorithm difficult to analyze. Like all SGD algorithms, the step-size for the LCCMA must be within a range for convergence in the mean, but deriving this range is an extremely involved process. The equation of the evolution of the expectation of the weight-error vector involves the covariance matrix of the weight-error, which highly complicates the equation. Zečević [80] did not report any instances of misconvergence of the algorithm.

[5] We may prove Equation (4.103) by showing that identical transformations to the left-hand side (LHS) and right-hand side (RHS) lead to the same result. After postmultiplying the LHS by $\mathbf{s}_1$, we get

$$\mathbf{W}_s\mathbf{W}_s^H\mathbf{s}_1 = \mathbf{0}$$

using Equation (4.94). Doing the same for the RHS, we get

$$\left(\mathbf{I} - \frac{\mathbf{s}_1\mathbf{s}_1^H}{\mathbf{s}_1^H\mathbf{s}_1}\right)\mathbf{s}_1 = \mathbf{s}_1 - \frac{\mathbf{s}_1^H\mathbf{s}_1}{\mathbf{s}_1^H\mathbf{s}_1}\mathbf{s}_1 = \mathbf{0}.$$

The above two equations hold for all $\mathbf{s}_1$.

4.4 Comparison Between CDMA and Adaptive Array Algorithms

Algorithms used for MAI rejection in code-on-pulse (COP) CDMA systems are similar to algorithms used for *beamforming* with narrowband equi-spaced linear (NEL) antenna arrays. The analogy stems from the similarity of signal processing operations performed in the two types of systems. Signal extraction in the two instances involves filtering: temporal FIR filtering in CDMA interference rejection and spatial filtering in beamforming. In the following discussion, we investigate the similarities in the two systems that help us to develop new algorithms for MAI rejection. We also explore the differences between the two systems, which impose limitations on the analogy. We maintain a very strict analogy between the two systems, which allows for the direct application of adaptive array algorithms to CDMA systems. More general comparisons broaden the scope but limit the extent to which the theory from one area can draw from the other.

4.4.1 Introduction

Figure 4.4 shows a NEL array receiver. The M antenna elements are uniformly spaced along a straight line. The RF signal received by each antenna element is independently downconverted to baseband and sampled to obtain complex data. The RF front ends are assumed to be identical and the signals in the M channels are sampled simultaneously. As will be seen in Section 4.4.2, the equally spaced separation of the antenna elements causes linear phase shifts in the signals sampled in successive channels. The baseband processor weights and combines the signals in the M channels to yield the recovered signal y. This processing amounts to shaping the *beampattern* of the antenna array, or the actual pattern depending on the weights used, and hence is termed *beamforming* [90, 91, 92]. The baseband processor shown is used for processing narrowband signals [90]; for broadband signals, the single weight in each channel is replaced by a FIR filter.

A CDMA receiver is depicted in Figure 4.5. The receiver has a single antenna element. The signal received by the antenna is downconverted to baseband by the single-channel RF front end and is sampled to obtain a complex data stream. Following synchronization, a buffer of N successive samples, equally spaced in time, is processed at a time by the baseband processor, which weights and combines the N samples to yield the recovered symbol stream y.

Comparison of the two figures reveals that in both cases the baseband processor weights and combines equally spaced (in space or time) samples to yield the recovered signal. However, two analogies can be drawn between COP CDMA interference rejection and beamforming with NEL arrays based on different considerations. One is based on the similarity of filter response characterization in the two systems while the other is based on

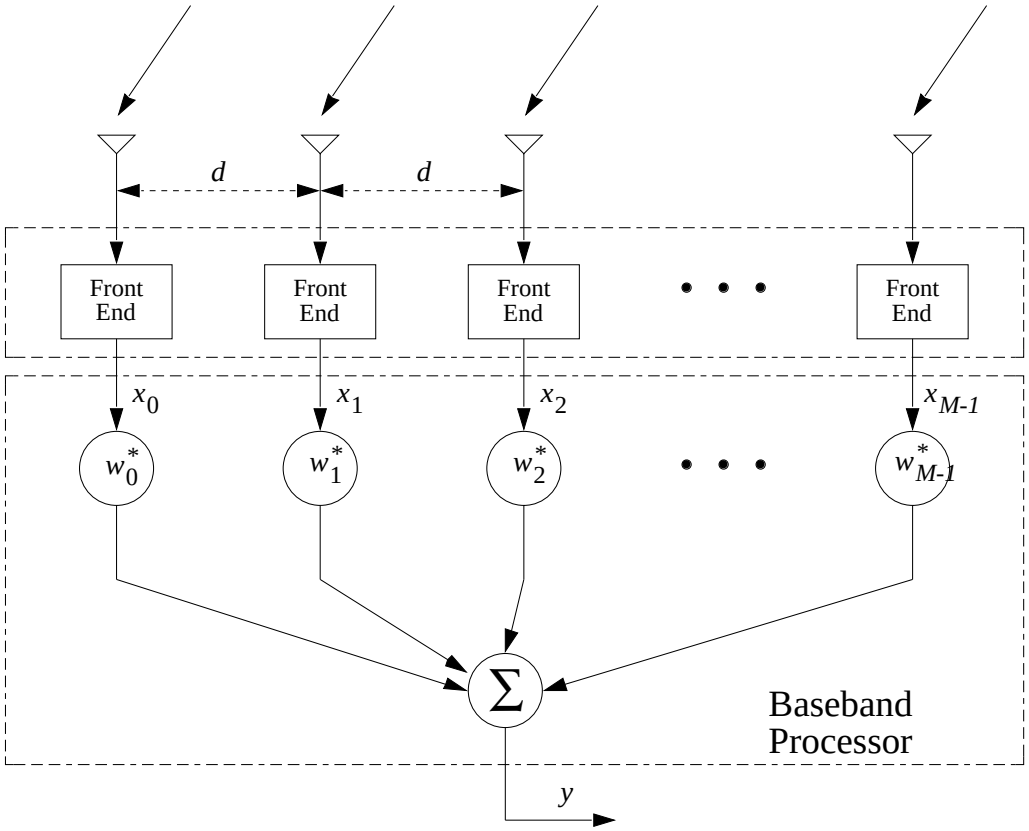

Figure 4.4: A NEL Array Receiver.

the similarity of their signal models. In the first analogy, the correspondence is between the NEL array and the FIR filter in the frequency domain, whereas in the second analogy the NEL array corresponds to the FIR filter in the time domain. The frequency domain analogy is briefly addressed below and the time domain analogy, which provides a direct mapping of filtering operations in the two types of receivers, is discussed in the next section.

The frequency domain analogy maps the frequency response of an FIR filter to the *beamformer response*, at a specific frequency, of the spatial filter [90], i.e., the beamformer response of a narrowband array. The analogy is appropriate because of the similarities of the definitions of the responses in their respective domains. The frequency response of the FIR filter defines the gain of the filter for all frequencies, whereas the beamformer response defines the gain of the spatial filter for all angles of arrival. The similarity also extends to the transforms that define these responses. However, the limitation of this analogy bears noting. With respect to the spatial filter, a signal source in AWGN is characterized by a single angle of arrival (AOA). Thus, this frequency domain analogy is most appropriate

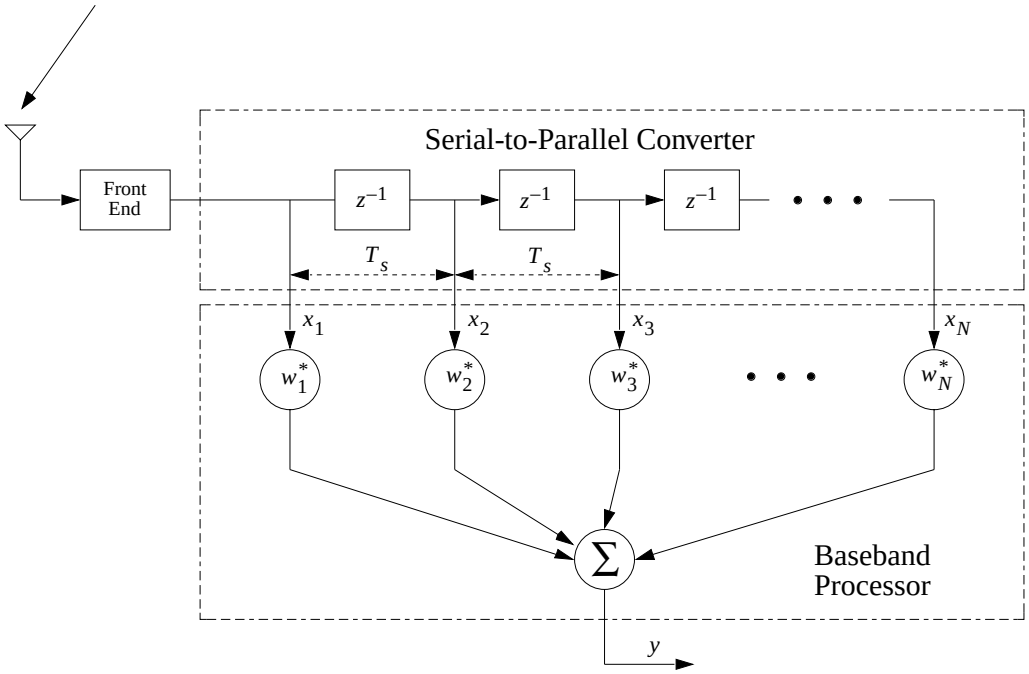

Figure 4.5: A CDMA Receiver.

when the signal processed by the FIR filter is a single tone. Furthermore, it is suitable for only AWGN channels because multipath is characterized by an angular spread [91], which does not map onto an equivalent in the case of the FIR filter. However, this frequency domain analogy is not useful for developing CDMA interference rejection algorithms.

Another frequency domain analogy worth mentioning is discussed by Zečević [80]. Zečević notes that the exploitation of spatial diversity by the beamformer is similar to the exploitation of spectral diversity in despreading a spread spectrum signal. The spreading operation may be viewed as frequency-shifting scaled versions of the data signal by integer multiples of the code repeat rate. Despreading with a time-varying filter is then the inverse operation, consisting of frequency-shifting filtered versions of different spectral portions of the spread signal to the data bandwidth and combining them, as depicted in Figure 3.1. This is similar to combining the filtered versions of the spatially sampled signal in a wideband array. Although this analogy may be exploited for general time-variant filtering, it is not very useful here since the FRESH filter of Figure 3.1 does not exploit the reduction in complexity gained by sampling the despread signal only once every symbol.

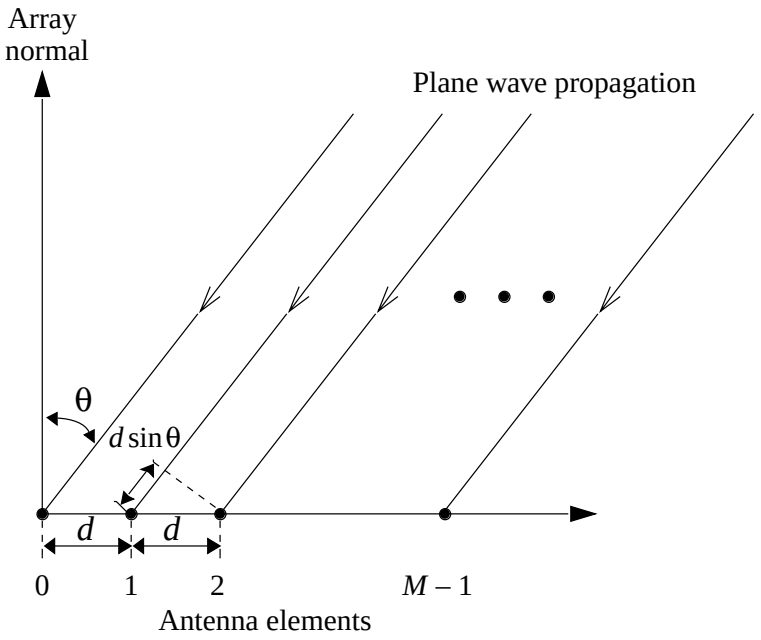

Figure 4.6: Arrival of a Plane Wavefront at the NEL Array.

4.4.2 Analogy Between a NEL Array and a CDMA Receiver in the Time Domain

The time domain analogy was first noted by Agee [93] and is best explained by comparing the signal models at the inputs of the two systems. We first consider the NEL array (with AWGN as the assumed channel). Figure 4.6 illustrates the incidence of a plane wavefront on the NEL array. θ is the angle made by the direction of arrival (DOA) with the normal to the array, and is termed the AOA. The separation between successive elements is represented as d. It is clear from the figure that the path difference between adjacent elements is $d \sin\theta$. Using the phase of the wave impinging on element 0 as the reference, the phase lag of the wave impinging on element m is $m\kappa d \sin\theta$ where $\kappa = 2\pi/\lambda$ (λ being the wavelength).

Consider a single source environment with AWGN. Let the sampled signal received at element 0 at time instant k be represented as

$$x_0(k) = s(k) + \nu_0(k) \tag{4.105}$$

where $s(k)$ is the signal due to a source with an AOA θ and $\nu_0(k)$ is the spatially uncor-

related noise. Then the sampled signal received at element m is

$$x_m(k) = s(k)\, e^{-jm\kappa d \sin\theta} + \nu_m(k). \tag{4.106}$$

Thus, the input signal vector may be represented by

$$\mathbf{x}(k) = s(k)\, \mathbf{a}(\theta) + \boldsymbol{\nu}(k) \tag{4.107}$$

where $\boldsymbol{\nu}(k)$ is the appropriately defined M-element noise vector and

$$\mathbf{d}(\theta, \omega) \triangleq \begin{bmatrix} 1 \\ e^{-j\kappa d \sin\theta} \\ e^{-j2\kappa d \sin\theta} \\ \vdots \\ e^{-j(M-1)\kappa d \sin\theta} \end{bmatrix} \tag{4.108}$$

is known as the *steering vector* or the *array response vector*. The steering vector defines the source of the incident signal $s(k)$ and, for a given array configuration and frequency, is a function of only the AOA θ.

Similarly, in a multiple source environment, the input signal vector may be expressed as

$$\mathbf{x}(k) = \sum_{i=1}^{L} s_i(k)\, \mathbf{a}_i + \boldsymbol{\nu}(k) \tag{4.109}$$

where L is the number of signal sources, $s_i(k)$ is the received signal due to the ith source, and $\mathbf{a}_i$ is the steering vector of the ith source. We assume that the sources are spatially separated so that each source has a unique AOA. Thus, the signal sources are distinguished from each other through their steering vectors, which may then be referred to as the *signature vectors*.

Next consider a CDMA system with L asynchronous signals. The received signal may be represented with an equivalent synchronous model as

$$\mathbf{x}(k) = \sum_{i=1}^{K} d_i(k)\, \mathbf{c}_i + \boldsymbol{\nu}(k) \tag{4.110}$$

where $K = 2L - 1$ is the number of equivalent synchronous signals[6], $d_i(k)$ is the information signal of the ith equivalent signal, and $\mathbf{c}_i$ is the spreading code of the ith equivalent

[6]There is one vector due to the desired signal and $2(L-1)$ vectors due to the $L-1$ MAI signals. This assumes that their delays are different from the delay of the desired signal.

signal. Recall that the signals are distinguished through their spreading codes, which are the *signature vectors* in this case.

Note the similarity between Equations (4.109) and (4.110). In each case, the ith signal is formed by the product of the information signal ($s_i(k)$ or $d_i(k)$) and its respective signature vector ($\mathbf{a}_i$ or $\mathbf{c}_i$). The input signal is formed by the summation of all the signals and noise. We further note that each element of the signature vector has a modulus of unity.

Without loss of generality, let the first signal be the desired signal. In both cases, the input signal is filtered in the receiver to obtain the estimated signal and this is expressed by

$$y(k) = \mathbf{w}^H \mathbf{x}(k) \tag{4.111}$$

where $\mathbf{w}$ is the weight vector. Furthermore, in both cases, $\mathbf{w}$ is chosen through an optimization procedure so that the estimated signal $y(k)$ closely approximates the information signal of interest ($s_1(k)$ or $d_1(k)$). The NEL array accomplishes this task by forming nulls in directions of the interference sources, while the CDMA receiver forms "nulls" towards the MAI signals. In either case, the task is accomplished by selecting a weight vector $\mathbf{w}$ that is approximately orthogonal to all of the interference signature vectors.

Thus, under the conditions assumed, it is clear that the signal processing algorithms developed for a NEL array operating in an AWGN channel to extract one of the many received signals may also be employed in a CDMA receiver to extract the desired signal received with MAI. Furthermore, if the information signals $s_i(k)$ and $d_i(k)$ share a common characteristic, a beamforming algorithm that exploits this characteristic may also be employed for CDMA interference rejection. Some algorithms that are commonly used in both receivers are the LMS algorithm, the recursive least-squares (RLS) algorithm, and the decision-directed algorithm. Zečević has successfully adopted Griffiths' algorithm and the LCCMA, both traditionally used for beamforming, for CDMA interference rejection [80].

4.4.3 Limitations of the Analogy

In the preceding discussion, it was assumed that the channel was AWGN. The analogy is not easily extended to multipath channels. Multipath propagation causes fading that may be either flat or frequency-selective depending on the bandwidth of the signal relative to the bandwidth of the channel [5]. Flat fading results when the bandwidth of the signal is less than the bandwidth of the channel; frequency-selective fading occurs when the bandwidth of the signal is greater than the bandwidth of the channel. In the

case of flat fading, the signal strength at the receiver fluctuates over time while spectral characteristics of the original signal are preserved. With frequency-selective fading, multiple delayed and scaled versions of the transmitted signal, each of which fades independently, arrive at the receiver. This phenomenon results in the alteration of the spectral characteristics of the transmitted signal.

Multipath components arrive at the NEL array from different directions depending on the location of the local scatterers causing multipath. Thus, multipath is characterized by its *angular spread* [91]. This angular spread, which depends on the distance between the mobile and the basestation relative to the radius of the scatterers, is small on the forward link in an outdoor mobile channel but is relatively large in an indoor channel.When the angular spread is negligible, multipath can be assumed to be coming from a single direction. This is similar to but not the same as assuming flat fading in the case of the CDMA receiver. Frequency-selective fading in the case of the array is not relevant to this discussion because the signals received by the array are assumed to be narrowband.

Let us consider a comparison of the NEL array in an outdoor mobile flat fading channel and the CDMA receiver in a flat fading channel. Ignoring mutual coupling between antenna elements and envelope correlation between signals at different elements, the signal received at each element of the array is independently faded. In the case of the CDMA receiver, however, all the samples processed by the filter are part of the same fading envelope. The independent fading of signals at the different elements is beneficial to the array in its exploitation of spatial diversity since the probability of the signal undergoing a deep fade at all elements *simultaneously* is very low. The adaptation algorithm used for beamforming also performs optimal combining by using small weights for less reliable samples, i.e., signal samples during a fade, and larger weights for more reliable samples. In contrast, the correlated nature of the samples in the input signal vector can be detrimental to the performance of the CDMA receiver. When the signal processed by the CDMA receiver undergoes a fade, all of the input vector samples will be faded with a high probability, greatly reducing the signal-to-noise ratio. The adaptation algorithm cannot do much in this situation and a high bit error rate results. Furthermore, some algorithms can fail catastrophically when processing the CDMA signal during a deep fade. The decision-directed algorithm is well known for this problem. Thus, the analogy between the two systems fails in this situation.

In the case of an indoor mobile flat fading channel, the NEL array receives the same signal from different directions. Thus, the composite signal from the desired source is the sum of scaled versions of the same information signal $s_1(k)$ multiplied by different steering vectors $\mathbf{a}_i$. The NEL array can combine the correlated signals arriving from different directions to enhance the estimated signal. The CDMA equivalent of this situation corresponds to receiving the sum of scaled versions of the same information signal $d_1(k)$ multiplied by different spreading codes $\mathbf{c}_i$. This situation occurs in frequency-selective fading channels where the correlated part of a delayed multipath component appears as the information signal $d_1(k)$ multiplied by a segment of a cyclically shifted version of

the code (cf. Chapter 6). The equivalent code vector is different from the original code vector. The uncorrelated part of a delayed component appears as an interference vector. Although the analogy is not perfect—interference vectors are introduced in the case of CDMA—algorithms used in a NEL array for indoor flat fading channels can be used in a CDMA receiver for frequency-selective fading channels. An example is the LMS algorithm, which is derived from the MSE cost function and can exploit the inherent temporal diversity of multipath signals. In both systems, the LMS algorithm combines correlated received signals to enhance the estimated signal.

4.5 Summary

An overview of adaptation algorithms used for CDMA interference rejection was provided. Adaptation algorithms can be classified as block or recursive. Stochastic gradient descent (SGD) algorithms are attractive due their simplicity. CDMA interference rejection use the following SGD algorithms: the least-mean square (LMS) algorithm (which converges to the minimum mean-squared error solution provided by the Wiener filter), the normalized LMS (NLMS) algorithm, the decision-directed algorithm, the minimum output-energy (MOE) algorithm, Griffiths' algorithm, and the linearly constrained constant modulus algorithm (LCCMA). Except for the LMS and the NLMS algorithms, the above algorithms are blind; they do not require a training signal to be transmitted. The cost functions that the above algorithms minimize were discussed, and a brief analysis of their convergence was presented. The relationship between these algorithms was shown. A comparison between adaptive array and CDMA interference rejection algorithms was provided. The analogy of CDMA systems with adaptive array systems was presented. The similarities between the systems were explained to show how adaptive array algorithms can be directly applied for CDMA interference rejection. The limitations of this analogy were discussed. A very strict analogy was presented to limit the scope of the theoretical applications of this analogy.

Chapter 5

Blind CDMA Interference Rejection in Multipath Channels

5.1 Introduction

The increasing interest in CDMA systems for mobile radio has spawned a great deal of research in recent years in the area of exploitation of multipath in conjunction with the mitigation of MAI. While a Rake receiver can coherently combine multipath, it is susceptible to degradation caused by near-far effects [94, 95] and is still limited by the MAI since it does not perform any interference mitigation. Most of the research efforts for overcoming these limitations have been concentrated on receiver architectures for the base station because of the high complexity.

As noted in Chapter 2, a multiuser receiver can reduce MAI yielding significant performance gains over a simple correlation receiver [22, 27, 28]. If multipath is present, a multistage Rake receiver can cancel interference as well as combine multipath [31]. However, the computational complexity of these receivers precludes their use in a single user receiver such as a mobile unit, which requires low power consumption and a small physical size. Adaptive MMSE receivers have been known to exploit multipath [50, 55] and many employ the relatively simple LMS algorithm for adaptation. Unfortunately, most of these receivers require a training sequence.

The LCCMA, Griffiths' algorithm, and the MOE algorithm do not require a training sequence (cf. Chapter 4). These algorithms have been shown to perform very well, and closely match the decision-directed algorithm following training, in stationary AWGN channels and even in near-far situations [78, 80]. Although these algorithms are simple and effective in MAI they do not exploit multipath.

In this chapter, the stationary points of the LCCM cost function are analyzed to demon-

strate that the LCCMA attempts to suppress multipath of the desired user's signal rather than exploit it. Analysis is performed both with and without the assumption that the received signal is Gaussian to obtain the same conclusion. A new *blind* algorithm that is suitable for multipath channels is proposed. This algorithm, called the multi-channel LCCMA (MLCCMA), is a modification of the LCCMA and employs multiple constraints to combine multipath components. The improvement in performance of this algorithm over LCCMA is significant. It is shown here that the performance of the algorithm is better than that of the conventional Rake receiver combining the same number of multipath components and approaches that of an adaptive receiver in the decision-directed mode following training.

5.2 Stationary Points of the Linearly Constrained Constant Modulus Cost Function

A *stationary point* of a cost function $J(\mathbf{w})$ is defined as the point described by $(\mathbf{w}_o, J(\mathbf{w}_o))$ where its gradient $\boldsymbol{\nabla}(J(\mathbf{w}))$ vanishes [73]. For a real-valued cost function of a complex weight-vector $\mathbf{w}$, it is necessary and sufficient if either the gradient with respect to $\mathbf{w}$ or the gradient with respect to $\mathbf{w}^*$ vanishes to determine the stationary point of $J(\mathbf{w})$ [96]. Stationary points may be categorized into *maxima*, *minima*, and *saddle points*. We now derive the stationary points of the linearly constrained constant modulus (LCCM) cost function.Analysis of the stationary points of the LCCM cost function is useful in determining how the LCCMA treat multipath components of the desired signal.

The LCCM cost function may be expressed as

$$J = \frac{1}{2}E[(|y|^2 - \delta)^2] + \lambda(1 - \mathbf{w}^H\mathbf{s}_1) \tag{5.1}$$

where λ is a Lagrange multiplier and y is the output given by

$$y = \mathbf{w}^H\mathbf{r}. \tag{5.2}$$

$\mathbf{w}$ is the weight vector and and $\mathbf{r}$ is the input signal vector. In the following discussion we use the definition $\boldsymbol{\nabla}_{\mathbf{w}^*} \triangleq \partial/\partial\mathbf{w}^*$ for the gradient operator, following the convention of [96], instead of the definition of Equation (4.10). Then, the gradient of the cost function with respect to $\mathbf{w}^*$ is given by

$$\boldsymbol{\nabla}(J) = E[(|y|^2 - \delta)\, y^*\, \mathbf{r}] - \lambda\mathbf{s}_1. \tag{5.3}$$

Thus, the condition for a stationary point is

$$E[(|y|^2 - \delta)\, y^*\, \mathbf{r}] - \lambda\mathbf{s}_1 = \mathbf{0}. \tag{5.4}$$

Premultiplying by $\mathbf{s}_1^H$ and rearranging, we get

$$\lambda = \frac{E[(|y|^2 - \delta)\, y^* \, \mathbf{s}_1^H \mathbf{r}]}{\mathbf{s}_1^H \mathbf{s}_1}. \tag{5.5}$$

When this result is used in Equation (5.4), we get

$$E[(|y|^2 - \delta)\, y^* \, \mathbf{r}] - \frac{E[(|y|^2 - \delta)\, y^* \, \mathbf{s}_1^H \mathbf{r}]}{\mathbf{s}_1^H \mathbf{s}_1} \mathbf{s}_1 = \mathbf{0}. \tag{5.6}$$

This may be rewritten as

$$E\left[(|y|^2 - \delta)\, y^* \, \left(\mathbf{I} - \frac{\mathbf{s}_1^H \mathbf{s}_1}{\mathbf{s}_1 \mathbf{s}_1^H}\right) \mathbf{r}\right] = \mathbf{0}. \tag{5.7}$$

Let

$$\mathbf{P} \triangleq \mathbf{I} - \frac{\mathbf{s}_1 \mathbf{s}_1^H}{\mathbf{s}_1^H \mathbf{s}_1}. \tag{5.8}$$

Then, using Equation (5.2), Equation (5.7) may be written as

$$\mathbf{P}(E[\mathbf{r}\mathbf{r}^H \mathbf{w}\mathbf{w}^H \mathbf{r}\mathbf{r}^H \mathbf{w}] - \delta E[\mathbf{r}\mathbf{r}^H \mathbf{w}]) = \mathbf{0}. \tag{5.9}$$

5.2.1 Using the Gaussian Assumption for the Input Signal

To evaluate the expectations in Equation (5.9), it is assumed that the input signal vector $\mathbf{r}$ consists of elements that are Gaussian random variables. This is a common assumption used for studying SGD algorithms for equalization applications and is somewhat justified in this instance when there is a large number of users in the CDMA system. Although only an approximation, it is very helpful in obtaining a closed form expression for the first expectation in Equation (5.9).

We may represent

$$E[\mathbf{r}\mathbf{r}^H \mathbf{w}\mathbf{w}^H \mathbf{r}\mathbf{r}^H \mathbf{w}] = \mathbf{A}\mathbf{w} \tag{5.10}$$

with

$$\mathbf{A} = \{a_{ij}\} \triangleq E[\mathbf{r}\mathbf{r}^H \mathbf{w}\mathbf{w}^H \mathbf{r}\mathbf{r}^H] \tag{5.11}$$

where a_{ij} denotes the (i, j) element of the matrix $\mathbf{A}$. Then

$$a_{ij} = \sum_{m=1}^{N_F}\sum_{n=1}^{N_F} E[r_i r_m^* w_m w_n^* r_n r_j^*] \tag{5.12}$$

$$= \sum_{m=1}^{N_F}\sum_{n=1}^{N_F} E[r_i r_m^* r_n r_j^*] w_m w_n^* \tag{5.13}$$

where r_m and w_m are the mth elements of $\mathbf{r}$ and $\mathbf{w}$, respectively. Using the results from the Gaussian moment factoring theorem for complex Gaussian random variables in [38], we get

$$E[r_i r_m^* r_n r_j^*] = E[r_i r_m^*]E[r_n r_j^*] + E[r_i r_j^*]E[r_n r_m^*]. \tag{5.14}$$

Denoting the (i,j) element of the correlation matrix $\mathbf{R}$ by γ_{ij},

$$\gamma_{ij} = E[r_i r_j^*] \tag{5.15}$$

and we can write

$$E[r_i r_m^* r_n r_j^*] = \gamma_{im}\gamma_{nj} + \gamma_{ij}\gamma_{mn}. \tag{5.16}$$

Then Equation (5.13) can be rewritten as

$$a_{ij} = \sum_{m=1}^{N_F}\sum_{n=1}^{N_F} \gamma_{im} w_m w_n^* \gamma_{nj} + \gamma_{ij}\sum_{m=1}^{N_F}\sum_{n=1}^{N_F} w_m \gamma_{mn} w_n^*. \tag{5.17}$$

From this equation, we can deduce that

$$\mathbf{A} = \mathbf{R}\mathbf{w}\mathbf{w}^H\mathbf{R} + \mathbf{R}\mathbf{w}^H\mathbf{R}\mathbf{w}, \tag{5.18}$$

where we have used the Hermitian property of $\mathbf{R}$. We also note that

$$E[\mathbf{r}\mathbf{r}^H\mathbf{w}] = E[\mathbf{r}\mathbf{r}^H]\mathbf{w} = \mathbf{R}\mathbf{w}. \tag{5.19}$$

Using Equations (5.10), (5.18), and (5.19) in Equation (5.9), the stationarity condition becomes

$$\mathbf{P}\left(2\mathbf{w}^H\mathbf{R}\mathbf{w}\mathbf{R}\mathbf{w} - \delta\mathbf{R}\mathbf{w}\right) = \mathbf{0} \tag{5.20}$$

or equivalently,

$$\left(2\mathbf{w}^H\mathbf{R}\mathbf{w} - \delta\right)\mathbf{P}\mathbf{R}\mathbf{w} = \mathbf{0} \tag{5.21}$$

Thus, at the stationary point, the weight vector satisfies, along with the linear constraint of Equation (4.91), either

$$2\mathbf{w}^H\mathbf{R}\mathbf{w} - \delta = 0 \tag{5.22}$$

or

$$\mathbf{P}\mathbf{R}\mathbf{w} = \mathbf{0}. \tag{5.23}$$

Equation (5.22) results in the stationarity condition

$$\mathbf{w}^H\mathbf{R}\mathbf{w} = \frac{\delta}{2} \tag{5.24}$$

which defines an N_F-dimensional *hyperellipsoid*. Equation (5.23) implies that the weight vector at the stationary point is the eigenvector associated with the eigenvalue zero of the singular matrix $\mathbf{PR}$. The vector

$$\mathbf{w}_{\text{opt}} = \frac{\mathbf{R}^{-1}\mathbf{s}_1}{\mathbf{s}_1^H\mathbf{R}^{-1}\mathbf{s}_1} \tag{5.25}$$

is such an eigenvector of $\mathbf{PR}$, since, using Equation (5.8),

$$\begin{aligned}
\mathbf{P}\mathbf{R}\mathbf{w}_{\text{opt}} &= \mathbf{R}\frac{\mathbf{R}^{-1}\mathbf{s}_1}{\mathbf{s}_1^H\mathbf{R}^{-1}\mathbf{s}_1} - \frac{\mathbf{s}_1\mathbf{s}_1^H}{\mathbf{s}_1^H\mathbf{s}_1}\mathbf{R}\frac{\mathbf{R}^{-1}\mathbf{s}_1}{\mathbf{s}_1^H\mathbf{R}^{-1}\mathbf{s}_1} \\
&= \frac{\mathbf{s}_1}{\mathbf{s}_1^H\mathbf{R}^{-1}\mathbf{s}_1} - \frac{\mathbf{s}_1}{\mathbf{s}_1^H\mathbf{R}^{-1}\mathbf{s}_1} \\
&= \mathbf{0}.
\end{aligned}$$

It should be noted that the weight vector of Equation (5.25) is proportional to the MMSE solution for an AWGN channel, which is $\mathbf{R}^{-1}\,\mathbf{s}_1$. Since the rank of the matrix $\mathbf{PR}$ is $N_F - 1$, there is only one eigenvalue equal to zero and therefore, there is only one unique solution that satisfies the stationarity condition of Equation (5.23), that of Equation (5.25).

Sufficient Conditions for Extrema of the Constrained Cost Function

The (N_F+1)th-order bordered Hessian matrix of the Lagrangian (constrained cost function of Equation (5.1)) is given by [73]

$$\mathbf{H}_J^{\mathbf{g}}(\mathbf{w}_{\text{opt}}, \lambda_{\text{opt}}) \triangleq \begin{bmatrix} \mathbf{H}_J(\mathbf{w}_{\text{opt}}, \lambda_{\text{opt}}) & \boldsymbol{\nabla}\mathbf{g}(\mathbf{w}_{\text{opt}}) \\ \boldsymbol{\nabla}\mathbf{g}(\mathbf{w}_{\text{opt}})^H & 0 \end{bmatrix} \tag{5.26}$$

where $(\cdot)$ denotes the matrix transpose operation, $\mathbf{w}_{\text{opt}}$ and λ_{opt} are the weight vector and the Lagrange multiplier, respectively, at the stationary point,

$$\mathbf{H}_J(\mathbf{w}, \lambda) \stackrel{\triangle}{=} \frac{\partial^2 J}{\partial \mathbf{w}^* \partial \mathbf{w}^H} \tag{5.27}$$

is the Hessian matrix of the LCCM cost function of Equation (5.1), and $\boldsymbol{\nabla}\mathbf{g}(\mathbf{w})$ is the gradient of the constraint function

$$\mathbf{g}(\mathbf{w}) \stackrel{\triangle}{=} 1 - \mathbf{w}^H \mathbf{s}_1. \tag{5.28}$$

From the theory of constrained optimization [73], the cost function J has a strong local extremum if

$$\begin{vmatrix} \mathbf{H}_J(\mathbf{w}_{\text{opt}}, \lambda_{\text{opt}})_{i,i} & \boldsymbol{\nabla}\mathbf{g}(\mathbf{w}_{\text{opt}})_i \\ \boldsymbol{\nabla}\mathbf{g}(\mathbf{w}_{\text{opt}})_i^H & 0 \end{vmatrix} \neq 0, \quad i = 2, \ldots, N_F \tag{5.29}$$

where $\mathbf{H}_J(\mathbf{w}_{\text{opt}}, \lambda_{\text{opt}})_{i,i}$ is the matrix obtained by taking the first i rows and the first i columns of $\mathbf{H}_J(\mathbf{w}_{\text{opt}}, \lambda_{\text{opt}})$ and $\boldsymbol{\nabla}\mathbf{g}(\mathbf{w}_{\text{opt}})_i$ is the vector of the first i elements of $\boldsymbol{\nabla}\mathbf{g}(\mathbf{w}_{\text{opt}})$. Furthermore,

1. if

$$\Delta_i = (-1)^i \begin{vmatrix} \mathbf{H}_J(\mathbf{w}_{\text{opt}}, \lambda_{\text{opt}})_{i,i} & \boldsymbol{\nabla}\mathbf{g}(\mathbf{w}_{\text{opt}})_i \\ \boldsymbol{\nabla}\mathbf{g}(\mathbf{w}_{\text{opt}})_i^H & 0 \end{vmatrix} > 0, \quad i = 2, \ldots, N_F \tag{5.30a}$$

   then J has a strong local maximum at $\mathbf{w}_{\text{opt}}$;

2. if

$$\Delta_i = \begin{vmatrix} \mathbf{H}_J(\mathbf{w}_{\text{opt}}, \lambda_{\text{opt}})_{i,i} & \boldsymbol{\nabla}\mathbf{g}(\mathbf{w}_{\text{opt}})_i \\ \boldsymbol{\nabla}\mathbf{g}(\mathbf{w}_{\text{opt}})_i^H & 0 \end{vmatrix} < 0, \quad i = 2, \ldots, N_F \tag{5.30b}$$

   then J has a strong local minimum at $\mathbf{w}_{\text{opt}}$.

The above two sufficient conditions for extrema are equivalent to the following two conditions [73]. For any $\mathbf{x}$ satisfying $\boldsymbol{\nabla}\mathbf{g}(\mathbf{w}_{\text{opt}})^H \mathbf{x} = 0$,

1. if

$$\mathbf{x}^H \mathbf{H}_J(\mathbf{w}_{\text{opt}}, \lambda_{\text{opt}}) \mathbf{x} > 0 \tag{5.31a}$$

   then J has a strong local minimum at $\mathbf{w}_{\text{opt}}$;

2. if

$$\mathbf{x}^H \mathbf{H}_J(\mathbf{w}_{\text{opt}}, \lambda_{\text{opt}})\, \mathbf{x} < 0 \tag{5.31b}$$

then J has a strong local maximum at $\mathbf{w}_{\text{opt}}$.

Thus, the sign definiteness of the quadratic form $\mathbf{x}^H \mathbf{H}_J(\mathbf{w}_{\text{opt}}, \lambda_{\text{opt}})\, \mathbf{x}$ for those $\mathbf{x}$ satisfying $\mathbf{g}(\mathbf{w}_{\text{opt}} + \mathbf{x}) = 0$ and hence $\boldsymbol{\nabla}\mathbf{g}(\mathbf{w}_{\text{opt}})^H \mathbf{x} = 0$ determines whether the extremum is a minimum or a maximum.

Determination of the Nature of the Stationary Point

The Hessian matrix $\mathbf{H}_J(\mathbf{w}, \lambda)$ defined in Equation (5.27) may be evaluated as follows:

$$\begin{aligned}
\mathbf{H}_J(\mathbf{w}, \lambda) &= \frac{\partial}{\partial \mathbf{w}^H}(\boldsymbol{\nabla} J) \\
&= E\left\{ \frac{\partial}{\partial \mathbf{w}^H} \left[(\mathbf{r}^H \mathbf{w}\mathbf{w}^H \mathbf{r} - \delta)\, \mathbf{r}\mathbf{r}^H \mathbf{w} \right] \right\} \\
&= E\left[(\mathbf{r}^H \mathbf{w}\mathbf{w}^H \mathbf{r} - \delta)\, \mathbf{r}\mathbf{r}^H \mathbf{I} + \mathbf{r}\mathbf{r}^H \mathbf{w}\ \mathbf{w}^H \mathbf{r}\mathbf{r}^H \right] \\
&= E\left[2\mathbf{r}\mathbf{r}^H \mathbf{w}\mathbf{w}^H \mathbf{r}\mathbf{r}^H - \delta \mathbf{r}\mathbf{r}^H \right] \\
&= 2\mathbf{R}\mathbf{w}\mathbf{w}^H \mathbf{R} + (2\mathbf{w}^H \mathbf{R}\mathbf{w} - \delta)\mathbf{R}.
\end{aligned} \tag{5.32}$$

Also,

$$\boldsymbol{\nabla}\mathbf{g}(\mathbf{w}) = -\mathbf{s}_1. \tag{5.33}$$

Evaluating the Hessian matrix at the stationary point defined in Equation (5.25), we get

$$\begin{aligned}
\mathbf{H}_J(\mathbf{w}_{\text{opt}}, \lambda_{\text{opt}}) &= \frac{\mathbf{s}_1}{\mathbf{s}_1^H \mathbf{R}^{-1} \mathbf{s}_1} \frac{\mathbf{s}_1^H}{\mathbf{s}_1^H \mathbf{R}^{-1} \mathbf{s}_1} + \left(2 \frac{\mathbf{w}_{\text{opt}}^H \mathbf{s}_1}{\mathbf{s}_1^H \mathbf{R}^{-1} \mathbf{s}_1} - \delta \right) \mathbf{R} \\
&= \frac{\mathbf{s}_1 \mathbf{s}_1^H}{(\mathbf{s}_1^H \mathbf{R}^{-1} \mathbf{s}_1)^2} + \left(\frac{2}{\mathbf{s}_1^H \mathbf{R}^{-1} \mathbf{s}_1} - \delta \right) \mathbf{R}
\end{aligned} \tag{5.34}$$

As noted in Section 4.3.7, δ should ideally be the actual output power. The optimum value of δ can be obtained by minimizing the cost function of Equation (5.1) with respect to δ and is given by [88]

$$\delta_{\text{opt}} = \mathbf{w}_{\text{opt}}^H \mathbf{R} \mathbf{w}_{\text{opt}}. \tag{5.35}$$

Substituting for $\mathbf{w}_{\text{opt}}$ from Equation (5.25) results in

$$\begin{aligned}\delta_{\text{opt}} &= \frac{\mathbf{s}_1^H\mathbf{R}^{-1}}{\mathbf{s}_1^H\mathbf{R}^{-1}\mathbf{s}_1}\mathbf{R}\frac{\mathbf{R}^{-1}\mathbf{s}_1}{\mathbf{s}_1^H\mathbf{R}^{-1}\mathbf{s}_1} \\ &= \frac{1}{\mathbf{s}_1^H\mathbf{R}^{-1}\mathbf{s}_1}. \end{aligned} \tag{5.36}$$

If this value of δ is used in Equation (5.34), we get

$$\mathbf{H}_J(\mathbf{w}_{\text{opt}}, \lambda_{\text{opt}}) = \frac{\mathbf{s}_1\mathbf{s}_1^H}{(\mathbf{s}_1^H\mathbf{R}^{-1}\mathbf{s}_1)^2} + \frac{1}{\mathbf{s}_1^H\mathbf{R}^{-1}\mathbf{s}_1}\mathbf{R}. \tag{5.37}$$

Defining

$$\mathbf{H}_1 \triangleq \frac{\mathbf{s}_1\mathbf{s}_1^H}{(\mathbf{s}_1^H\mathbf{R}^{-1}\mathbf{s}_1)^2} \tag{5.38}$$

$$\mathbf{H}_2 \triangleq \frac{1}{\mathbf{s}_1^H\mathbf{R}^{-1}\mathbf{s}_1}\mathbf{R}, \tag{5.39}$$

we note that since $\mathbf{R}$ is positive definite, so is $\mathbf{H}_2$. Furthermore, for $\mathbf{x} \in \mathcal{R}^{N_F}$,

$$\begin{aligned}\mathbf{x}^H\mathbf{H}_1\mathbf{x} &= \frac{\mathbf{x}^H\mathbf{s}_1\mathbf{s}_1^H\mathbf{x}}{(\mathbf{s}_1^H\mathbf{R}^{-1}\mathbf{s}_1)^2} \\ &= \frac{|\mathbf{x}^H\mathbf{s}_1|^2}{(\mathbf{s}_1^H\mathbf{R}^{-1}\mathbf{s}_1)^2} \\ &\geq 0 \quad \forall\, \mathbf{x}. \end{aligned} \tag{5.40}$$

Therefore, $\mathbf{H}_1$ is *positive semidefinite*. Since $\mathbf{H}_1$ is positive semidefinite and $\mathbf{H}_2$ is positive definite, $\mathbf{H}_J(\mathbf{w}_{\text{opt}}, \lambda_{\text{opt}})$ must be positive definite. Therefore,

$$\mathbf{x}^H\,\mathbf{H}_J(\mathbf{w}_{\text{opt}}, \lambda_{\text{opt}})\,\mathbf{x} > 0 \;\forall\; \mathbf{x} \tag{5.41}$$

and hence

$$\mathbf{x}^H\,\mathbf{H}_J(\mathbf{w}_{\text{opt}}, \lambda_{\text{opt}})\,\mathbf{x} > 0 \;\forall\; \mathbf{x} \text{ satisfying } \boldsymbol{\nabla}\mathbf{g}(\mathbf{w}_{\text{opt}})^H\,\mathbf{x} = 0. \tag{5.42}$$

Equation (5.42) implies that the stationary point of Equation (5.25) is a *minimum* of the LCCM cost function and therefore, the SGD adaptation algorithm for LCCMA will converge to this stationary point.

Equation (5.22) also defines stationary points. These are actually the stationary points of the CM cost function in the absence of the linear constraint. Clearly, when the optimal value of δ defined in Equation (5.35) is used, the condition for stationarity cannot be satisfied. This contradiction implies that the stationary points of Equation (5.22) do not pertain to global extrema of the LCCM cost function.

As noted earlier, the weight vector defined in Equation (5.25) is proportional to the MMSE solution for an AWGN channel, which suggests that any multipath of the signal of interest is not treated as desired signal[1]. That is, multipath components are treated as additional interference and are suppressed like the MAI signals. This is a major weakness of the LCCMA that prevents it from exploiting multipath diversity in fading channels.

5.2.2 Without Using the Gaussian Assumption

Analysis for AWGN Channels

Here we make no assumptions about the distribution of the received signal. We model the received signal vector $\mathbf{r}$ as the sum of the signals from K users and AWGN:

$$\mathbf{r} = \sum_{l=1}^{K} A_l b_l \mathbf{s}_l + \mathbf{n} \tag{5.43}$$

where A_l is the amplitude, b_l is the transmitted information bit, and $\mathbf{s}_l$ is the spreading code of the lth user. $\mathbf{n}$ is the zero-mean AWGN vector with covariance matrix $\sigma^2\mathbf{I}$. It may be noted that

$$E[b_l\mathbf{n}] = \mathbf{0}, \qquad l = 1, 2, \ldots, K. \tag{5.44}$$

We represent the mth user's spreading code as

$$\mathbf{s}_l \stackrel{\triangle}{=} \begin{bmatrix} s_{l1} \\ s_{l2} \\ \vdots \\ s_{lN_F} \end{bmatrix}. \tag{5.45}$$

Using the notation of Equation (5.11), we have

$$a_{ij} = \sum_{m=1}^{N_F} \sum_{n=1}^{N_F} E[r_i r_m^* w_m w_n^* r_n r_j^*]$$

[1]It is seen in Chapter 6 that the MMSE solution $\mathbf{w}_{\text{opt}} = \mathbf{R}^{-1}\mathbf{p} \neq \mathbf{R}^{-1}\mathbf{s}_1$ since $\mathbf{p} \neq \mathbf{s}_1$ in multipath channels. $\mathbf{p}$ includes contributions from the correlated parts of the delayed multipath components.

$$= \sum_{m=1}^{N_F}\sum_{n=1}^{N_F}\sum_{l=1}^{K}|A_l|^4 s_{li}s_{lm}^* w_m w_n^* s_{ln}s_{lj}^* + \sum_{m=1}^{N_F}\sum_{n=1}^{N_F}\sigma^4(\delta_{im}w_m w_n^*\delta_{nj} + \delta_{ij}w_m\delta_{mn}w_n^*). \quad (5.46)$$

The information bits of the different users are uncorrelated and this has been used to obtain the first term; the Gaussian moment factoring theorem (cf. Section 5.2.1) has been used to evaluate the second term. Also,

$$\delta_{ij} \stackrel{\triangle}{=} \begin{cases} 1, & i = j, \\ 0, & \text{otherwise.} \end{cases} \quad (5.47)$$

Thus,

$$\mathbf{A} = \sum_{l=1}^{K}|A_l|^4\mathbf{s}_l\mathbf{s}_l^H\mathbf{w}\mathbf{w}^H\mathbf{s}_l\mathbf{s}_l^H + \sigma^4(\mathbf{w}\mathbf{w}^H + \mathbf{w}^H\mathbf{w}\mathbf{I}). \quad (5.48)$$

Defining

$$\kappa_l \stackrel{\triangle}{=} \mathbf{w}^H\mathbf{s}_l \quad (5.49)$$

we get

$$\mathbf{A}\mathbf{w} = \sum_{l=1}^{K}|A_l|^4|\kappa_l|^2\kappa_l^*\mathbf{s}_l + 2\sigma^4\mathbf{w}^H\mathbf{w}\mathbf{w}. \quad (5.50)$$

Furthermore,

$$E[\mathbf{r}\mathbf{r}^H] = \sum_{l=1}^{K}|A_l|^2\mathbf{s}_l\mathbf{s}_l^H + \sigma^2\mathbf{I} \quad (5.51)$$

so that

$$E[\mathbf{r}\mathbf{r}^H\mathbf{w}] = \sum_{l=1}^{K}|A_l|^2\kappa_l^*\mathbf{s}_l + \sigma^2\mathbf{w}. \quad (5.52)$$

Using Equations (5.50) and (5.52) in Equation (5.9), the stationarity condition becomes

$$\sum_{l=1}^{K}|A_l|^2\kappa_l^*(|A_l|^2|\kappa_l|^2 - \delta)\mathbf{P}\mathbf{s}_l + \sigma^2(2\sigma^2\mathbf{w}^H\mathbf{w} - \delta)\mathbf{P}\mathbf{w} = \mathbf{0}. \quad (5.53)$$

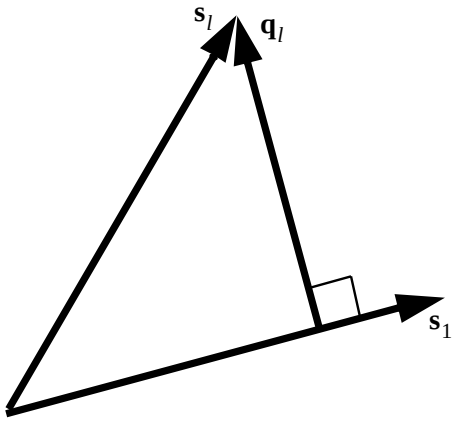

Figure 5.1: $\mathbf{q}_l$ is the The Component of $\mathbf{s}_l$ that is Orthogonal to $\mathbf{s}_1$.

We may note that

$$\begin{aligned}\mathbf{P}\mathbf{s}_1 &= \left(\mathbf{I} - \frac{\mathbf{s}_1\mathbf{s}_1^H}{\mathbf{s}_1^H\mathbf{s}_1}\right)\mathbf{s}_1 \\ &= \mathbf{s}_1 - \frac{\mathbf{s}_1^H\mathbf{s}_1}{\mathbf{s}_1^H\mathbf{s}_1}\mathbf{s}_1 \\ &= \mathbf{0} \end{aligned} \tag{5.54}$$

and for $l \neq 1$

$$\begin{aligned}\mathbf{P}\mathbf{s}_l &= \left(\mathbf{I} - \frac{\mathbf{s}_1\mathbf{s}_1^H}{\mathbf{s}_1^H\mathbf{s}_1}\right)\mathbf{s}_l \\ &= \mathbf{s}_l - \frac{\mathbf{s}_1^H\mathbf{s}_l}{\mathbf{s}_1^H\mathbf{s}_1}\mathbf{s}_1 \stackrel{\triangle}{=} \mathbf{q}_l. \end{aligned} \tag{5.55}$$

It should be noted that the vector $\mathbf{q}_l$ is the component of $\mathbf{s}_l$ that is orthogonal to $\mathbf{s}_1$, as depicted in Figure 5.1. Also,

$$\begin{aligned}\mathbf{P}\mathbf{w} &= \left(\mathbf{I} - \frac{\mathbf{s}_1\mathbf{s}_1^H}{\mathbf{s}_1^H\mathbf{s}_1}\right)\mathbf{w} \\ &= \mathbf{w} - \frac{\mathbf{s}_1}{\mathbf{s}_1^H\mathbf{s}_1} \stackrel{\triangle}{=} \mathbf{u}. \end{aligned} \tag{5.56}$$

It can be seen that $\mathbf{u}$ is the component of $\mathbf{w}$ that is orthogonal to the desired user's spreading code $\mathbf{s}_1$, as seen in Figure 5.2. Equation (5.53) now reduces to

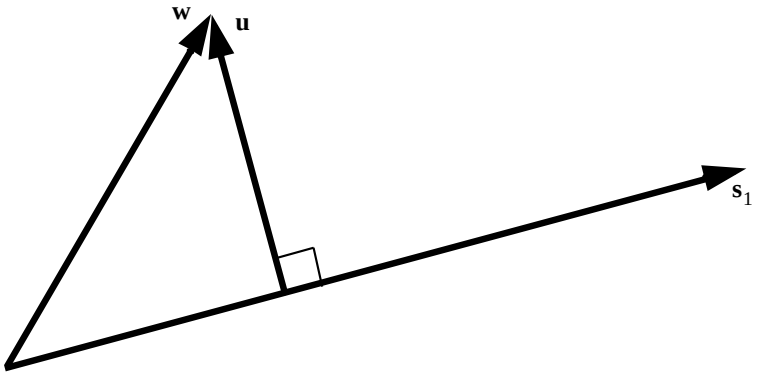

Figure 5.2: $\mathbf{u}$ is the The Component of $\mathbf{w}$ that is Orthogonal to $\mathbf{s}_1$.

$$\sum_{l=2}^{K} |A_l|^2 \kappa_l^* (|A_l|^2 |\kappa_l|^2 - \delta)\mathbf{q}_l + \sigma^2(2\sigma^2 \mathbf{w}^H \mathbf{w} - \delta)\mathbf{u} = \mathbf{0}. \tag{5.57}$$

Equation (5.57) shows that at the stationary point, the sum of the vectors $\mathbf{q}_l$, which are the components of the spreading codes $\mathbf{s}_l$ that are orthogonal to $\mathbf{s}_1$, weighted by functions of the corresponding crosscorrelation factors κ_l, and the vector $\mathbf{u}$, which is the component of the weight vector $\mathbf{w}$ orthogonal to $\mathbf{s}_1$, weighted by a function of the norm of the weight vector, is equal to the null vector.

It is interesting to look at two limiting cases. In the single user case, $K = 1$ and the first term of Equation (5.57) disappears. In this scenario, the stationary point is defined by $\mathbf{u} = \mathbf{0}$ or

$$\mathbf{w}_{\text{opt}} = \frac{\mathbf{s}_1}{\mathbf{s}_1^H \mathbf{s}_1}. \tag{5.58}$$

That is, the optimum weight vector is equal to the matched filter, which is an intuitively satisfying result.

In the second limiting case, we consider the noise to be either absent or negligible, so that the second term in Equation (5.57) vanishes. The optimum weight vector is now such that the weighted versions of $\mathbf{q}_l$ add up to the null vector. Clearly, the condition is satisfied if

$$\kappa_l^* = 0 \quad \forall\, l. \tag{5.59}$$

Writing the above set of equations in matrix form,

$$\begin{bmatrix} \mathbf{s}_2^H \\ \mathbf{s}_3^H \\ \vdots \\ \mathbf{s}_K^H \end{bmatrix} \mathbf{w}_{\text{opt}} = \mathbf{0}. \tag{5.60}$$

Assuming that $K \leq N_F$, if we construct a square matrix $\mathbf{C}$ as follows,

$$\mathbf{C} \stackrel{\triangle}{=} \begin{bmatrix} \mathbf{s}_2^H \\ \mathbf{s}_3^H \\ \vdots \\ \mathbf{s}_K^H \\ \mathbf{0}^H \\ \vdots \\ \mathbf{0}^H \end{bmatrix} \tag{5.61}$$

then the stationarity condition may be restated as

$$\mathbf{C}^H \mathbf{w}_{\text{opt}} = \mathbf{0}. \tag{5.62}$$

Thus the optimum weight vector is the eigenvector associated with one of the zero-eigenvalues of the matrix $\mathbf{C}^H$.

Analysis for Static Multipath Channels

It would be interesting to investigate the nature of the stationary points in multipath channels. Since the primary interest is in determining the impact of the multipath components and not that of the distribution of the envelope, it is assumed that the channel is static. For simplicity of analysis, only one delayed component is considered. The analysis can be extended for an arbitrary number of components to generalize the results. Furthermore, it is assumed that the delay of the multipath component is less than a symbol period in order to make it correlated with the main component within the reception window. Thus the received signal vector is now represented as

$$\mathbf{r} = \sum_{l=1}^{K} A_l b_l \mathbf{s}_l + \sum_{l=1}^{K} \tilde{A}_l (d_l \mathbf{s}_l^0 + b_l \mathbf{s}_l^1) + \mathbf{n} \tag{5.63}$$

where $\tilde{A}_l$ is the amplitude of the multipath component for the lth user, d_l is the previous information bit of the lth user, $\mathbf{s}_l^0$ and $\mathbf{s}_l^1$ are constructed by taking segments of the spreading code $\mathbf{s}_l$ that are modulated by the previous bit and the current bit, respectively,

$$\mathbf{s}_l^0 \triangleq \begin{bmatrix} s_{l(p_l)} \\ s_{l(p_l+1)} \\ \vdots \\ s_{lN_F} \\ 0 \\ \vdots \\ 0 \end{bmatrix} \tag{5.64}$$

and

$$\mathbf{s}_l^1 \triangleq \begin{bmatrix} 0 \\ \vdots \\ 0 \\ s_{l1} \\ s_{l2} \\ \vdots \\ s_{l(p_l-1)} \end{bmatrix} \tag{5.65}$$

where p_l is the delay, in samples, of the multipath component of the lth user. To keep the correlated components together, Equation (5.63) is rewritten in the following form:

$$\mathbf{r} = \sum_{l=1}^{K} A_l b_l \tilde{\mathbf{s}}_l + \sum_{l=1}^{K} \tilde{A}_l d_l \mathbf{s}_l^0 + \mathbf{n} \tag{5.66}$$

where

$$\tilde{\mathbf{s}}_l \triangleq \mathbf{s}_l + \frac{\tilde{A}_l}{A_l} \mathbf{s}_l^1. \tag{5.67}$$

Then it can be easily shown that

$$\begin{aligned} \mathbf{A} \;=\; & \sum_{l=1}^{K} |A_l|^4 \tilde{\mathbf{s}}_l \tilde{\mathbf{s}}_l^H \mathbf{w}\mathbf{w}^H \tilde{\mathbf{s}}_l \tilde{\mathbf{s}}_l^H \\ & + \sum_{l=1}^{K} |\tilde{A}_l|^4 \mathbf{s}_l^0 \mathbf{s}_l^{0H} \mathbf{w}\mathbf{w}^H \mathbf{s}_l^0 \mathbf{s}_l^{0H} + \sigma^4 (\mathbf{w}\mathbf{w}^H + \mathbf{w}^H \mathbf{w} \mathbf{I}) \end{aligned} \tag{5.68}$$

where $\mathbf{A}$ is as defined in Equation (5.11). Defining

$$\alpha_l = \mathbf{w}^H \tilde{\mathbf{s}}_l \tag{5.69}$$
$$\beta_l = \mathbf{w}^H \mathbf{s}_l^0 \tag{5.70}$$

we get

$$\mathbf{A}\mathbf{w} = \sum_{l=1}^{K} |A_l|^4 |\alpha_l|^2 \alpha_l^* \tilde{\mathbf{s}}_l + \sum_{l=1}^{K} |\tilde{A}_l|^4 |\beta_l|^2 \beta_l^* \mathbf{s}_l^0 + 2\sigma^4 \mathbf{w}^H \mathbf{w}\mathbf{w} \tag{5.71}$$

and

$$E[\mathbf{r}\mathbf{r}^H \mathbf{w}] = \sum_{l=1}^{K} |A_l|^2 \alpha_l^* \tilde{\mathbf{s}}_l + \sum_{l=1}^{K} |\tilde{A}_l|^2 \beta_l^* \mathbf{s}_l^0 + \sigma^2 \mathbf{w}. \tag{5.72}$$

This results in the stationarity condition

$$\begin{aligned} \sum_{l=1}^{K} |A_l|^2 \alpha_l^* (|A_l|^2 |\alpha_l|^2 - \delta) \mathbf{P}\tilde{\mathbf{s}}_l &+ \sum_{l=1}^{K} |\tilde{A}_l|^2 \beta_l^* (|\tilde{A}_l|^2 |\beta_l|^2 - \delta) \mathbf{P}\mathbf{s}_l^0 \\ &+ \sigma^2 (2\sigma^2 \mathbf{w}^H \mathbf{w} - \delta) \mathbf{P}\mathbf{w} = \mathbf{0}. \end{aligned} \tag{5.73}$$

We find that

$$\begin{aligned} \mathbf{P}\mathbf{s}_l^0 &= \left(\mathbf{I} - \frac{\mathbf{s}_1 \mathbf{s}_1^H}{\mathbf{s}_1^H \mathbf{s}_1} \right) \mathbf{s}_l^0 \\ &= \mathbf{s}_l - \frac{\mathbf{s}_1^H \mathbf{s}_l^0}{\mathbf{s}_1^H \mathbf{s}_1} \mathbf{s}_1 \triangleq \mathbf{q}_l^0. \end{aligned} \tag{5.74}$$

$\mathbf{q}_l^0$ is that component of the uncorrelated segment of the multipath component that is orthogonal to $\mathbf{s}_1$. Furthermore,

$$\begin{aligned} \mathbf{P}\tilde{\mathbf{s}}_l &= \left(\mathbf{I} - \frac{\mathbf{s}_1 \mathbf{s}_1^H}{\mathbf{s}_1^H \mathbf{s}_1} \right) \left(\mathbf{s}_l + \frac{\tilde{A}_l}{A_l} \mathbf{s}_l^1 \right) \\ &= \left(\mathbf{s}_l - \frac{\mathbf{s}_1^H \mathbf{s}_l}{\mathbf{s}_1^H \mathbf{s}_1} \mathbf{s}_1 \right) + \frac{\tilde{A}_l}{A_l} \left(\mathbf{s}_l^1 - \frac{\mathbf{s}_1^H \mathbf{s}_l^1}{\mathbf{s}_1^H \mathbf{s}_1} \mathbf{s}_1 \right) \triangleq \mathbf{q}_l + \frac{\tilde{A}_l}{A_l} \mathbf{q}_l^1. \end{aligned} \tag{5.75}$$

Here $\mathbf{q}_l^1$ is that component of the correlated segment of the multipath component that is orthogonal to $\mathbf{s}_1$. Finally,

$$\begin{aligned} \mathbf{P}\tilde{\mathbf{s}}_1 &= \left(\mathbf{I} - \frac{\mathbf{s}_1 \mathbf{s}_1^H}{\mathbf{s}_1^H \mathbf{s}_1} \right) \left(\mathbf{s}_1 + \frac{\tilde{A}_1}{A_1} \mathbf{s}_1^1 \right) \\ &= \left(\mathbf{s}_1 - \frac{\mathbf{s}_1^H \mathbf{s}_1}{\mathbf{s}_1^H \mathbf{s}_1} \mathbf{s}_1 \right) + \frac{\tilde{A}_1}{A_1} \left(\mathbf{s}_1^1 - \frac{\mathbf{s}_1^H \mathbf{s}_1^1}{\mathbf{s}_1^H \mathbf{s}_1} \mathbf{s}_1 \right) = \frac{\tilde{A}_1}{A_1} \mathbf{q}_1^1. \end{aligned} \tag{5.76}$$

Using Equations (5.74), (5.75), and (5.76) in Equation (5.73), we find that the stationarity condition reduces to

$$\sum_{l=2}^{K} |A_l|^2 \alpha_l^* (|A_l|^2 |\alpha_l|^2 - \delta)\mathbf{q}_l + \sum_{l=1}^{K} A_l^* \tilde{A}_l \alpha_l^* (|A_l|^2 |\alpha_l|^2 - \delta)\mathbf{q}_l^1 + \sum_{l=1}^{K} |\tilde{A}_l|^2 \beta_l^* (|\tilde{A}_l|^2 |\beta_l|^2 - \delta)\mathbf{q}_l^0 + \sigma^2 (2\sigma^2 \mathbf{w}^H \mathbf{w} - \delta)\mathbf{u} = \mathbf{0} \tag{5.77}$$

where $\mathbf{u}$ is as defined before. From the second term on the left hand side of this equation, we see that at the stationary point, the correlated multipath component of the desired user is treated the same as those of the other users, i.e., as interference. The optimum weight vector, therefore, is such that the multipath component of the desired user is also canceled. It is easy to see how this analysis can be extended for an arbitrary number of multipath components. Thus, due to the linear constraint of Equation (4.91), only the principal component of the desired user is the signal of interest; everything else is interference.

The preceding analysis reinforces the analysis of Section 5.2.1, which yielded the same conclusion. The importance of the Gaussian assumption on the input signal is underlined by these results; the Gaussian assumption is not always completely accurate, but it makes analysis tractable and allows us to obtain very useful results.

5.3 The Multi-Channel Linearly Constrained Constant Modulus Algorithm

Since the linear constraint of Equation (4.91) ensures that the multipath components of the desired user are canceled at the stationary point of the LCCM cost function, the SGD LCCMA attempts to do the same. Also, when operating in a time-varying channel, since the adaptive portion of the weight vector does not operate in the desired-signal subspace, any fading on the signal results in the eye closing. However, in a multipath channel, there is an inherent diversity since the multipath components fade independently. The diversity offered by multipath is exploited in a Rake receiver and also by some adaptive receivers. We now propose the blind MLCCMA receiver that exploits this diversity by extracting individual multipath components and combining them.

Figure 5.3 a GSC structure that may be used to extract two synchronized multipath components and adaptively combine them. There is a constrained weight vector $\mathbf{w}_{qi},\ i = 1, 2$ in each arm of the multi-channel GSC that extracts the signal in that component. The common blocking matrix $\tilde{\mathbf{W}}_s$ "blocks" all the components. This structure is simpler than one that uses a separate blocking matrix for each component. The unconstrained adaptive weight vector $\mathbf{w}_{ai}$ in each channel suppresses the residual interference at the

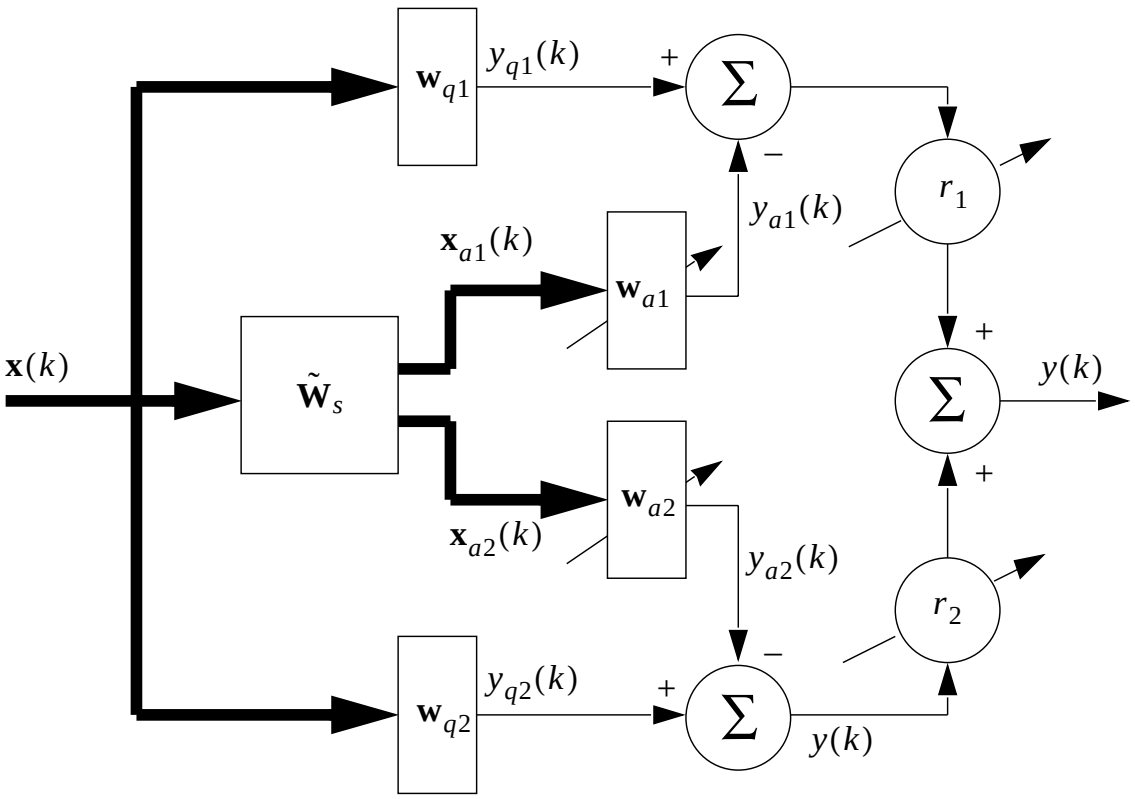

Figure 5.3: GSC Receiver Structure for Extracting and Combining Two Multipath Components.

output of $\mathbf{w}_{qi}$. The adaptive weights r_i appropriately weight the extracted components, which are then combined.

The structure of Figure 5.3 may be equivalently represented as in Figure 5.4, where the weight vectors have been combined into weight matrices. Additionally, differential detection is incorporated into this structure. The GSC structure yields a vector of outputs each derived from a different multipath component. The vector output of the GSC structure is weighted and summed to obtain the demodulated signal,

$$\hat{d}(k) = \mathbf{h}^H(k)\,\mathbf{z}(k) \tag{5.78}$$

where $\mathbf{h}(k)$ is the weight vector and $\mathbf{z}(k)$ is the vector output from the GSC structure obtained by

$$\mathbf{z}(k) = \mathbf{W}^H(k)\,\mathbf{r}(k). \tag{5.79}$$

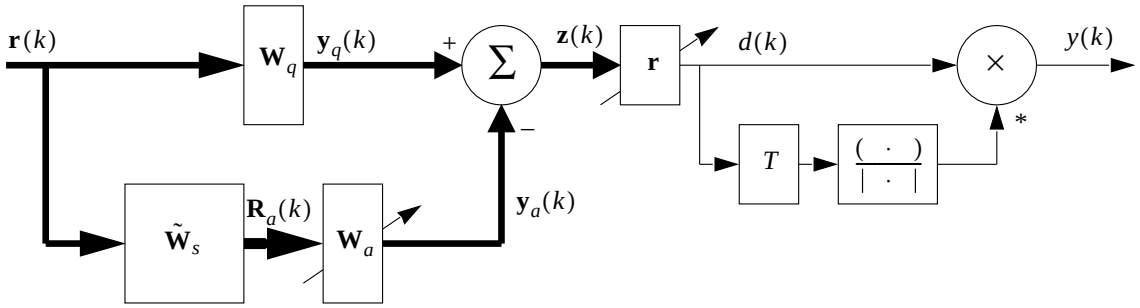

Figure 5.4: The Proposed Multi-Channel Receiver Structure.

Differential encoding and decoding is used to combat phase ambiguity created by the CMA and the channel. The differentially detected signal is

$$y(k) = \hat{d}(k)\,\frac{\hat{d}^*(k-1)}{|\hat{d}(k-1)|}. \tag{5.80}$$

The weight matrix $\mathbf{W}$ is decomposed as

$$\mathbf{W} = \mathbf{W}_q - \tilde{\mathbf{W}}_s\,\mathbf{W}_a. \tag{5.81}$$

Equation (5.81) is similar to Equation (4.92) for the LCCMA with the exception that the weight *matrices* $\mathbf{W}$, $\mathbf{W}_q$ and $\mathbf{W}_a$ contain multiple columns, the number of which is equal to L, the number of multipath components being combined. The constraint equation here is

$$\mathbf{C}^H\,\mathbf{W} = \mathbf{I} \tag{5.82}$$

where $\mathbf{I}$ is the identity matrix of dimension L and $\mathbf{C}$ is the constraint matrix which is of the form

$$\mathbf{C} = [\ \mathbf{s}_{11}\ \ \cdots\ \ \mathbf{s}_{1L}\ ]. \tag{5.83}$$

The ith column $\mathbf{s}_{1i}$ consists of the sampled spreading code coefficients of the desired user preceded by zeros whose number is equal to the delay (in number of samples) of the ith multipath component. Zeros fill any remaining rows in the column.

The constrained weight matrix $\mathbf{W}_q$ is again obtained using

$$\mathbf{W}_q = \mathbf{C}\,(\mathbf{C}^H\mathbf{C})^{-1}, \tag{5.84}$$

and the blocking matrix $\tilde{\mathbf{W}}_s$ spans the left null space of $\mathbf{C}$.

The weight matrix $\mathbf{W}_a$ is adapted to minimize the CM error criterion of (4.90). An important modification is that the error after differential detection is minimized (cf. Chapter 8). This results in the update equation

$$\mathbf{W}_a(k+1) = \mathbf{W}_a(k) + \mu_1 \left(|y(k)|^2 - \delta\right) y^*(k) \frac{\hat{d}^*(k-1)}{|\hat{d}(k-1)|} \mathbf{R}_a(k)\, \mathbf{h}^H(k) \tag{5.85}$$

where $\mathbf{R}_a(k) = \tilde{\mathbf{W}}_s\, \mathbf{r}(k)$ and μ_1 is the step-size.

The weight vector $\mathbf{h}$ is adapted to minimize the error criterion

$$J_{\mathbf{h}} = \frac{1}{4} E[(|\Re\{y\}|^2 - \delta)^2], \tag{5.86}$$

where $\Re\{\cdot\}$ denotes extraction of the real part. Since fading channels impart a random phase shift in the signal and the complex version of the CMA is insensitive to phase, a moving constellation results. In spite of differential encoding and decoding, this phase drift diminishes the performance. However, projecting the real part of the output onto a constant modulus enables the imaginary part to be ignored in the decision process, yielding improved performance. The resulting update equation is

$$\mathbf{h}(k+1) = \mathbf{h}(k) - \mu_2 \left(|\Re\{y(k)\}|^2 - \delta\right) y^*(k) \frac{\hat{d}^*(k-1)}{|\hat{d}(k-1)|} \mathbf{z}(k). \tag{5.87}$$

μ_2 is the step-size and is not necessarily equal to μ_1. In fact μ_2 is made large enough for tracking the time-varying channel, whereas μ_1 is set to a smaller value so that the weights $\mathbf{W}_a$ change more slowly than the weights $\mathbf{r}$.

Due to the nonlinear nature of Equations (5.85) and (5.87), and interdependence of $\mathbf{W}_a$ and $\mathbf{r}$, a convergence analysis of the algorithms is difficult to perform. However, no problems with convergence were encountered in simulations when μ_1 was set smaller than μ_2.

5.4 The System Model

Since the forward link is being considered, the signals of all the users transmitted by the base station are bit and chip synchronous. Furthermore, all the signals pass through the same channel. Although this is the model used in this work, all discussion pertaining to algorithms are applicable to asynchronous reverse links as well. Near-far situations arise

on the reverse link, but LCCMA has been shown to be near-far resistant [80] and it is reasonable to assume that the MLCCMA is also near-far resistant.

COP binary modulation is assumed. The sampled received signal $r(k)$ at the kth instant is modeled by

$$r(k) = \sum_{j=1}^{L} A_j(k) \sum_{i=1}^{K} d_i(k - m_j)\, s_i(k - m_j) + n(k) \tag{5.88}$$

where $A_j(k)$ is the amplitude of the jth multipath component at the kth sampling instant, $d_i(k)$ is the modulating bit of the ith user, $s_i(k)$ is the sampled spreading code of the ith user at the kth sampling instant, m_j is the delay in samples of the jth multipath component, $n(k)$ is the sampled noise, L is the number of multipath components, and K is the number of users. The length N_F of the received signal vector $\mathbf{x}(k)$ is large enough to completely accommodate the last multipath component of interest.

5.5 Simulation Results

The data is encoded before spreading at the transmitter and the demodulated data is decoded as shown in Figure 5.4. A two-ray Rayleigh fading channel is chosen as an example. Furthermore, perfect synchronization with the multipath components is assumed (synchronization is a requirement for a Rake receiver as well). In other words, the delays are assumed to be known. The channel impulse response is

$$h_l = \delta_l + 0.5\, \delta_{l+29}\, e^{-j2\pi f_c 29} \tag{5.89}$$

where f_c is the normalized carrier frequency. The 29-sample delay of the multipath component corresponds to 5 μs at the above sample rate, a typical value for an urban channel. The two components are independently faded. The bit rate is 128 kb/s and the processing gain is 15, resulting in a chip rate of 1.92 Mc/s. The signal is sampled at 5.76 Msamples/s (3 samples/chip).

The carrier frequency is 2.05 GHz. The mobile is assumed to be traveling at a speed of 45 km/h, resulting in a maximum Doppler of about 85 Hz. The E_b/N_0 is 23 dB. The spreading gain is 15. Spreading codes were generated using two m-sequences in a manner similar to the generation of Gold codes, and these codes were found to have Gold-like properties. The Rake receiver and the MLCCMA receiver make use of both multipath components. Maximal ratio combining was used for the Rake receiver.

Figure 5.5 shows the BER simulation results for the matched filter (MF) receiver, the LCCMA receiver, and the decision-directed NLMS (DD-NLMS) algorithm with a CLFSR.

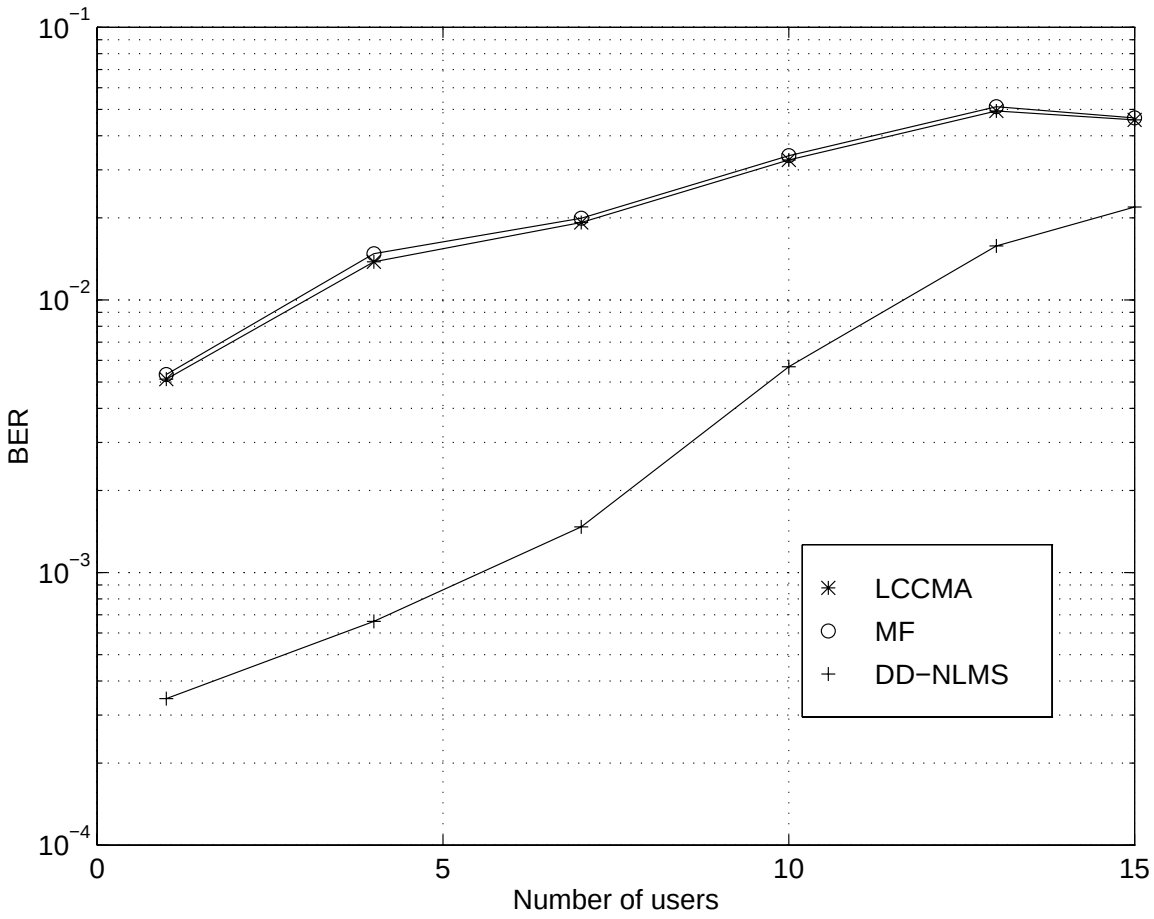

Figure 5.5: Performance of the LCCMA in a Two-Ray Rayleigh Channel.

The MF receiver performance is extremely poor with the BER remaining above 10^{-2} for four or more users. The CLFSR adapted by the DD-NLMS exhibits a superior performance, but it should be noted that some of the simulation points were obtained after repeated trials since the algorithm failed catastrophically many times, often when the signal went into deep fades. For the LCCMA, a small step size (0.005) was used since it was found that larger step sizes resulted in more errors. LCCMA performs only slightly better than the MF but is still highly inferior to DD-NLMS because LCCMA does not combine multipath and fading of the main component results in the eye closing.

The plots of BER versus number of users for the Rake, the MLCCMA receiver, and the DD-NLMS receivers are illustrated in Figure 5.6. While the Rake receiver is better than the MF receiver, it is still limited by the MAI due to its inability to cancel interference. The MLCCMA outdoes DD-NLMS by a small margin in performance at higher levels of interference and is consistently better than the Rake receiver except in the first two simulation points. In these cases, a small step-size would allow the adaptive receivers to approach the performance of the Rake receiver but would diminish the performance for higher numbers of users. Furthermore, the first two simulation points are indicative of the greater effectiveness of the Rake receiver in combining multipath energy at low levels of interference. If the acceptable BER is 10^{-2}, then about four users can be supported with the MF receiver and the LCCMA receiver with an E_b/N_0 of 23 dB. About eight users can be supported with the Rake receiver. However, twelve to thirteen users can be supported with the DD-NLMS receiver and the MLCCMA receiver. Thus the MLCCMA yields a significant capacity increase over the conventional receivers and matches the performance of the DD-NLMS receiver. DD-NLMS is known to combine multipath. The MLCCMA algorithm does this explicitly and, hence, is able to match DD-NLMS. Furthermore, the algorithm converged in all cases in which it was tested. It was observed that when all the multipath components went into simultaneous deep fades, the eye of the output sometimes closed temporarily but re-opened when the signal came out of the fade. The algorithm then continued to track the signal.

Figure 5.7 shows the outputs $z_1(k)$ and $z_2(k)$, the elements of the estimated vector $\mathbf{z}(k)$ defined in Equation(5.79), and the estimated data signal $y(k)$. It is observed that although the amplitudes of the individual components extracted are not constant, they are combined to obtain a constant modulus output. Thus, temporal diversity is exploited to maintain an open eye.

In the second example, a three-ray multipath channel is used. The first two components undergo Rayleigh fading, and the third component has a Gaussian Doppler spectrum, which is typical for an urban channel [97]. The delays of the multipath components are 0.6 μs and 1.6 μs. The channel impulse response is

$$h_l = \delta_l + 0.79\,\delta_{l+3}\,e^{-j2\pi f_c 3} + 0.5\,\delta_{l+9}\,e^{-j2\pi f_c 9}. \tag{5.90}$$

The other simulation parameters are the same.

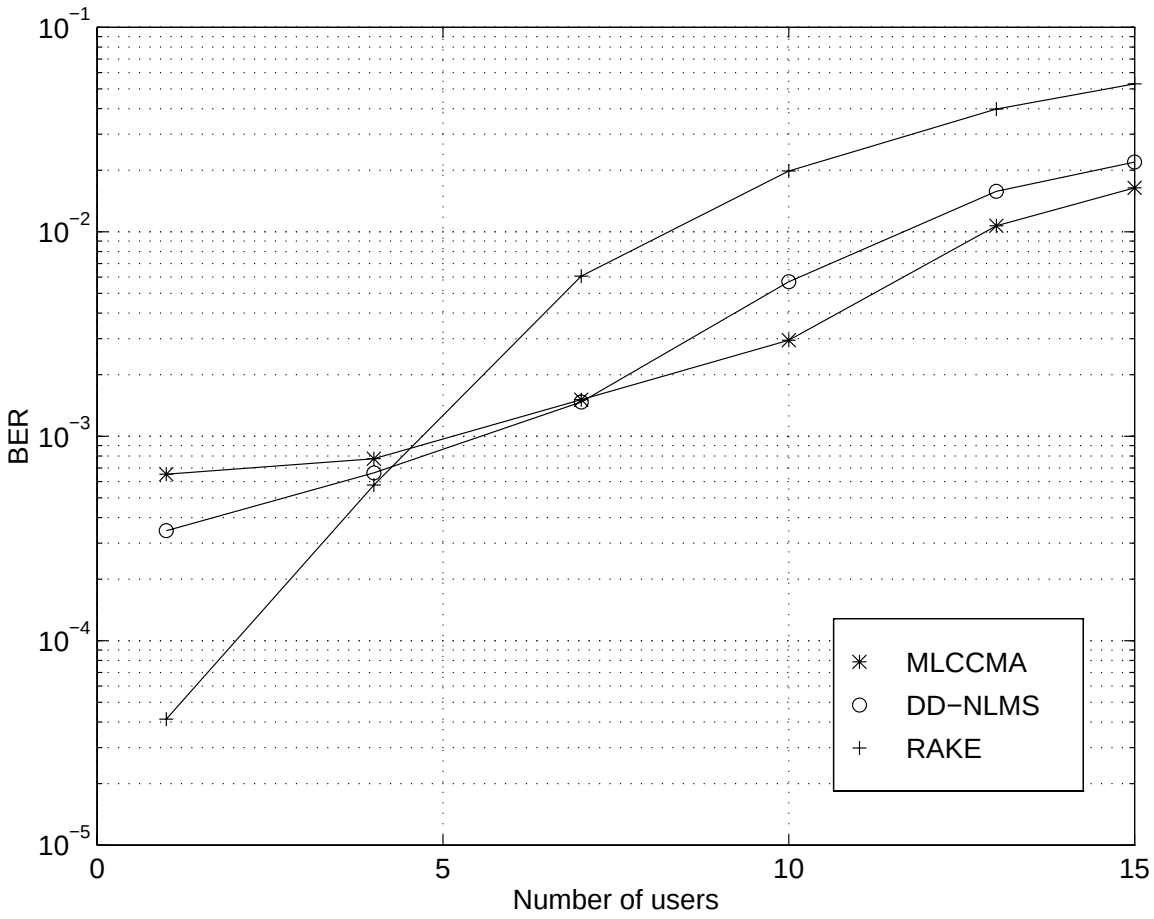

Figure 5.6: Performance of the MLCCMA in a Two-Ray Rayleigh Channel.

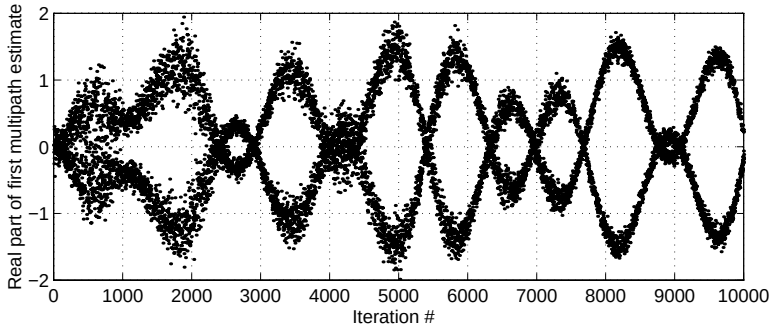

(a)

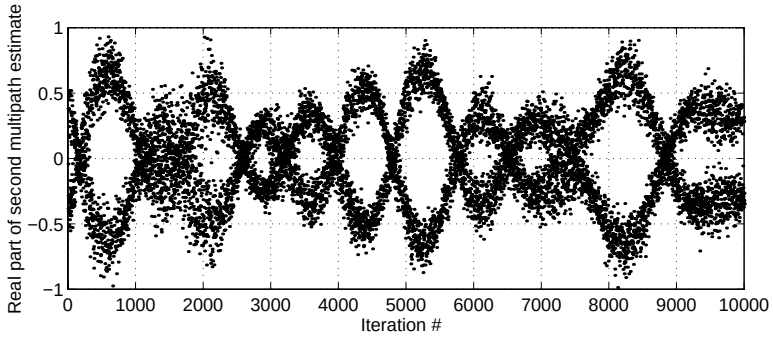

(b)

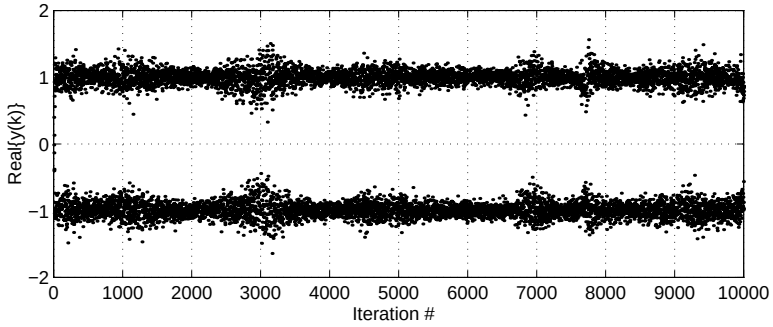

(c)

Figure 5.7: Combining of Multipath Components: (a) real part of the first multipath estimate (first element of $\mathbf{z}(k)$ (b) real part of the second multipath estimate (second element of $\mathbf{z}(k)$ (c) real part of combined estimate y(k).

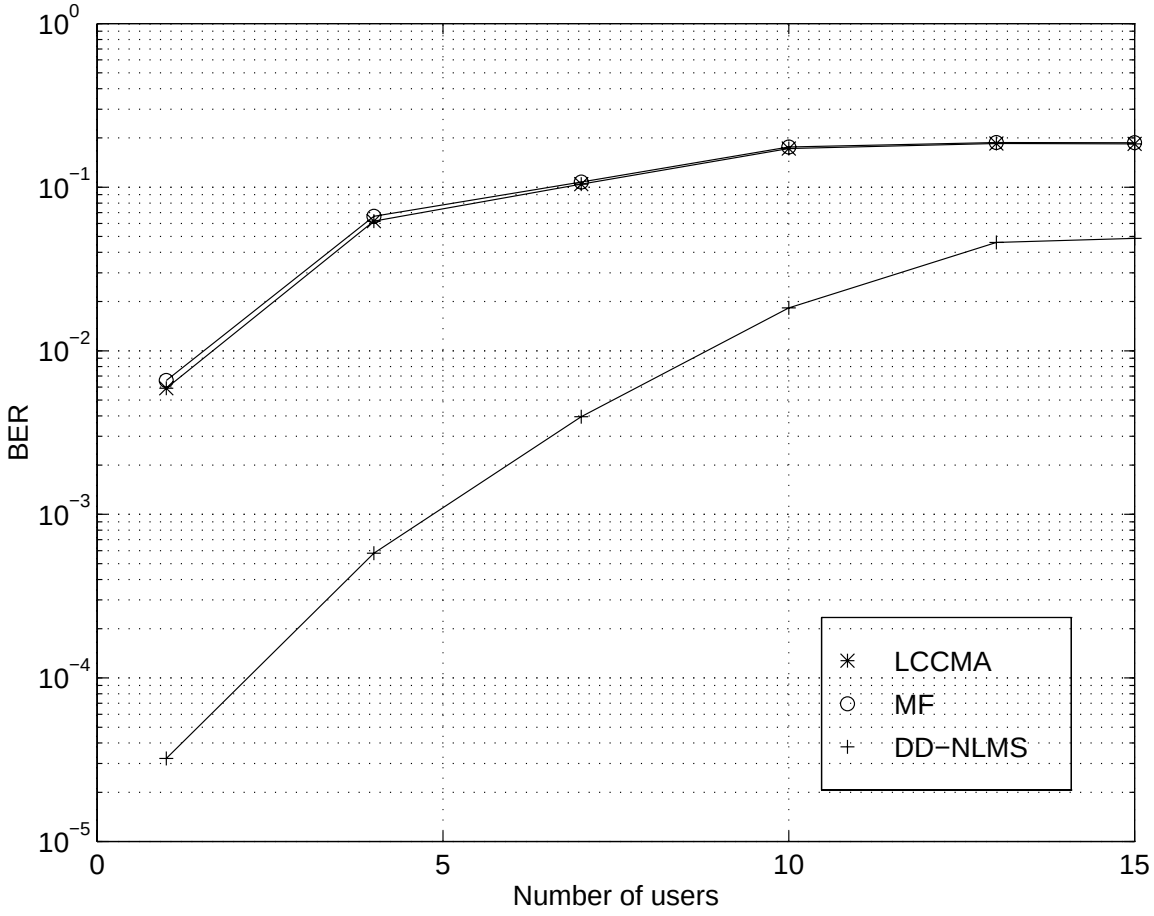

Figure 5.8: Performance of LCCMA in a Three-Ray Multipath Channel.

Figure 5.8 compares the performances of the MF receiver, the LCCMA receiver and the DD-NLMS receiver. At a BER of 10^{-2}, the MF and the LCCMA receivers can support only a single user, but the DD-NLMS receiver is able to support about nine users.

The BER results for the Rake and the MLCCMA receivers are shown in Figure 5.9. The Rake receiver is able to support about five users. The DD-NLMS and the MLCCMA receivers support about eight users. Again the MLCCMA is seen to match the performance of the DD-NLMS, and both adaptive receivers offer an improved capacity over the Rake receiver. For a lower number of users, the performances of the adaptive receivers in the three-ray channel are better than in the two-ray channel due to the increased temporal diversity. However, for higher levels of interference, the dominant effect of the multipath interference of the more hostile channel results in an degraded performance compared to the two-ray channel. Despite gradient noise effects degrading the performance of the adaptive receivers, they do not perform much worse than the Rake receiver in the single

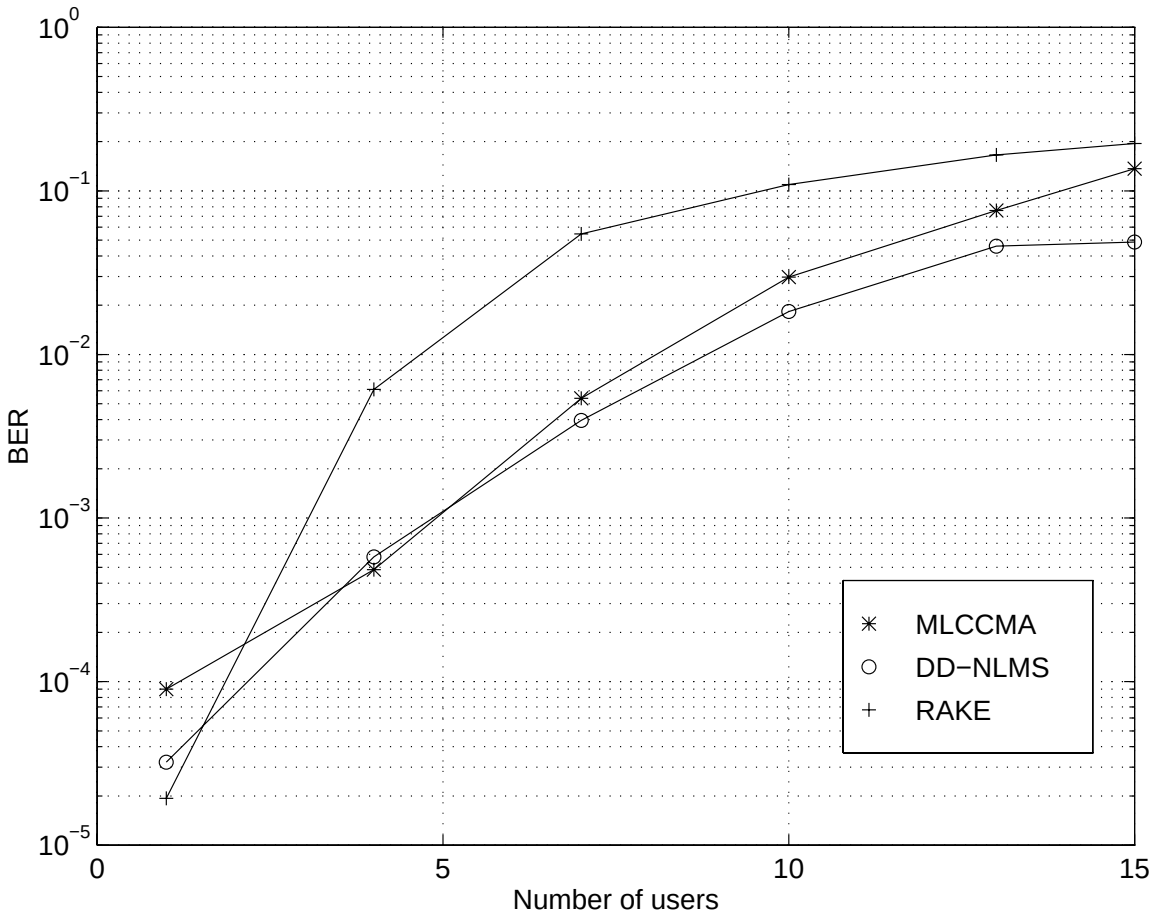

Figure 5.9: Performance of the MLCCMA in a Three-Ray Multipath Channel.

user case, which is affected by the more significant interference due to multipath in this channel.

5.6 Summary

Rake receivers exploit multipath, but their performance is limited by multiple access interference. Multi-stage Rake receivers are too complex for a mobile unit. Adaptive receivers that employ the least mean-square algorithm require the transmission of a training sequence, which may not be feasible, and the blind decision-directed algorithm is susceptible to deep fades. Therefore an improved blind algorithm is desirable. The stationary points of the linearly constrained constant modulus cost function were investigated. Using the Gaussian assumption for the input signal, it was shown that the minimum mean-squared error solution for additive white Gaussian noise channels, which does not exploit the correlated nature of multipath, is a minimum of this cost function and hence the adaptation algorithm will converge to it. Without the Gaussian assumption, it was shown that at the stationary points, the multipath components of the desired user's signal are treated as interference. Thus the adaptation algorithm, due to its linear constraint, attempts to suppress multipath energy rather than exploit it. The multi-channel linearly constrained constant modulus algorithm for multipath channels with known characteristics was proposed. This algorithm exploits the temporal diversity in multipath channels, and its performance approaches that of the decision-directed algorithm after training. An important advantage of the multi-channel linearly constrained constant modulus algorithm over the decision-directed algorithm is that deep fades on the signal do not result in the failure of the tracking process of the algorithm. No problems with the convergence of the algorithm were observed.

Chapter 6

Minimum Mean-Squared Error Analysis of the Optimum Receiver

6.1 Introduction

Wiener filter theory is a mature subject, extensively studied by scholars in many diverse fields. Many applications for employing Wiener filters exist, but the basic elements remain the same. The concept of the MMSE cost function and the optimal solution that minimizes this cost function were briefly addressed in Chapter 4. Greater insight into the theory may be obtained by reading the vast body of literature available. Haykin [38] and Widrow and Stearns [39] are good sources with which to begin.

As Chapters 2 and 4 indicated, the use of MMSE receivers for CDMA interference mitigation has been investigated for several years now. Focus on theoretical analysis, however, is a feature of recent years. Some key results on the MMSE receiver are provided by Madhow and Honig [46], where the authors discuss the MMSE in terms of code cross-correlations. However, the purpose of this work is to follow a new approach to clearly establish the dependence of the MMSE on three independent parameters: code crosscorrelations, interference-to-signal power ratios, and the SNR. With this relationship established, it is easy to study the impact of any individual parameter (or set of parameters) on the MMSE. This approach is first used to derive the MMSE in AWGN channels and then to extend the result to static multipath channels. The "gain" yielded by multipath is evaluated and it is thereby proven that the MMSE receiver exploits multipath. Thus, the object of this work is to provide greater insight into the dependence of the MMSE on the three aforementioned channel parameters and multipath characteristics. Some assumptions are made to simplify the expression for the MMSE. The simplified expression is used to demonstrate the near-far resilience of the MMSE receiver. A similar analysis is performed on the matched filter receiver to show that it is not near-far resistant.

6.2 Model of the CDMA System

The CDMA system is assumed to consist of K users. The intent is to analyze a generic system, so no assumption is made on the synchronism of the signals from the different users. Thus an asynchronous channel is considered. Moreover, no form of power control is assumed, so that the signals can have widely varying powers. In this chapter, all the users are assumed to have the same symbol rate, and the signals are assumed to be COP. No pulse shaping is assumed. The received signal $r(t)$ at the input of the receiver is modeled by the following equation:

$$r(t) = \sum_{k=1}^{K} a_k(t)\, d_k(t-\tau_k)\, c_k(t-\tau_k) \cos(\omega_c(t-\tau_k) + \phi_k) + n(t) \tag{6.1}$$

where

$a_k(t)$ = amplitude of the kth user,
$d_k(t)$ = data signal of kth user,
$c_k(t)$ = spreading signal of kth user,
ω_c = carrier frequency,
τ_k = time delay of kth user's signal, uniformly distributed over $[0, T_d)$,
ϕ_k = phase of kth user's signal, uniformly distributed over $[0, 2\pi)$,
$n(t)$ = AWGN.

At the receiver, the signal is downconverted to baseband. Perfect knowledge of the carrier frequency is assumed. Following the downconversion, the signal is digitized. The sampling frequency is assumed to be higher than the Nyquist frequency. Thus the signal is sampled at least two times per chip. A vector of signal samples is collected for processing with the adaptive receiver. This vector of N samples is assumed to span one symbol period. The sampled received signal vector at time instant n may be represented as

$$\mathbf{r}(n) = \sum_{k=1}^{K} a_k(n)\mathbf{s}_k(n)\, e^{j\psi_k} + \boldsymbol{\nu}(n) \tag{6.2}$$

where

$$a_k(n) = a_k^c(n) + j\, a_k^s(n) \tag{6.3}$$

is the amplitude of the kth user and is assumed to remain constant during the symbol period, $a_k^c(n)$ and $a_k^s(n)$ are Gaussian random variables, $\mathbf{s}_k(n)$ is the kth user's signal vector,

$$\psi_k = \phi_k - \omega_c \tau_k \tag{6.4}$$

is the phase of kth user's signal, uniformly distributed over $[0, 2\pi)$, and $\boldsymbol{\nu}(n)$ is the AWGN vector whose samples are zero-mean random variables with a variance σ_ν^2.

If $\mathbf{c}_k$ is the sampled spreading code of the kth user, it can be represented as

$$\mathbf{c}_k \triangleq \begin{bmatrix} c_{k,1} \\ c_{k,2} \\ \vdots \\ c_{k,N} \end{bmatrix}. \tag{6.5}$$

Without loss of generality, we assume that the first user is the desired user. We further assume that the receiver is perfectly synchronized to the desired user's spreading code. If $d_k(n)$ is the kth user's data bit, then

$$\mathbf{s}_1(n) = d_1(n)\,\mathbf{c}_1. \tag{6.6}$$

Also, the asynchronous interference signal vectors may be represented as equivalent synchronous interference vectors by

$$\mathbf{s}_k(n) \triangleq b_k(n)\,\tilde{\mathbf{c}}_k, \tag{6.7}$$

$$\tilde{\mathbf{c}}_k = \begin{cases} \mathbf{c}_k^{(1)} & \text{if } d_k(n) = d_k(n-1) \\ \mathbf{c}_k^{(2)} & \text{if } d_k(n) = -d_k(n-1) \end{cases}, \tag{6.8}$$

$$b_k(n) = d_k(n) \tag{6.9}$$

where

$$\mathbf{c}_k^{(1)} \triangleq \begin{bmatrix} c_{k,N-m_k+1} \\ c_{k,N-m_k+2} \\ c_{k,N} \\ c_{k,1} \\ \vdots \\ c_{k,N-m_k} \end{bmatrix}, \tag{6.10a}$$

$$\mathbf{c}_k^{(2)} \triangleq \begin{bmatrix} -c_{k,N-m_k+1} \\ -c_{k,N-m_k+2} \\ -c_{k,N} \\ c_{k,1} \\ \vdots \\ c_{k,N-m_k} \end{bmatrix}, \tag{6.10b}$$

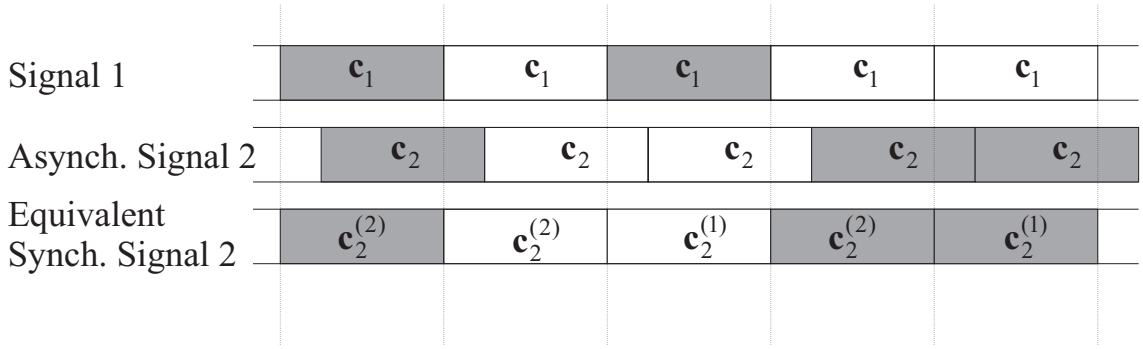

Figure 6.1: Equivalent Synchronous Representation of Asynchronous Signals.

and m_k is the time delay in samples of the kth user's signal, uniformly distributed over $[0, N-1]$. It should be noted that

$$\tilde{\mathbf{c}}_1 = \mathbf{c}_1 \tag{6.11}$$

$$b_1(n) = d_1(n). \tag{6.12}$$

Figure 6.1 illustrates how an asynchronous signal may be represented by an equivalent synchronous signal.

Assuming that the signal powers are not time varying, i.e., $a_k(n)$ is not a random variable, if P_k is the received power for the kth user's signal, the received signal vector can be represented by

$$\mathbf{r}(n) = \sum_{k=1}^{K} \sqrt{\frac{P_k}{2}}\, b_k(n)\, e^{j\psi_k}\, \tilde{\mathbf{c}}_k + \boldsymbol{\nu}(n). \tag{6.13}$$

6.3 Computation of the Correlation Matrix

The correlation matrix of the input signal vector is given by

$$\begin{aligned}
\mathbf{R} &\triangleq E\left[\mathbf{r}(n)\mathbf{r}^H(n)\right] \\
&= E\left[\left(\sum_{k=1}^{K} \sqrt{\frac{P_k}{2}}\, b_k(n)\, e^{j\psi_k}\, \tilde{\mathbf{c}}_k + \boldsymbol{\nu}(n)\right)\right. \\
&\qquad \left.\cdot \left(\sum_{k=1}^{K} \sqrt{\frac{P_k}{2}}\, b_k(n)\, e^{-j\psi_k}\, \tilde{\mathbf{c}}_k^H + \boldsymbol{\nu}^H(n)\right)\right]
\end{aligned}$$

$$
\begin{aligned}
= \; & E\left[\sum_{k=1}^{K} \frac{P_k}{2} \left(b_k(n)\right)^2 \tilde{\mathbf{c}}_k \, \tilde{\mathbf{c}}_k^H\right] \\
& + E\left[\boldsymbol{\nu}(n)\boldsymbol{\nu}^H(n)\right] \\
& + E\left[\sum_{i=1}^{K}\sum_{j=1}^{K} \sqrt{\frac{P_i P_j}{4}} \, b_i(n) \, b_j(n) \, e^{j(\psi_i - \psi_j)} \, \tilde{\mathbf{c}}_i \, \tilde{\mathbf{c}}_j^H\right] \\
& + E\left[\sum_{k=1}^{K} \sqrt{\frac{P_k}{2}} \, b_k(n) \, e^{j\psi_k} \, \tilde{\mathbf{c}}_k \, \boldsymbol{\nu}^H(n)\right] \\
& + E\left[\sum_{k=1}^{K} \sqrt{\frac{P_k}{2}} \, b_k(n) \, e^{-j\psi_k} \, \boldsymbol{\nu}(n) \, \tilde{\mathbf{c}}_k^H\right]. \qquad (6.14)
\end{aligned}
$$

Noting that the symbols $b_k(n)$ of the different users are uncorrelated with each other, and the symbols $b_k(n)$ are uncorrelated with the noise vector $\boldsymbol{\nu}(n)$, the last three terms vanish. We note that

$$E\left[\boldsymbol{\nu}(n)\boldsymbol{\nu}^H(n)\right] = \sigma_\nu^2 \, \mathbf{I}_N \qquad (6.15)$$

where $\mathbf{I}_N$ is the order-N identity matrix. Furthermore, for the interference signals, it can be verified that

$$\mathbf{R}_k \stackrel{\triangle}{=} E[\tilde{\mathbf{c}}_k \, \tilde{\mathbf{c}}_k^H] = \frac{1}{2}\mathbf{c}_k^{(1)} \, \mathbf{c}_k^{(1)^H} + \frac{1}{2}\mathbf{c}_k^{(2)} \, \mathbf{c}_k^{(2)^H}. \qquad (6.16)$$

Equation (6.16) can be interpreted as the contribution of the two spreading codes $\mathbf{c}_k^{(1)}$ and $\mathbf{c}_k^{(2)}$, each of which appears in the signal half the time on average or each of which has half the total power for that user. Thus, each *asynchronous* interference signal (with spreading code $\mathbf{c}_k$) arriving at the receiver is perceived by the receiver as two interference signals (with different spreading codes $\mathbf{c}_k^{(1)}$ and $\mathbf{c}_k^{(2)}$), each with half of the power of the original interference signal. Therefore, the receiver perceives the number of interference signals to be[1] $2K - 2$. Equation (6.14) now reduces to

$$
\begin{aligned}
\mathbf{R} \; & = \; \sum_{k=1}^{K} \frac{P_k}{2} \, \mathbf{R}_k + \sigma_\nu^2 \, \mathbf{I}_N \\
& = \; \frac{P_1}{2} \, \tilde{\mathbf{c}}_1 \, \tilde{\mathbf{c}}_1^H + \sum_{k=2}^{K} \frac{P_k}{4} \left[\mathbf{c}_k^{(1)} \, \mathbf{c}_k^{(1)^H} + \mathbf{c}_k^{(2)} \, \mathbf{c}_k^{(2)^H}\right] + \sigma_\nu^2 \, \mathbf{I}_N \\
& = \; \sum_{k=1}^{2K-1} \sigma_k^2 \hat{\mathbf{c}}_k \, \hat{\mathbf{c}}_k^H + \sigma_\nu^2 \, \mathbf{I}_N \qquad (6.17)
\end{aligned}
$$

[1]It is assumed here that the delays of the signals are, in general, different. It is easy to see that depending on how many delays are equal, the number of interference signals perceived by the receiver can vary from $K - 1$ to $2(K - 1) = 2K - 2$.

where

$$\hat{\mathbf{c}}_k = \begin{cases} \tilde{\mathbf{c}}_1, & k = 1, \\ \mathbf{c}_k^{(1)}, & k = 2, \ldots, K, \\ \mathbf{c}_{k-K+1}^{(2)}, & k = K+1, \ldots, 2K-1 \end{cases} \tag{6.18}$$

is the effective code seen by the receiver, and

$$\sigma_k^2 = \begin{cases} \dfrac{P_1}{2}, & k = 1, \\ \dfrac{P_k}{4}, & k = 2, \ldots, K, \\ \dfrac{P_{k-K+1}}{4}, & k = K+1, \ldots, 2K-1. \end{cases} \tag{6.19}$$

If two signals have identical spreading codes (and delays), the $\mathbf{R}_k$ term is the same for both signals. The two terms have different coefficients for $\mathbf{R}_k$, however, in the summation of Equation (6.17). The cumulative effect of the two terms results in a coefficient of $\mathbf{R}_k$ now being the sum of the two coefficients. In other words, the σ_k^2 for the two signals add up.

We now introduce the diagonal matrix $\hat{\mathbf{C}}_k$, whose diagonal elements are the elements of the vector $\hat{\mathbf{c}}_k$, and the square matrix $\mathbf{E}_N$ of order N, which has all elements equal to unity. Then Equation (6.17) may be rewritten as[2]

$$\mathbf{R} = \sum_{k=1}^{2K-1} \sigma_k^2 \hat{\mathbf{C}}_k \, \mathbf{E}_N \, \hat{\mathbf{C}}_k^H + \sigma_\nu^2 \, \mathbf{I}_N \tag{6.20}$$

$$= \mathbf{C} \, \mathbf{D} \, \mathbf{C}^H + \sigma_\nu^2 \, \mathbf{I}_N \tag{6.21}$$

where

$$\mathbf{C} \triangleq \begin{bmatrix} \hat{\mathbf{C}}_1 & \hat{\mathbf{C}}_2 & \ldots & \hat{\mathbf{C}}_{K_1} \end{bmatrix}, \tag{6.22}$$

$$\mathbf{D} \triangleq \sigma_1^2 \begin{bmatrix} \mathbf{E}_N & \mathbf{0}_N & \ldots & \ldots & \mathbf{0}_N \\ \mathbf{0}_N & \dfrac{\sigma_2^2}{\sigma_1^2}\mathbf{E}_N & \mathbf{0}_N & \ldots & \vdots \\ \vdots & \mathbf{0}_N & \ddots & \ddots & \vdots \\ \vdots & \vdots & \ddots & \ddots & \mathbf{0}_N \\ \mathbf{0}_N & \ldots & \ldots & \mathbf{0}_N & \dfrac{\sigma_{K_1}^2}{\sigma_1^2}\mathbf{E}_N \end{bmatrix}, \tag{6.23}$$

[2]The assistance of Mark von Tress, who responded to the author's queries on Usenet newsgroups, in formulating the correlation matrix as in Equation (6.21) is gratefully acknowledged.

with $\mathbf{0}_N$ being the square null matrix of order N and

$$K_1 \triangleq 2K - 1. \tag{6.24}$$

It may be noted that $\mathbf{C}$ is an $N \times K_1 N$ matrix and $\mathbf{D}$ is a $K_1 N \times K_1 N$ matrix. Furthermore, the rank of $\mathbf{D}$ is K_1. Consider the eigenvalue decomposition of $\mathbf{D}$:

$$\mathbf{D} = \mathbf{U}\,\mathbf{S}\,\mathbf{U}^{-1} \tag{6.25}$$

where $\mathbf{S}$ is the diagonal matrix whose diagonal elements are the eigenvalues of $\mathbf{D}$ and $\mathbf{U}$ is the modal matrix, whose columns are the eigenvectors of $\mathbf{D}$. Since $\mathbf{D}$ is a real matrix, it is also a normal matrix ($\mathbf{D}\,\mathbf{D}^H = \mathbf{D}^H\,\mathbf{D}$), and its eigenvectors are orthogonal. Therefore,

$$\mathbf{U}^H\,\mathbf{U} = \mathbf{I} \tag{6.26}$$

and hence

$$\mathbf{U}^{-1} = \mathbf{U}^H. \tag{6.27}$$

Using this result in Equation (6.24), we get

$$\mathbf{D} = \mathbf{U}\,\mathbf{S}\,\mathbf{U}^H. \tag{6.28}$$

Since the rank of $\mathbf{D}$ is K_1, it has only K_1 nonzero eigenvalues, and $\mathbf{S}$ is of the form

$$\mathbf{S} = \begin{bmatrix} \lambda_1 & 0 & \dots & & & & \\ 0 & \lambda_2 & 0 & \dots & & & \\ \vdots & 0 & \ddots & \ddots & & & \\ & \vdots & \ddots & \lambda_{K_1} & & & \\ & & & & 0 & & \\ & & & & & \ddots & \\ & & & & & & 0 \end{bmatrix} \tag{6.29}$$

where

$$\lambda_k = \sigma_k^2 N, \qquad k = 1, 2, \dots, K_1, \tag{6.30}$$

and it is assumed that $K_1 < N$. A dimension reduction of Equation (6.28) yields

$$\mathbf{D} = N\sigma_1^2\,\mathbf{T}\,\mathbf{L}\,\mathbf{T}^H, \tag{6.31}$$

where we now define

$$\mathbf{L} \triangleq \begin{bmatrix} \tilde{\lambda}_1 & 0 & \dots & \\ 0 & \tilde{\lambda}_2 & 0 & \dots \\ \vdots & 0 & \ddots & \ddots \\ & \vdots & \ddots & \tilde{\lambda}_{K_1} \end{bmatrix}, \tag{6.32}$$

$$\tilde{\lambda}_k \triangleq \frac{\sigma_k^2}{\sigma_1^2} \qquad k = 1, 2, \dots, K_1, \tag{6.33}$$

and

$$\mathbf{T} \triangleq \begin{bmatrix} \mathbf{u}_1 & \mathbf{u}_2 & \dots & \mathbf{u}_{K_1} \end{bmatrix} \tag{6.34}$$

where $\mathbf{u}_k$ ($k = 1, 2, \dots, K_1$) are the unit-norm eigenvectors associated with the eigenvalues λ_i. Using Equation (6.31) in Equation (6.21), we get

$$\begin{aligned} \mathbf{R} &= \sigma_\nu^2 \mathbf{I}_N + N\sigma_1^2 \mathbf{C}\,\mathbf{T}\,\mathbf{L}\,\mathbf{T}^H\,\mathbf{C}^H \\ &= \sigma_\nu^2 \left(\mathbf{I}_N + N\frac{\sigma_1^2}{\sigma_\nu^2} \mathbf{Q}\,\mathbf{L}\,\mathbf{Q}^H \right) \end{aligned} \tag{6.35}$$

where

$$\mathbf{Q} \triangleq \mathbf{C}\,\mathbf{T}. \tag{6.36}$$

We may note that $\mathbf{C}$ is an $N \times K_1 N$ matrix, $\mathbf{T}$ is a $K_1 N \times K_1$ matrix, $\mathbf{Q}$ is an $N \times K_1$ matrix, and $\mathbf{L}$ is a $K_1 \times K_1$ matrix.

6.4 Computation of the MMSE

From Chapter 4, we may recall that the MMSE obtained with the optimum receiver is given by

$$J_{\min} = 1 - \mathbf{p}^H\,\mathbf{R}^{-1}\,\mathbf{p} \tag{6.37}$$

where $\mathbf{p}$ is the crosscorrelation vector, and it has been assumed without loss of generality that the power of the desired symbol sequence is unity. To evaluate $\mathbf{R}^{-1}$, we invoke the well-known *matrix inversion lemma* [98]. According to this lemma, if $\mathbf{A}$ and $\mathbf{F}$ are nonsingular square matrices and the product $\mathbf{BFG}$ exists, then

$$(\mathbf{A} + \mathbf{BFG})^{-1} = \mathbf{A}^{-1} - \mathbf{A}^{-1}\mathbf{B}(\mathbf{GA}^{-1}\mathbf{B} + \mathbf{F}^{-1})^{-1}\mathbf{DA}^{-1}. \tag{6.38}$$

This is used to evaluate $\mathbf{R}^{-1}$ in the following manner:

$$\begin{aligned}\mathbf{R}^{-1} &= \frac{1}{\sigma_\nu^2}\left[\mathbf{I}_N - \mathbf{I}_N\,\mathbf{Q}\left(\mathbf{Q}^H\,\mathbf{I}_N\,\mathbf{Q} + \left(N\frac{\sigma_1^2}{\sigma_\nu^2}\,\mathbf{L}\right)^{-1}\right)^{-1}\mathbf{Q}^H\,\mathbf{I}_N\right] \\ &= \frac{1}{\sigma_\nu^2}\left[\mathbf{I}_N - \mathbf{Q}\left(\mathbf{Q}^H\,\mathbf{Q} + \frac{\sigma_\nu^2}{N\sigma_1^2}\,\mathbf{L}^{-1}\right)^{-1}\mathbf{Q}^H\right]. \qquad (6.39)\end{aligned}$$

For a given phase ψ_1 of the desired signal, we see From Equation (6.13) that the cross-correlation vector is given by

$$\mathbf{p} = \sigma_1\,e^{j\psi_1}\,\tilde{\mathbf{c}}_1 \qquad (6.40)$$

so that the MMSE is obtained from Equation (6.37) as

$$\begin{aligned}J_{\min} &= 1 - \sigma_1^2\,\hat{\mathbf{c}}_1^H\,\mathbf{R}^{-1}\,\hat{\mathbf{c}}_1 \qquad (6.41)\\ &= 1 - \frac{\sigma_1^2}{\sigma_\nu^2}\,\hat{\mathbf{c}}_1^H\left[\mathbf{I}_N - \mathbf{Q}\left(\mathbf{Q}^H\,\mathbf{Q} + \frac{\sigma_\nu^2}{N\sigma_1^2}\,\mathbf{L}^{-1}\right)^{-1}\mathbf{Q}^H\right]\hat{\mathbf{c}}_1 \\ &= 1 - \frac{\sigma_1^2}{\sigma_\nu^2}\left[N - N\,\frac{\hat{\mathbf{c}}_1^H}{\sqrt{N}}\,\mathbf{Q}\left(\mathbf{Q}^H\,\mathbf{Q} + \frac{\sigma_\nu^2}{N\sigma_1^2}\,\mathbf{L}^{-1}\right)^{-1}\mathbf{Q}^H\,\frac{\hat{\mathbf{c}}_1}{\sqrt{N}}\right] \\ &= 1 - \gamma\left[1 - \frac{\hat{\mathbf{c}}_1^H}{\sqrt{N}}\,\mathbf{Q}\left(\mathbf{Q}^H\,\mathbf{Q} + \frac{1}{\gamma}\,\mathbf{L}^{-1}\right)^{-1}\mathbf{Q}^H\,\frac{\hat{\mathbf{c}}_1}{\sqrt{N}}\right], \qquad (6.42)\end{aligned}$$

utilizing

$$\hat{\mathbf{c}}_1^H\,\hat{\mathbf{c}}_1 = N \qquad (6.43)$$

and

$$\gamma \triangleq N\frac{\sigma_1^2}{\sigma_\nu^2}, \qquad (6.44)$$

the SNR of the desired signal.

We now attempt to simplify Equation (6.42). We first consider

$$\mathbf{Q}^H\,\mathbf{Q} = \mathbf{T}^H\,\mathbf{C}^H\,\mathbf{C}\,\mathbf{T}. \qquad (6.45)$$

But,

$$\begin{aligned}\mathbf{C}^H\mathbf{C} &= \begin{bmatrix} \hat{\mathbf{C}}_1^H \\ \hat{\mathbf{C}}_2^H \\ \vdots \\ \hat{\mathbf{C}}_{K_1}^H \end{bmatrix} \begin{bmatrix} \hat{\mathbf{C}}_1 & \hat{\mathbf{C}}_2 & \dots & \hat{\mathbf{C}}_{K_1} \end{bmatrix} \\ &= \begin{bmatrix} \hat{\mathbf{C}}_1^H\hat{\mathbf{C}}_1 & \hat{\mathbf{C}}_1^H\hat{\mathbf{C}}_2 & \dots & \hat{\mathbf{C}}_1^H\hat{\mathbf{C}}_{K_1} \\ \hat{\mathbf{C}}_2^H\hat{\mathbf{C}}_1 & \hat{\mathbf{C}}_2^H\hat{\mathbf{C}}_2 & & \\ \vdots & & \ddots & \\ \hat{\mathbf{C}}_{K_1}^H\hat{\mathbf{C}}_1 & & & \hat{\mathbf{C}}_{K_1}^H\hat{\mathbf{C}}_{K_1} \end{bmatrix}. \end{aligned} \tag{6.46}$$

Recalling that $\hat{\mathbf{C}}_k$ is a diagonal matrix whose diagonal elements are the elements of $\hat{\mathbf{c}}_k$,

$$\hat{\mathbf{C}}_k \triangleq \begin{bmatrix} \hat{c}_{k,1} & 0 & \dots & \\ 0 & \hat{c}_{k,2} & \ddots & \\ \vdots & \ddots & \ddots & \\ & & & \hat{c}_{k,N} \end{bmatrix} \tag{6.47}$$

we may rewrite Equation (6.46) as

$$\mathbf{C}^H\mathbf{C} = \left[\begin{array}{ccc|c|ccc} \hat{c}_{1,1}^2 & 0 & \dots & & \hat{c}_{1,1}\hat{c}_{K_1,1} & 0 & \dots \\ 0 & \ddots & \ddots & \dots & 0 & \ddots & \ddots \\ \vdots & \ddots & \hat{c}_{1,N}^2 & & \vdots & \ddots & \hat{c}_{1,N}\hat{c}_{K_1,N} \\ \hline & \vdots & & \ddots & & \vdots & \\ \hline \hat{c}_{K_1,1}\hat{c}_{1,1} & 0 & \dots & & \hat{c}_{K_1,1}^2 & 0 & \dots \\ 0 & \ddots & \ddots & \dots & 0 & \ddots & \ddots \\ \vdots & \ddots & \hat{c}_{K_1,N}\hat{c}_{1,N} & & \vdots & \ddots & \hat{c}_{K_1,N}^2 \end{array}\right]. \tag{6.48}$$

Furthermore, we find that

$$\mathbf{u}_i = \frac{1}{\sqrt{N}} \begin{bmatrix} 0 \\ \vdots \\ 0 \\ \hline 0 \\ \vdots \\ 0 \\ \hline 1 \\ \vdots \\ 1 \\ \hline 0 \\ \vdots \\ 0 \\ \hline 0 \\ \vdots \\ 0 \end{bmatrix} \begin{array}{l} \\ \\ \text{1st set of } N \text{ rows} \\ \\ \\ \\ \vdots \\ \\ \\ \\ i\text{th set of } N \text{ rows} \\ \\ \\ \\ \vdots \\ \\ \\ \\ K_1\text{th set of } N \text{ rows} \\ \\ \end{array} \tag{6.49}$$

so that

$$\mathbf{T} = \frac{1}{\sqrt{N}} \left[\begin{array}{c|c|c|c} 1 & 0 & & 0 \\ \vdots & \vdots & \cdots & \vdots \\ 1 & 0 & & 0 \\ \hline 0 & 1 & & 0 \\ \vdots & \vdots & \cdots & \vdots \\ 0 & 1 & & 0 \\ \hline 0 & 0 & & 0 \\ \vdots & \vdots & \ddots & \vdots \\ 0 & 0 & & 0 \\ \hline 0 & 0 & & 1 \\ \vdots & \vdots & \cdots & \vdots \\ 0 & 0 & & 1 \end{array}\right]. \tag{6.50}$$

Using Equations (6.48) and (6.50) in Equation (6.45), we get

$$\mathbf{Q}^H \mathbf{Q} = \frac{1}{N} \begin{bmatrix} \sum_{i=1}^{N} \hat{c}_{1,i}^2 & \sum_{i=1}^{N} \hat{c}_{1,i}\hat{c}_{2,i} & \cdots & \sum_{i=1}^{N} \hat{c}_{1,i}\hat{c}_{K_1,i} \\ \sum_{i=1}^{N} \hat{c}_{2,i}\hat{c}_{1,i} & \sum_{i=1}^{N} \hat{c}_{2,i}^2 & & \vdots \\ \vdots & & \ddots & \\ \sum_{i=1}^{N} \hat{c}_{K_1,i}\hat{c}_{1,i} & \cdots & & \sum_{i=1}^{N} \hat{c}_{K_1,i}^2 \end{bmatrix} \triangleq \mathbf{X}. \tag{6.51}$$

An examination of Equation (6.51) reveals that $\mathbf{X}$ is the matrix of crosscorrelations between the normalized effective spreading codes, $\hat{\mathbf{c}}_k/\sqrt{N}$ $(k = 1, 2, \ldots, K_1)$. Thus, the (i, j)th element of $\mathbf{X}$ is the crosscorrelation value between the codes $\hat{\mathbf{c}}_i/\sqrt{N}$ and $\hat{\mathbf{c}}_j/\sqrt{N}$.

Now we consider

$$\mathbf{Q}^H \frac{\hat{\mathbf{c}}_1}{\sqrt{N}} = \frac{1}{\sqrt{N}} \mathbf{T}^H \mathbf{C}^H \hat{\mathbf{c}}_1. \tag{6.52}$$

We see that

$$\mathbf{C}^H \hat{\mathbf{c}}_1 = \begin{bmatrix} \hat{c}_{1,1}^2 \\ \hat{c}_{1,2}^2 \\ \vdots \\ \hat{c}_{1,N}^2 \\ \hline \hat{c}_{1,1}\hat{c}_{2,1} \\ \hat{c}_{1,2}\hat{c}_{2,2} \\ \vdots \\ \hat{c}_{1,N}\hat{c}_{2,N} \\ \hline \vdots \\ \hline \hat{c}_{1,1}\hat{c}_{K_1,1} \\ \hat{c}_{1,2}\hat{c}_{K_1,2} \\ \vdots \\ \hat{c}_{1,N}\hat{c}_{K_1,N} \end{bmatrix} \tag{6.53}$$

and Equation (6.52) becomes

$$\mathbf{Q}^H \frac{\hat{\mathbf{c}}_1}{\sqrt{N}} = \frac{1}{N} \begin{bmatrix} \sum_{i=1}^{N} \hat{c}_{1,i}^2 \\ \sum_{i=1}^{N} \hat{c}_{1,i}\hat{c}_{2,i} \\ \vdots \\ \sum_{i=1}^{N} \hat{c}_{1,i}\hat{c}_{K_1,i} \end{bmatrix} \triangleq \mathbf{x}. \tag{6.54}$$

It can be seen from Equation (6.54) that $\mathbf{x}$ is a vector of crosscorrelations between the normalized spreading code of the desired user, $\hat{\mathbf{c}}_1/\sqrt{N}$, and the normalized effective spreading codes of all the users, $\hat{\mathbf{c}}_k/\sqrt{N}$ $(k = 1, 2, \ldots, K_1)$. The ith element of $\mathbf{x}$ is the crosscorrelation value between $\hat{\mathbf{c}}_1/\sqrt{N}$ and $\hat{\mathbf{c}}_i/\sqrt{N}$. Furthermore, $\mathbf{x}$ is the first column of $\mathbf{X}$.

Using Equations (6.51) and (6.54) in Equation (6.42), we get

$$J_{\min} = 1 - \gamma \left[1 - \mathbf{x}^H \left(\mathbf{X} + \frac{1}{\gamma} \mathbf{L}^{-1} \right)^{-1} \mathbf{x} \right]. \tag{6.55}$$

Equation (6.55) shows that the MMSE depends on the SNR γ, crosscorrelations between the codes (as evidenced by the presence of $\mathbf{x}$ and $\mathbf{X}$ in the equation), and the ratios between the power of each of the effective interference signals and the power of the desired user's signal (due to the presence of $\mathbf{L}$ in the equation).

6.5 Numerical Example

We consider a CDMA system with four users. For simplicity, we assume that channel is synchronous, so that we have four effective users with the following spreading codes, each of length 15 chips:

$$\begin{aligned}
\hat{\mathbf{c}}_1 &= \{1, 1, -1, -1, 1, -1, 1, 1, 1, 1, -1, 1, -1, -1, 1\}, \\
\hat{\mathbf{c}}_2 &= \{1, 1, 1, 1, -1, -1, -1, 1, -1, -1, -1, 1, 1, -1, 1\}, \\
\hat{\mathbf{c}}_3 &= \{-1, 1, -1, -1, -1, 1, -1, -1, 1, -1, -1, -1, 1, -1, 1\}, \\
\hat{\mathbf{c}}_4 &= \{1, -1, 1, -1, 1, 1, 1, 1, 1, -1, 1, -1, 1, -1, -1\}.
\end{aligned}$$

Assuming that there are two samples per chip, the correlation matrix is

$$\mathbf{X} = \begin{bmatrix} 1.0000 & -0.0667 & -0.0667 & -0.0667 \\ -0.0667 & 1.0000 & -0.0667 & -0.0667 \\ -0.0667 & -0.0667 & 1.0000 & -0.0667 \\ -0.0667 & -0.0667 & -0.0667 & 1.0000 \end{bmatrix}.$$

Assuming that the powers of the four users are 1, 4, 10, and 0.1, respectively, the matrix $\mathbf{L}$ is

$$\mathbf{L} = \begin{bmatrix} 1 & 0 & 0 & 0 \\ 0 & 4 & 0 & 0 \\ 0 & 0 & 10 & 0 \\ 0 & 0 & 0 & 0.1 \end{bmatrix}.$$

$\mathbf{x}$ is the first column of $\mathbf{X}$. For a SNR of 10 dB, i.e., $\gamma = 10$, the MMSE using Equation (6.55) is

$$J_{\min} = 0.0919.$$

We note that for the given parameters, $\sigma_\nu^2 = 30/10 = 3$. Since the channel is synchronous, the correlation matrix may be expressed as

$$\mathbf{R} = \sum_{k=1}^{4} \sigma_k^2 \, \hat{\mathbf{c}}_k \, \hat{\mathbf{c}}_k^H$$

where $\sigma_k^2,\ k = 1, 2, 3, 4$, are the powers of the users, which are also the diagonal elements of $\mathbf{L}$. Due to the constraints of space, we merely present the optimum weight vector:

$$\begin{aligned} \mathbf{w}_{\text{opt}} &= \mathbf{R}^{-1} \, \hat{\mathbf{c}}_1 \\ &= [0.0318, 0.0318, 0.0295, 0.0295, -0.0295, -0.0295, -0.0318, -0.0318, \\ &\quad 0.0274, 0.0274, -0.0294, -0.0294, 0.0274, 0.0274, 0.0318, 0.0318, \\ &\quad 0.0318, 0.0318, 0.0250, 0.0250, -0.0339, -0.0339, 0.0294, 0.0294, \\ &\quad -0.0250, -0.0250, -0.0363, -0.0363, 0.0339, 0.0339]^T. \end{aligned}$$

Using the well known expression of Equation (6.37) to find the MMSE and noting that $\mathbf{p} = \hat{\mathbf{c}}_1$, we get

$$\begin{aligned} J_{\min} &= 1 - \hat{\mathbf{c}}_1^H \, \mathbf{R}^{-1} \, \hat{\mathbf{c}}_1 = 1 - \hat{\mathbf{c}}_1^H \, \mathbf{w}_{\text{opt}} \\ &= 0.0919, \end{aligned}$$

which is the same as what we got using Equation (6.55). Thus, the accuracy of the expression of Equation (6.55) is validated.

6.6 Near-Far Resistance Capability of the MMSE Receiver

The MMSE receiver has been shown to be near-far resistant through simulations [55]. Theoretical discussions of near-far resistance of the MMSE receiver have tended to be abstract [46], defining a quantity termed near-far resistance as the asymptotic efficiency evaluated for worst case energies. The asymptotic efficiency is a measure, as the noise level tends to zero, of how well the receiver performs in the presence of MAI relative to

its performance in the absence of MAI. Madhow and Honig [46] also go on to discuss near-far resistance in terms of signal and interference subspaces.

A more intuitive understanding of the mechanism of near-far resistance is desirable. We seek to show in more practical terms that the MMSE receiver is near-far resistant. To accomplish this, further simplification of Equation (6.55) is necessary. Since,

$$\mathbf{X} + \frac{1}{\gamma}\mathbf{L}^{-1} = \mathbf{X}\left(\mathbf{I} + \frac{1}{\gamma}\mathbf{X}^{-1}\mathbf{L}^{-1}\right),$$

we may write

$$\left(\mathbf{X} + \frac{1}{\gamma}\mathbf{L}^{-1}\right)^{-1} = \left(\mathbf{I} + \frac{1}{\gamma}\mathbf{X}^{-1}\mathbf{L}^{-1}\right)^{-1}\mathbf{X}^{-1}. \tag{6.56}$$

Next, we make use of the following lemma, which is well-known in matrix perturbation theory [99, 100]:

Lemma Suppose $\mathbf{F} \in \Re^{n\times n}$ and that $\|\cdot\|$ is a norm satisfying the following submultiplicative property for conformable matrices $\mathbf{A}$ and $\mathbf{B}$:

$$\|\mathbf{AB}\| \leq \|\mathbf{A}\|\,\|\mathbf{B}\|. \tag{6.57}$$

If $\|\mathbf{F}\| < 1$, then $\mathbf{I} - \mathbf{F}$ is nonsingular and

$$(\mathbf{I} - \mathbf{F})^{-1} = \sum_{k=1}^{\infty}\mathbf{F}^k. \tag{6.58}$$

Equation (6.58), known as the *von Neumann series*[3], can also be written as

$$(\mathbf{I} + \mathbf{F})^{-1} = \mathbf{I} - \mathbf{F} + \mathbf{F}^2 - \mathbf{F}^3 + \ldots. \tag{6.59}$$

[3]The author is grateful to Peter Spellucci for referring him to the von Neumann series. Peter Spellucci responded to the author's queries on Usenet newsgroups.

To use Equation (6.59) to simplify Equation (6.56), we assume that[4]

$$\left\| \frac{1}{\gamma} \mathbf{X}^{-1} \mathbf{L}^{-1} \right\|_2 < 1, \tag{6.60}$$

noting that the 2-norm satisfies the above submultiplicative property. Then we may write Equation (6.56) as

$$\begin{aligned} \left(\mathbf{X} + \frac{1}{\gamma} \mathbf{L}^{-1} \right)^{-1} &= \left(\mathbf{I} - \frac{1}{\gamma} \mathbf{X}^{-1} \mathbf{L}^{-1} + \frac{1}{\gamma^2} \mathbf{X}^{-1} \mathbf{L}^{-1} \right. \\ &\quad - \frac{1}{\gamma^3} \mathbf{X}^{-1} \mathbf{L}^{-1} \mathbf{X}^{-1} \mathbf{L}^{-1} \mathbf{X}^{-1} \mathbf{L}^{-1} \\ &\quad \left. + \text{smaller terms} \right) \mathbf{X}^{-1}. \end{aligned} \tag{6.61}$$

If

$$\mathbf{e}_1 \triangleq \begin{bmatrix} 1 \\ 0 \\ \vdots \\ 0 \end{bmatrix} \tag{6.62}$$

then, since $\mathbf{X}$ is Hermitian,

$$\mathbf{x} = \mathbf{X} \mathbf{e}_1 \tag{6.63}$$

so that

$$\begin{aligned} \mathbf{x}^H \left(\mathbf{X} + \frac{1}{\gamma} \mathbf{L}^{-1} \right)^{-1} \mathbf{x} &= \mathbf{e}_1^H \mathbf{X} \left(\mathbf{I} - \frac{1}{\gamma} \mathbf{X}^{-1} \mathbf{L}^{-1} + \frac{1}{\gamma^2} \mathbf{X}^{-1} \mathbf{L}^{-1} \mathbf{X}^{-1} \mathbf{L}^{-1} \right. \\ &\quad \left. - \frac{1}{\gamma^3} \mathbf{X}^{-1} \mathbf{L}^{-1} \mathbf{X}^{-1} \mathbf{L}^{-1} \mathbf{X}^{-1} \mathbf{L}^{-1} + \ldots \right) \mathbf{X}^{-1} \mathbf{X} \mathbf{e}_1 \\ &= \mathbf{e}_1^H \mathbf{X} \mathbf{e}_1 - \frac{1}{\gamma} \mathbf{e}_1^H \mathbf{L}^{-1} \mathbf{e}_1 + \frac{1}{\gamma^2} \mathbf{e}_1^H \mathbf{L}^{-1} \mathbf{X}^{-1} \mathbf{L}^{-1} \mathbf{e}_1 \\ &\quad - \frac{1}{\gamma^3} \mathbf{e}_1^H \mathbf{L}^{-1} \mathbf{X}^{-1} \mathbf{L}^{-1} \mathbf{X}^{-1} \mathbf{L}^{-1} \mathbf{e}_1 + \ldots . \end{aligned} \tag{6.64}$$

[4]This assumption holds for a large class of cases, including when

1. the SNR γ is "high", and
2. the interference-to-signal ratios, $\sigma_k^2/\sigma_1^2,\ k = 2, 3, \ldots, K_1$, are "high."

The former case is the interference-limited case. The latter case implies that the interference signals are strong; this is an interesting scenario as well. Thus, the problem is not necessarily oversimplified by this assumption.

We note that

$$\mathbf{e}_1^H \mathbf{X} \mathbf{e}_1 = \mathbf{e}_1^H \mathbf{x} = \frac{1}{N} \sum_{i=1}^{N} \hat{c}_{1,i}^2 = 1 \tag{6.65}$$

$$\mathbf{L}^{-1} \mathbf{e}_1 = \mathbf{e}_1 \tag{6.66}$$

$$\mathbf{e}_1^H \mathbf{L}^{-1} \mathbf{e}_1 = 1 \tag{6.67}$$

$$\mathbf{e}_1^H \mathbf{L}^{-1} \mathbf{X}^{-1} \mathbf{L}^{-1} \mathbf{e}_1 = \mathbf{e}_1^H \mathbf{X}^{-1} \mathbf{e}_1 \tag{6.68}$$

$$\mathbf{e}_1^H \mathbf{L}^{-1} \mathbf{X}^{-1} \mathbf{L}^{-1} \mathbf{X}^{-1} \mathbf{L}^{-1} \mathbf{e}_1 = \mathbf{e}_1^H \mathbf{X}^{-1} \mathbf{L}^{-1} \mathbf{X}^{-1} \mathbf{e}_1 \tag{6.69}$$

so Equation (6.64) simplifies to

$$\begin{aligned} \mathbf{x}^H \left(\mathbf{X} + \frac{1}{\gamma} \mathbf{L}^{-1} \right)^{-1} \mathbf{x} &= 1 - \frac{1}{\gamma} + \frac{1}{\gamma^2} \mathbf{e}_1^H \mathbf{X}^{-1} \mathbf{e}_1 \\ &\quad - \frac{1}{\gamma^3} \mathbf{e}_1^H \mathbf{X}^{-1} \mathbf{L}^{-1} \mathbf{X}^{-1} \mathbf{e}_1 + \text{higher order terms.} \end{aligned} \tag{6.70}$$

Using Equation (6.70) in Equation (6.55), we get

$$\begin{aligned} J_{\min} &= 1 - \gamma \left[1 - \left(1 - \frac{1}{\gamma} + \frac{1}{\gamma^2} \mathbf{e}_1^H \mathbf{X}^{-1} \mathbf{e}_1 - \frac{1}{\gamma^3} \mathbf{e}_1^H \mathbf{X}^{-1} \mathbf{L}^{-1} \mathbf{X}^{-1} \mathbf{e}_1 \right. \right. \\ &\quad \left. \left. + \frac{1}{\gamma^4} \mathbf{e}_1^H \mathbf{X}^{-1} \mathbf{L}^{-1} \mathbf{X}^{-1} \mathbf{L}^{-1} \mathbf{X}^{-1} \mathbf{e}_1 - \ldots \right) \right] \\ &= \frac{1}{\gamma} \mathbf{e}_1^H \mathbf{X}^{-1} \mathbf{e}_1 - \frac{1}{\gamma^2} \mathbf{e}_1^H \mathbf{X}^{-1} \mathbf{L}^{-1} \mathbf{X}^{-1} \mathbf{e}_1 \\ &\quad + \frac{1}{\gamma^3} \mathbf{e}_1^H \mathbf{X}^{-1} \mathbf{L}^{-1} \mathbf{X}^{-1} \mathbf{L}^{-1} \mathbf{X}^{-1} \mathbf{e}_1 - \ldots \end{aligned} \tag{6.71}$$

where the ellipsis indicates smaller terms that are negligible compared with the preceding terms.

Thus, Equation (6.71) is the simplified expression for the MMSE, in terms of the SNR γ, the inverse of the crosscorrelation matrix $\mathbf{X}$, and the inverse of the diagonal matrix $\mathbf{L}$, whose diagonal elements are the signal-to-interference power ratios. It is easy to see from this equation that the MMSE is dominated by the first term of the infinite series. For moderate SNRs, the series can be truncated after the third term with little loss in accuracy, and for higher SNRs, even the third term can be omitted. For most practical cases of interest, it is safe to consider only the first two terms of the series for analysis.

If we denote

$$\mathbf{X}^{-1} \triangleq \{\tilde{x}_{ij}\}, \tag{6.72}$$

then we may write

$$J_{\min} \approx \frac{1}{\gamma}\,\tilde{x}_{11} - \frac{1}{\gamma^2}\,\sum_{i=1}^{K_1} \eta_i\,\tilde{x}_{i1}^2 \tag{6.73}$$

where $\eta_i,\ i = 1, 2, \ldots, K_1$, are the diagonal elements of $\mathbf{L}^{-1}$. They are, in fact, the signal-to-interference power ratios. The sensitivity of the MMSE to change in an signal-to-interference ratio may be measured by its partial derivate with respect to η_j:

$$\frac{\partial J_{\min}}{\partial \eta_j} \approx -\frac{1}{\gamma^2}\,\tilde{x}_{j1}^2. \tag{6.74}$$

This equation shows that with a decrease in the signal-to-interference power ratio there is an increase in the MMSE and the rate of change is $\tilde{x}_{i1}^2/\gamma^2$. Thus, if $\tilde{x}_{j1}^2$ is insignificant compared to γ^2, then the MMSE solution is insensitive to change in the signal-to-interference ratio, i.e., it is near-far resistant. The dependence of the elements of $\mathbf{X}^{-1}$ on the matrix $\mathbf{X}$ is investigated in the following paragraphs. In the limiting case where noise is absent, i.e., $\gamma = \infty$, the MMSE receiver is completely near-far resistant. The receiver achieves this because the MMSE solution in this case is perfectly orthogonal to all the interference vectors.

The concept of *condition number* of a matrix [99] is briefly introduced here to explain the significance of Equation (6.74). The condition number $\kappa(\mathbf{A})$ of a matrix $\mathbf{A}$ is defined by

$$\kappa(\mathbf{A}) \stackrel{\triangle}{=} \|\mathbf{A}\|\,\|\mathbf{A}^{-1}\| \tag{6.75}$$

where $\|\cdot\|$ is any matrix norm. The condition number depends on the norm used. When the 2-norm is used,

$$\kappa_2(\mathbf{A}) \stackrel{\triangle}{=} \|\mathbf{A}\|_2\,\|\mathbf{A}^{-1}\|_2. \tag{6.76}$$

The norm is a measure of the "size" of the matrix, i.e., of its elements. The 2-norm is given by

$$\|\mathbf{A}\|_2 = \sqrt{\lambda_{\max}(\mathbf{A}^H\,\mathbf{A})}. \tag{6.77}$$

If $\mathbf{A}$ is Hermitian, then,

$$\|\mathbf{A}\|_2 = \lambda_{\max}(\mathbf{A}) \tag{6.78}$$

where $\lambda_{\max}(\mathbf{A})$ is the largest eigenvalue of $\mathbf{A}$, and

$$\|\mathbf{A}^{-1}\|_2 = \lambda_{\max}(\mathbf{A}^{-1}) = \frac{1}{\lambda_{\min}(\mathbf{A})} \tag{6.79}$$

where $\lambda_{\min}(\mathbf{A})$ is the smallest eigenvalue of $\mathbf{A}$. Then Equation (6.76) may be expressed as

$$\kappa_2(\mathbf{A}) = \frac{\lambda_{\max}(\mathbf{A})}{\lambda_{\min}(\mathbf{A})}. \tag{6.80}$$

From Equation (6.76), we have

$$\|\mathbf{A}^{-1}\|_2 = \frac{\kappa_2(\mathbf{A})}{\|\mathbf{A}\|_2}. \tag{6.81}$$

We know that the absolute values of all the non-diagonal elements of the matrix $\mathbf{X}$ are less than unity, so $\|\mathbf{X}\|_2$ is well bounded. Therefore, $\|\mathbf{X}^{-1}\|_2$ can vary widely depending upon $\kappa_2(\mathbf{X})$. A unitary matrix $\mathbf{V}$ ($\mathbf{V}^H\mathbf{V} = 1$) has the smallest possible condition number with $\kappa_2(\mathbf{V}) = 1$. Thus the greater the "deviation" of $\mathbf{X}$ from a unitary matrix (for example, if $\|\mathbf{X} - \mathbf{I}\|_2$ is large compared to unity), the larger the condition number of $\mathbf{X}$. If the set of effective codes $\hat{\mathbf{c}}_k$, $k = 1, 2, \ldots, K_1$ have good code crosscorrelation properties, the matrix $\mathbf{X}$ has low values for its non-diagonal elements, which also result in a low condition number $\kappa_2(\mathbf{X})$ and hence a low value for $\|\mathbf{X}^{-1}\|_2$. This implies that the individual elements of $\mathbf{X}^{-1}$ are not likely to be very large, leading to a near-far resistant receiver.

6.7 Equivalent Near-Far Resistance Analysis for a Matched Filter Receiver

It is interesting to perform a similar analysis on the conventional matched filter receiver. Although it is of greater interest to look at the dependence of the BER of the matched filter receiver on the interference-to-signal power ratio, an examination of the dependence of the MSE at the matched filter output on the interference-to-signal power ratio can provide a useful comparison with the MMSE receiver.

The MSE at the matched filter output is given by

$$\varepsilon = E\left[\left|d(n) - \mathbf{w}_{\mathrm{MF}}^H\,\mathbf{r}(n)\right|^2\right] \tag{6.82}$$

where $d(n) \in \{+1, -1\}$ and the matched filter weight vector $\mathbf{w}_{\mathrm{MF}}$ is given by

$$\mathbf{w}_{\mathrm{MF}} = \frac{e^{-j\psi}}{\sigma_1 N}\,\hat{\mathbf{c}}_1. \tag{6.83}$$

Evaluation of Equation (6.82) yields

$$\varepsilon = 1 - \frac{e^{j\psi}}{\sigma_1 N}\,\hat{\mathbf{c}}_1^H\,\mathbf{p} - \frac{e^{-j\psi}}{\sigma_1 N}\,\mathbf{p}^H\,\hat{\mathbf{c}}_1 + \frac{1}{\sigma_1^2 N}\,\mathbf{c}_1^H\,\mathbf{R}\,\mathbf{c}_1. \tag{6.84}$$

Using Equation (6.35), the last term is

$$\begin{aligned}
\frac{1}{\sigma_1^2 N}\,\hat{\mathbf{c}}_1^H\,\mathbf{R}\,\mathbf{c}_1 &= \frac{1}{\sigma_1^2 N}\,\mathbf{c}_1^H\left[\sigma_\nu^2\left(\mathbf{I}_N + N\frac{\sigma_1^2}{\sigma_\nu^2}\,\mathbf{Q}\,\mathbf{L}\,\mathbf{Q}^H\right)\right]\hat{\mathbf{c}}_1 \\
&= \frac{\sigma_\nu^2}{\sigma_1^2 N}\left[\frac{\hat{\mathbf{c}}_1^H\,\hat{\mathbf{c}}_1}{N} + \gamma\,\frac{\hat{\mathbf{c}}_1^H}{\sqrt{N}}\,\mathbf{Q}\,\mathbf{L}\,\mathbf{Q}^H\,\frac{\hat{\mathbf{c}}_1}{\sqrt{N}}\right] \\
&= \frac{1}{\gamma}\left[1 + \gamma\,\mathbf{x}^H\,\mathbf{L}\,\mathbf{x}\right] \\
&= \frac{1}{\gamma} + \mathbf{x}^H\,\mathbf{L}\,\mathbf{x}.
\end{aligned} \tag{6.85}$$

Using the expression

$$\mathbf{p} = e^{j\psi}\,\sigma_1\,\mathbf{c}_1 \tag{6.86}$$

and Equation (6.85) in Equation (6.84), we obtain

$$\begin{aligned}
\varepsilon &= 1 - \frac{\hat{\mathbf{c}}_1^H\,\hat{\mathbf{c}}_1}{N} - \frac{\hat{\mathbf{c}}_1^H\,\hat{\mathbf{c}}_1}{N} + \frac{1}{\gamma} + \mathbf{x}^H\,\mathbf{L}\,\mathbf{x} \\
&= \mathbf{x}^H\,\mathbf{L}\,\mathbf{x} + \frac{1}{\gamma} - 1.
\end{aligned} \tag{6.87}$$

Using the notation

$$\mathbf{x} \triangleq \{x_i\} \tag{6.88}$$

where x_i is the normalized crosscorrelation between the desired spreading code and the ith effective spreading code, the MSE at the matched filter output may be expressed as

$$\varepsilon = \sum_{i=1}^{K_1} \tilde{\lambda}_i\,x_i^2 + \frac{1}{\gamma} - 1 \tag{6.89}$$

where $\tilde{\lambda}_i,\ i = 1, 2, \ldots, K_1$, are the diagonal elements of $\mathbf{L}$ and are the interference-to-signal power ratios for the effective interference signals. As before, the partial derivative of the MSE with respect to the $\tilde{\lambda}_j$ may be used to obtain a measure of the of the sensitivity of the MSE to changes in the jth interference-to-signal power ratio and is found to be

$$\frac{\partial \varepsilon}{\partial \tilde{\lambda}_j} = x_j^2. \tag{6.90}$$

Thus, the MSE at the matched filter output increases with the interference-to-signal power ratio. Equation (6.90) shows that the rate of change of the MSE with the jth interference-to-signal power ratio is x_i^2, i.e., it is dependent *only* on the crosscorrelation of the desired signal's spreading code with the jth signal's spreading code. Thus, the higher this crosscorrelation, the more the matched filter's MSE is affected by changes in the interference power. A large SNR does not aid the matched filter receiver in improving its near-far resilience.

The preceding argument does not imply that the BER of the matched filter is affected to the same extent. However, it does suggest that the matched filter is not near-far resistant and this measure provides for a comparison with the MMSE receiver. The MMSE receiver is near-far resistant if the SNR is high or if the crosscorrelations are reasonably low, whereas the matched filter receiver is highly susceptible to the near-far problem if the code crosscorrelations are not insignificant.

Figure 6.2 shows the variation of the the MMSE of the optimum filter and the MSE of the matched filter with the standard deviation of the powers of the MAI signals. The plots are obtained by averaging the results of 1000 trials. In each trial, seven users are considered. Random codes of length 15 are generated for the users and powers for the MAI signals are lognormally distributed with mean zero and the specified standard deviation. The figure demonstrates that the MMSE receiver is near-far resistant whereas the matched filter receiver is susceptible to the near-far problem.

6.8 MMSE Analysis for Multipath Channels

In Section 6.4, an expression for the MMSE in an AWGN channel was derived in terms of the SNR, the crosscorrelations between the effective code vectors of all the signals, and the signal-to-interference power ratios. In this section, the analysis is extended to multipath channels. Multipath is a form of diversity that the MMSE receiver is able to exploit and this has been reported in the literature. Exploitation of multipath diversity has been demonstrated through simulations. However, MMSE analysis can provide further insight into this topic.

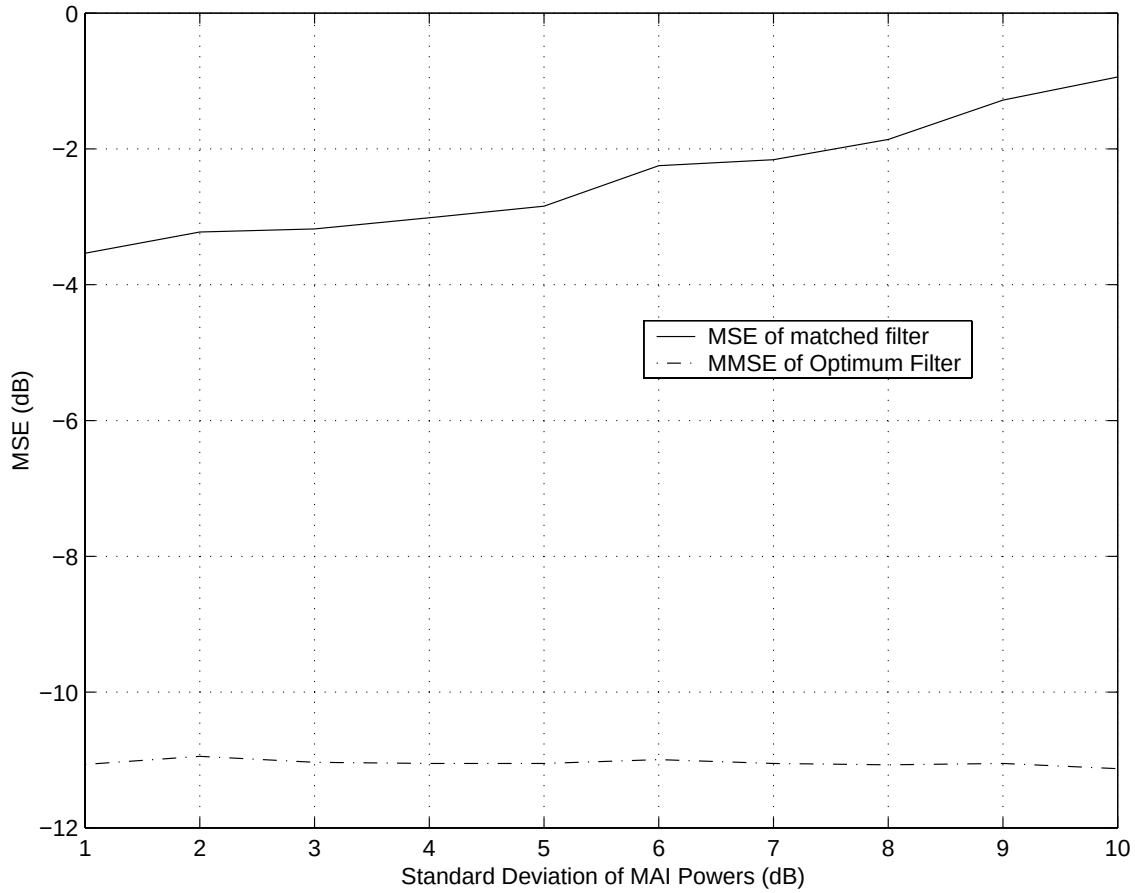

Figure 6.2: Variation of the MMSE of the Optimum Receiver and the MSE of the Matched Filter Receiver with Standard Deviation of the Powers of the MAI Signals.

Following the notation of Section 6.2, the CDMA signal at the receiver is modeled as

$$r(t) = \sum_{k=1}^{K} \sum_{l=1}^{L} A_{kl}\, d_k(t - \tau_{kl})\, c_k(t - \tau_{kl}) \cos(\omega_c(t - \tau_{kl}) + \phi_k) + n(t) \tag{6.91}$$

where L is the number of multipath components, A_{kl} is the time-invariant amplitude of the lth component of the kth user's signal, and τ_{kl} is the time delay of the lth component of the kth user's signal. It is assumed that there is no frequency offset on any of the signals. Assuming perfect knowledge of the carrier frequency, the sampled baseband received signal vector at time instant n is represented as

$$\mathbf{r}(n) = \sum_{k=1}^{K} \sum_{l=1}^{L} A_{kl}\, \mathbf{s}_{kl}(n)\, e^{j\psi_{kl}} + \boldsymbol{\nu}(n) \tag{6.92}$$

where $\mathbf{s}_{kl}(n)$ is the signal vector due to the lth multipath component of the kth user and

$$\psi_{kl} = \phi_k - \omega_c \tau_{kl} \tag{6.93}$$

is the phase of the lth multipath component of the kth user's signal uniformly distributed over $[0, 2\pi)$. Defining the complex amplitude as

$$a_{kl} \triangleq A_{kl}\, e^{j\psi_{kl}}, \tag{6.94}$$

we may write

$$\mathbf{r}(n) = \sum_{k=1}^{K} \sum_{l=1}^{L} a_{kl}\, \mathbf{s}_{kl}(n) + \boldsymbol{\nu}(n). \tag{6.95}$$

Again, recalling the notation of Section 6.2, we have

$$\mathbf{s}_{11}(n) = d_1(n)\, \mathbf{c}_1 \tag{6.96}$$

and

$$\mathbf{s}_{k1}(n) = b_k(n)\, \tilde{\mathbf{c}}_k \tag{6.97}$$

where $\mathbf{c}_k$, $\tilde{\mathbf{c}}_k$, and $b_k(n)$ are defined in Equations (6.5), (6.8), and (6.9), respectively. We now introduce the notation $\tilde{\mathbf{c}}_k^L$ and $\tilde{\mathbf{c}}_k^R$ defined by

$$\tilde{\mathbf{c}}_{kl}^L \triangleq \begin{bmatrix} \tilde{c}_{k,N-m_{kl}+1} \\ \tilde{c}_{k,N-m_{kl}+1} \\ \vdots \\ \tilde{c}_{k,N} \\ 0 \\ \vdots \\ 0 \end{bmatrix}, \tag{6.98}$$

$$\tilde{\mathbf{c}}_{kl}^R \triangleq \begin{bmatrix} 0 \\ \vdots \\ 0 \\ \tilde{c}_{k,1} \\ \tilde{c}_{k,2} \\ \vdots \\ \tilde{c}_{k,N-m_{kl}} \end{bmatrix} \tag{6.99}$$

where $\tilde{c}_{k,i}$ is the ith element of the equivalent synchronous code vector $\tilde{\mathbf{c}}_k$ of the kth user and m_{kl} is the time delay in samples of the lth multipath component of the kth user's signal relative to the signal's first component. For the purpose of this analysis, we assume that the delay of the last component with respect to the first component is less than a symbol period, i.e., $m_{kL} < N$. This ensures that each multipath component vector of the desired signal is correlated with the first component vector[5]. This assumption does not influence the effect of the interference, however, because each multipath component of the MAI signals is an uncorrelated interference. Furthermore, for the interference signals ($k \neq 1$), we have

$$\tilde{\mathbf{c}}_{kl}^{R} = \begin{cases} \mathbf{c}_{kl}^{R(1)}, & d_k(n) = d_k(n-1), \\ \mathbf{c}_{kl}^{R(2)}, & d_k(n) = -d_k(n-1), \end{cases} \tag{6.100}$$

$$\tilde{\mathbf{c}}_{kl}^{L} = \begin{cases} \mathbf{c}_{kl}^{L(1)}, & d_k(n) = d_k(n-1), \\ \mathbf{c}_{kl}^{L(2)}, & d_k(n) = -d_k(n-1), \end{cases} \tag{6.101}$$

where $\mathbf{c}_{kl}^{R(\cdot)}$ and $\mathbf{c}_{kl}^{L(\cdot)}$ are defined in a manner similar to Equations (6.10a) and (6.10b).

Equation (6.94) is now rewritten as

$$\begin{aligned} \mathbf{r}(n) &= \sum_{k=1}^{K} a_{k1}\, b_k(n)\, \tilde{\mathbf{c}}_k \\ &\quad + \sum_{k=1}^{K} \sum_{l=2}^{L} a_{kl} \left(b_k(n-1)\, \tilde{\mathbf{c}}_{kl}^{L} + b_k(n)\, \tilde{\mathbf{c}}_{kl}^{R} \right) + \boldsymbol{\nu}(n). \end{aligned} \tag{6.102}$$

The first term on the right side is due to the first multipath components of all signals. The second term is due to the delayed multipath components of all signals. The two terms in the parentheses indicate the contributions from two adjacent symbols, the "previous" and "current" symbols[6]. Equation (6.100) is rearranged to combine correlated vectors,

$$\begin{aligned} \mathbf{r}(n) &= \sum_{k=1}^{K} a_{k1}\, b_k(n) \left(\tilde{\mathbf{c}}_k + \sum_{l=2}^{L} \frac{a_{kl}}{a_{k1}}\, \tilde{\mathbf{c}}_{kl}^{R} \right) \\ &\quad + \sum_{k=1}^{K} \sum_{l=2}^{L} a_{kl}\, b_k(n-1)\, \tilde{\mathbf{c}}_{kl}^{L} + \boldsymbol{\nu}(n) \\ &= \sum_{k=1}^{K} a_{k1}\, b_k(n)\, \mathbf{g}_k + \sum_{k=1}^{K} \sum_{l=2}^{L} a_{kl}\, b_k(n-1)\, \tilde{\mathbf{c}}_{kl}^{L} + \boldsymbol{\nu}(n) \end{aligned} \tag{6.103}$$

[5]Uncorrelated multipath due to the desired signal behaves like interference.

[6]Since multipath delay does not exceed a symbol period, there is no contribution from other symbols.

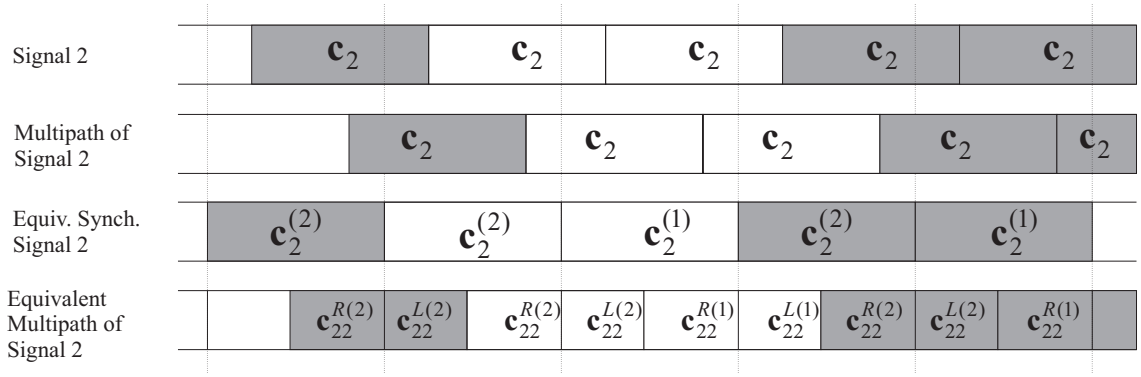

Figure 6.3: Equivalent Synchronous Representation of Asynchronous Signals and Their Multipath Components.

where we now define

$$\mathbf{g}_k \stackrel{\triangle}{=} \tilde{\mathbf{c}}_k + \sum_{l=2}^{L} \frac{a_{kl}}{a_{k1}} \tilde{\mathbf{c}}_{kl}^{R}. \tag{6.104}$$

Figure 6.3 shows an example of an asynchronous signal (Signal 2) and its delayed multipath component. Equivalent synchronous representations of the first and delayed components are illustrated. The vertical lines indicate the received signal window, i.e., the symbol boundaries of the desired signal (Signal 1). Each rectangular block represents a symbol. The dark blocks represents the symbol $+1$, while the white blocks represent the symbol -1. The first row depicted is the first component of Signal 2. The second row is a delayed multipath component of this signal. The third and fourth rows are equivalent synchronous representations of the first and delayed components, respectively, of Signal 2.

The correlation matrix in this case is given by

$$\begin{aligned}
\mathbf{R} &\stackrel{\triangle}{=} E\left[\mathbf{r}(n)\,\mathbf{r}^H(n)\right] \\
&= \sum_{k=1}^{K} E\left[|a_{k1}|^2\,\mathbf{g}_k\,\mathbf{g}_k^H\right] + \sum_{k=1}^{K}\sum_{l=2}^{L} E\left[|a_{kl}|^2\,\tilde{\mathbf{c}}_{kl}^{L}\,(\tilde{\mathbf{c}}_{kl}^{L})^H\right] + E\left[\boldsymbol{\nu}(n)\,\boldsymbol{\nu}^H(n)\right] \\
&= \underbrace{|a_{11}|^2\,\mathbf{g}_1\,\mathbf{g}_1^H}_{A} + \underbrace{\sum_{k=2}^{K} \frac{|a_{k1}|^2}{2}\left[\mathbf{g}_k^{(1)}\,\mathbf{g}_k^{(1)H} + \mathbf{g}_k^{(2)}\,\mathbf{g}_k^{(2)H}\right]}_{B} + \underbrace{\sum_{l=2}^{L} |a_{1l}|^2\,\tilde{\mathbf{c}}_{1l}^{L}\,(\tilde{\mathbf{c}}_{1l}^{L})^H}_{C} \\
&\quad + \underbrace{\sum_{k=2}^{K}\sum_{l=2}^{L} \frac{|a_{kl}|^2}{2}\left[\mathbf{c}_{kl}^{L(1)}\,\mathbf{c}_{kl}^{L(1)H} + \mathbf{c}_{kl}^{L(2)}\,\mathbf{c}_{kl}^{L(2)H}\right]}_{D} + \underbrace{\sigma_\nu^2\,\mathbf{I}_N}_{E}
\end{aligned} \tag{6.105}$$

where

$$\mathbf{g}_k^{(1)} \triangleq \mathbf{c}_k^{(1)} + \sum_{l=2}^{L} \frac{a_{kl}}{a_{k1}} \mathbf{c}_{kl}^{R(1)}, \tag{6.106a}$$

$$\mathbf{g}_k^{(2)} \triangleq \mathbf{c}_k^{(2)} + \sum_{l=2}^{L} \frac{a_{kl}}{a_{k1}} \mathbf{c}_{kl}^{R(2)}. \tag{6.106b}$$

The terms of Equation (6.105) need further explanation. The term labeled A is the signal of interest. It includes the contribution from all of the correlated multipath. The term labeled B is due to multiple access interference. Each term of the summation includes the first component and the correlated parts of all other multipath components of that user's signal. The term labeled C is due to the sum of all the uncorrelated parts of the desired signal's multipath components. Term D comprises the contributions of the uncorrelated parts of the multipath components of the MAI signals. Finally, the term labeled E is due to AWGN. Equation (6.105) can now be rewritten as

$$\mathbf{R} = \sum_{k=1}^{4K-2} \sigma_k^2 \, \hat{\mathbf{c}}_k \, \hat{\mathbf{c}}_k^H + \mathbf{I}_N \tag{6.107}$$

where the new code vector[7] $\hat{\mathbf{c}}_k$ is defined as

$$\hat{\mathbf{c}}_k \triangleq \begin{cases} \mathbf{g}_1, & k = 1, \\ \mathbf{g}_k^{(1)}, & k = 2, \ldots, K, \\ \mathbf{g}_{k-K+1}^{(2)}, & k = K+1, \ldots, 2K-1, \\ \sum\limits_{l=2}^{L} |a_{1l}|^2 \, \tilde{\mathbf{c}}_{1l}^{L}, & k = 2K, \\ \sum\limits_{l=2}^{L} |a_{(k-2K+1)l}|^2 \, \mathbf{c}_{(k-2K+1)l}^{L(1)}, & k = 2K+1, \ldots, 3K-1, \\ \sum\limits_{l=2}^{L} |a_{(k-3K+2)l}|^2 \, \mathbf{c}_{(k-3K+2)l}^{L(2)}, & k = 3K, \ldots, 4K-2, \end{cases} \tag{6.108}$$

[7]This definition of $\hat{\mathbf{c}}$ is an extension of the definition of Equation (6.18) for the multipath case. As in Section 6.3, it is assumed that the delays of the signals are different. This gives rise to one term from A of Equation (6.105), $2(K-1) = 2K-2$ terms from B, one term from C, and $2K-2$ terms from D, for a total of $4K-2$ terms in the summation.

and σ_k^2 is defined as

$$\sigma_k^2 \triangleq \begin{cases} |a_{11}|^2, & k = 1, \\ \dfrac{|a_{k1}|^2}{2}, & k = 2, \ldots, K, \\ \dfrac{|a_{(k-K+1)1}|^2}{2}, & k = K+1, \ldots, 2K-1, \\ 1, & k = 2K, \\ \dfrac{1}{2}, & k = 2K+1, \ldots, 3K-1, \\ \dfrac{1}{2}, & k = 3K, \ldots, 4K-2. \end{cases} \tag{6.109}$$

Note that all of the vectors on the right side of Equation (6.108) do not have the same norm. The norms of the vectors strongly depend on the multipath characteristics. Furthermore, the powers defined in Equation (6.109) depend on the amplitudes of the first components of the signals. The first three sets of powers on the right side of the equation correspond to the main components.

Using the definitions in Section 6.3, the correlation matrix $\mathbf{R}$ can again be represented as in Equation (6.21), but with the difference that K_1 is now given by

$$K_1 \triangleq 4K - 2. \tag{6.110}$$

The correlation matrix may be expressed as in Equation (6.35). From Equation (6.37), the MMSE of the optimum receiver is given by

$$J_{\min} = 1 - \mathbf{p}^H \mathbf{R}^{-1} \mathbf{p}$$

where $\mathbf{p}$ is the crosscorrelation vector. Using Equation (6.103) and noting that $d_1(n) = b_1(n)$, we have

$$\begin{aligned} \mathbf{p} &= E[d_1(n)\,\mathbf{r}(n)] \\ &= E\left[d_1(n)\left(a_{11}\,d_1(n)\,\mathbf{g}_1 + \sum_{k=2}^{K} a_{k1}\,b_k(n)\,\mathbf{g}_k \right.\right. \\ &\qquad \left.\left. + \sum_{k=1}^{K}\sum_{l=2}^{L} a_{kl}\,b_k(n-1)\,\tilde{\mathbf{c}}_{kl}^{L} + \boldsymbol{\nu}(n)\right)\right]. \end{aligned} \tag{6.111}$$

Since $d_1(n)$ is uncorrelated with $b_k(n), k \neq 1$ and $b_k(n-1)$ for all values of k, this reduces to

$$\mathbf{p} = a_{11}\,\mathbf{g}_1 = a_{11}\,\hat{\mathbf{c}}_1. \tag{6.112}$$

Using Equation (6.112) and Equation (6.39) for $\mathbf{R}^{-1}$ in Equation (6.37), we get

$$\begin{aligned}
J_{\min} &= 1 - |a_{11}|^2 \, \hat{\mathbf{c}}_1^H \, \mathbf{R}^{-1} \, \hat{\mathbf{c}}_1 \\
&= 1 - \frac{\sigma_1^2}{\sigma_\nu^2} \, \hat{\mathbf{c}}_1^H \left[\mathbf{I}_N - \mathbf{Q} \left(\mathbf{Q}^H \, \mathbf{Q} + \frac{\sigma_\nu^2}{N \sigma_1^2} \, \mathbf{L}^{-1} \right)^{-1} \mathbf{Q}^H \right] \hat{\mathbf{c}}_1 \\
&= 1 - \frac{\sigma_1^2}{\sigma_\nu^2} \left[\gamma_m \, N - \gamma_m \, N \, \frac{\hat{\mathbf{c}}_1^H}{\sqrt{\gamma_m \, N}} \, \mathbf{Q} \right. \\
&\qquad \left. \cdot \left(\mathbf{Q}^H \, \mathbf{Q} + \frac{\sigma_\nu^2}{N \sigma_1^2} \, \mathbf{L}^{-1} \right)^{-1} \mathbf{Q}^H \, \frac{\hat{\mathbf{c}}_1}{\sqrt{\gamma_m \, N}} \right] \\
&= 1 - \gamma_m \, \gamma \left[1 - \frac{\hat{\mathbf{c}}_1^H}{\sqrt{\gamma_m \, N}} \, \mathbf{Q} \left(\mathbf{Q}^H \, \mathbf{Q} + \frac{1}{\gamma} \, \mathbf{L}^{-1} \right)^{-1} \mathbf{Q}^H \, \frac{\hat{\mathbf{c}}_1}{\sqrt{\gamma_m \, N}} \right] \\
&= 1 - \gamma_m \, \gamma \left[1 - \frac{\hat{\mathbf{c}}_1^H}{\sqrt{\gamma_m \, N}} \, \frac{\mathbf{Q}}{\sqrt{\gamma_m}} \right. \\
&\qquad \left. \cdot \left(\frac{1}{\gamma_m} \, \mathbf{Q}^H \, \mathbf{Q} + \frac{1}{\gamma_m \, \gamma} \, \mathbf{L}^{-1} \right)^{-1} \frac{\mathbf{Q}^H}{\sqrt{\gamma_m}} \, \frac{\hat{\mathbf{c}}_1}{\sqrt{\gamma_m \, N}} \right]
\end{aligned} \tag{6.113}$$

where we have used

$$\hat{\mathbf{c}}_1^H \, \hat{\mathbf{c}}_1 = \gamma_m \, N, \tag{6.114}$$

γ_m being the "gain" due to multipath[8]. The multipath "gain" is further analyzed in Section 6.9. In Equation (6.113), the SNR γ is as defined in Equation (6.44). Equation (6.51) may be used to evaluate $\mathbf{Q}^H \, \mathbf{Q}$, resulting in

$$\frac{1}{\gamma_m} \, \mathbf{Q}^H \, \mathbf{Q} = \frac{1}{\gamma_m \, N} \begin{bmatrix} \sum_{i=1}^{N} \hat{c}_{1,i}^2 & \sum_{i=1}^{N} \hat{c}_{1,i} \hat{c}_{2,i} & \cdots & \sum_{i=1}^{N} \hat{c}_{1,i} \hat{c}_{K_1,i} \\ \sum_{i=1}^{N} \hat{c}_{2,i} \hat{c}_{1,i} & \sum_{i=1}^{N} \hat{c}_{2,i}^2 & & \vdots \\ \vdots & & \ddots & \\ \sum_{i=1}^{N} \hat{c}_{K_1,i} \hat{c}_{1,i} & \cdots & & \sum_{i=1}^{N} \hat{c}_{K_1,i}^2 \end{bmatrix} \triangleq \mathbf{X}. \tag{6.115}$$

Thus, $\mathbf{X}$ is the matrix of crosscorrelations between the normalized effective spreading codes $\hat{c}_k / \sqrt{\gamma_m \, N}$ $(k = 1, 2, \ldots, K_1)$. The normalization is with respect to the 2-norm of $\hat{\mathbf{c}}_1$ given in Equation (6.114). Equation (6.54) provides the expression for $\mathbf{Q}^H \, \hat{\mathbf{c}}_1 / \sqrt{N}$, so

[8] γ_m reduces to 1 in the absence of multipath.

that

$$\frac{\mathbf{Q}^H}{\sqrt{\gamma_m}}\,\frac{\hat{\mathbf{c}}_1}{\sqrt{\gamma_m\,N}} = \frac{1}{\gamma_m\,N}\begin{bmatrix} \sum_{i=1}^{N}\hat{c}_{1,i}^2 \\ \sum_{i=1}^{N}\hat{c}_{1,i}\hat{c}_{2,i} \\ \vdots \\ \sum_{i=1}^{N}\hat{c}_{1,i}\hat{c}_{K_1,i} \end{bmatrix} \stackrel{\triangle}{=} \mathbf{x}. \tag{6.116}$$

$\mathbf{x}$ is the vector of crosscorrelations between the normalized spreading code of the desired user, $\hat{c}_1/\sqrt{\gamma_m\,N}$, and the normalized effective spreading codes of all the users, $\hat{c}_k/\sqrt{\gamma_m\,N}$ $(k = 1, 2, \ldots, K_1)$.

Using Equations (6.115) and (6.116) in Equation (6.113) yields

$$\begin{aligned} J_{\min} &= 1 - \gamma_m\,\gamma\left[1 - \mathbf{x}^H\left(\mathbf{X} + \frac{1}{\gamma_m\,\gamma}\,\mathbf{L}^{-1}\right)^{-1}\mathbf{x}\right] \\ &= 1 - \gamma_{\text{eff}}\left[1 - \mathbf{x}^H\left(\mathbf{X} + \frac{1}{\gamma_{\text{eff}}}\,\mathbf{L}^{-1}\right)^{-1}\mathbf{x}\right] \end{aligned} \tag{6.117}$$

where

$$\gamma_{\text{eff}} \stackrel{\triangle}{=} \gamma_m\,\gamma. \tag{6.118}$$

Equation (6.118) is identical to Equation (6.55) with the exception that γ_{eff} replaces γ. Hence γ_{eff} may be termed the "effective" SNR. Clearly, $\gamma_{\text{eff}} = \gamma$ in the absence of correlated multipath. An important difference between the two equations is, the elements of both $\mathbf{X}$ and $\mathbf{x}$ in Equation (6.118) are the normalized crosscorrelation values between the effective spreading code vectors defined in Equation (6.108), which include the effects of multipath, whereas the corresponding elements in Equation (6.55) do not include multipath effects. $\mathbf{L}$ is still defined as in Equation (6.32) but σ_k^2 is now defined by Equation (6.109).

6.9 Impact of Multipath on the MMSE

As seen in Section 6.8, multipath increases the effective SNR in the MMSE receiver but also increases interference. The increased interference comes from the uncorrelated portions of the multipath of the desired signal and the multipath components of the

MAI signals. Clearly, the gain is more when the multipath components are highly correlated with the first component, i.e., when the multipath delays are small compared with the symbol period. When there a is strong uncorrelated multipath component, it can harm the performance of the MMSE receiver. Thus, the propagation channel determines whether multipath contributes as a form of diversity or as increased interference. In this section, we consider a few examples and evaluate the impact of multipath on the performance of the MMSE receiver.

From Equation (6.114), γ_m is defined by

$$\begin{aligned}
\gamma_m &\triangleq \frac{1}{N}\,\hat{\mathbf{c}}_1^H\,\hat{\mathbf{c}}_1 \\
&= \frac{1}{N}\,\mathbf{g}_1^H\,\mathbf{g}_1 \\
&= \frac{1}{N}\left(\mathbf{c}_1+\sum_{l=2}^{L}\frac{a_{1l}}{a_{11}}\,\tilde{\mathbf{c}}_{1l}^R\right)^H\left(\mathbf{c}_1+\sum_{l=2}^{L}\frac{a_{1l}}{a_{11}}\,\tilde{\mathbf{c}}_{1l}^R\right) \\
&= \frac{1}{N}\left(\mathbf{c}_1^H\,\mathbf{c}_1+\sum_{l=2}^{L}\left|\frac{a_{1l}}{a_{11}}\right|^2(\tilde{\mathbf{c}}_{1l}^R)^H\,\tilde{\mathbf{c}}_{1l}^R+2\,\Re\left\{\sum_{l=2}^{L}\frac{a_{1l}}{a_{11}}\,\mathbf{c}_1^H\,\tilde{\mathbf{c}}_{1l}^R\right\}\right. \\
&\qquad \left.+\sum_{\substack{l=2\\ l\neq p}}^{L}\sum_{p=2}^{L}\frac{a_{1l}^*\,a_{1p}}{|a_{11}|^2}\,(\tilde{\mathbf{c}}_{1l}^R)^H\,\tilde{\mathbf{c}}_{1p}^R\right) \\
&= \underbrace{1}_{A}+\underbrace{\sum_{l=2}^{L}\left|\frac{a_{1l}}{a_{11}}\right|^2\frac{(N-m_{1l})}{N}}_{B}+\underbrace{\frac{2}{N}\,\Re\left\{\sum_{l=2}^{L}\frac{a_{1l}}{a_{11}}\sum_{i=m_{1l}+1}^{N}c_{1i}^*\,c_{1(i-m_{1l})}\right\}}_{C} \\
&\qquad \underbrace{+\frac{1}{N}\sum_{\substack{l=2\\ l\neq p}}^{L}\sum_{p=2}^{L}\frac{a_{1l}^*\,a_{1p}}{|a_{11}|^2}\sum_{i=\max(m_{1l},m_{1p})+1}^{N}c_{1(i-m_{1l})}^*\,c_{1(i-m_{1p})}}_{D}
\end{aligned} \tag{6.119}$$

The first term, labeled A, is the autocorrelation of the first component. The term labeled B is the sum of the autocorrelations of the correlated portion of each multipath component and is positive. C is the sum of the partial crosscorrelations between the first component and the correlated portion of each of the other components. The result of the inner summation can be either positive or negative. Finally, term D is the sum of the delayed multipath components. The result of the innermost summation can be positive or negative (for real spreading codes). Given the pseudorandom property of the spreading codes and the random nature of the delays, terms C and D are small compared with the sum of the first two terms and may be neglected when multipath components are separated by more than one chip period. Under this assumption, Equation (6.119)

may be approximated to

$$\gamma_m \approx 1 + \sum_{l=2}^{L} \left| \frac{a_{1l}}{a_{11}} \right|^2 \left(1 - \frac{m_{1l}}{N} \right). \tag{6.120}$$

While correlated multipath gives rise to the multipath gain discussed above, uncorrelated portions add up to form an interference signal (with code vector $\hat{\mathbf{c}}_{2K}$ in Equation (6.108)). Thus, interference exists even in the absence of MAI. We examine the impact of multipath interference in the absence of MAI. In this case, the matrix of crosscorrelations becomes

$$\mathbf{X} = \begin{bmatrix} 1 & \chi^* \\ \chi & 1 \end{bmatrix} \tag{6.121}$$

where χ is the normalized crosscorrelation between the sum of the correlated components of the desired signal, $\hat{\mathbf{c}}_1$, and the sum of its uncorrelated components, $\hat{\mathbf{c}}_2$, expressed as

$$\begin{aligned}
\chi &\triangleq \frac{1}{\gamma_m N} \hat{\mathbf{c}}_1^H \hat{\mathbf{c}}_2 \\
&= \frac{1}{\gamma_m N} \left(\mathbf{c}_1 + \sum_{l=2}^{L} \frac{a_{1l}}{a_{11}} \tilde{\mathbf{c}}_{1l}^R \right)^H \left(\sum_{p=2}^{L} a_{1p} \tilde{\mathbf{c}}_{1l}^L \right) \\
&= \frac{1}{\gamma_m N} \sum_{p=2}^{L} a_{1p} \mathbf{c}_1^H \tilde{\mathbf{c}}_{1l}^L + \frac{1}{\gamma_m N} \sum_{l=2}^{p-1} \sum_{p=3}^{L} \frac{a_{1l}^* a_{1p}}{a_{11}} (\tilde{\mathbf{c}}_{1l}^R)^H \tilde{\mathbf{c}}_{1l}^L \\
&= \frac{1}{\gamma_m N} \sum_{l=2}^{L} a_{1l} \sum_{i=1}^{m_{1l}} c_{1i}^* c_{1(N-m_{1l}+i)} \\
&\quad + \frac{1}{\gamma_m N} \sum_{p=3}^{L} \sum_{l=2}^{p-1} \frac{a_{1l}^* a_{1p}}{a_{11}} \sum_{i=1}^{m_{1p}-m_{1l}} c_{1i}^* c_{1(N-m_{1p}+m_{1l}+i)}.
\end{aligned} \tag{6.122}$$

In many cases, the second term is negligible when compared with the first. Then, an approximate version of the above expression is

$$\chi \approx \frac{1}{\gamma_m N} \sum_{p=2}^{L} a_{1p} \sum_{i=1}^{m_{1l}} c_{1i}^* c_{1(N-m_{1l}+i)}. \tag{6.123}$$

We now recall Equation (6.73), which is an approximate expression for the MMSE. To use this expression, $\mathbf{X}^{-1}$ must determined. We find

$$\mathbf{X}^{-1} = \begin{bmatrix} \frac{1}{1-|\chi|^2} & \frac{\chi}{1-|\chi|^2} \\ \frac{\chi}{1-|\chi|^2} & \frac{1}{1-|\chi|^2} \end{bmatrix} \tag{6.124}$$

and

$$\begin{aligned} J_{\min} &\approx \frac{1}{\gamma_{\text{eff}}}\,\tilde{x}_{11} - \frac{1}{\gamma_{\text{eff}}^2}\sum_{i=1}^{K_1}\eta_i\,|\tilde{x}_{1i}|^2 \\ &= \frac{1}{\gamma_{\text{eff}}}\,\frac{1}{1-|\chi|^2} - \frac{1}{\gamma_{\text{eff}}^2}\left(\frac{1}{(1-|\chi|^2)^2} + \frac{|a_{11}^2|\,|\chi|^2}{(1-|\chi|^2)^2}\right) \\ &= \frac{1}{\gamma_{\text{eff}}\,(1-|\chi|^2)} - \frac{1+|a_{11}^2|\,|\chi|^2}{\gamma_{\text{eff}}^2\,(1-|\chi|^2)^2}. \end{aligned} \tag{6.125}$$

Finally, if $|a_{11}^2|\,|\chi|^2 \ll \gamma_{\text{eff}}^2\,(1-|\chi|^2)^2$, Equation (6.125) may be further approximated as

$$J_{\min} \approx \frac{1}{\gamma\,\gamma_m\,(1-|\chi|^2)} - \frac{1}{(\gamma\,\gamma_m\,(1-|\chi|^2))^2}. \tag{6.126}$$

Recall that in the absence of multipath

$$J_{\min} \approx \frac{1}{\gamma} - \frac{1}{\gamma^2}. \tag{6.127}$$

Thus, with regard to the MMSE in the single-user case, multipath has the effect of multiplying the SNR γ by the factor $\gamma_m\,(1-|\chi|^2)$. $(1-|\chi|^2)$ may be identified as the "multipath loss factor" since it effectively causes a loss in the SNR due to uncorrelated multipath of the desired signal. Note that in Equation (6.122), χ is inversely scaled by γ_m. This implies that the larger the multipath gain γ_m, the smaller the loss due to multipath.

The preceding analysis is illustrated through several examples.

Example 1: A Two-Ray Channel

We consider the following Gold code of length 15:

$$\mathbf{c}_1 = \{1,1,-1,-1,1,-1,1,1,1,1,-1,1,-1,-1,1\}^T.$$

Let the received signal be sampled at two times the chip rate, so that $N = 30$. Consider a two-ray channel with the impulse response

$$h(k) = \delta(k) + 0.5\,e^{-j2\pi\frac{f_c}{f_s}m_{12}}\,\delta(k-m_{12})$$

where f_c is the carrier frequency, f_s is the sampling frequency, and m_{12} is the delay (in samples) of the second component. If $f_c = 2.05$ GHz, $f_s = 3.84$ Msamples/s, and

$m_{12} = 21$ (corresponding to a delay of 10.5 chip periods, i.e., a delay of about 5.5 μs), then the impulse response becomes

$$h(k) = \delta(k) + 0.5\, e^{-j5.8905}\, \delta(k - 21).$$

From this impulse response, we have

$$\begin{aligned} a_{11} &= 1, \\ a_{12} &= 0.5\, e^{-j5.8905}. \end{aligned}$$

Then,

$$\begin{aligned} \gamma_m &= 1 + \left(\frac{0.5}{1}\right)^2 \frac{30 - 21}{30} + \frac{2}{30}\, \Re\left\{ \frac{0.5\, e^{-j5.8905}}{1}\, 3 \right\} \\ &\approx 1 + 0.0750 + 0.0924 \\ &\approx 1.1674. \end{aligned}$$

On a decibel scale, the gain due to multipath is $\gamma_m \approx 0.67$ dB.

To determine the multipath loss factor, we first compute χ:

$$\begin{aligned} \chi &= \frac{1}{(1.1674)(30)}\, 0.5\, e^{-j5.8905}\, (-5) \\ &= -0.0660 - j\, 0.0273. \end{aligned} \tag{6.128}$$

The loss factor is $1 - |\chi|^2 = 0.9949$, which corresponds to approximately -0.02 dB. Thus, the overall gain with multipath is about 0.65 dB.

We now evaluate the multipath gain when the delay is changed to 11 samples, i.e., $m_{12} = 11$, which corresponds to 5.5 chip periods or about 2.9 μs. In this case,

$$a_{12} = 0.5\, e^{-j2.4871}$$

and

$$\begin{aligned} \gamma_m &= 1 + \left(\frac{0.5}{1}\right)^2 \frac{30 - 11}{30} + \frac{2}{30}\, \Re\left\{ \frac{0.5\, e^{-j2.4871}}{1}\, (-3) \right\} \\ &\approx 1 + 0.1583 + 0.0793 \\ &\approx 1.2377. \end{aligned}$$

Thus, the multipath gain is $\gamma_m \approx 0.93$ dB in this case.

Further,

$$\begin{aligned}\chi &= \frac{1}{(1.2377)(30)}\,0.5\,e^{-j2.4871}\,(1) \\ &= -0.0107 - j\,0.0082. \end{aligned} \tag{6.129}$$

The loss factor is then $1 - |\chi|^2 = 0.9998$, i.e., approximately -0.0008 dB, which is negligible. The overall gain due to multipath remains at approximately 0.93 dB. The above results reinforce the intuitive notion that the higher the multipath gain γ_m, the lower the loss factor $1 - |\chi|^2$.

In both of the above cases for the two different multipath delays, the third term in Equation (6.119) is negligible compared with the sum of the first two terms, thus validating the approximation of Equation (6.120). Furthermore, uncorrelated multipath causes negligible degradation and the overall gain is close to γ_m.

Figure 6.4 illustrates how the multipath gain varies with the delay of the second multipath component. The figure demonstrates that for a given set of parameters, such as the carrier frequency, sample rate, and the spreading code, the multipath gain is not a monotonic function of the delay. The gain can differ significantly for a change in delay by a single sample. The variation of the MMSE with the multipath delay is shown in Figure 6.5 where the approximate expressions of Equations (6.126) and (6.127) have been used. This figure demonstrates the improvement in MMSE due to multipath. It can be seen that multipath does not always yield a gain. For a multipath delay of 16 samples, for example, the improvement is almost 0 dB. For a multipath delay of 29 samples, there is a degradation of the MMSE due to the highly uncorrelated multipath causing a greater loss than the gain it yields.

The variation of the *average* MMSE over a set of fifteen Gold codes with the delay of the multipath component is illustrated in Figure 6.6. As expected, the average MMSE exhibits a decreasing trend with increasing multipath delay, a result of the increasing multipath gain. It is interesting to note that the MMSE increases by about 1 dB when the delay is reduced from two samples to one sample, which is a result of the increase in the degree of correlation between the two multipath components.

Example 2: The COST-207 Rural Channel

In this example, the multipath gain is evaluated for the COST-207 Rural channel model [97]. The impulse response of this channel is provided by Table 6.1. The impulse response of the channel, after rounding the delays to the nearest sample, is

$$\begin{aligned} h(k) &= \delta(k) + 0.7937\,e^{-j5.3669}\,\delta(k-1) \\ &\quad + 0.3162\,e^{-j4.4506}\,\delta(k-2) + 0.1\,e^{-j4.4506}\,\delta(k-2) \end{aligned}$$

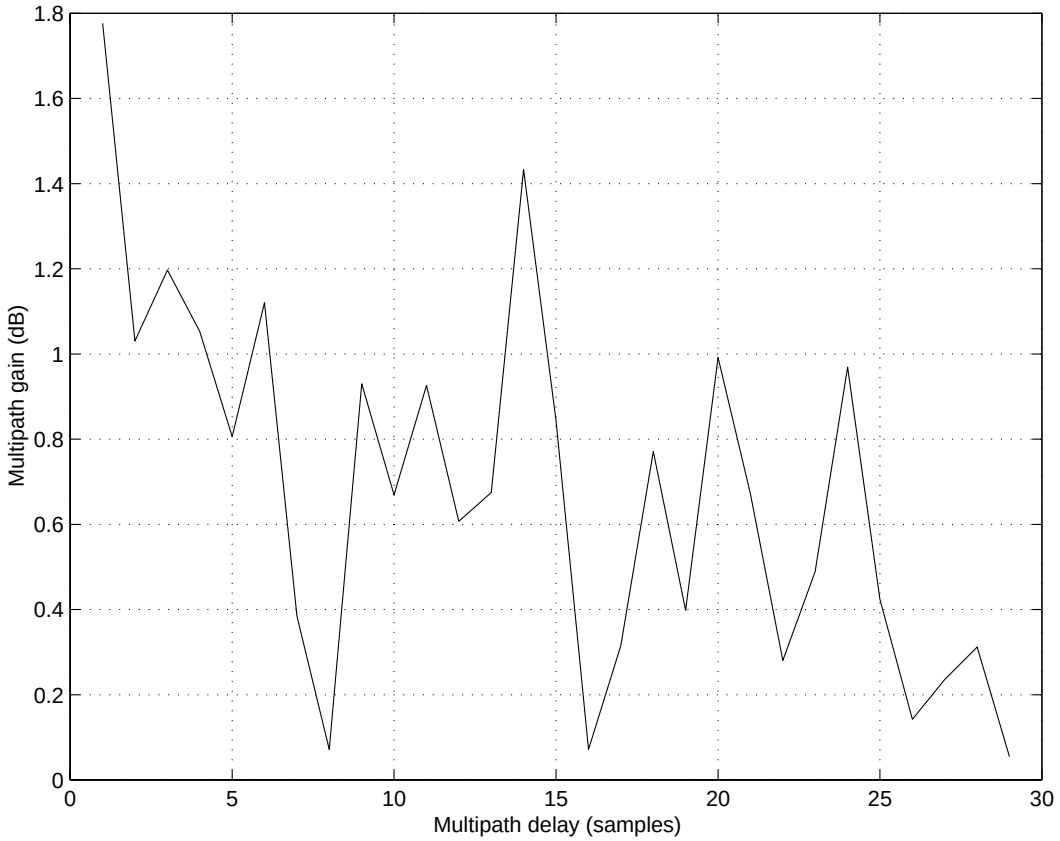

Figure 6.4: Variation of Multipath Gain with Multipath Delay for the Chosen Gold Code.

$$= \delta(k) + 0.7937\, e^{-j5.3669}\, \delta(k-1) + 0.4162\, e^{-j4.4506}\, \delta(k-2).$$

Therefore, we have

$$\begin{aligned} a_{11} &= 1, \\ a_{12} &= 0.7937\, e^{-j5.3669}, \\ a_{13} &= 0.4162\, e^{-j4.4506}, \end{aligned}$$

so that

$$\begin{aligned} \gamma_m &= 1 + \left[\left(\frac{0.7937}{1} \right)^2 \frac{30-1}{30} + \left(\frac{0.4162}{1} \right)^2 \frac{30-2}{30} \right] \\ &\quad + \frac{2}{30}\, \Re \left\{ \frac{0.7937\, e^{-j5.3669}}{1}\, (13) + \frac{0.4162\, e^{-j4.4506}}{1}\, (-4) \right\} \end{aligned}$$

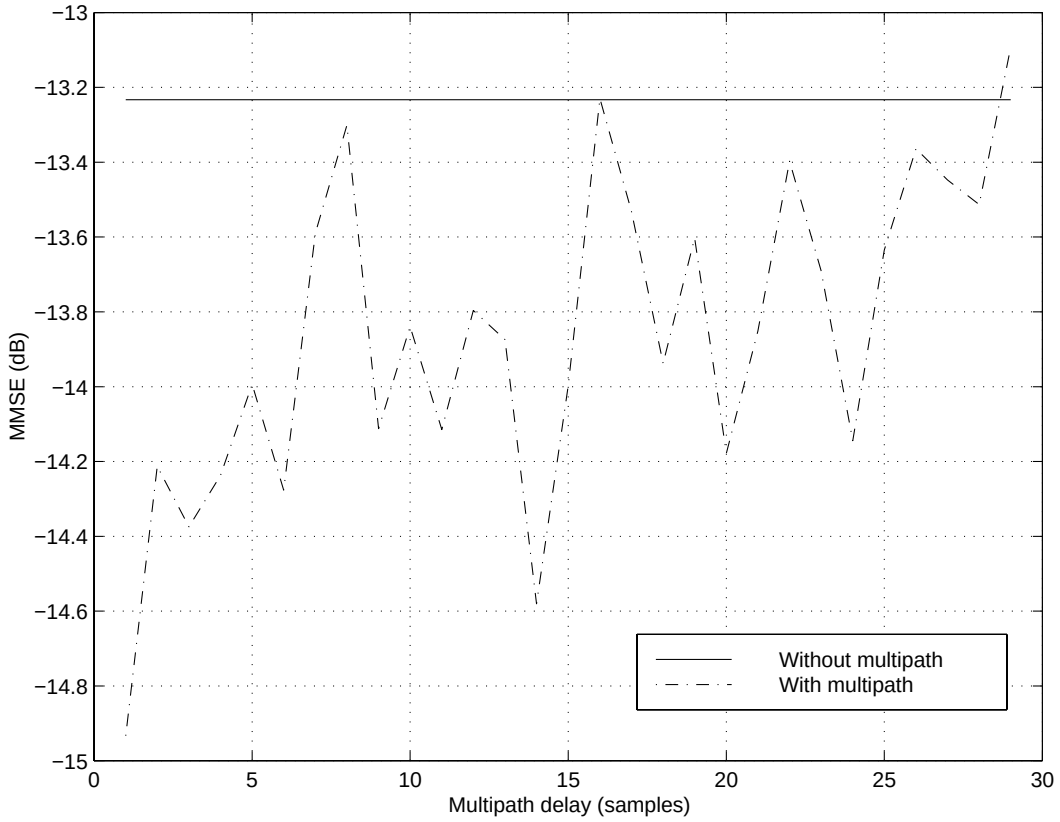

Figure 6.5: Variation of the MMSE with Multipath Delay for the Chosen Gold Code.

$$
\begin{aligned}
&+ \frac{1}{30}\left[\frac{0.7937\, e^{j5.3669}\, 0.4162\, e^{-j4.4506}}{1}\,(12)\right. \\
&\qquad\left. + \frac{0.4162\, e^{j4.4506}\, 0.7937\, e^{-j5.3669}}{1}\,(12)\right] \\
\approx\ & 1 + 0.7706 + 0.4475 + 0.1609 \\
\approx\ & 2.3790.
\end{aligned}
$$

That is, the gain is $\gamma_m \approx 3.76$ dB, which is significant. Such a large multipath gain is due to the highly correlated nature of the multipath, since all three delayed components arrive within one chip period of the first component. In this case, it is important to note that the terms C and D in Equation (6.119) are not insignificant compared with the sum of the first two terms. Term C is due to the crosscorrelation between the first component and other components and is substantial due to the large correlation between the first two components, since the second component has a delay of half a chip period. Term D is due to the crosscorrelation between the second and third effective components and is

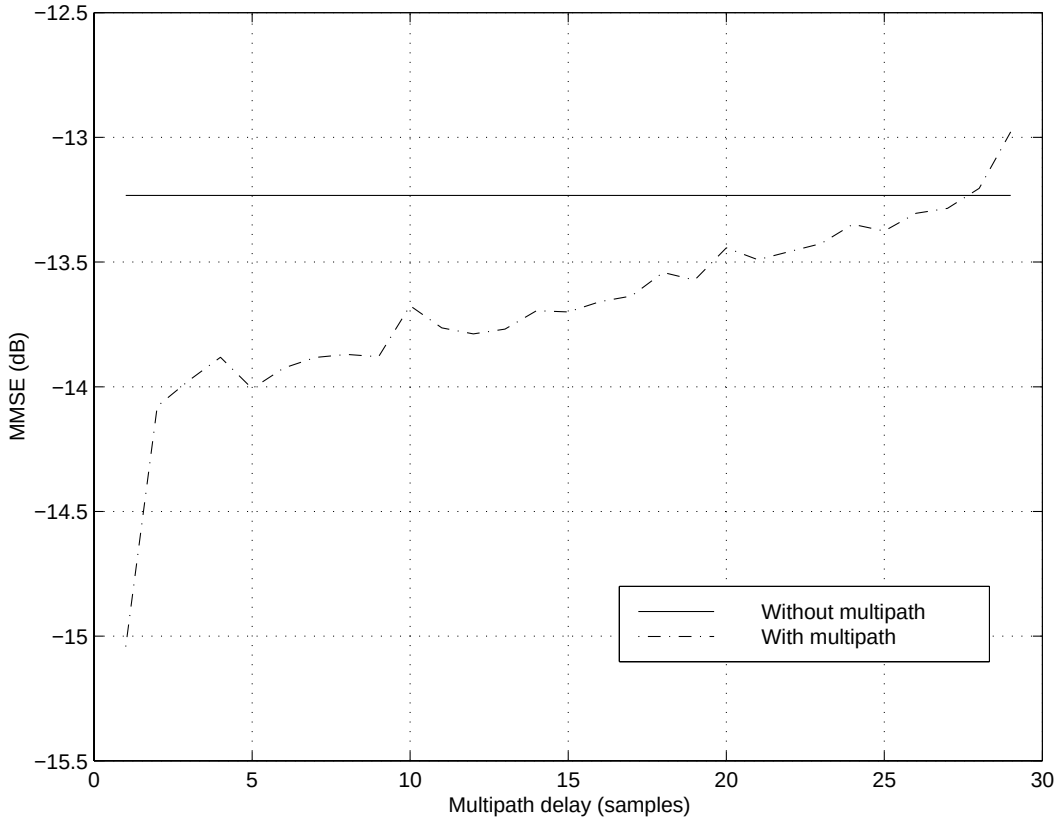

Figure 6.6: Variation of the MMSE Averaged over a Set of Fifteen Gold Codes with Multipath Delay.

large despite their relatively small magnitudes because of the large correlation between them, since the third component is half a chip behind the second component.

In this case, we have

$$\begin{aligned}\chi &= \frac{1}{(2.3790)(30)}\left[0.7937\,e^{-j5.3669}\,(1) + 0.4162\,e^{-j4.4506}\,(2)\right] \\ &\quad + \frac{1}{(2.3790)(30)}\left[\frac{0.7937\,e^{-j5.3669}\,0.4162\,e^{-j4.4506}}{1}\,(1)\right] \\ &\approx (0.0038 + j\,0.0201) + (0.0028 + j\,0.0037) \\ &\approx 0.0066 + j\,0.0238.\end{aligned}$$

The loss factor is $1 - |\chi|^2 = 0.9994$, i.e., approximately -0.003 dB. The loss due to multipath is again negligible and the overall gain is about 3.76 dB. The multipath delays

Table 6.1: COST-207 Rural Channel Model Parameters

Multipath Delay (μs)	**Multipath Amplitude**
0.0	1.0
0.2	0.7937
0.4	0.3162
0.6	0.1

Table 6.2: COST-207 Urban Channel Model Parameters

Multipath Delay (μs)	**Multipath Amplitude**
0.0	0.7071
0.2	1.0
0.6	0.7937
1.6	0.5
2.4	0.4
5.0	0.3162

are very small and as a result, there is substantial gain and only an insignificant loss due to multipath.

Example 3: The COST-307 Urban Channel

We now evaluate the multipath gain for the COST-207 Urban channel [97] described by Table 6.2. This yields the impulse response

$$\begin{aligned} h(k) &= 0.7071\,\delta(k) + e^{-j5.3669}\,\delta(k-1) + 0.7937\,e^{-j4.4506}\,\delta(k-2) \\ &\quad + 0.5\,e^{-j0.7854}\,\delta(k-6) + 0.4\,e^{-j4.3197}\,\delta(k-9) \\ &\quad + 0.3162\,e^{-j1.4399}\,\delta(k-19) \end{aligned}$$

and

$$\begin{aligned} a_{11} &= 0.7071, \\ a_{12} &= e^{-j5.3669}, \\ a_{13} &= 0.7937\,e^{-j4.4506}, \end{aligned}$$

$$
\begin{aligned}
a_{14} &= 0.5\,e^{-j0.7854}, \\
a_{15} &= 0.4\,e^{-j4.3197}, \\
a_{16} &= 0.3162\,e^{-j1.4399}.
\end{aligned}
$$

Therefore,

$$
\begin{aligned}
\gamma_m &= 1 + \left[\left(\frac{1}{0.7071}\right)^2 \frac{30-1}{30} + \left(\frac{0.7937}{0.7071}\right)^2 \frac{30-2}{30} + \left(\frac{0.5}{0.7071}\right)^2 \frac{30-6}{30}\right. \\
&\qquad \left. + \left(\frac{0.4}{0.7071}\right)^2 \frac{30-9}{30} + \left(\frac{0.3162}{0.7071}\right)^2 \frac{30-19}{30}\right] \\
&\quad + \frac{2}{30}\Re\left\{\frac{e^{-j5.3669}}{0.7071}(13) + \frac{0.7937\,e^{-j4.4506}}{0.7071}(-4) + \frac{0.5\,e^{-j0.7854}}{0.7071}(4)\right. \\
&\qquad \left. + \frac{0.4\,e^{-j4.3197}}{0.7071}(-5) + \frac{0.3162\,e^{-j1.4399}}{0.7071}(1)\right\} \\
&\quad + \frac{1}{30}\sum_{\substack{l=2 \\ l\neq p}}^{6}\sum_{p=2}^{6} \frac{a_{1l}^* a_{1p}}{(0.7071)^2} \sum_{i=\max(m_{1l},m_{1p})+1}^{30} c_{1(i-m_{1l})}^* c_{1(i-m_{1p})} \\
&\approx 1 + 3.8067 + 1.0330 + 0.4362 \\
&\approx 6.2758.
\end{aligned}
$$

On a decibel scale, $\gamma_m \approx 7.98$ dB. This is a very large gain due to strong multipath. Note that two of the delayed components are stronger than the first component. Here again, terms C and D are not insignificant because of the high crosscorrelation between components that are within a chip period of each other.

We now compute the loss factor.

$$
\begin{aligned}
\chi &= \frac{1}{(6.2758)(30)}\left[e^{-j5.3669}(1) + 0.7937\,e^{-j4.4506}(2) + 0.5\,e^{-j0.7854}(-6)\right. \\
&\qquad \left. + 0.4\,e^{-j4.3197}(3) + 0.3162\,e^{-j1.4399}(-3)\right] \\
&\quad + \frac{1}{(6.2758)(30)}\sum_{p=3}^{6}\sum_{l=2}^{p-1} \frac{a_{1l}^* a_{1p}}{1} \sum_{i=1}^{m_{1p}-m_{1l}} c_{1i}^* c_{1(N-m_{1p}+m_{1l}+i)} \\
&\approx (-0.0133 - j\,0.0345) + (-0.0033 - j\,0.0068) \\
&\approx -0.0166 - j\,0.0413. \qquad (6.130)
\end{aligned}
$$

The loss factor is, therefore, $1 - |\chi|^2 = 0.9980$, which corresponds to about -0.009 dB. Again, the loss factor is negligible and the overall gain is approximately 7.97 dB. In this example, the insignificant loss factor is not a result of small multipath delays but rather due to the large multipath gain.

It is interesting to note that the multipath gain can be greater when multipath components are not resolvable in the conventional sense, i.e., when multipath delay is less than a chip period, as demonstrated in Example 1. Furthermore, a strong crosscorrelation between components can also lead to a reduction of the overall gain when it has canceling effect, i.e., when their phase relationship is such that the crosscorrelation between them is negative.

The examples discussed above demonstrate how multipath improves the effective SNR by yielding a multipath gain. The correlated portions of the multipath provide this gain, whereas the uncorrelated portions cause interference to the desired signal. In the single-user case, the degradation due to the uncorrelated multipath can be characterized in the form of a loss factor. As the examples showed, this degradation is often negligible. Multipath components of the MAI signals cause additional interference, which further degrades the MMSE. The impact of multipath components of the MAI is more serious because these components are entirely uncorrelated with the desired signal. Rather than provide specific examples to examine this degradation, we point the interested reader to [55], where the BER performance of adaptive MMSE receivers for various multipath channels has been demonstrated.

6.10 Summary

Although the minimum mean-squared error (MMSE) achieved by the adaptive receiver has been investigated in the literature, there is a need to study the dependence of the MMSE on the crosscorrelations between the spreading codes of the users in the system. An additive white Gaussian noise channel model for the code division multiple access system was described. The asynchronous interference signal vectors were modeled as contributions due to equivalent synchronous spreading code vectors. An expression for the correlation matrix of the input signal matrix was obtained. Using this, the MMSE was expressed in terms of the signal-to-noise ratio of the desired signal, the matrix of correlations between the effective spreading codes, and the diagonal matrix whose diagonal elements are equal to signal-to-interference power ratios. Using reasonable assumptions of the relationship between these parameters, the von Neumann series was used to simplify the expression for the MMSE. This series was further used to show how the MMSE receiver is near-far resistant. A similar analysis was performed for the matched filter receiver to show that the receiver lacks near-far resilience. An expression for the MMSE for multipath channels was derived following the principles of the previous analysis. This analysis demonstrated how correlated multipath improves the receiver signal-to-noise ratio in the form of a "multipath gain." An expression for the multipath gain was derived. The "loss factor," which accounts for the degradation due to multipath in the single-user case was examined. Several examples were presented to illustrate the impact of multipath. The multipath gain was seen to be significant in the Urban channel, which is character-

ized by strong multipath. Thus, the analysis presented here examines the dependence of the MMSE of the MMSE receiver on channel characteristics, such as the signal-to-noise ratio of the desired signal, the crosscorrelations between the effective spreading codes, the interference-to-signal power ratios of the MAI signals, and multipath characteristics.

Chapter 7

Adaptive MMSE Receiver for Multi-Rate Systems

7.1 Introduction

The MMSE receiver has been proposed and extensively studied for use in CDMA systems in which the signals are COP or modulation-on-symbol where the same spreading code repeats for every transmitted symbol and the code lengths of all the users are equal. The reason for this assumption is obvious: conventional CDMA systems investigated in the literature fall under this category. Furthermore, this assumption applied to deriving the optimal time-varying receiver leads to a highly simplified implementation, a fractionally spaced FIR filter, which has been comprehensively analyzed for channel equalization. The simplification results from the ability to sample the receiver output only once every symbol period of the desired signal, which is also equal to the symbol period of each interference signal (cf. Chapter 3).

The interest in CDMA systems with different data rates and unequal code lengths is growing. Of particular relevance is the development of third generation PCS systems, which hope to provide a wide range of data rates with variable quality of service [2, 4, 101, 102]. In such systems, the cyclostationary properties of the signals of the different users in the system vary, resulting in the breakdown of the assumptions that lead to the simple complex FIR filter being the optimum TDAF structure. Consequently, a single FIR filter yields a highly degraded performance when interference signals have dissimilar rate parameters.

A heuristic explanation for the performance degradation is that interference patterns do not remain constant over successive symbol intervals, and the adaptive receiver has to overcome a much higher number of effective interference signals, which it can do only to a certain extent. This is illustrated through Figure 7.1. The figure shows four users, each

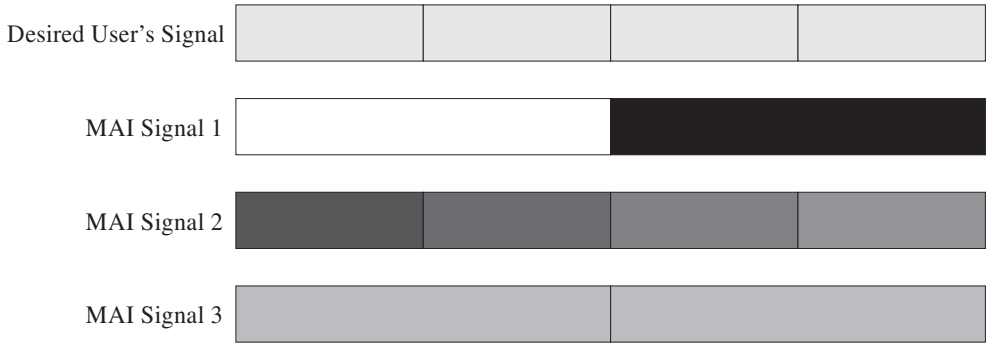

Figure 7.1: Example of a Multi-Rate CDMA System. Each block represents a symbol, each shade represents a unique spreading code segment.

with a different type of spread signal. The desired user's signal is COP. The first MAI signal has double the symbol period and four times the code length of the desired user. The symbol period of the second MAI signal is equal to that of the desired user, while its code length is also equal to four times that of the desired user's signal or four times its own symbol period. Finally, the third MAI signal is also COP, but its code length is twice that of the desired user's signal. Looking at the figure, it is easy to see that the receiver sees different MAI patterns during four successive symbol periods. It sees four interference patterns due to each of the first two MAI signals and two interference patterns due to the third MAI signal. Thus, an adaptive receiver with an input signal window equal to one symbol period has to overcome *ten* different interference patterns, not three. The limited degrees of freedom in the adaptive receiver prevent it from easily surmounting this problem. Thus, the performance deteriorates rapidly with increasing users in the system. Asynchronous channels pose an even bigger challenge because of the increased number of effective interference patterns to be suppressed.

Interest in an adaptive receiver for such a scenario is also spawned in ad hoc networks with little coordination between users in the system, precluding the use of multi-user receivers that exploit the knowledge of signal parameters. This chapter presents the optimum receiver structure for a given CDMA environment and demonstrates its performance through simulation results for a variety of signal environments.

7.2 System Description

The system is assumed to consist of K users. The spreading code of the kth user contains N_k chips. If $T_{c,k}$ is the chip interval for the kth user's signal, T_s is the sampling interval,

and $N_{s,k}$ is the corresponding number of samples/chip, then

$$T_{c,k} = N_{s,k}\, T_s, \qquad k = 1, 2, \ldots, K. \tag{7.1}$$

The code repetition period of the kth user is

$$T_{r,k} = N_k T_{c,k} = N_k N_{s,k}\, T_s. \tag{7.2}$$

Furthermore, it is assumed that the code length for any user is an integer multiple of the processing gain S_k. If $N_{b,k}$ is the number of samples per symbol period of the kth user, then

$$N_{b,k} = S_k N_{s,k}. \tag{7.3}$$

7.3 Derivation of the Optimum Time-Variant Filter

From Equation (3.63), we find that the cycle frequencies of the kth user's signal are given by

$$\tilde{\alpha}_k = \frac{p}{N_k N_{s,k} T_s} \tag{7.4}$$

for all integer values of p. The fundamental cycle frequency α_0 is such that all other cycle frequencies are its integer multiples. Therefore, the fundamental cycle frequency is given by

$$\alpha_0 = \frac{1}{M T_s} \tag{7.5}$$

where M is the least common multiple (LCM) of $N_1 N_{s,1}, N_2 N_{s,2}, \ldots, N_K N_{s,K}$. The set of cycle frequencies is

$$\bar{\alpha} = \left\{ 0, \frac{1}{MT_s}, \frac{2}{MT_s}, \ldots, \frac{(M-1)}{MT_s} \right\}. \tag{7.6}$$

Using Equation (3.65), the signal at the output of the optimal time-variant filter at time instant m may be expressed as

$$z(m) = \sum_{i=0}^{M-1} \sum_{l=0}^{N_F-1} w_i(l)\, r(m-l)\, e^{j2\pi \frac{i}{MT_s}(m-l)T_s} \tag{7.7}$$

where N_F is the length of each of the FIR filters, $w_i(m)$ is the ith filter's impulse response at time instant m, and $r(m)$ is the sampled received signal at time instant m. Thus, the output signal $z(m)$ is produced at the sampling rate. However, it is sufficient for the filter output $z(m)$ to be optimum only once every symbol period of the desired user, since this output sample can be used to make a decision on the symbol. Therefore, the output signal is sampled once every $N_{b,1}$ samples, i.e., for $m = N_{b,1}n$ where n is an integer. This sampled estimated signal $y(n) = z(N_{b,1}n)$ is given by

$$\begin{aligned} y(n) &= \sum_{i=0}^{M-1} \sum_{l=0}^{N_F-1} w_i(l)\, r(nN_{b,1} - l)\, e^{j2\pi \frac{i}{M}(nN_{b,1}-l)}, && (7.8) \\ &= \sum_{l=0}^{N_F-1} r(nN_{b,1} - l) \sum_{i=0}^{M-1} w_i(l)\, e^{j2\pi \frac{i}{M}(nN_{b,1}-l)}. && (7.9) \end{aligned}$$

Noting that M is an integer multiple of $N_{b,1}$, we may define an integer L such that

$$M = L\, N_{b,1}. \tag{7.10}$$

Further defining integers p and q such that

$$i = qL + p, \tag{7.11}$$

we may rewrite the inner summation in Equation (7.9) as

$$\begin{aligned} \sum_{i=0}^{M-1} w_i(l)\, e^{j2\pi \frac{i}{M}(nN_{b,1}-l)} &= \sum_{q=0}^{N_{b,1}-1} \sum_{p=0}^{L-1} w_{qL+p}(l)\, e^{j\frac{2\pi}{M}(nN_{b,1}-l)(qL+p)} \\ &= \sum_{q=0}^{N_{b,1}-1} \sum_{p=0}^{L-1} w_{qL+p}(l)\, e^{j\frac{2\pi}{M}qmM}\, e^{-j\frac{2\pi}{M}lqL}\, e^{j\frac{2\pi}{M}(nN_{b,1}-l)p}. \end{aligned}$$

Since $e^{j\frac{2\pi}{M}qmM} = 1$, the above equation simplifies to

$$\begin{aligned} \sum_{i=0}^{M-1} w_i(l)\, e^{j2\pi \frac{i}{M}(nN_{b,1}-l)} &= \sum_{p=0}^{L-1} \sum_{q=0}^{N_{b,1}-1} w_{qL+p}(l)\, e^{-j\frac{2\pi}{N_{b,1}}lq}\, e^{j\frac{2\pi}{M}(nN_{b,1}-l)p} \\ &= \sum_{p=0}^{L-1} \tilde{w}_p(l)\, e^{j\frac{2\pi}{M}(nN_{b,1}-l)p} && (7.12) \end{aligned}$$

where we define

$$\tilde{w}_p(l) \triangleq \sum_{q=0}^{L-1} w_{qL+p}(l)\, e^{-j\frac{2\pi}{N_{b,1}}lq}. \tag{7.13}$$

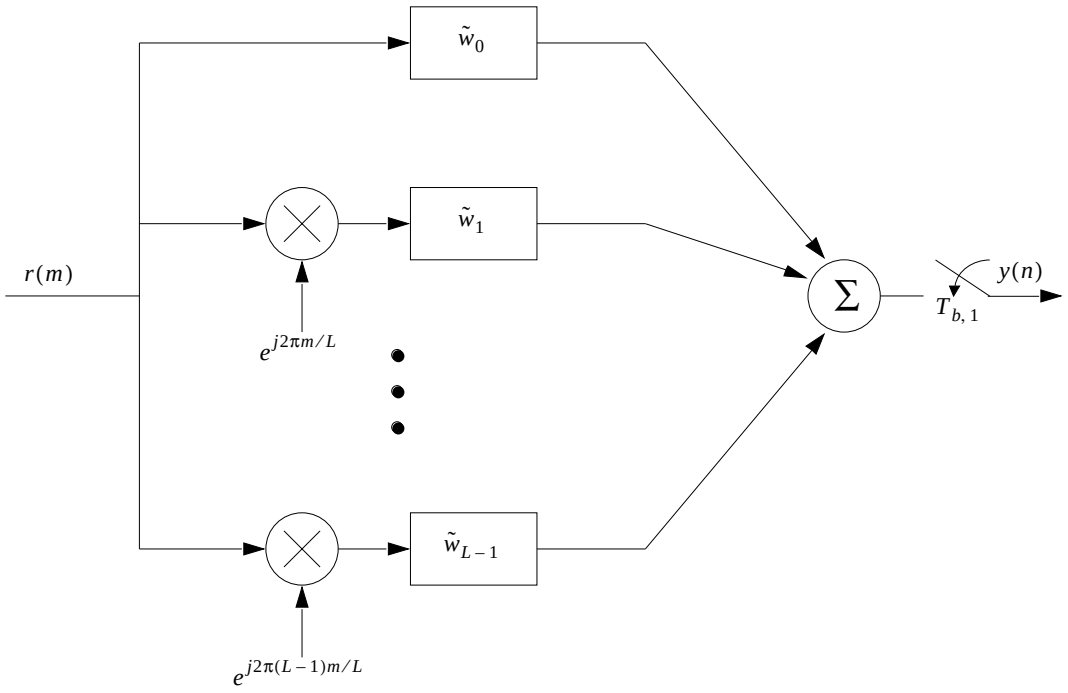

Figure 7.2: FRESH Filter Implementation of TDAF for System with Multiple Rates and Code Lengths.

Using Equation (7.12) in Equation (7.9), we get

$$\begin{aligned} y(n) &= \sum_{l=0}^{N_F-1} r(nN_{b,1}-l) \sum_{p=0}^{L-1} \tilde{w}_p(l)\, e^{j\frac{2\pi}{M}(nN_{b,1}-l)p} \\ &= \sum_{p=0}^{L-1} \sum_{l=0}^{N_F-1} \tilde{w}_p(l)\, r(nN_{b,1}-l)\, e^{j\frac{2\pi}{M}(nN_{b,1}-l)p} \\ &= \sum_{p=0}^{L-1} \left[r(nN_{b,1})\, e^{j\frac{2\pi}{M}npN_{b,1}} \right] \otimes \tilde{w}_p(nN_{b,1}) \\ &= \sum_{p=0}^{L-1} \left[r(nN_{b,1})\, e^{j\frac{2\pi}{L}np} \right] \otimes \tilde{w}_p(nN_{b,1}). \end{aligned} \tag{7.14}$$

The above equation may be recognized as a periodically time-varying filtering operation. The FRESH filter implementation of this filtering operation is depicted in Figure 7.2.

We show below that Equation (7.14) can be rewritten in the form

$$y(n) = \sum_{p=0}^{L-1} \left[r(nN_{b,1}) \otimes h_p(nN_{b,1}) \right] \, \delta_p(n), \tag{7.15}$$

where

$$\delta_p(n) \stackrel{\triangle}{=} \begin{cases} 1, & n = p, p \pm L, p \pm 2L, \ldots, \\ 0, & \text{otherwise}, \end{cases} \tag{7.16}$$

and $h_p(\cdot)$ is the impulse response of the pth filter. We follow the analysis in [103]. Noting that $\delta_p(n)$ may be represented by

$$\delta_p(n) = \frac{1}{L} \sum_{i=0}^{L-1} e^{j\frac{2\pi}{L} i(n-p)}, \tag{7.17}$$

we may rewrite Equation (7.15) as

$$y(n) = \sum_{p=0}^{L-1} \left[r(nN_{b,1}) \otimes h_p(nN_{b,1}) \right] \cdot \frac{1}{L} \sum_{i=0}^{L-1} e^{j\frac{2\pi}{L} i(n-p)}. \tag{7.18}$$

Taking z-transforms on both sides yields

$$\begin{aligned} Y(z) &= \frac{1}{L} \sum_{i=0}^{L-1} \sum_{p=0}^{L-1} e^{-j\frac{2\pi}{L} ip} \sum_{n=-\infty}^{\infty} \left[r(nN_{b,1}) \otimes h_p(nN_{b,1}) \right] \, e^{j\frac{2\pi}{L} in} \, z^{-n} \\ &= \frac{1}{L} \sum_{i=0}^{L-1} \sum_{p=0}^{L-1} e^{-j\frac{2\pi}{L} ip} \, R(z\, e^{-j\frac{2\pi}{L} i}) \, H_p(z\, e^{-j\frac{2\pi}{L} i}) \end{aligned} \tag{7.19}$$

where $R(z)$ and $H_p(z)$ are the z-transforms of $r(nN_{b,1})$ and $h_p(nN_{b,1})$, respectively. This expression may be rewritten as

$$Y(z) = \sum_{i=0}^{L-1} R(z\, e^{-j\frac{2\pi}{L} i}) \, \frac{1}{L} \sum_{p=0}^{L-1} H_p(z\, e^{-j\frac{2\pi}{L} i}) \, e^{-j\frac{2\pi}{L} ip}. \tag{7.20}$$

Now taking inverse z-transforms on both sides, we get

$$y(n) = \sum_{i=0}^{L-1} \left[r(nN_{b,1}) \, e^{j\frac{2\pi}{L} in}) \right] \otimes \left[\frac{1}{L} \sum_{p=0}^{L-1} h_p(nN_{b,1}) \, e^{j\frac{2\pi}{L} i(n-p)} \right]. \tag{7.21}$$

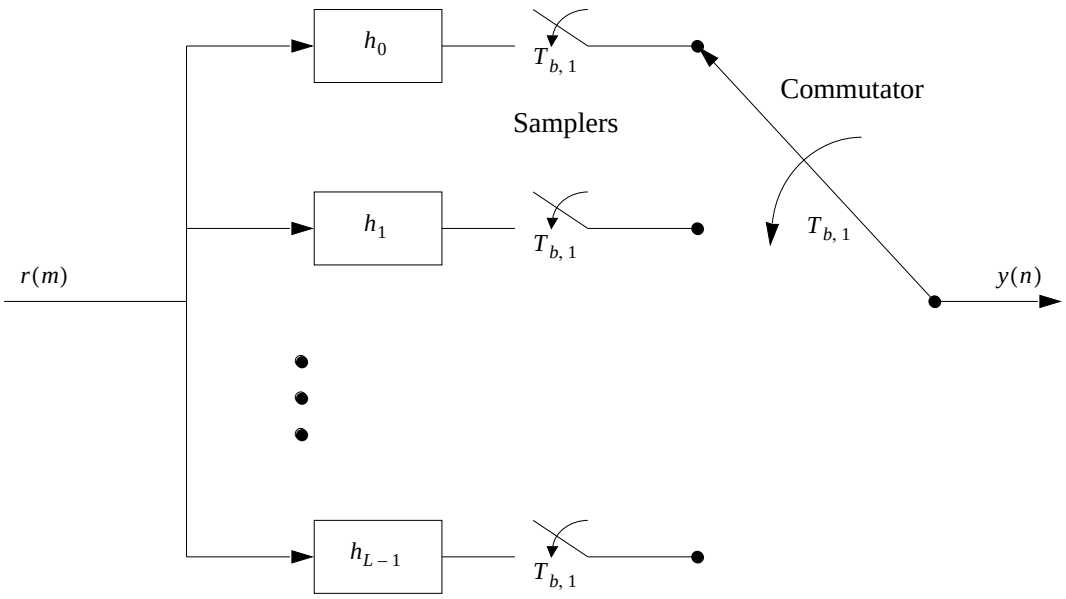

Figure 7.3: Filter Bank Implementation of TDAF for System with Multiple Rates and Code Lengths.

Defining

$$\tilde{w}_i(nN_{b,1}) \triangleq \frac{1}{L}\sum_{p=0}^{L-1} h_p(nN_{b,1})\, e^{j\frac{2\pi}{L}i(n-p)} \tag{7.22}$$

and changing the dummy variable i to p, we get Equation (7.14). We have thus proved that Equations (7.14) and (7.15) are equivalent.

The implementation of Equation (7.15) is illustrated in Figure 7.3. The receiver consists of a bank of filters. There are L filters in the filter bank, and the sampling of the output of successive filters is staggered by the symbol period of the desired user, $T_{b,1}$, or $N_{b,1}$ samples. Thus, each filter is sampled once every M samples. A commutator selects the sampled symbol estimate and passes it on to the decision device. This structure is intuitively satisfying because there are as many filters as the number of *distinct* aggregate interference patterns and each filter operates on a different periodically repeating aggregate interference pattern. A transmultiplexer implementation of this periodically time-varying filter can be realized [103].

7.4 Comparison of MMSEs of a Filter Bank and a Single Filter for Multi-Rate Systems

7.4.1 Analytical Model

The received signal is the sum of K transmitted signals, the kth signal having the attributes described in Section 7.2. An AWGN channel is considered. The vector of received signal samples is represented as in Equation (6.13) by

$$\mathbf{r}(n) = \sum_{k=1}^{K} \sqrt{\frac{P_k}{2}}\, b_k(n)\, e^{j\psi_k}\, \tilde{\mathbf{c}}_k(n) + \boldsymbol{\nu}(n) \tag{7.23}$$

where P_k is the received power of the kth user's signal, $b_k(n)$ is the *apparent* symbol of the kth user, $\tilde{\mathbf{c}}_k(n)$ is the code *segment*[1] of the kth user at the nth instant, and $\boldsymbol{\nu}(n)$ is the vector of noise samples with variance σ_ν^2. We make the following assumptions that make the analysis in this section tractable.

Assumption 1 The transmission of each user is COP, i.e., $N_k = S_k$.

Assumption 2 The signals are synchronous, i.e., the symbols of all the users begin coincidentally every M samples where M is as defined in Section 7.3. Thus, starting from time instant zero, every M samples contain an integer number of *complete* symbols of all users.

Assumption 3 The length of the spreading code of the kth signal is an integer multiple L_k of the length of the desired signal's spreading code. Therefore, $b_k(n)$ remains constant for L_k successive code periods of the desired signal, during which the receiver sees L_k different code segments from the kth user.

Although the above assumptions simplify the analytical representation of signals and make the analysis less general, they do not devalue the results of this section, which seeks to draw a comparison between the MMSEs of two different receivers when signals have different rates. The general asynchronous case can be worse than those falling within the purview of the above assumptions but is exemplified well by the results of this section. The above assumptions are for the purpose of tractable MMSE analysis in this section only; the BER performance of the receivers is investigated through simulations for both synchronous and asynchronous channels in Section 7.6.

[1]Since the spreading code repetition period, $T_{r,k}$, of the kth user is different, in general, from the desired user's code repetition period, the receiver sees a number of different segments of the kth user's code, each of which repeats periodically.

7.4.2 MMSE of the Single Filter Receiver

Following a development similar to that in Section 6.3, the correlation matrix may be expressed in the form

$$\mathbf{R} = \sum_{k=1}^{K} \frac{P_k}{2} \mathbf{R}_k + \sigma_\nu^2 \mathbf{I}_{N_F}, \tag{7.24}$$

$$\mathbf{R}_k \triangleq E[\tilde{\mathbf{c}}_k \tilde{\mathbf{c}}_k^H] = \frac{1}{L_k} \sum_{i=0}^{L_k} \mathbf{c}_k^{(i)} \mathbf{c}_k^{(i)H}, \tag{7.25}$$

where $\mathbf{c}_k^{(i)}$ is the ith code segment of the kth user. Thus the summation in Equation (7.24) actually consists of $\tilde{K}$ terms where

$$\tilde{K} = \sum_{k=1}^{K} L_k. \tag{7.26}$$

Equation (7.24) can now rewritten as

$$\mathbf{R} = \sum_{k=1}^{\tilde{K}} \sigma_k^2 \hat{\mathbf{c}}_k \hat{\mathbf{c}}_k^H + \sigma_\nu^2 \mathbf{I}_{N_F}. \tag{7.27}$$

Again as in Section 6.3, $\hat{\mathbf{c}}_k$ is the effective code segment seen by the receiver, and σ_k^2 is the power due to that code segment. Furthermore,

$$\hat{\mathbf{c}}_1 = \mathbf{c}_1, \tag{7.28}$$

$$\sigma_1^2 = \frac{P_1}{2}. \tag{7.29}$$

Reverting back to Chapter 6 for the rest of the analysis, the MMSE of the single filter receiver may be deduced to be given by

$$J_{\min}^{(S)} = 1 - \gamma \left[1 - \mathbf{x}_S^H \left(\mathbf{X}_S + \frac{1}{\gamma} \mathbf{L}_S^{-1} \right)^{-1} \mathbf{x}_S \right] \tag{7.30}$$

where, as before, γ is the SNR defined in Equation (6.44), $\mathbf{x}_S$ is the vector of normalized crosscorrelations defined in Equation (6.54), $\mathbf{X}_S$ is the matrix of normalized crosscorrelations defined in Equation (6.51), and $\mathbf{L}_S$ is a diagonal matrix whose diagonal elements are $\{1, \sigma_2^2/\sigma_1^2, \ldots, \sigma_{\tilde{K}}^2/\sigma_1^2\}$. Note that $\mathbf{x}_S$ is a $\tilde{K} \times 1$ vector and $\mathbf{X}_S$ and $\mathbf{L}_S$ are $\tilde{K} \times \tilde{K}$ matrices.

7.4.3 MMSE of the Filter Bank Receiver

Recall that the filter bank receiver consists of L filters, and the output of these filters are sampled sequentially when obtaining successive symbol estimates. The overall MMSE of the receiver is the average of the MMSEs of the individual filters. The input correlation matrices for these filters are different from each other in the combination of spreading code segments that affect them. A salient feature of this receiver is that each of the filters sees only one code segment of each received signal. Thus, the correlation matrix for the pth filter is of the form

$$\mathbf{R}_p = \sum_{k=1}^{K} \frac{P_k}{2} \mathbf{R}_{p,k} + \sigma_\nu^2 \mathbf{I}_N, \tag{7.31}$$

$$\mathbf{R}_{p,k} \stackrel{\triangle}{=} E[\tilde{\mathbf{c}}_{p,k} \tilde{\mathbf{c}}_{p,k}^H] = \mathbf{c}_k^{(p)} \mathbf{c}_k^{(p)H} \tag{7.32}$$

where $\mathbf{c}_k^{(p)}$ is the code segment of the kth user seen by the pth filter. Equation (7.31) may be rewritten as

$$\mathbf{R} = \sum_{k=1}^{K} \sigma_k^2 \mathbf{c}_k^{(p)} \mathbf{c}_k^{(p)H} + \sigma_\nu^2 \mathbf{I}_N \tag{7.33}$$

where σ_k^2 is the power of the kth user's signal, and

$$\mathbf{c}_1^{(p)} = \mathbf{c}_1, \tag{7.34}$$

$$\sigma_1^2 = \frac{P_1}{2}. \tag{7.35}$$

The MMSE of the pth filter is given by

$$J_{\min}^{(p)} = 1 - \gamma \left[1 - \mathbf{x}_p^H \left(\mathbf{X}_p + \frac{1}{\gamma} \mathbf{L}^{-1} \right)^{-1} \mathbf{x}_p \right] \tag{7.36}$$

where γ is the SNR, $\mathbf{x}_p$ is the vector of normalized crosscorrelations at the pth filter, $\mathbf{X}_p$ is the matrix of normalized crosscorrelations at the pth filter, $\mathbf{L}$ is a diagonal matrix whose diagonal elements are $\{1, \sigma_2^2/\sigma_1^2, \ldots, \sigma_K^2/\sigma_1^2\}$. $\mathbf{x}_p$ is a $K \times 1$ vector, and $\mathbf{X}_p$ and $\mathbf{L}$ are $K \times K$ matrices. Since the overall MMSE of the filter bank receiver is the average of the MMSE at the L filters, the MMSE is given by

$$J_{\min}^{(B)} = \frac{1}{L} \sum_{p=1}^{L} J_{\min}^{(p)}$$

$$
\begin{aligned}
&= \frac{1}{L}\sum_{p=1}^{L} 1-\gamma\left[1-\mathbf{x}_p^H\left(\mathbf{X}_p+\frac{1}{\gamma}\mathbf{L}^{-1}\right)^{-1}\mathbf{x}_p\right] \\
&= 1-\frac{1}{L}\sum_{p=1}^{L}\gamma\left[1-\mathbf{x}_p^H\left(\mathbf{X}_p+\frac{1}{\gamma}\mathbf{L}^{-1}\right)^{-1}\mathbf{x}_p\right]. \qquad (7.37)
\end{aligned}
$$

7.4.4 Comparison of MMSEs

Making the assumptions of Section 6.6, the approximate expression of Equation (6.73) for the MMSE may be used. Then the MMSE of the single filter receiver may be expressed as

$$J_{\min}^{(S)} \approx \frac{1}{\gamma}\,\tilde{\chi}_{11} - \frac{1}{\gamma^2}\sum_{i=1}^{\tilde{K}}\tilde{\eta}_i\,\tilde{\chi}_{i1}^2 \qquad (7.38)$$

where $\tilde{\eta}_i$ are the diagonal elements of $\mathbf{L}_S^{-1}$ and $\tilde{\chi}_{i1}$ are the elements of the first column of $\mathbf{X}_S^{-1}$. A similar expression for the filter bank receiver is

$$J_{\min}^{(B)} \approx \frac{1}{L}\sum_{p=1}^{L}\left(\frac{1}{\gamma}\,\chi_{11}^{(p)} - \frac{1}{\gamma^2}\sum_{i=1}^{K}\eta_i\,\chi_{i1}^{(p)^2}\right) \qquad (7.39)$$

where η_i are the diagonal elements of $\mathbf{L}^{-1}$ (the interference-to-signal power ratios) and $\chi_{i1}^{(p)}$ are the elements of the first column of $\mathbf{X}_p^{-1}$.

If the crosscorrelations between the desired user's spreading code and different segments of the interference signals' spreading codes are about the same, then $\mathbf{X}_p$, $p = 1, 2, \ldots, L$ can be be considered approximately equal so that $J_{\min}^{(B)}$ is approximately equal to $J_{\min}^{(p)}$. Furthermore, $\tilde{\chi}_{11}$ and $\chi_{11}^{(p)}$ are the dominant terms of the above two MMSEs, and the magnitude of $\tilde{\chi}_{11}$ is greater than that of $\chi_{11}^{(p)}$ because the much higher order of $\mathbf{X}_S$ results in higher magnitudes for the elements of $\mathbf{X}_S^{-1}$ as compared with $\mathbf{X}_p^{-1}$ when the off-diagonal elements of both $\mathbf{X}_S$ and $\mathbf{X}_p$ are all approximately the same. This leads to a higher value for $J_{\min}^{(S)}$ compared with $J_{\min}^{(B)}$. A heuristic explanation is that the single filter receiver has to overcome many more interference patterns than each of the filters in the filter bank receiver. That is, the interference subspace is much larger for the former than for the latter, enabling the filter bank receiver to better suppress the interference and thus have a lower MMSE than the single filter receiver.

7.4.5 Numerical Example

The MMSE improvement is illustrated by way of a numerical example. We consider the scenario of Figure 7.1. Four random spreading codes are chosen:

$$\begin{aligned}
\mathbf{c}_1 &= \{1,1,-1,-1,1,1,1,-1\},\\
\mathbf{c}_2 &= \{1,-1,1,1,1,-1,-1,1,1,-1,-1,-1,1,1,-1,-1,\\
&\quad -1,1,-1,-1,1,1,-1,-1,1,1,1,-1,-1,-1,-1,-1\},\\
\mathbf{c}_3 &= \{-1,1,-1,1,1,-1,1,1,-1,-1,1,-1,1,-1,-1,1,\\
&\quad 1,1,-1,-1,1,-1,-1,1,-1,-1,1,-1,-1,1,1,1\},\\
\mathbf{c}_4 &= \{-1,-1,-1,1,-1,-1,-1,1,-1,1,-1,-1,1,1,-1,1\}
\end{aligned}$$

where $\mathbf{c}_1$ is the desired user's spreading code. The four codes have lengths equal to 8, 32, 32, and 16, respectively. We break up $\mathbf{c}_2$, $\mathbf{c}_3$, and $\mathbf{c}_4$ into segments of length eight (the length of $\mathbf{c}_1$).

Noting that the single filter receiver sees four different segments of $\mathbf{c}_2$ and $\mathbf{c}_3$ and two different segments of $\mathbf{c}_4$, the crosscorrelation matrix $\mathbf{X}_S$ is

$$\mathbf{X}_S = \begin{bmatrix}
1.00 & 0 & 0 & 0 & 0.50 & 0 & 0.75 & 0.50 & 0.75 & 0 & -0.25\\
0 & 1.00 & 0 & 0.50 & 0 & 0.50 & -0.25 & -0.50 & 0.25 & 0 & -0.25\\
0 & 0 & 1.00 & 0 & -0.50 & 0 & 0.25 & 0 & 0.25 & -0.50 & -0.25\\
0 & 0.50 & 0 & 1.00 & 0 & 0 & -0.25 & -0.50 & 0.25 & 0 & -0.25\\
0.50 & 0 & -0.50 & 0 & 1.00 & 0 & 0.25 & 0.50 & 0.25 & 0 & -0.25\\
0 & 0.50 & 0 & 0 & 0 & 1.00 & 0.25 & 0 & 0.25 & 0 & 0.25\\
0.75 & -0.25 & 0.25 & -0.25 & 0.25 & 0.25 & 1.00 & 0.75 & 0.50 & -0.25 & 0\\
0.50 & -0.50 & 0 & -0.50 & 0.50 & 0 & 0.75 & 1.00 & 0.25 & 0 & -0.25\\
0.75 & 0.25 & 0.25 & 0.25 & 0.25 & 0.25 & 0.50 & 0.25 & 1.00 & 0.25 & -0.50\\
0 & 0 & -0.50 & 0 & 0 & 0 & -0.25 & 0 & 0.25 & 1.00 & -0.25\\
-0.25 & -0.25 & -0.25 & -0.25 & -0.25 & 0.25 & 0 & -0.25 & -0.50 & -0.25 & 1.00
\end{bmatrix}.$$

Assuming that all of the signals are received with equal power, the matrix $\mathbf{L}_S$ is

$$\mathbf{L}_S = \text{diag}\{1.00, 0.25, 0.25, 0.5, 0.25, 0.25, 0.5, 0.25, 0.25, 0.25, 0.25\}.$$

For a SNR of 10 dB, i.e., $\gamma = 10$, noting that $\mathbf{x}_S$ is the first column of $\mathbf{X}_S$, the MMSE of the single filter from Equation (7.30) is computed to be

$$J_{\min}^{(S)} = 0.2788,$$

which corresponds to about -5.5 dB.

For the filter bank receiver, we note that $L = 4$ so that

$$\mathbf{X}_1 = \begin{bmatrix} 1.00 & 0 & 0 & 0 \\ 0 & 1.00 & 0 & 0.50 \\ 0 & 0 & 1.00 & 0 \\ 0 & 0.50 & 0 & 1.00 \end{bmatrix}, \quad \mathbf{X}_3 = \begin{bmatrix} ,1.00 & 0.50 & 0.75 & 0 \\ 0.50 & 1.00 & 0.25 & -0.50 \\ 0.75 & 0.25 & 1.00 & 0.25 \\ 0 & -0.50 & 0.25 & 1.00 \end{bmatrix},$$

$$\mathbf{X}_2 = \begin{bmatrix} 1.00 & 0.50 & 0 & 0.75 \\ 0.50 & 1.00 & 0 & 0.25 \\ 0 & 0 & 1.00 & 0.25 \\ 0.75 & 0.25 & 0.25 & 1.00 \end{bmatrix}, \quad \mathbf{X}_4 = \begin{bmatrix} 1.00 & 0 & -0.25 & 0.75 \\ 0 & 1.00 & -0.25 & -0.25 \\ -0.25 & -0.25 & 1.00 & 0 \\ 0.75 & -0.25 & 0 & 1.00 \end{bmatrix},$$

and

$$\mathbf{L} = \text{diag}\{1.00, 0.25, 0.25, 0.5\}.$$

Noting that $\mathbf{x}_p$ is the first column of $\mathbf{X}_p$, the MMSE of the filter bank receiver is computed using Equation (7.37) and is found to be

$$J_{\min}^{(B)} = 0.1551,$$

which corresponds to about -8.1 dB. Thus, for the codes considered, the gain yielded by a filter bank receiver over a single filter receiver is about 2.6 dB, which is significant.

7.5 Simulation of BER Performance of Filter Bank Receivers

7.5.1 Preliminary Remarks

The lower MMSE obtained with a filter bank receiver translates to lower BERs as well. Since the interference characteristics are assumed to be unknown to the receiver, the optimal solution cannot be computed. Therefore, an adaptive implementation is more practical. Performance of filter bank receivers in both AWGN and multipath fading channels are presented. The soft decision-directed algorithm [76] is used after training with the NLMS algorithm. We ignore the overhead due to the use of a training sequence.

In the soft decision-directed algorithm, the following function is used as the error signal:

$$e(n) = \frac{e^{2\,y(n)/\sigma^2} - 1}{e^{2\,y(n)/\sigma^2} + 1} - y(n) \tag{7.40}$$

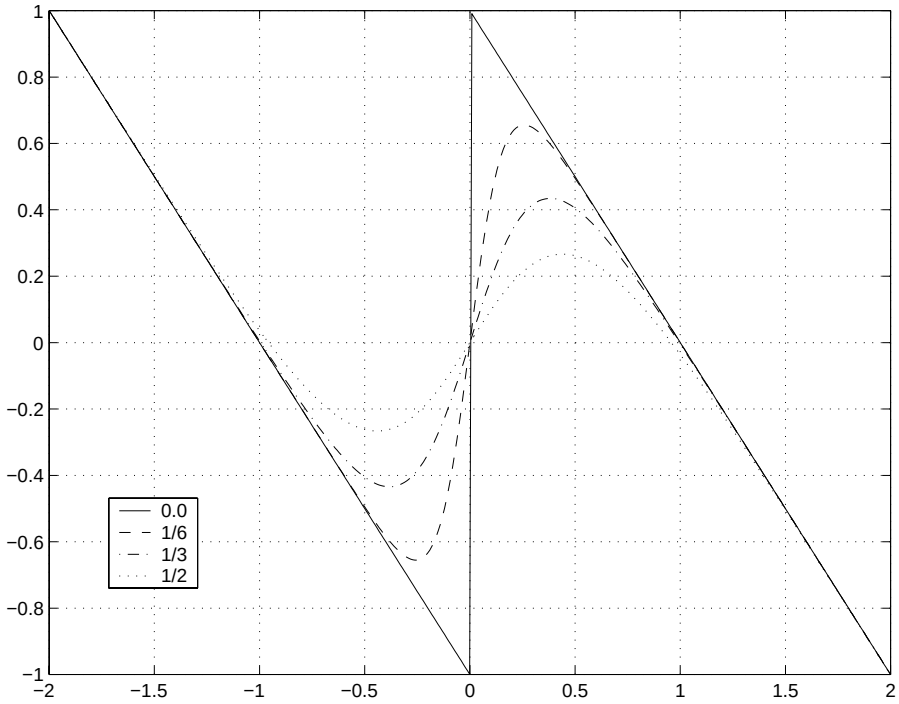

Figure 7.4: The Modified Error Function in the Soft Decision-Directed Algorithm for Different Values of σ^2.

where $y(n)$ is the filter output. In Figure 7.4, $e(n)$ is plotted as a function of $y(n)$ for different values of σ^2. $\sigma^2 = 0$ corresponds to the conventional decision-directed algorithm. A non-zero value of σ^2 effectively weights the conventional error function $(\text{sgn}\{y(n)\} - y(n))$, giving a large weight when $|y(n)|$ is close to 1, i.e., when the filter output is highly reliable, and a small weight when $|y(n)|$ is small, or, when the output is less reliable. The larger the value of σ^2, the smaller is the weight of the error for less reliable outputs. Using a high value of σ^2 reduces the probability of the algorithm losing convergence but degrades the algorithm's tracking ability in time-varying channels. For all of the simulation results presented here, $\sigma^2 = 1/3$ is used.

Compared with the single adaptive filter receiver, the adaptive filter bank receiver does not have additional *computational* overhead because the number of filter weights in each filter of the filter bank is the same as the number of weights in the single adaptive filter receiver. Also, only one filter within the bank is used in making a symbol estimate. Thus, the number of computations in both filtering and adaptation of weights per symbol remain unchanged. However, there is increased overhead in the form of storage of filter weights; instead of N_F filter weights, $L\,N_F$ weights have to be stored. This is usually not a problem as long as this number is not very large. In most cases, computational

complexity rather than storage would be the limiting factor. In addition to increased storage requirements, there may also be some overhead due to switching from one filter to the next during successive symbols, depending on the implementation. For example, in a DSP implementation, an extra pointer may be required to keep track of the current filter within the filter bank.

An important aspect of the filter bank receiver is the relatively longer convergence time, a result of multiple filters being adapted sequentially rather than concurrently. This may become an important consideration if the number of filters is large. However, when the filter weights are initialized to the matched filter coefficients and when the NLMS algorithm is used, each filter converges rapidly and the total convergence time is not prohibitively long. Furthermore, when convergence is slow, techniques to speed up convergence can be applied to overcome this problem.

7.5.2 Simulation Parameters

1. Spreading codes of four different lengths, 16, 32, 64, and 128, are used in the simulations. Each set of length 2^m codes ($\in \{+1, -1\}$) is created by first aligning Gold codes [14, 104] of length $2^m - 1$ so that the normalized crosscorrelations between any two codes is $-1/(2^m - 1)$, and then appending $+1$ to each sequence, resulting in a set of *orthogonal* codes of length 2^m. There are $2^m - 1$ codes in each set. The orthogonal codes have good crosscorrelation properties for all relative cyclic shifts, not quite as good as those of the Gold codes used to generate them but still better than those of random codes. The orthogonality between codes of the same length should help in reducing the MSEs of both adaptive receivers in the cases where multiple codes of the same length are used and when the signals are synchronous. Even in the asynchronous cases, the good crosscorrelation properties of codes of the same length should aid in reducing the MSE of each receiver.

2. For each set of simulation results, the total number of users considered is divided into four different categories, each with a specific code length or a specific chip rate. Thus, for each simulation point (barring the single user case), the number of users considered is an integer multiple of four.

3. Each simulation point is obtained by averaging the results of 96 independent trials.

4. Systems with signals of different bandwidths resulting from different *chip rates* are also considered. The use of a filter bank in such situations is demonstrated through results here.

5. The availability of a coherent reference for the carrier is not assumed. Therefore, differential detection is employed at the receiver, with corresponding differential encoding of the transmitted symbols. The LMS algorithm is modified slightly

to incorporate the differential decoding within the algorithm as discussed in Section 8.5.

6. For the synchronous cases, spreading codes for each group are randomly chosen in every trial while ensuring that no two users are assigned the same spreading code. Furthermore, all of the signals are assigned the same carrier phase, which is randomly generated every trial.

7. For the asynchronous cases, each signal is assigned a random carrier phase, the phase being uniformly distributed over $[0, 2\pi)$. Each signal is also assigned a random time shift, which is uniformly distributed over the length of the code. Signals are assigned codes randomly picked from the corresponding set. These parameters are randomly generated every trial.

8. All of the signals are assumed to be COP.

9. The pulse shaping is rectangular and the sampling rate is selected such that all of the signals are sampled at least two times per chip.

10. The BER performance of the adaptive filter bank receiver (AFBR), the single adaptive filter receiver (SAFR), and the matched filter receiver (MFR) are provided in each case for comparison.

7.6 Simulation Results for an AWGN Channel

So far, the investigation has focused on the performance gains that the filter bank receiver yields for multi-rate CDMA systems in an AWGN channel. This section presents the simulation results for this scenario. It will be shown that these gains are often significant and, considering the moderate increase in the overall receiver complexity, demonstrate the importance of the approach. Misconvergence/divergence problems are not anticipated when the NLMS algorithm is operated in the decision-directed mode. Performance results in this section are provided for two values of E_b/N_0: 9 dB and 10 dB.

7.6.1 Performance When Users Have Different Code Lengths

Here, all of the signals are assumed to have the same chip rate and, hence, bandwidth. They have different symbol rates and, since they are COP signals, they have different code lengths as well. The BERs of the three receivers are determined for a system with one, four, eight, twelve, and sixteen users in the system. Several scenarios are considered, some with each of the four groups of users having a different code length, and others with multiple groups sharing the same code length. Results for both synchronous and asynchronous channels are presented.

Case 1: Synchronous System in Which Users Have Four Different Code Lengths

Simulations results are first demonstrated for the synchronous case as defined in Assumption 2 of Section 7.4.1. All of the signals are assumed to have equal powers and are assigned the same randomly generated phase offset in each trial. Except for the single user case, each of the other cases has one quarter of the users assigned a code with length 16, 32, 64, and 128. The desired user has a spreading code of length 16, i.e., the shortest of the codes. It is easily seen that the number of filters needed for the filter bank receiver is $128/16 = 8$.

Figure 7.5 shows the BERs of the receivers versus the number of users in the system. The increase in the load on the system clearly has a highly detrimental effect on the performance of the MFR for both SNRs. The SAFR is marginally better than the matched filter receiver, with the improvement increasing with the SNR. The performance of the AFBR is substantially better. Again, the BER improvement is magnified when the SNR is increased. The AFBR is less interference limited than the other two receivers and hence this result. If the desired BER is 5×10^{-3}, for example, assuming adequate error correction coding, then for $E_b/N_0 = 9$ dB, no more than two or three users are permissible in the system with a MFR. The SAFR tolerates one additional user at most. In contrast, the AFBR can provide adequate performance with six users. Thus, the capacity is at least doubled by using the AFBR. Similar observations can be made for $E_b/N_0 = 10$ dB. For most of the range of system loads, increasing the E_b/N_0 from 9 to 10 dB leaves the performance of the SAFR well short of that of the AFBR at 9 dB. From the figure, the performance gain yielded by the the AFBR over the SAFR in the useful range of system load appears to be at least 3 dB, which is significant.

Figure 7.6 illustrates the variation of the BERs of the three receivers with SNR when there are eight users in the system. If the desired BER is 10^{-2}, this figure shows that with eight users, the AFBR yields a gain of about 3.5 dB. Furthermore, the separation between the performance curves increases with SNR. Thus, the AFBR yields higher gains over the SAFR at higher SNRs.

Case 2: Synchronous System in Which Users Have Two Different Code Lengths

In this case, users are synchronous but have one of two code lengths. Two examples are presented. Except for the single user case, each of the other cases has one quarter of the users being assigned a code with length 16, and the rest being assigned a different code length. The desired user has a spreading code of length 16.

In the first example, the second group of users has a code of length 32. Therefore, the number of filters in the filter bank receiver is $32/16 = 2$. The plot of Figure 7.7

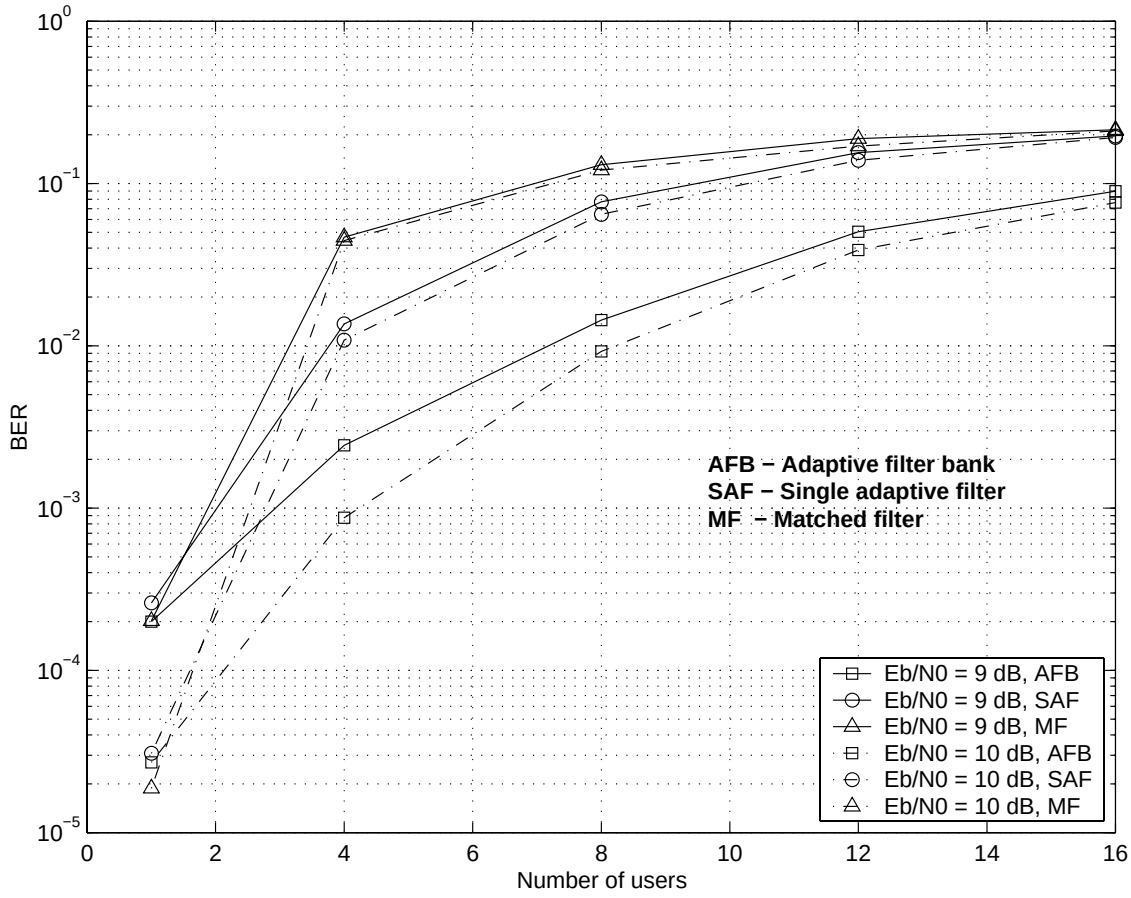

Figure 7.5: BER Performance of the Three Receivers in a Synchronous Channel with 25% of Users Having Each of the Code Lengths of 16, 32, 64, and 128 (the Desired User's Code Length is 16).

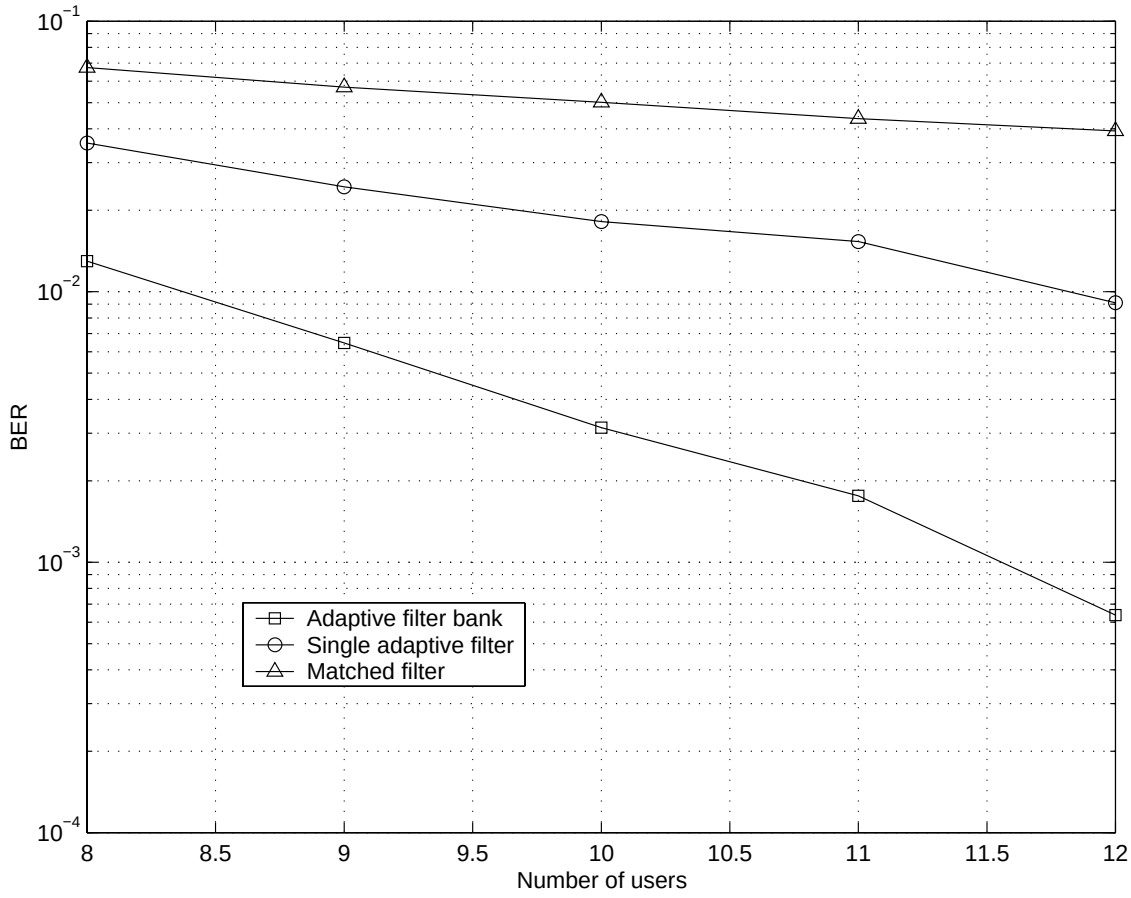

Figure 7.6: Variation of BERs of the Three Receivers with SNR in a Synchronous Channel with Two Users Having Each of the Code Lengths of 16, 32, 64, and 128 (the Desired User's Code Length is 16).

demonstrates the performance of the receivers. At low system loads, the gain provided by the AFBR over the SAFR is marginal, about 1 dB. At higher levels of interference, the improvement amounts to several dB. Furthermore, as observed in Case 1, the performance improvement increases with the SNR. The SAFR performs better here than in Case 1 because of the fewer effective interference patterns that need to be suppressed. The AFBR exhibits a performance very similar to Case 1. If the desired BER at $E_b/N_0 =$ 9 dB is 5×10^{-3}, the MFR can support about two users. The SAFR provides the desired performance with four users or less, whereas the AFBR can provide the desired performance with six users. The performance gain yielded by the AFBR over the SAFR ranges from 1 dB to several dB for the system loads of interest.

In the second example, the code length for the second group of users is 64 and, hence, there are $64/16 = 4$ filters in the filter bank receiver. The performance results are depicted in Figure 7.8. A comparison with Figure 7.7 shows that AFBR yields larger gains over the SAFR than in the previous example. The poorer performance of the SAFR is due to the increased number of effective interference patterns it has to suppress. The BER of the SAFR degrades rapidly with increasing interference. Whereas in the previous example the SAFR performed better than the MFR for all system loads, in this case the two receivers yield the same BER with twelve or more users. The performances are similar to those of Case 1. The gain with the AFBR is again several dB over the SAFR. These two examples demonstrate that the AFBR is very useful even when the code length disparity is moderate.

Figure 7.9 shows the variation of the BERs of the three receivers with SNR when there are eight users in the system. This figure is similar to Figure 7.6. If a BER of 10^{-2} is desired with eight users, the AFBR again yields an improvement of about 3.5 dB.

Case 3: Asynchronous System in Which Users Have Four Different Code Lengths

As explained earlier, this case is characterized by a different random phase offset and time shift for each user. The code lengths of users and the assignment of codes are as in the Case 1. In the first two examples, it is assumed that there is no carrier frequency offset on the signals. Simulation results are first provided for the case with perfect power control, i.e., all the signals have equal powers. In this case, the interference is not as severe as in the synchronous case since each interference signal is out of phase with respect to the desired signal, so it has an orthogonal component that does not harm the desired signal. This is reflected in the BER performance of the three receivers in Figure 7.10. Again, it is observed that the SAFR is slightly better than the MFR. The AFBR outdoes the SAFR in BER performance by a modest margin. In the range of interest, the AFBR can tolerate about twice the system load as the SAFR. For $E_b/N_0 = 9$ dB, the AFBR can provide a BER of 5×10^{-3} with seven users in the system as opposed to three or four

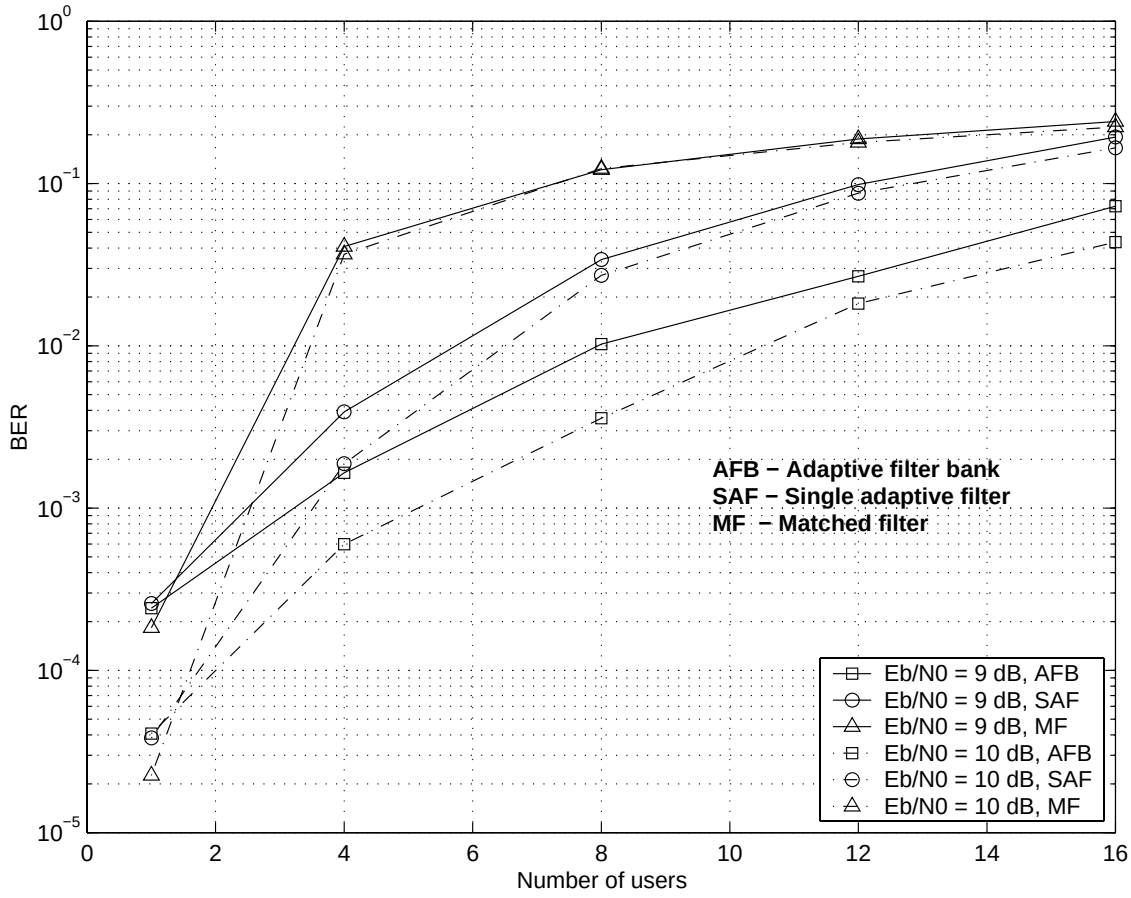

Figure 7.7: BER Performance of the Three Receivers in a Synchronous Channel with 25% of Users Having the Code Lengths of 16 and the Others Having a Code Length of 32 (the Desired User's Code Length is 16).

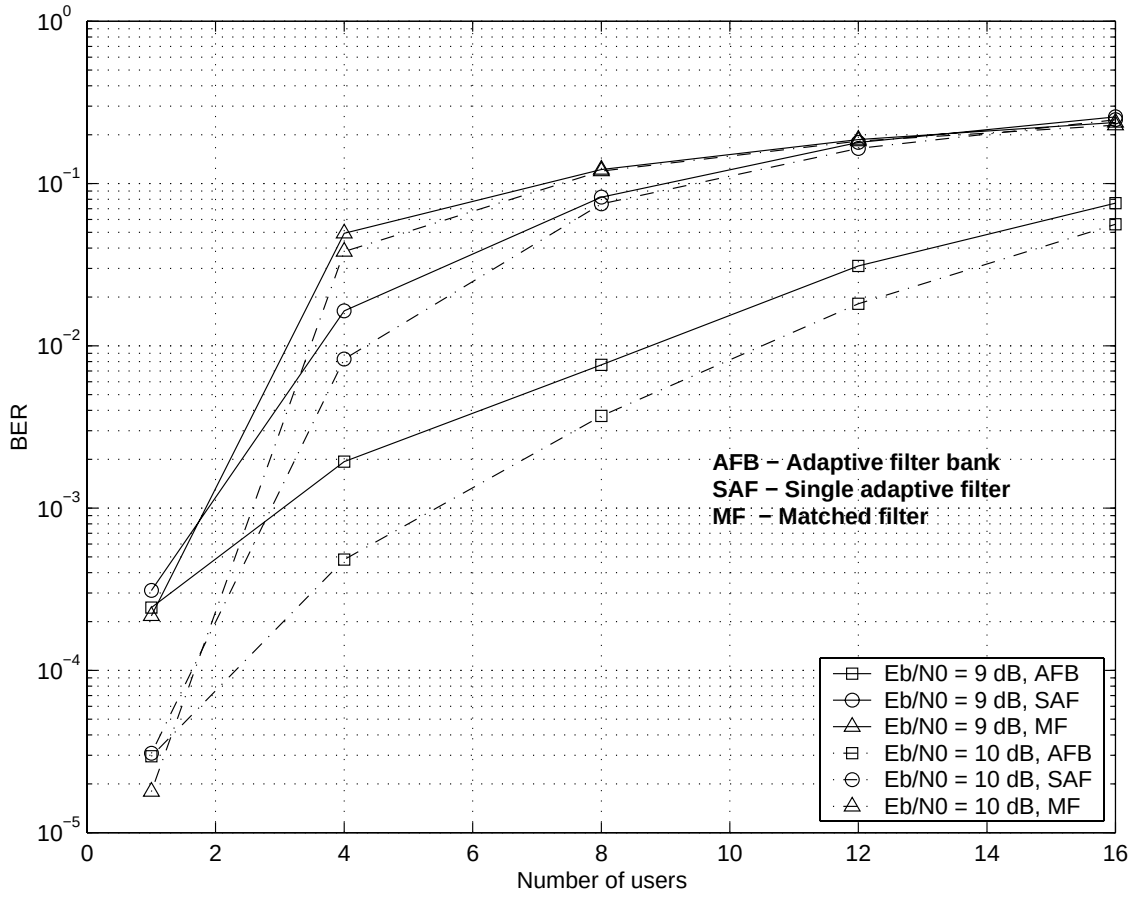

Figure 7.8: BER Performance of the Three Receivers in a Synchronous Channel with 25% of Users Having the Code Lengths of 16 and the Others Having a Code Length of 64 (the Desired User's Code Length is 16).

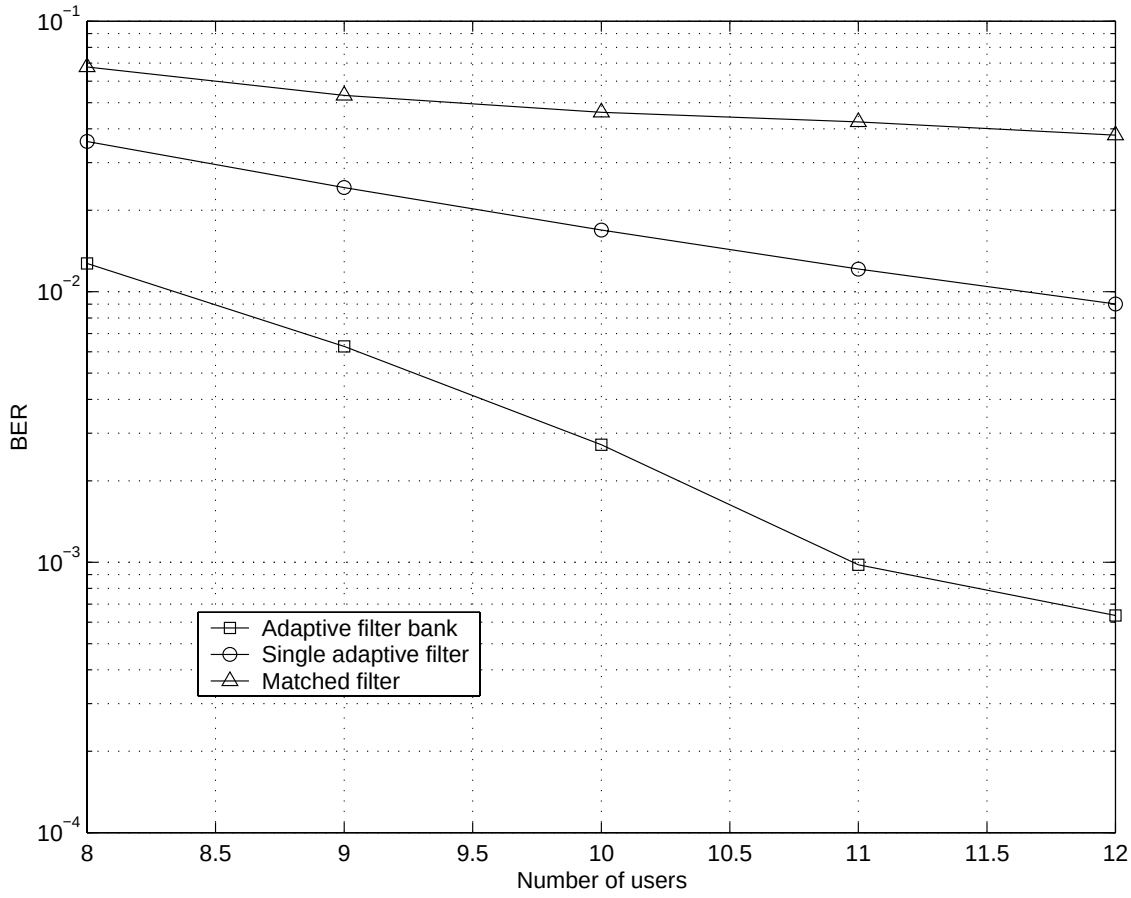

Figure 7.9: Variation of BERs of the Three Receivers with SNR in a Synchronous Channel with Two Users Having a Code Length of 16, and the Others Having a Code Length 64 (the Desired User's Code Length is 16).

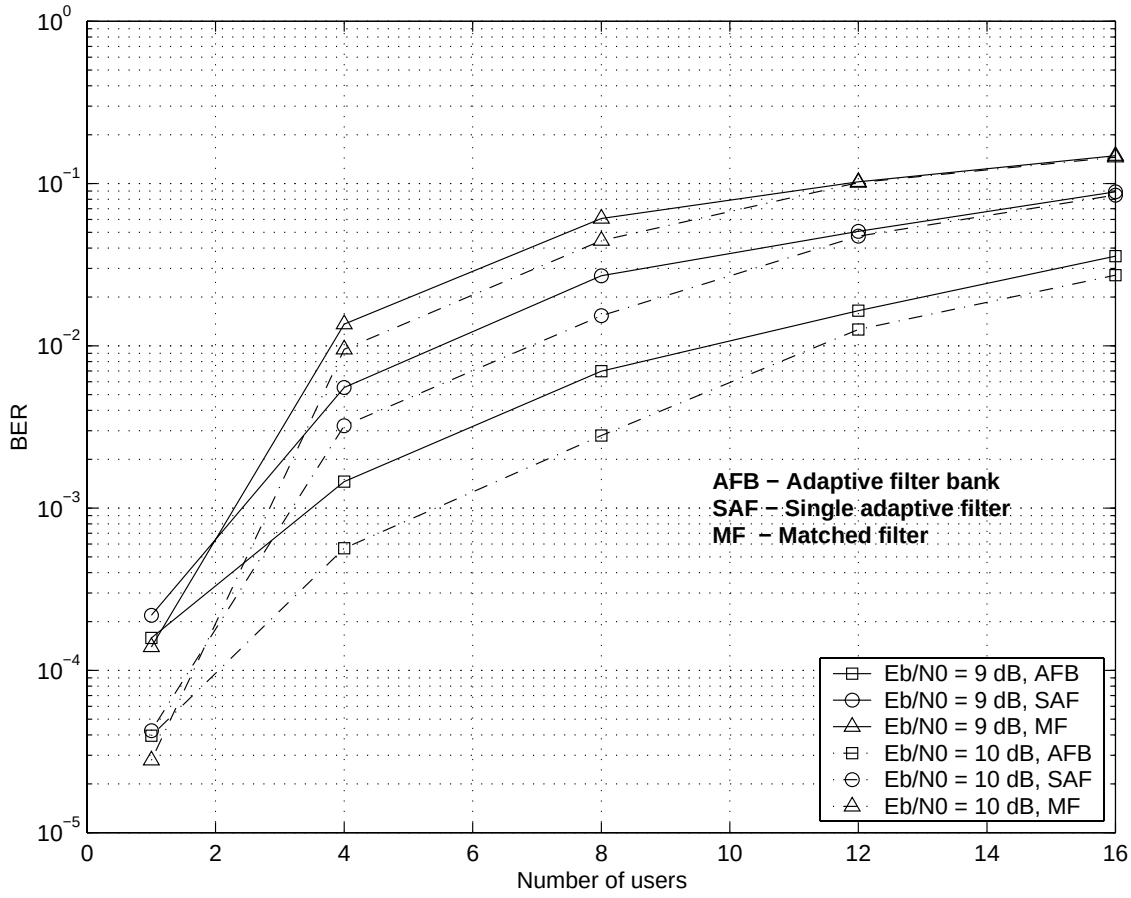

Figure 7.10: BER Performance of the Three Receivers in an Asynchronous Channel with No Carrier Offset and with 25% of Users Having Each of the Code Lengths of 16, 32, 64, and 128 (the Desired User's Code Length is 16). Perfect power control is assumed.

users in the case of the SAFR. For $E_b/N_0 = 10$ dB, the corresponding numbers are four and eight. The performance gain appears to be 2 to 3 dB over the region of interest in this case as well.

Figure 7.11 shows the simulation results when the power control is "loose". For these results, it is assumed that the powers of all the signals are lognormally distributed with a mean of zero and a variance of ten. BER curves are provided only for $E_b/N_0 = 9$ dB. A comparison of Figures 7.10 and 7.11 shows that the performance gains of the AFBR are similar even in this scenario, suggesting that the receiver is near-far resilient, which is not surprising.

In addition to the characteristics of the first example, the signals are also assumed to have carrier frequency offsets in the next example. Each signal has a random frequency offset that is uniformly distributed over [−5000 Hz, +5000 Hz] (a maximum offset of about ±2.5% of the carrier frequency), and the symbol rate of the desired user is 50 kbps. Different frequency offsets are used in each trial. The performance curves are depicted in Figure 7.12. Comparing the curves of Figures 7.10 and 7.12 shows that the performance of the receivers with frequency offsets on signals remains almost the same as without offsets. ±5 kHz is about ±4% of the the symbol rate and differential detection of the received symbols appears to adequately compensate for this offset. Note that the *maximum* frequency offset is ±5 kHz and the actual offset is a random variable and can have a very small value as well.

7.6.2 Performance When Users Have Different Chip Rates

We now consider the use of an adaptive filter bank receiver in a system where users have different bandwidths resulting from different chip rates. When a user demands a lower data rate and lower quality of service, there may be no need to grant the same bandwidth as for a higher data rate user. If the same processing gain is used for the two users, they end up with different chip rates. Figure 7.13 illustrates an example system in which signals have three different bandwidths. The power spectral densities of the signals are represented. The example shows signals with equal powers, so when the bandwidth is doubled, the power spectral density is halved.

For all of the following simulation results, spreading codes of length 16 are used. Several different scenarios are considered with users in the four groups assigned different symbol rates and corresponding bandwidths. The ratio of the bandwidth of any signal to the bandwidth of any lower bandwidth signal is always a power of two.

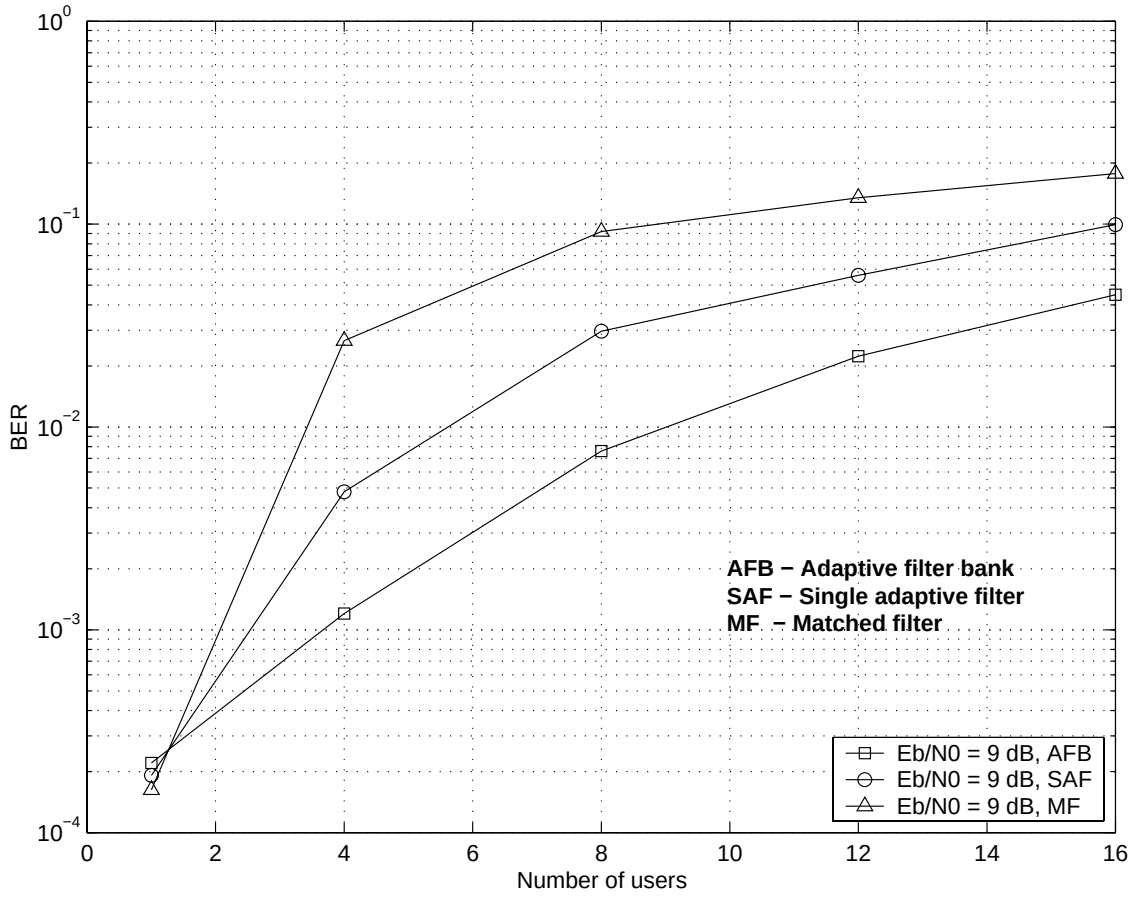

Figure 7.11: BER Performance of the Three Receivers in an Asynchronous Channel with No Carrier Offset and with 25% of Users Having Each of the Code Lengths of 16, 32, 64, and 128 (the Desired User's Code Length is 16). "Loose" power control is assumed.

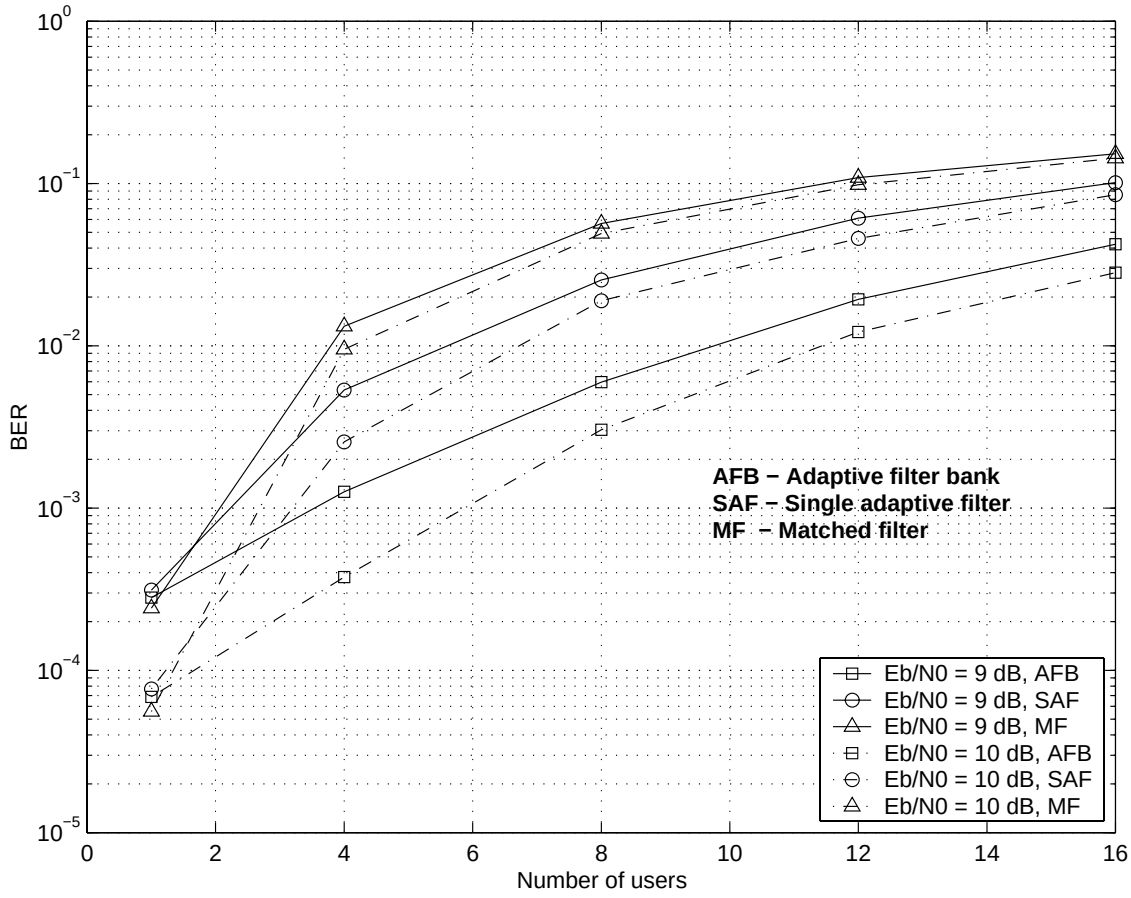

Figure 7.12: BER Performance of the Three Receivers in an Asynchronous Channel with Carrier Offset and with 25% of Users Having Each of the Code Lengths of 16, 32, 64, and 128 (the Desired User's Code Length is 16).

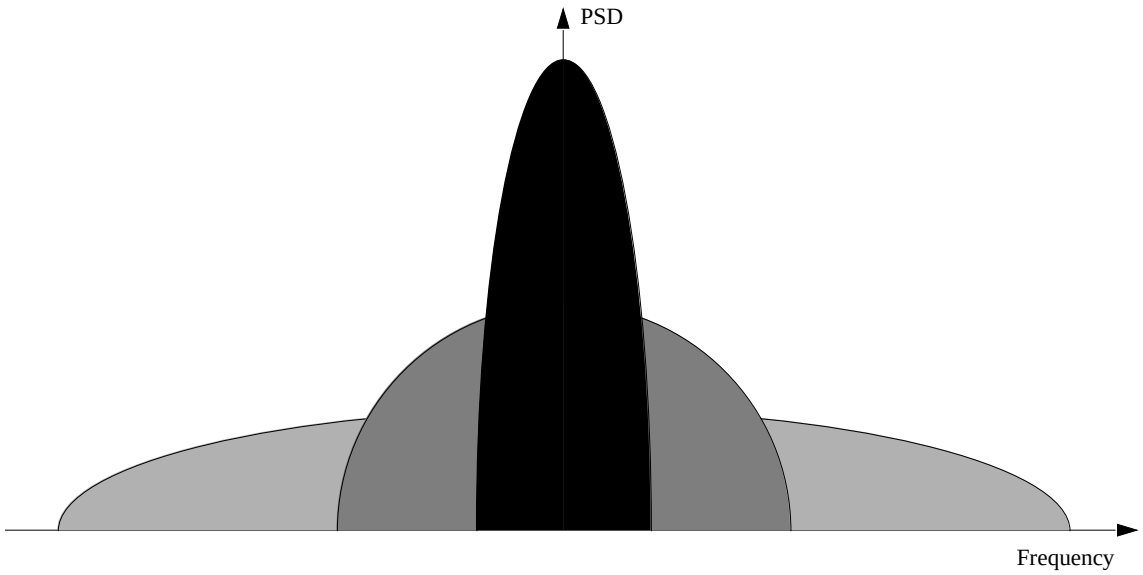

Figure 7.13: Power Spectra of Three Signals with Equal Powers but Different Chip Rates.

Case 1: Synchronous System

In this case, signals have four different bandwidths. The chip rates normalized to the sampling rate are 1/2, 1/4, 1/8, and 1/16, with the desired user falling in the first group (having the highest chip rate).

Figure 7.14 shows the results for the synchronous case. It is interesting to compare these results with those of the synchronous case with different code lengths (Figure 7.5). The MFR performs poorly again, with the BER rapidly deteriorating. In fact, the performance is almost identical in both cases. The biggest improvement is in the case of the SAFR. The AFBR outdoes the SAFR in BER performance by only a small margin. The curves for both $E_b/N_0 = 9$ dB and $E_b/N_0 = 10$ dB show that the improvement hovers around 1 dB over the entire range of system loads. At $E_b/N_0 = 9$ dB and for a desired BER of 5×10^{-2}, the MFR, the SAFR, and the AFBR can tolerate approximately three, five, and seven users in the system, respectively, and the corresponding numbers of users for $E_b/N_0 = 10$ dB are roughly three, six, and nine, respectively.

The improvement in the performance of the SAFR may be explained by the following considerations. When the chip rate of a group of MAI signals is low relative to that of the desired user, the number of pseudorandom chips of the MAI signals per symbol of the desired user also reduces. This reduces the number of interference patterns that the SAFR must suppress. To clarify, consider the set of MAI signals that have a normalized chip rate of 1/16 as compared with 1/2 for the desired signal, i.e., each of these interference

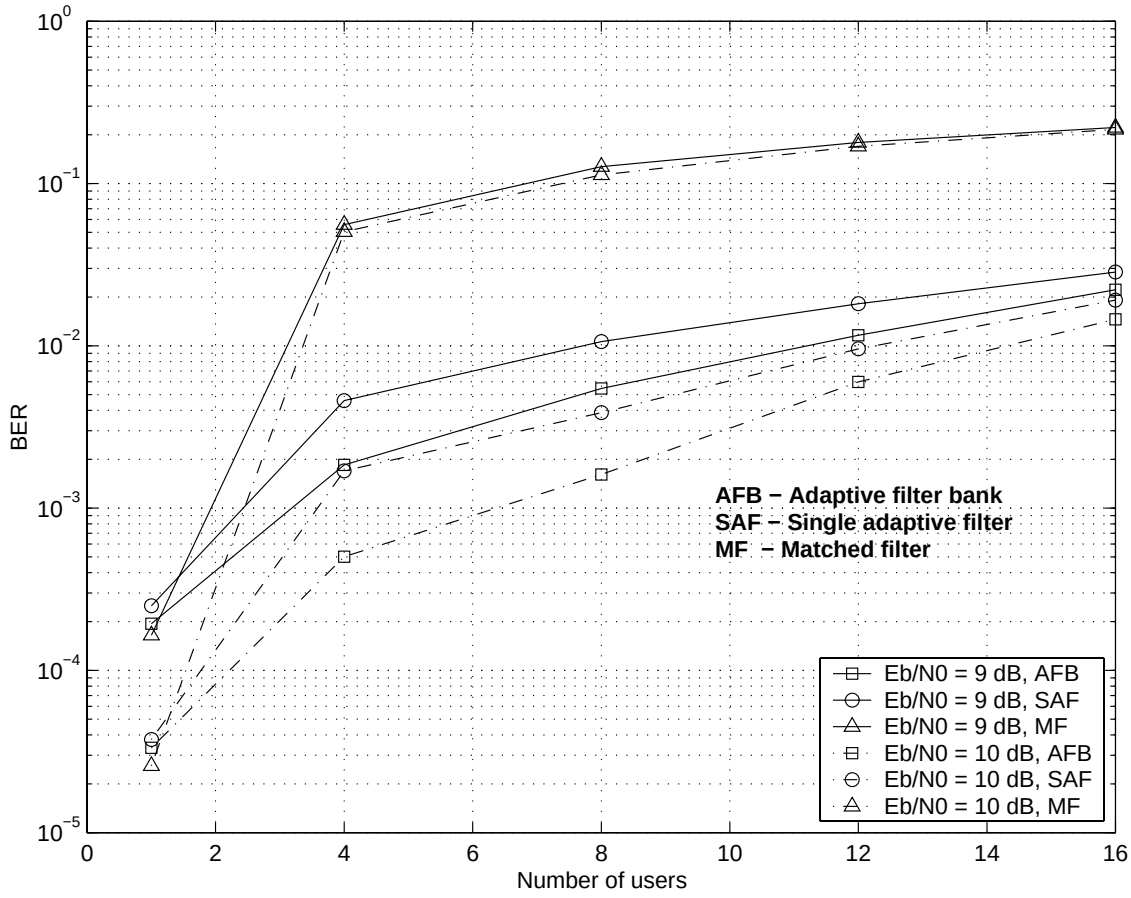

Figure 7.14: BER Performance of the Three Receivers in a Synchronous Channel with 25% of Users Having Each of the Normalized Chip Rates of 1/2, 1/4, 1/8, and 1/16 (the Desired User's Normalized Chip Rate is 1/2).

signals has one chip for every eight chips of the desired signal, or two chips over the entire code length (symbol period). The only two combinations of two chips are $\{+1, -1\}$ and $\{+1, +1\}$, since their inverses do not count as new interference patterns. Thus, regardless of the actual number of MAI signals that have this chip rate, the actual number of MAI patterns within this group that the SAFR must overcome is two. The increased number of identical interference patterns is perceived by the receiver as merely a higher power contribution due to each pattern, which does not affect the receiver much given its near-far resilience. In the extreme case, if a set of MAI signals has a normalized chip rate of 1/32 (or a submultiple of 1/32), the SAFR would have to suppress only one interference pattern due to this set: +1 over the entire code length. Therefore, the overall impact of the MAI signals is less, resulting in the SAFR's performance approaching that of the AFBR.

Case 2: Asynchronous System in Which Users Have Four Different Chip Rates

In this case, the distribution of users' chip rates is the same as for the synchronous case. It is assumed that the signals have equal powers. The simulation results are given in Figure 7.15. It is again seen that the performance of the MFR is as poor as in Case 2 of Section 7.6.1. Its performance is better than in the synchronous case, since the asynchronous MAI signals have components orthogonal to the desired signal due to their unique phases. The SAFR shows a marked improvement over the MFR, closely approaching the AFBR in performance. However, the AFBR does perform better than the SAFR. The performance gain is less than 1 dB, which is less than in the synchronous case. The performance of the SAFR approaches that of the AFBR for the same reason it did in the synchronous case.

Case 3: Asynchronous System in Which Users Have Two Different Chip Rates

To study the effect of the chip rates of the interference signals, the users are divided into only two groups, each with a different chip rate. Two cases are considered.

In the first scenario, a quarter of all the users, including the desired user, have a normalized chip rate of 1/2, whereas the rest of the users have a normalized chip rate of 1/4, or half that of the first group. Figure 7.16 shows the BERs of the three receivers. In the next case, a quarter of all the users, including the desired user, have a normalized chip rate of 1/2, whereas the rest of the users have a normalized chip rate of 1/8, a quarter of that of the first group. The results are illustrated in Figure 7.17.

A comparison of Figures 7.16 and 7.17 demonstrates the effect of the chip rates of the MAI signals on receiver performance. The performance of the MFR is virtually the same in both cases. However, the performance curves are shifted down slightly for the other

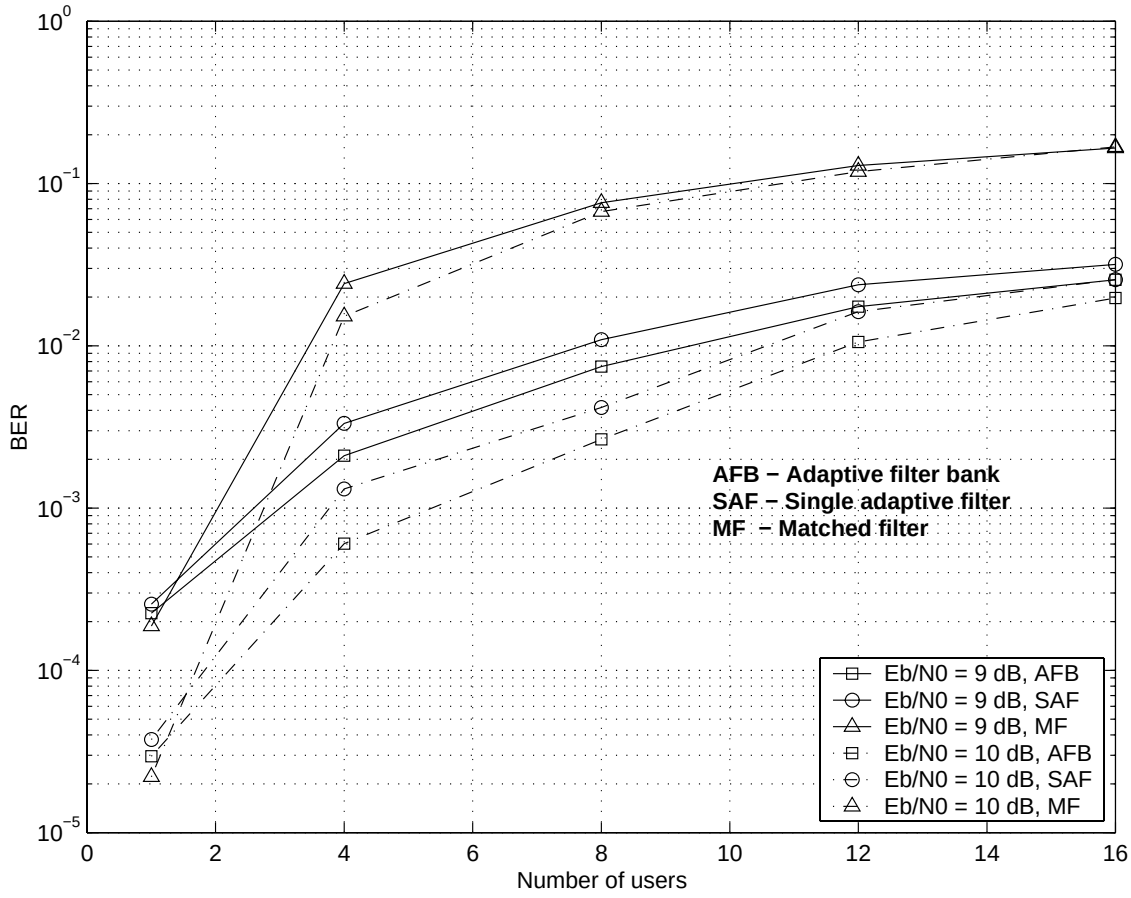

Figure 7.15: BER Performance of the Three Receivers in an Asynchronous Channel with 25% of Users Having Each of the Normalized Chip Rates of 1/2, 1/4, 1/8, and 1/16 (the Desired User's Normalized Chip Rate is 1/2).

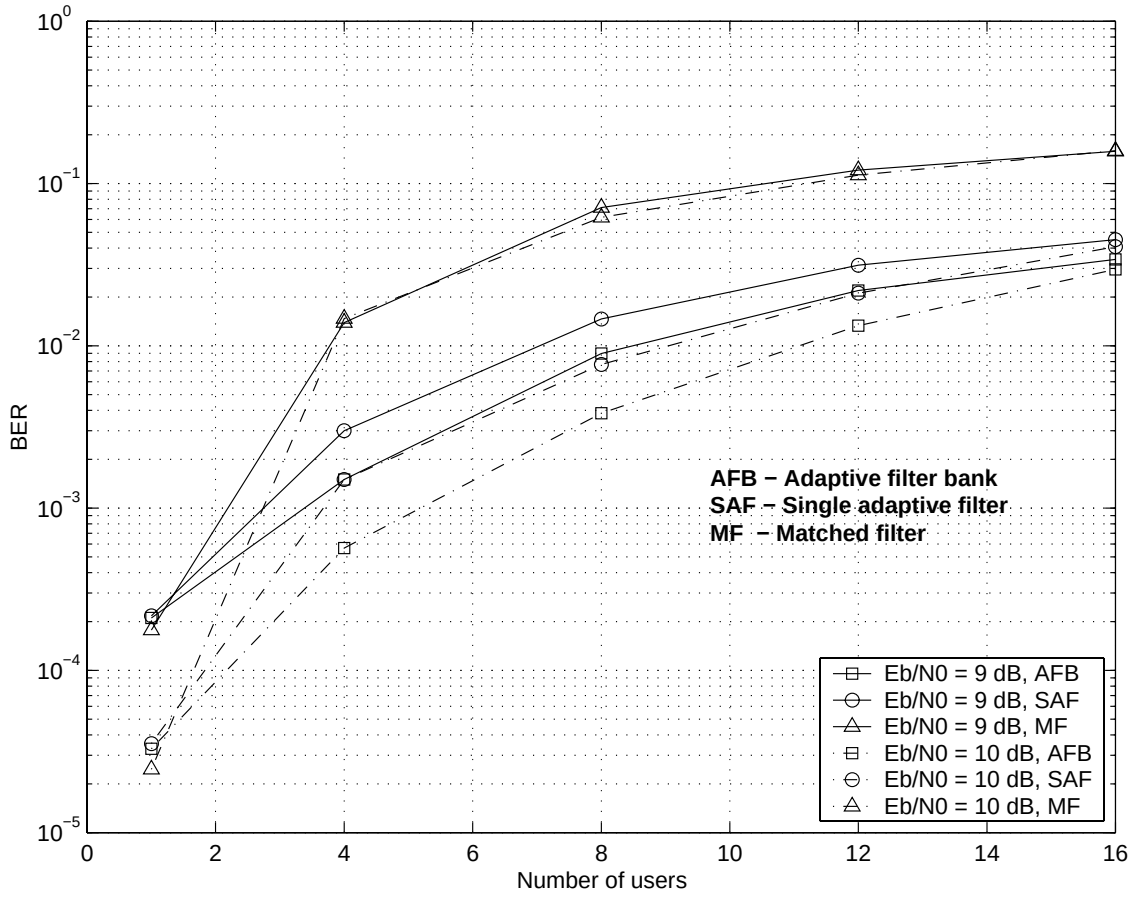

Figure 7.16: BER Performance of the Three Receivers in an Asynchronous Channel with 25% of Users Having a Normalized Chip Rate of 1/2 and the Others Having a Normalized Chip Rate of 1/4 (the Desired User's Normalized Chip Rate is 1/2).

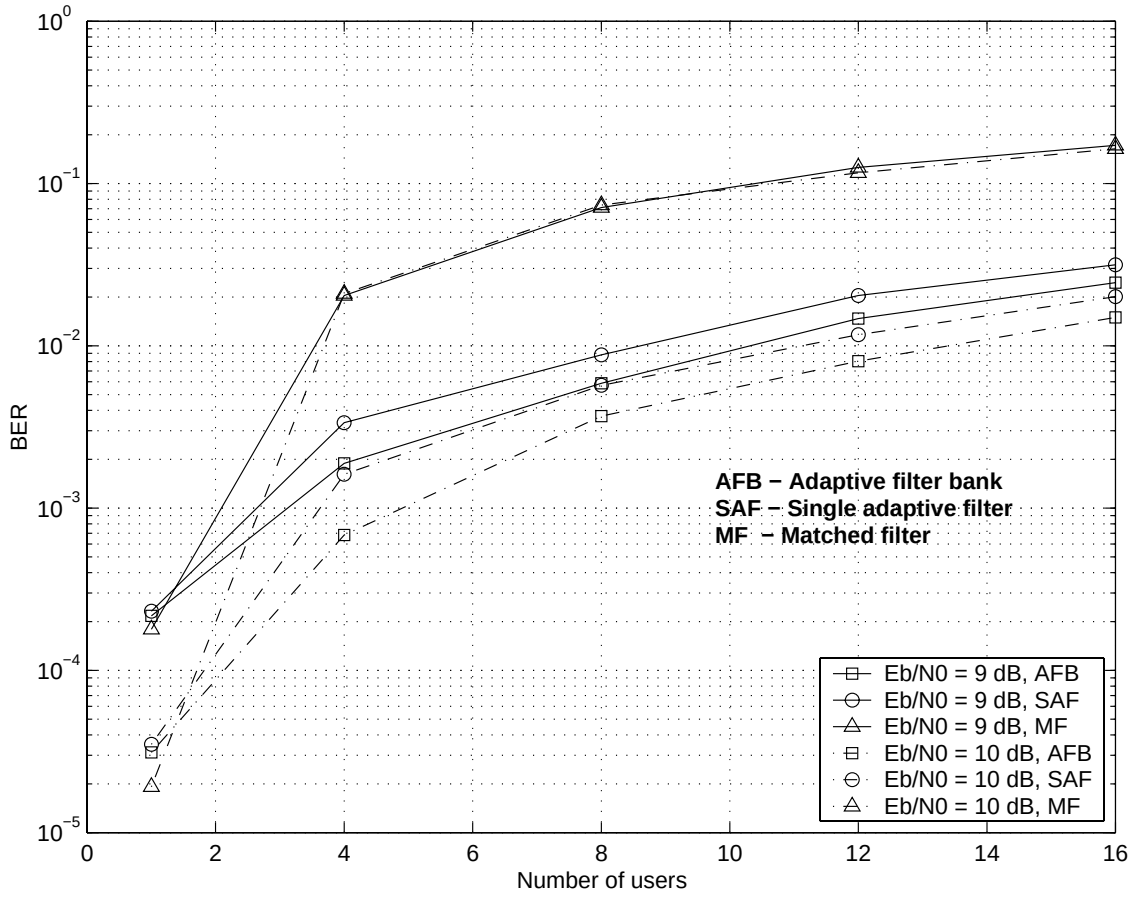

Figure 7.17: BER Performance of the Three Receivers in an Asynchronous Channel with 25% of Users Having a Normalized Chip Rate of 1/2 and the Others Having a Normalized Chip Rate of 1/8 (the Desired User's Normalized Chip Rate is 1/2).

Table 7.1: Simulations Parameters.

Carrier frequency	2.050 GHz
Data rate	128 kbps
Chip rate	1.92 Mcps
Sample rate	3.84 Mcps

two receivers in Figure 7.17 compared with Figure 7.16. While the advantage of the AFBR over the SAFR is about 1 dB in the first case, this margin is reduced in the second case, at least for light system loads. For heavier loads, the AFBR maintains a gain of about 1 dB. These results demonstrate that as the chip rates of the MAI signals decrease, the SAFR is better able to suppress the interference.

7.7 Simulation Results for Multipath Fading Channels

The main weakness of the AFBR in fading channels is its restricted ability to track time-varying channels. Of the L filters in the filter bank, only the filter that is used to demodulate the received signal is adapted. Thus, each weight vector is updated only once every L symbols. Therefore, the more the number of filters in the filter bank, the less frequently each filter can be adapted and the poorer its tracking ability. This limitation is important when considering the performance of the AFBR in rapidly time-varying channels.

In this section, the performances of the receivers are compared in different multipath fading channels. Both synchronous and asynchronous links are considered. For the synchronous forward link, the same propagation channel is used for all of the users. For the asynchronous reverse link, an independent channel is used for each user. The same delay profile is employed for all of the users but the signals are independently faded. Also, all the mobiles are assumed to travel at the same speed with respect to the base station. While this last assumption may not represent a practical scenario, the results obtained with it may be used as realistic performance limits. Some of the general signal parameters used for the simulations are given in Table 7.1. Others are specific to each case.

Two multipath channel models are used for the simulations. The channel parameters are described by Table 7.2. In each case, the SNR (E_b/N_0) is measured with respect to the first multipath component. The first channel has a large delay spread with just two components, whereas the second channel has a very small delay spread with four

Table 7.2: Multipath Channel Models Used for Simulations.

Channel Model	**Component**	**Multipath Delay** (μs)	**Multipath Amplitude**	**Type of Fading**
Two-Ray Rayleigh	1	0.0	1	Rayleigh
	2	5.0	0.5	Rayleigh
COST-207 Rural	1	0.0	1.0	Ricean
	2	0.2	0.7937	Rayleigh
	3	0.4	0.3162	Rayleigh
	4	0.6	0.1	Rayleigh

components. As seen in Chapter 6, the Rural channel can provide a large multipath gain.

The problem encountered with the decision-directed algorithm in fading channels was described in Chapter 5. When the signal goes through a deep fade or when there is strong interference, the weight vector is adapted on decisions made in a closed eye situation, which do not have a very high probability of being correct. This can cause loss of convergence of the algorithm. The adaptation algorithm can either get trapped in an undesirable local minimum or suffer catastrophic failure, leading to a BER of 0.5. Although the soft decision-directed algorithm used here alleviates the problem to some extent, it does not completely overcome it. Infrequent update of the weight vectors in the AFBR aggravates the problem. Hence, the AFBR cannot operate effectively in rapidly time-varying channels, something that a more robust algorithm could enable. There is no simple method for penalizing the receiver, which is ideally desirable, for catastrophic failure of the algorithm. Counting all of the errors is a harsh penalty since receivers are normally capable of detecting very high BERs and the receiver can request for retraining. We take the approach of limiting each simulation trial to 10000 bits, i.e., the filter is re-trained every 10000 bits. If the BER of the receiver exceeds 0.25 during any 1000 bit period within the trial, the algorithm is regarded to have "failed" and the errors accrued in that simulation trial are discounted.

Although only a single filter is necessary in the single-user case, L filters are used in the AFBR for the single-user case in all simulations, where L is the number of filters required for the multiple-user cases. This maintains consistency and also helps to demonstrate the impact of using a bank of filters in the single-user case with each filter being adapted infrequently. Consequently, simulation results for a single user may not match up for two examples using different numbers of filters in the AFBR.

7.7.1 Performance When Users Have Different Code Lengths

The signal model here is the same as that in Section 7.6.1. Several cases are considered for both forward and reverse links.

Case 1: Synchronous System with Mobile Speeds of 10 km/h

Except for the single-user case, in all of the cases one quarter of the users have spreading codes of length 16, and the remaining users have other code lengths, the distribution of code lengths varying for different examples. The mobile speed is 10 km/h in this case, which causes a maximum Doppler frequency of about 19 Hz.

In the first example, three quarters of the users are assigned codes of length 32. The performance of the receivers is illustrated in Figure 7.18. Figure 7.18(a) demonstrates the performances in a two-ray Rayleigh fading channel while Figure 7.18(b) shows the performances in a Rural channel. The performance of the AFBR in the first channel is marginally better (by a few dB) than that of the SAFR. The BERs of the receivers in the multipath fading channels are primarily determined by their performances in the noise-limited deep-fade situations because most of the bit errors occur during these times. Increasing the SNR helps the AFBR more than it does the other two receivers. The lack of improvement of the BER of the SAFR may be attributed to the poor performance of the decision-directed algorithm at low BERs. The AFBR, however, does exhibit an improvement. In the second channel, the performance of both adaptive receivers is enhanced by multipath gain. However, the relative performance of the AFBR compared with the SAFR is even better than in the two-ray channel. The SAFR suffers from greater interference due to multipath of the MAI signals. It should be noted that each filter in the AFBR is adapted once every two symbols.

In the second example, three quarters of the users have codes of length 64. The results for the two channels in this case are plotted in Figure 7.19. The figures show that the SAFR performs worse than in the previous example as a result of the increased number of interference patterns. Neither does the AFBR maintain its performance, a result of the more infrequent update of each filter weight vector—each of the four weight vectors is updated once every *four* symbols. Nevertheless, the AFBR is vastly superior to the SAFR over most of the range of system loads.

In the final example of this case, one quarter of the users are assigned spreading codes of each of the lengths 16, 32, 64, and 128. Figure 7.20 shows the simulation results. The performance of the AFBR in this example, while surprising at first, is easily explained. We note that the AFBR consists of eight filters, each of which is adapted once every *eight* symbols. The channel does not vary rapidly, yet the channel changes fast enough to degrade the AFBR's performance. The result is that the AFBR performs worse than the SAFR with one and four users despite having better interference rejection capability.

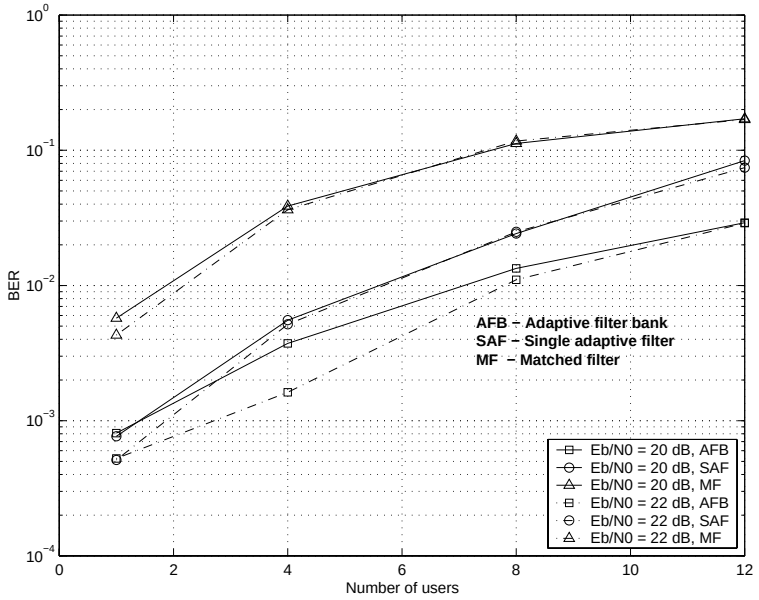

(a)

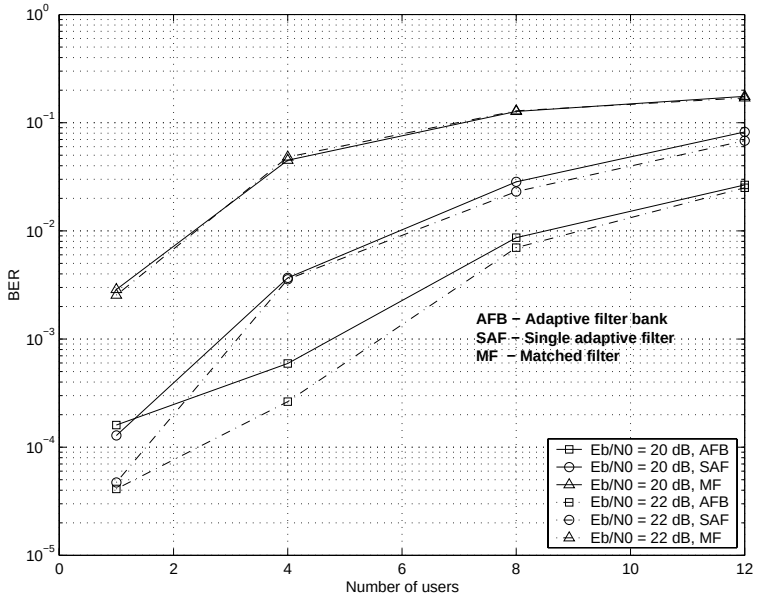

(b)

Figure 7.18: BER Performance of the Three Receivers in a Synchronous (a) Two-Ray Rayleigh Fading Channel and (b) COST-207 Rural Channel with 25% of Users Having Codes of Length 16 and the Others Having Codes of Length 32 (the Desired User's Code Length 16).

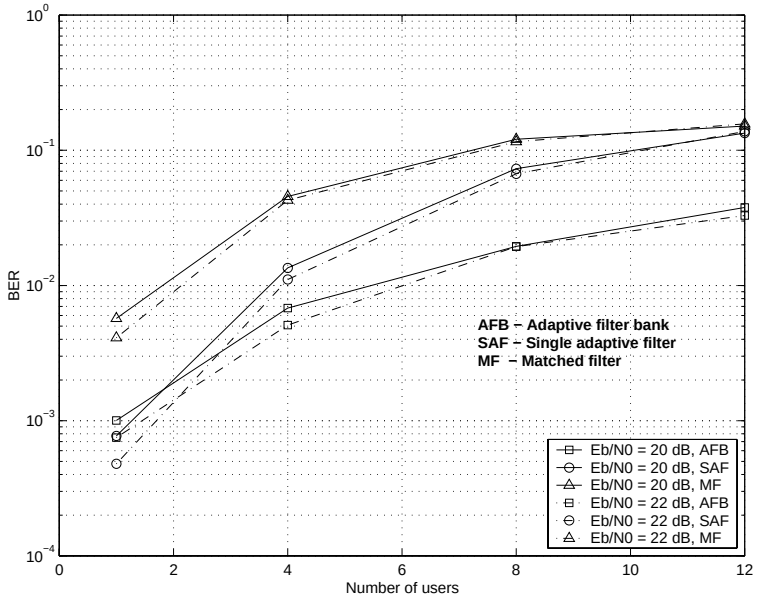

(a)

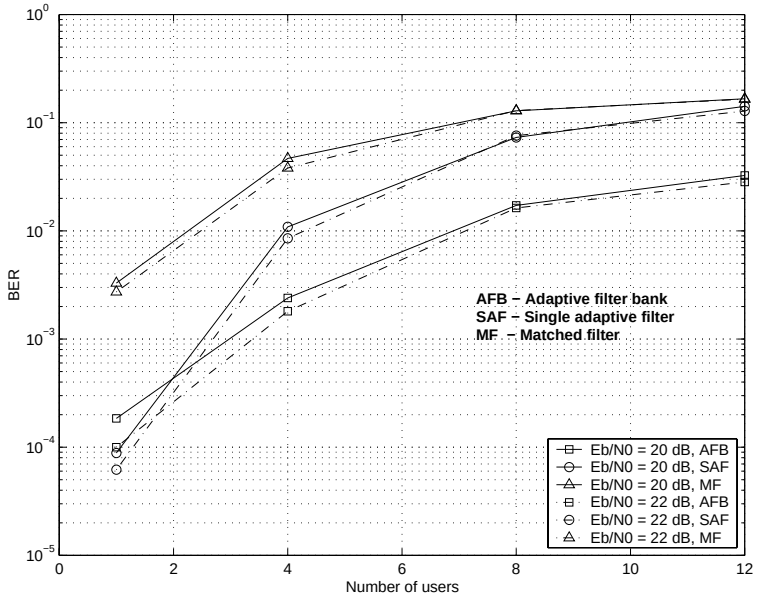

(b)

Figure 7.19: BER Performance of the Three Receivers in a Synchronous (a) Two-Ray Rayleigh Fading Channel and (b) COST-207 Rural Channel with 25% of Users Having Codes of Length 16 and the Others Having Codes of Length 64 (the Desired User's Code Length 16).

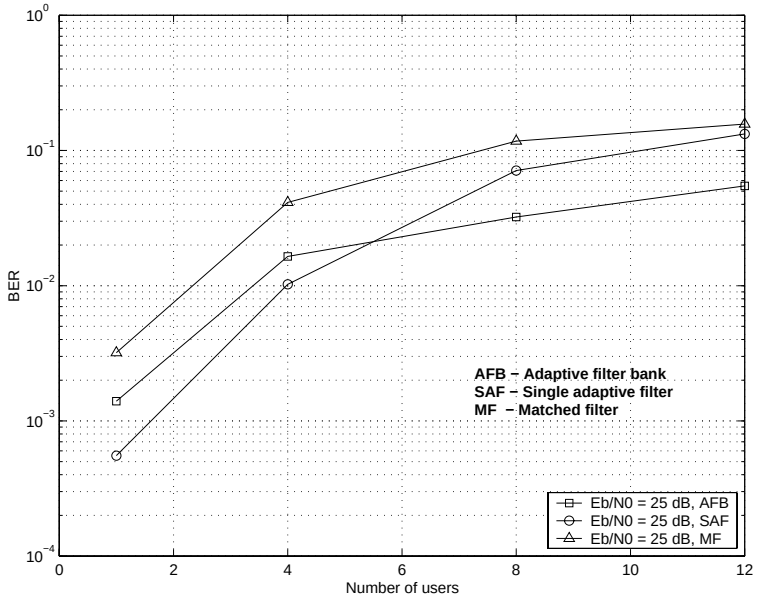

(a)

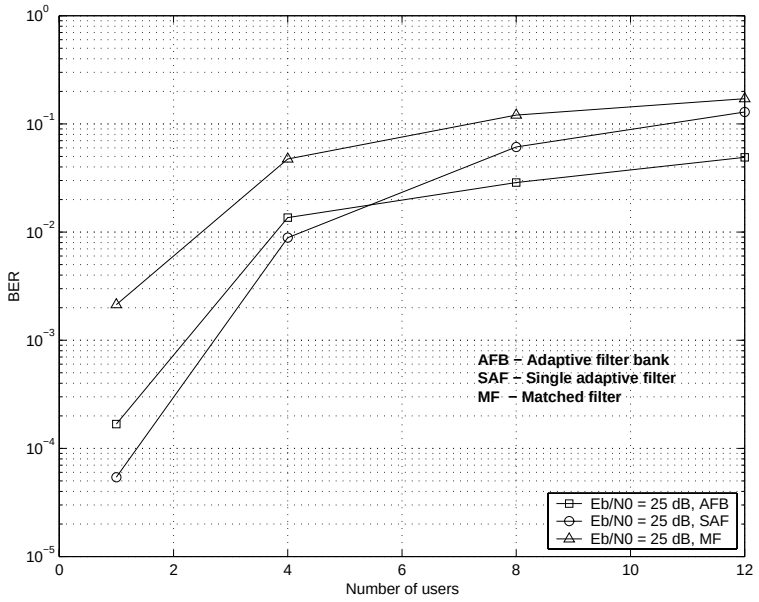

(b)

Figure 7.20: BER Performance of the Three Receivers in a Synchronous (a) Two-Ray Rayleigh Fading Channel and (b) COST-207 Rural Channel with 25% of Users Having Codes of Lengths 16, 32, 64, and 128. (the Desired User's Code Length 16).

However, for higher system loads, the superiority of the AFBR in suppressing MAI signals overrides the degradation resulting from poor tracking. Thus, the BER curves for the SAFR and AFBR cross between five and six users. Similar observations can be made for both channels except that the performance of the adaptive receivers is slightly better in the Rural channel due to a higher effective SNR. Increasing the step-size for the AFBR slightly improves its tracking ability, but increases the probability of catastrophic failure of the soft decision-directed algorithm, i.e., increases the failure rate. The overhead due to increased failure rate outweighs the gain purchased by BER improvement. For this reason, a step-size of $\mu_0 = 0.1$ for the NLMS algorithm is used for all of the simulations.

The results of this case highlight the strengths of the AFBR and also its weakness. The AFBR is significantly superior to the SAFR if its weight vectors can be frequently updated. If the disparity between code lengths is large, the number of interference patterns that have to be suppressed is also large, which maximizes the utility of the AFBR. At the same time, the number of filters in the filter bank is high, which leads to infrequent adaptation of the filters, reducing the effectiveness of the AFBR in suppressing interference if the channel changes rapidly. It must be emphasized that the performance of each adaptive receiver is limited by the ability of the soft decision-directed algorithm to *reliably* track the channel. A more robust but complex adaptation algorithm can be expected to diminish this problem and yield better results.

Case 2: Synchronous System with Mobile Speeds of 20 km/h

In this case, the mobile velocity is increased to 20 km/h, resulting in a maximum Doppler frequency of about 38 Hz. A higher SNR is used for the simulations to reduce the failure rate.

The first example presented here is similar to the first example of Case 1. Figure 7.21 shows the results. The AFBR yields a marginal improvement over the SAFR. The relatively poor performance of the AFBR is due to its inability to effectively track the channel.

The second example in this case is similar to the second example of Case 1. The results are plotted in Figure 7.22. The weakness of the AFBR already begins to show here with the single-user BER being worse for the AFBR than for the SAFR. When there is MAI, the AFBR is only slightly superior to the SAFR. When we compare this example with the preceding example, we see that the gain yielded by the AFBR is greater here, as expected.

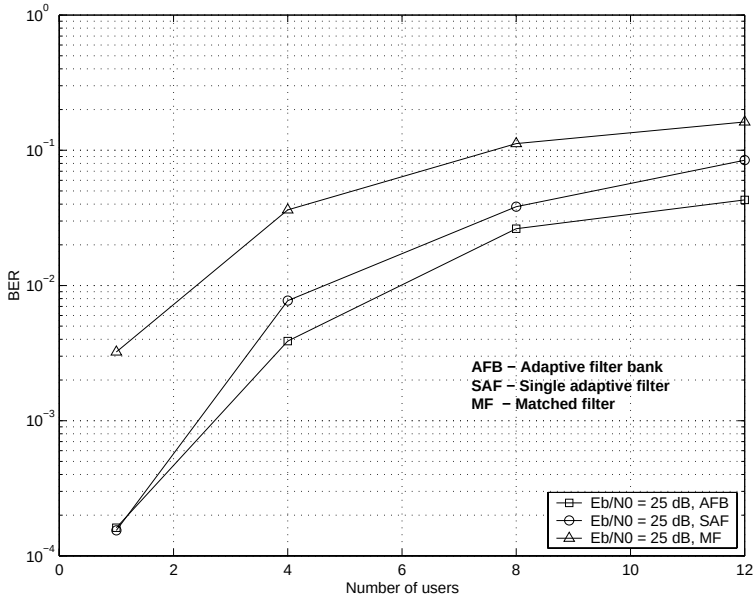

(a)

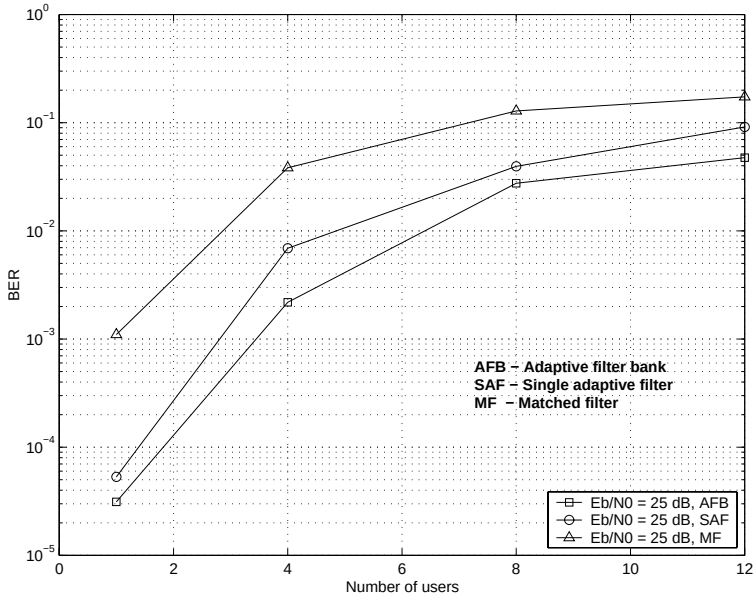

(b)

Figure 7.21: BER Performance of the Three Receivers in a Synchronous (a) Two-Ray Rayleigh Fading Channel and (b) COST-207 Rural Channel with 25% of Users Having Codes of Length 16 and the Others Having Codes of Length 32 (the Desired User's Code Length 16).

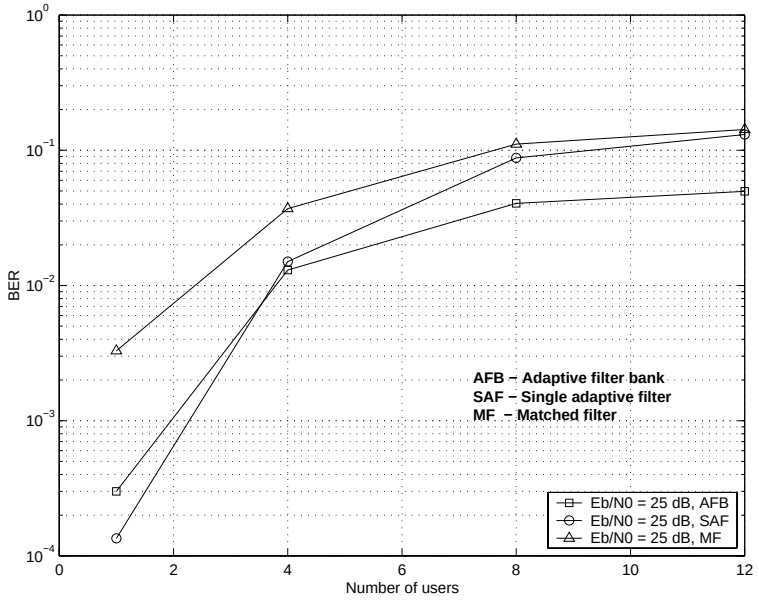

(a)

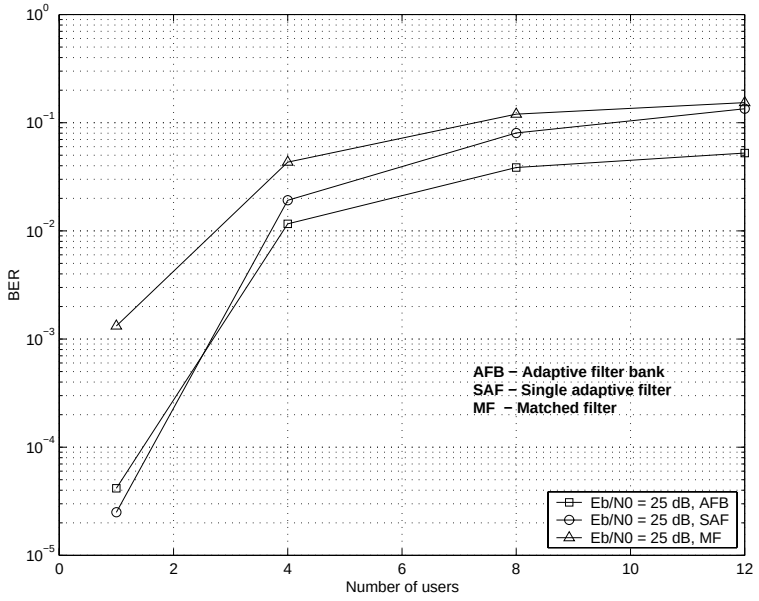

(b)

Figure 7.22: BER Performance of the Three Receivers in a Synchronous (a) Two-Ray Rayleigh Fading Channel and (b) COST-207 Rural Channel with 25% of Users Having Codes of Length 16 and the Others Having Codes of Length 64 (the Desired User's Code Length 16).

Case 3: Asynchronous System with Mobile Speeds of 10 km/h

In each case, except for the single user case, one quarter of the users have a code with length 16, and the others have a different code length. The mobile speed is 10 km/h.

In the first example, the second group, comprising three quarters of all users, is assigned codes of length 32. The simulation results are depicted in Figure 7.23. In the two-ray Rayleigh fading channel, the AFBR yields a very small improvement over the SAFR. Since the signal from each user propagates over an independent channel, the interference is very dynamic. The optimum solution varies more dynamically here than in the synchronous link because both the SNR and the signal-to-interference ratios vary over time. Each filter weight vector in the AFBR is updated every other symbol and this proves debilitating to the AFBR. The performance of the AFBR is slightly better in the Rural channel because of the increased effective SNR.

In the next example, the second group of users is assigned codes of length 64. Figure 7.24 illustrates the performances of the receivers in this case. Here the performance of the AFBR is barely better than that of the SAFR. The AFBR weight vectors are updated only once every four symbols, which degrades its performance. Thus, the gain provided by the AFBR over the SAFR is almost completely nullified in this example by the time-varying channel.

7.7.2 Performance When Users Have Different Chip Rates

The signal model here is the same as that in Section 7.6.2. Simulation results are provided for only the forward link.

Figure 7.25 shows the performance of the receivers when one quarter of the users, including the desired user, have a normalized chip rate of 1/2 and the rest have a normalized chip rate of 1/4. The AFBR yields almost negligible gain over the SAFR in the two-ray Rayleigh fading channel. However, the BER improvement is better in the Rural channel.

Figure 7.26 illustrates the performance of the receivers when three quarters of the users have a normalized chip rate of 1/8. In this case, the AFBR has eight filters, each of which is adapted once every eight symbols. The AWGN channel results of Section 7.6.2 show that the gain yielded by the AFBR in this instance is small. This, coupled with the infrequent weight vector update, ensures that the AFBR performs worse than the SAFR in both multipath channels being considered. The performance of the AFBR can be expected to be worse in asynchronous channels and, hence, we do not present simulation results for these channels.

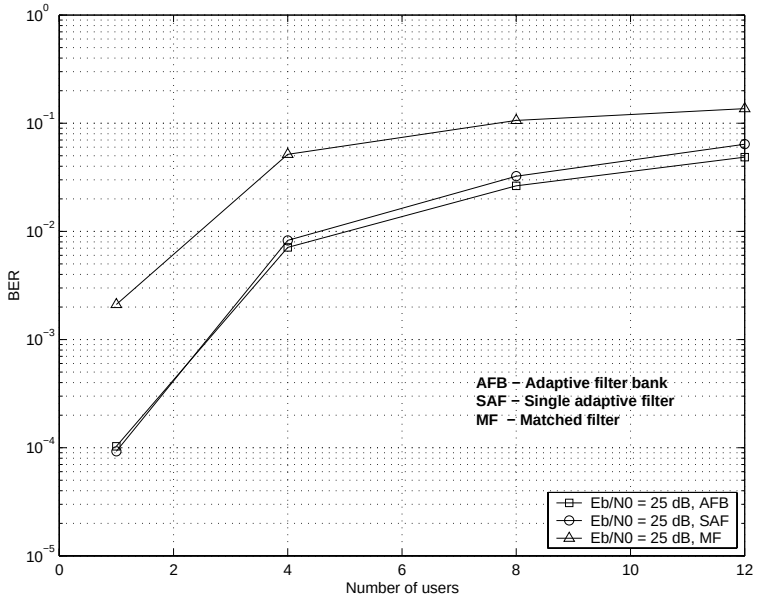

(a)

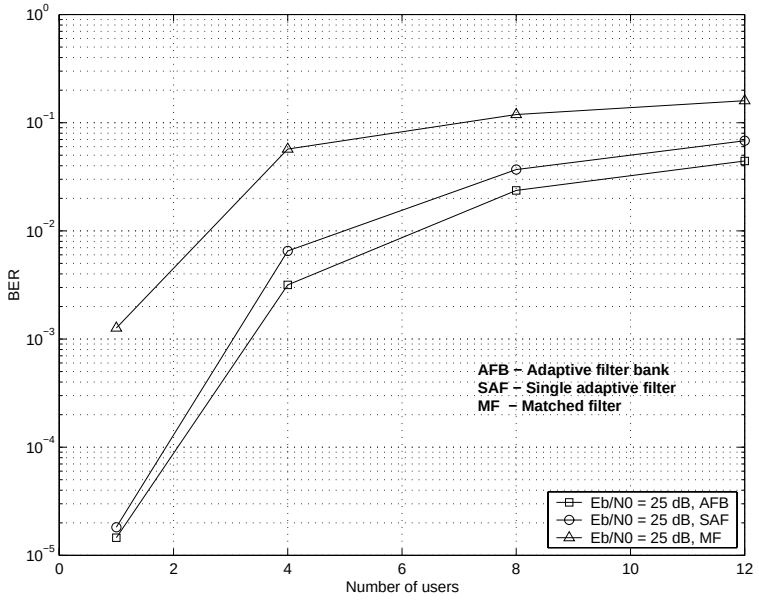

(b)

Figure 7.23: BER Performance of the Three Receivers in an Asynchronous (a) Two-Ray Rayleigh Fading Channel and (b) COST-207 Rural Channel with 25% of Users Having Codes of Length 16 and the Others Having Codes of Length 32 (the Desired User's Code Length 16).

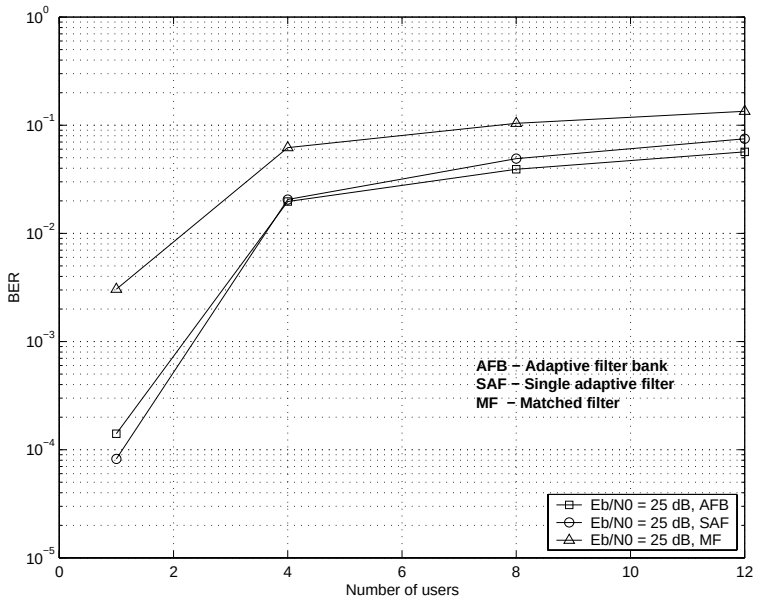

(a)

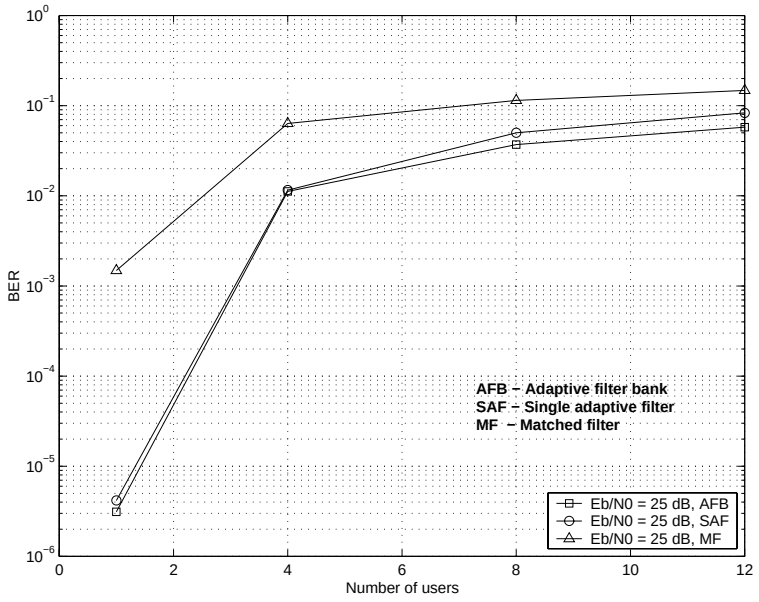

(b)

Figure 7.24: BER Performance of the Three Receivers in an Asynchronous (a) Two-Ray Rayleigh Fading Channel and (b) COST-207 Rural Channel with 25% of Users Having Codes of Length 16 and the Others Having Codes of Length 64 (the Desired User's Code Length 16).

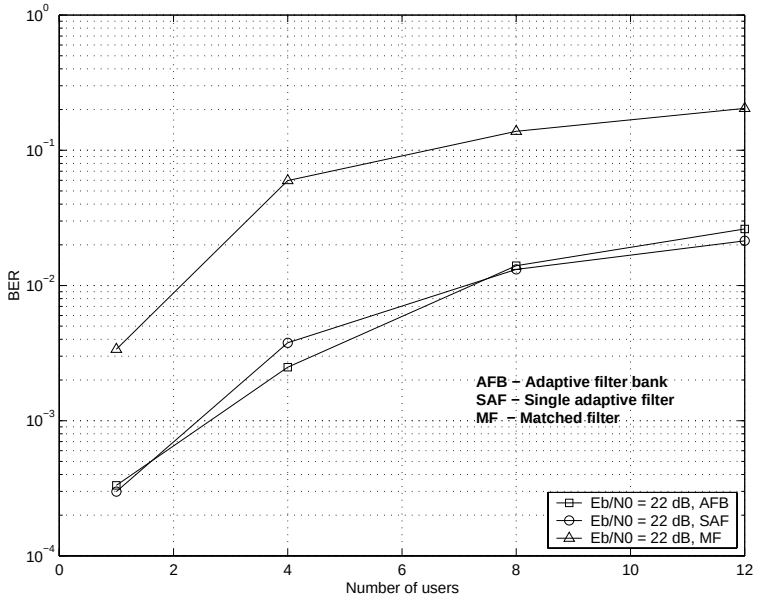

(a)

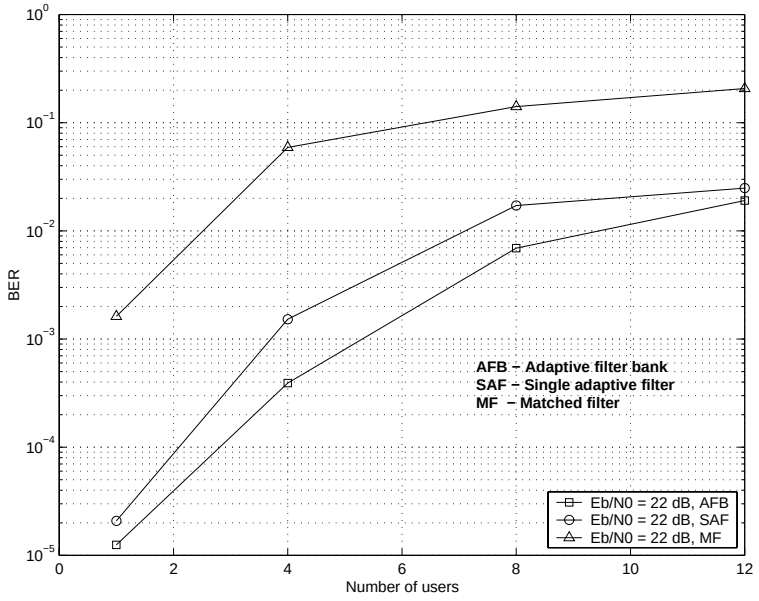

(b)

Figure 7.25: BER Performance of the Three Receivers in a Synchronous (a) Two-Ray Rayleigh Fading Channel and (b) COST-207 Rural Channel with 25% of Users Having a Normalized Chip Rate of 1/2 and the Others Having a Normalized Chip Rate of 1/4 (the Desired User's Normalized Chip Rate is 1/2).

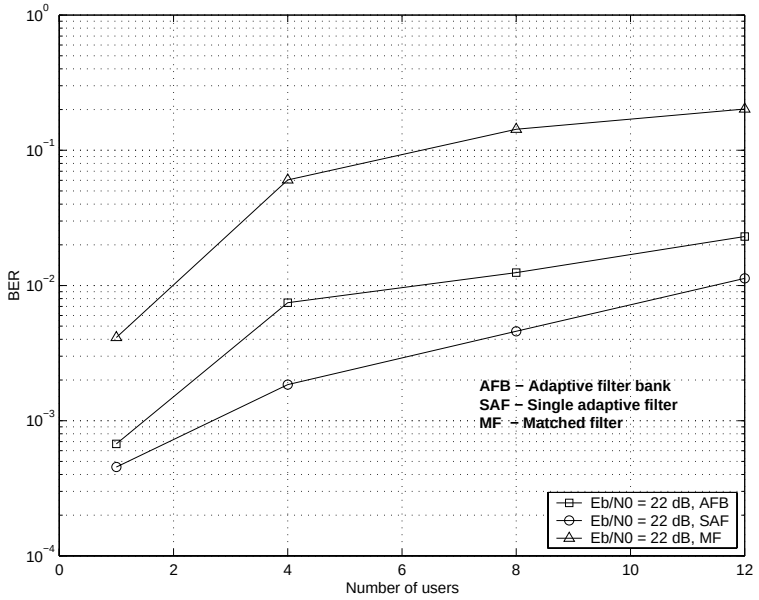

(a)

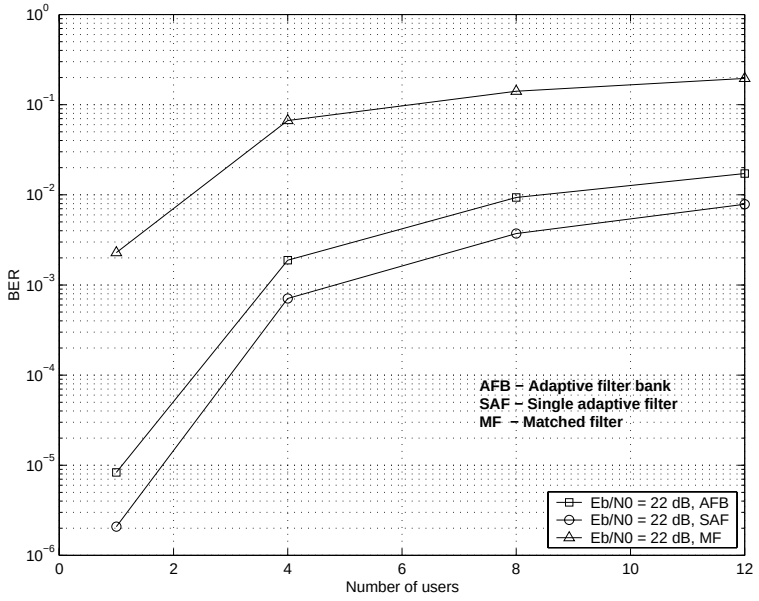

(b)

Figure 7.26: BER Performance of the Three Receivers in a Synchronous (a) Two-Ray Rayleigh Fading Channel and (b) COST-207 Rural Channel with 25% of Users Having a Normalized Chip Rate of 1/2 and the Others Having a Normalized Chip Rate of 1/8 (the Desired User's Normalized Chip Rate is 1/2).

7.8 Use of Filter Bank Receivers in Third Generation Wideband CDMA Systems

Third-generation (3G) PCS systems aim at providing a wide range of services, including paging, audio, video, and data services [1, 2, 101, 105]. There is a provision for a flexible physical layer that can support a large range of varying bit rates so that bandwidth can be provided on demand. Furthermore, users with different rates also have different quality of service requirements [4]. Spreading factors are adjusted to yield the same spread bandwidth for all users. Thus, users of the multi-rate system can have different code lengths. As seen in this chapter, adaptive filter bank receivers are useful in improving the performance of matched filter receivers or single adaptive filter receivers in such systems.

Several concepts for the radio interface were investigated by European research programs. An outcome of this research was the decision to employ the Future Radio Wideband Multiple Access System (FRAMES) technology for the Universal Mobile Telecommunications System (UMTS) [3]. Two modes are proposed:

- FMA1—wideband TDMA with and without spreading
- FMA2—direct sequence wideband CDMA

The European Telecommunications Standards Institute (ETSI) Special Mobile Group (SMG2) set up five concept groups [1] for radio interface, one of which is the wideband CDMA (WCDMA) concept group, to which FRAMES contributed FMA2. The Association of Radio Industries and Businesses (ARIB) for the 3G systems standardization in Japan also contributed to this proposal, leading to a common proposal between ETSI and ARIB for the WCDMA parameters [4]. The ETSI proposal yielded the main uplink parameters while ARIB contributed the main downlink parameters. Both frequency-division duplex (FDD) mode and time-division duplex (TDD) mode, harmonized to have the same chip rate, fame length, and number of slots per frame, have been proposed [4].

Third-generation systems have provisions for multi-user detection techniques on the reverse link or uplink and FMA2 has made spreading with long codes optional to facilitate advanced receiver technologies. As a result, multi-rate signals without long code spreading retain strong cyclostationary features, which enables the use of filter bank receivers instead of matched filter receivers or Rake receivers to enhance receiver performance and thus improve system capacity.

Figure 7.27 shows the spreading and modulation on the uplink of FMA2. The dedicated physical data channel (DPDCH) and the dedicated physical control channel (DPCCH) are carried on the same signal. As the figure shows, each is spread by a different channelization code ($\mathbf{c}_{\mathrm{D}}$ or $\mathbf{c}_{\mathrm{C}}$). Orthogonal variable spreading factors (OVSFs) are used for

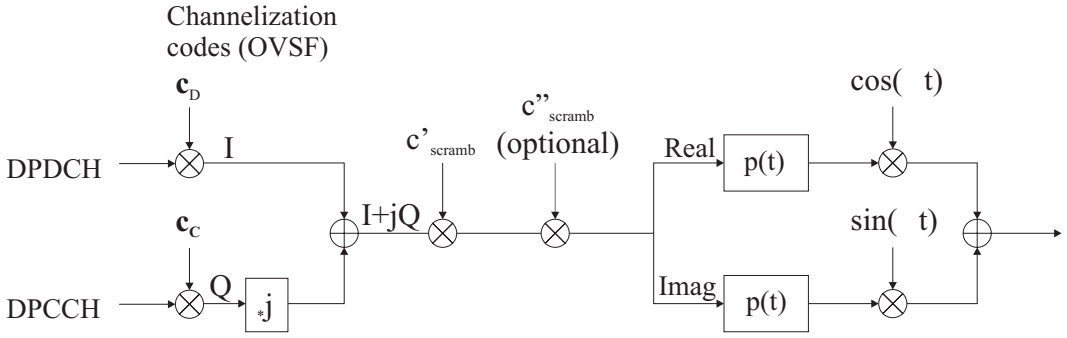

Figure 7.27: Uplink Spreading and Modulation in WCDMA.

channelization [1]. The length of the channelization codes is 2^k, where $k = 0, 1, \ldots, 8$ and depends on the data rate (the chip rate is always 4.096 Mcps). The two spread channels are combined to form a complex signal of the form $\mathrm{I} + j\,\mathrm{Q}$. To maintain good spectral properties, the complex spread signal is scrambled by a complex code, whose real and imaginary components are constructed from the extended Very Large Kasami set of length 256. Due to its better interference averaging properties, the long scrambling code is used in receivers that do not perform interference cancellation. Thus, when only a short scrambling code is used, the DPDCH (DPCCH) may be considered to have been spread by a composite code $\mathbf{c}_{\mathrm{D}}\,\mathbf{c}'_{\mathrm{scramb}}$ ($\mathbf{c}_{\mathrm{C}}\,\mathbf{c}'_{\mathrm{scramb}}$) of length 256. It is noted that the rates and, hence, the spreading factors for the I and Q channels can be different. When users have different rates, we have a multi-rate system where the interference vectors for any signal change cyclically over time. A filter bank receiver can be employed to suppress the periodically time-varying interference. However, since the I and Q channels are spread by different composite codes, the I and Q data should be demodulated by two independent filter bank receivers. Since the two channels are orthogonal to each other, they do not interfere with each other. Lastly, the DPDCH has pilot symbols whereas the DPCCH does not. Therefore, trained algorithms can be used for the DPDCH whereas blind algorithms should be used for the DPCCH. Further investigation of the application of adaptive filter bank receivers in 3G systems is beyond the scope of this work and is recommended for future research.

7.9 Summary

This chapter presented the optimal receiver structure for a CDMA system in which the cyclostationary characteristics of the various users in the system differ. When the spreading code of each signal in the system repeats every symbol period of the desired user's signal, the optimum minimum mean-squared error (MMSE) receiver is a single

filter. However, when the code repeat rates of the signals differ, the optimum MMSE receiver is, in fact, a bank of filters. This was shown through an analytical derivation. The MMSEs of a single filter receiver and a filter bank receiver were compared. A numerical example was used to illustrate how the MMSE of the filter bank receiver is better than that of a single filter receiver when users have different code lengths.

Extensive simulation results were provided to demonstrate the performance of the matched filter receiver, an adaptive single filter receiver, and an adaptive filter bank receiver, where the normalized least mean square algorithm was used for initial adaptation. Simulation results were provided for both additive white Gaussian noise (AWGN) channels and multipath fading channels. Two sets of cases were considered: users having different code lengths and users have different chip rates. In the first set of cases, the adaptive filter bank receiver (AFBR) was shown to yield a performance gain of about 3 dB over the single adaptive filter receiver (SAFR) in synchronous AWGN channels. In the second set of cases, the performance gain was shown to be about 1 dB in AWGN channels. The relative improvement of the performance of the SAFR was explained as a mitigated effect of interference signals with a lower chip rate. In multipath fading channels, the AFBR yields large performance gains over the SAFR if the channel is slowly time-varying. When there is a large disparity in the code lengths and chip rates of the desired user and multiple access interference users, the number L of filters in the AFBR is larger and each filter is adapted once every L symbols, which may not be frequent enough. Furthermore, the poor performance of the decision-directed algorithm when the eye is closed in fading channels tends to further degrade the performance of the AFBR. Adaptation algorithms that are more robust in fading channels can improve the performance of the AFBR. Simulation results show that the AFBR is not substantially better than the SAFR and can be worse than the SAFR in some scenarios. Thus, the large gains that the AFBR can potentially yield when L is large are offset to some extent by the receiver's weakness in fading channels. The interference rejection performance is traded off for better tracking ability in these dynamic systems. Nevertheless, there are many situations where the AFBR proves vastly superior to the SAFR. Overall, it was seen that the adaptive filter bank receiver warrants employment in multi-rate systems since it does not incur any overhead in computational complexity and incurs only a minor overhead in the form of increased storage over the adaptive single filter receiver. Furthermore, since each filter of the L-filter AFBR is adapted once every L symbols, the training period for the AFBR is longer than that for the SAFR. Since the filter weights converge rapidly when initialized with the spreading code coefficients, this is not considered a serious disadvantage.

Third-generation systems are adopting CDMA technology. The wideband CDMA technology proposed by ETSI and ARIB has provisions for advanced receivers. The variable rate signals on the uplink of the proposed wideband CDMA have the option of being spread by only a short code, in which case the signals reduce to the form of multi-rate signals investigated in this chapter. Hence, filter bank receivers can be employed instead of conventional receivers to suppress interference and improve system performance.

Chapter 8

Adaptive Receivers for Signals with Carrier Frequency Offsets

8.1 Introduction

The recovery of a digital communications signal transmitted over a wireless medium requires the knowledge of certain parameters of the signal of interest. One such parameter is the carrier frequency of the signal, which is needed so that, upon downconversion, the original baseband signal is recovered with additive ambient and receiver noise and interference. Most signal processing techniques are effective when the carrier frequency is either known or can be estimated.

Some signal detection techniques require the knowledge of the *phase* of the carrier signal in addition to the knowledge of the carrier frequency. Therefore, carrier *tracking*, which establishes accurate knowledge of the instantaneous carrier phase and thereby, frequency of the signal of interest, must be implemented at the receiver. Such schemes are termed *phase-coherent* detection techniques [18, 106]. Effective phase-coherent detection will maximize receiver performance.

Unfortunately, the establishment of a phase-coherent carrier reference at the receiver is often either impractical or impossible. Factors that influence this aspect of the implementation include constraints on the receiver complexity as well as economic considerations. In these circumstances, *noncoherent detection* techniques may be used to receive the information signal [18, 106]. As the name suggests, these schemes do not require tracking the carrier phase. Compared with the phase-coherent detection schemes, these techniques suffer from a performance penalty.

In PSK signaling systems there is yet another class of detection techniques that may be employed when the carrier reference signal is known to within a fixed phase. Known as

differentially coherent detection techniques [106], they are useful when it is not possible to resolve this fixed phase ambiguity. Differentially coherent detection is implemented when information is encoded in the phase *difference* between successive transmitted symbols. Thus, detection of the phase differences between successive symbols in the received signal amounts to recovery of the original information signal. These techniques are also accompanied by a performance degradation in comparison with the phase-coherent techniques because each detected symbol is influenced by more than one demodulated symbol.

In mobile communications, where there is relative motion between the transmitter and the receiver, the *Doppler* effect contributes to a carrier frequency offset at the receiver. A practical receiver is not devoid of imperfections even if the radio propagation channel is assumed to be ideal. One source of error is the local oscillator used to generate the carrier frequency in the transmitter. Even the most stable local oscillators are subject to small drifts over time and with temperature changes. Even if the transmitter local oscillator is assumed to be ideal, the transmitted carrier frequency is insufficient information for the receiver since it is impossible to have an ideal local oscillator at the receiver. Economic considerations have a bearing on the quality of the local oscillator at the transmitter and the receiver and hence on their stabilities. The conclusion is, regardless of the oscillator stabilities, there is bound to be a frequency offset on the signal recovered by the receiver. Optimum receiver performance, therefore, calls for some form of compensation of carrier offset to be implemented at the receiver.

In this chapter, a brief outline of conventionally used carrier recovery schemes is provided. An extensive survey of the literature in this area may be found in [17]. The objective here is to introduce the schemes that are applicable in CDMA systems and to investigate their performances when used in adaptive receivers for mobile radio channels. These schemes are viewed as carrier offset compensation techniques, rather than carrier recovery techniques, based on the assumption that some *a priori* information about the carrier is available to the receiver. The MMSE solution of the optimum receiver in the presence of carrier frequency offsets is derived. The MSE obtained with a coherent adaptive receiver using the LMS is analyzed. The stationary points of the cost function corresponding to the differentially coherent implementation of the LMS algorithm are examined. Simulation results of the receiver structures presented here, obtained during joint work with Nicoloso [17], show that an adaptive receiver in conjunction with differentially coherent detection can also compensate for frequency offsets, obviating a separate offset compensation scheme altogether. The BER performances of these various receiver implementations in a variety of radio propagation channels are studied through extensive simulations.

8.2 Traditional Techniques for Frequency Offset Compensation

Frequency offset compensation schemes fall under two main categories: *open-loop* schemes and *closed-loop* schemes. Closed-loop schemes rely on a feedback control system to correct for frequency offsets. These techniques are based on the phase-locked loop (PLL), which consists of a loop filter that filters the error signal, which in turn is obtained by mixing the incoming signal whose phase is to be estimated with the reference signal. The filtered signal drives the voltage-controlled oscillator that generates the reference signal. Thus, a PLL attempts to drive the error signal—in this case the difference between the instantaneous *phases* of the input and reference signals—to zero at steady-state. A PLL can also correct for frequency offsets since a frequency offset may also be construed as a continuous phase offset. Techniques for automatic frequency control (AFC) are similar to PLLs but differ in that the error signal in these schemes measures the *frequency* difference, rather than the *phase* difference, between the input and reference signals. Open-loop schemes, on the other hand, do not involve any feedback. They employ conventional techniques for parameter estimation. In particular, the incoming signal is used to derive an estimate, such as a *maximum-likelihood* (ML) estimate or a *maximum a posteriori* (MAP) estimate, of the instantaneous frequency or phase, which is then appropriately used for compensation. An exhaustive literature survey on open-loop and closed-loop compensation techniques is provided by Nicoloso [17], but we discuss here only those that yielded adequate performance in CDMA environments receivers, both conventional and adaptive, while maintaining reasonable complexity. In the following sections, the Costas loop and open-loop maximum likelihood phase estimators are outlined.

8.2.1 Costas Loop

The Costas loop [106] performs the dual functions of tracking a suppressed carrier and demodulating the signal. Figure 8.1 is a depiction of the analog implementation of the Costas loop. When the input signal $s(t) = \sqrt{2P}\, d(t)\, cos(2\pi f_c t + \theta)$ where $d(t)$ is a binary information signal, then $i(t)$ is of the form $\sqrt{P/2}\, d(t)\, \cos(\theta - \hat{\theta})$ since the double frequency term produced during mixing is removed by the low-pass filter (LPF). Similarly, $q(t)$ is of the form $\sqrt{P/2}\, d(t)\, \sin(\theta - \hat{\theta})$. To remove the modulating signal $d(t)$, $i(t)$ and $q(t)$ are mixed together to obtain $e(t) = (P/4)\, \sin(2\phi)$ where $\phi = \theta - \hat{\theta}$ is the phase difference between the input signal and the reference signal. When $e(t)$ is small, $e(t) \approx 2\phi$. Thus, the error signal driving the voltage controlled oscillator (VCO) is proportional to the phase difference. At steady-state, this error is small and $i(t) \approx \sqrt{P/2}\, d(t)$ since $\cos(\phi) \approx 1$. Thus, if the LPF bandwidth is made equal to the information signal bandwidth, out-of-band noise is removed and $i(t)$ yields the demodulated signal.

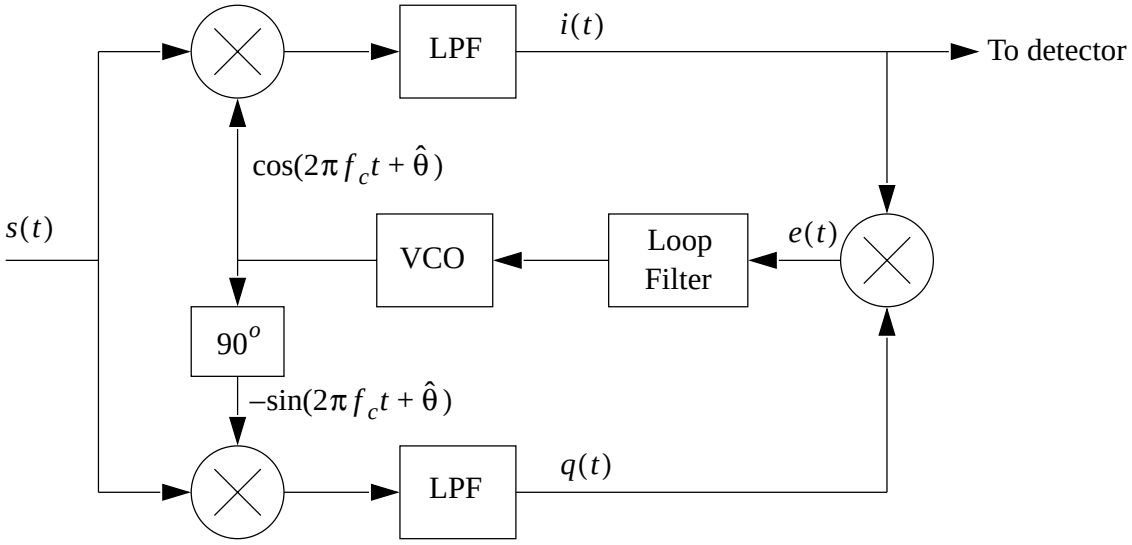

Figure 8.1: Analog Implementation of the Costas Loop.

Figure 8.2 shows the discrete-time implementation of the Costas loop. The variance of the phase estimate in the Costas loop has a contribution from *squaring loss*, which is attributed to the squaring operation performed on noise when computing $e(t)$, the product of $i(t)$ and $q(t)$ [17]. This loss, while negligible for high input SNRs, is significant for low SNRs, and imposes constraints on the loop bandwidth. The integrate-and-dump filters (IDFs) indicated in the discrete-time implementation improve the SNR seen by the loop, assuming correct symbol synchronization. When the pulse shape is not rectangular, these IDFs are replaced with symbol-matched filters. It is to be noted that the loop operates at the symbol rate and is characterized by a longer acquisition time than a sample-rate implementation. Hardlimiting in the I-arm of the loop is common when the input SNR is high, making the error term proportional to ϕ rather than 2ϕ, and the analysis of the Costas loop more closely follows that of a PLL. Furthermore, the output of the hardlimiter yields the bit estimate directly in the case of BPSK modulation.

8.2.2 Open-Loop Phase Estimators

Divsalar and Simon [107] proposed a number of open-loop phase estimation schemes based on maximum likelihood (ML) estimation theory. A first-order[1] ML phase estimator applied to binary modulation is illustrated in Figure 8.3. The output of the matched filter is sampled at the symbol rate. N successive symbol estimates where N is an arbitrary

[1]Nicoloso used the term "order" in [17] to describe these various estimators, noting the analogies between these estimators and PLLs of different orders.

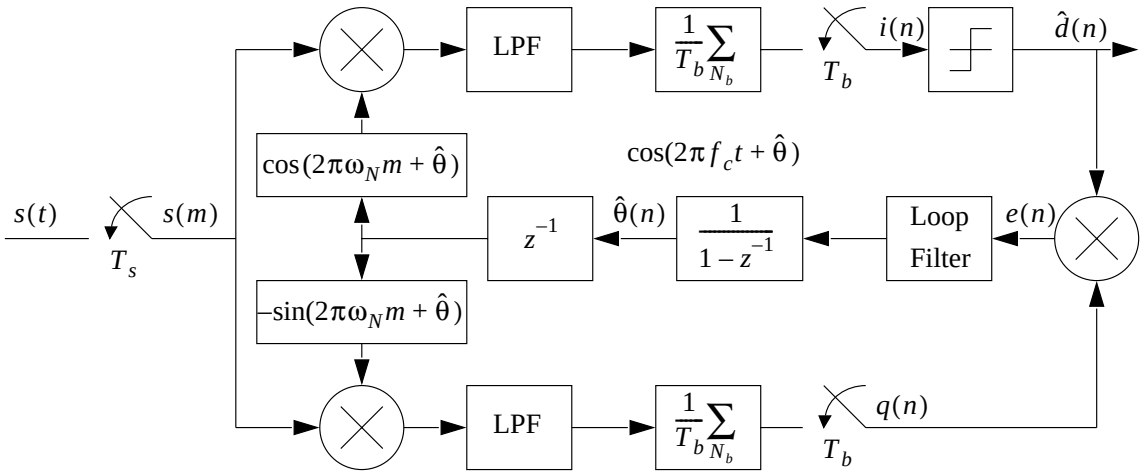

Figure 8.2: Discrete-Time Implementation of the Costas Loop.

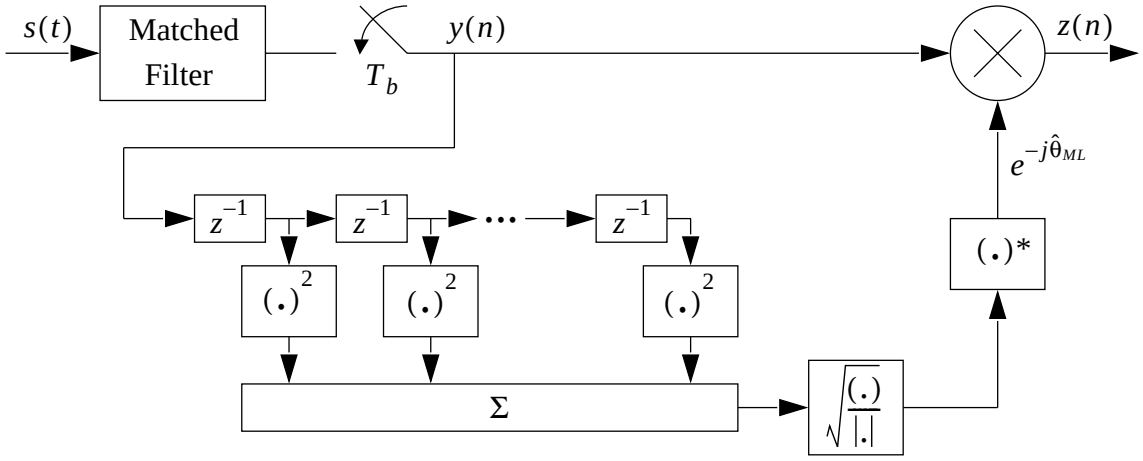

Figure 8.3: First-Order ML Phase Estimation Scheme.

parameter, are squared and averaged. The squaring results in doubling the phase of each sample. Thus, what results after the square-root operation is an estimate of the phase of the matched filter output samples with a 180° phase ambiguity. The matched filter output is multiplied with the conjugate of the resultant estimate to remove its residual phase. Differentially coherent detection may be used to overcome the phase ambiguity. It can be shown [17] that the phase estimate is in fact the ML estimate if the input SNR is assumed to be low. Nicoloso has discussed the analogy between the ML estimator and the Costas loop.

When there is a residual frequency offset on the input signal, the carrier phase θ changes over the N-symbol averaging period and the steady-state errors of the first-order ML phase estimator structures do not have zero mean. The actual carrier phase at the symbol sampling instant may be modeled as a linearly increasing parameter over time. When the frequency offset is assumed to be uniformly distributed over $(-f_{\max}, f_{\max})$, where $f_{\max}$ is the maximum expected frequency offset, it can be shown that a low SNR assumption results in the ML estimation structure given in Figure 8.4 [107]. In this figure, $\gamma_i = \text{sinc}(4f_{\max}iT_b)$. The 180° phase-jump detector observes when a symbol crosses the imaginary axis and multiplies the phase estimate by ± 1 as appropriate. Phase estimation errors caused by the squaring operation followed by the square root operation[2], are, thereby, eliminated. For optimal performance, this scheme requires that the maximum frequency offset $f_{\max}$ be known to the receiver. Moreover, it is suitable only when the residual frequency offset is "small."

8.3 MMSE Solution in the Presence of Frequency Offsets on the Signals

The residual frequency offsets on downconverted signals are generally different for the users on the reverse link. The complex sampled received signal at baseband $r(n)$ at time instant m may be represented as

$$r(m) = \sum_{k=1}^{K} a_k \, e^{j\left(2\pi \frac{f_k}{f_s} m + \psi_k\right)} \, d_k(m - m_k) \, c_k(m - m_k) + \nu(m) \tag{8.1}$$

where K is the total number of users, a_k is the amplitude of the kth user's signal, f_k is the carrier frequency offset on the kth user's signal, ψ_k is the phase offset on the kth user's signal, f_s is the sampling frequency. In Equation (8.1), $d_k(m)$ is the kth user's information signal, $c_k(m)$ is the kth user's spreading signal, m_k is the delay of the kth user's signal, and $\nu(m)$ is the sampled noise. We note that samples of any element of

[2]The combination of these two operations limits the phase estimate to the $(-\pi, \pi]$ range, whereas the actual phase is continuous in the complex plain.

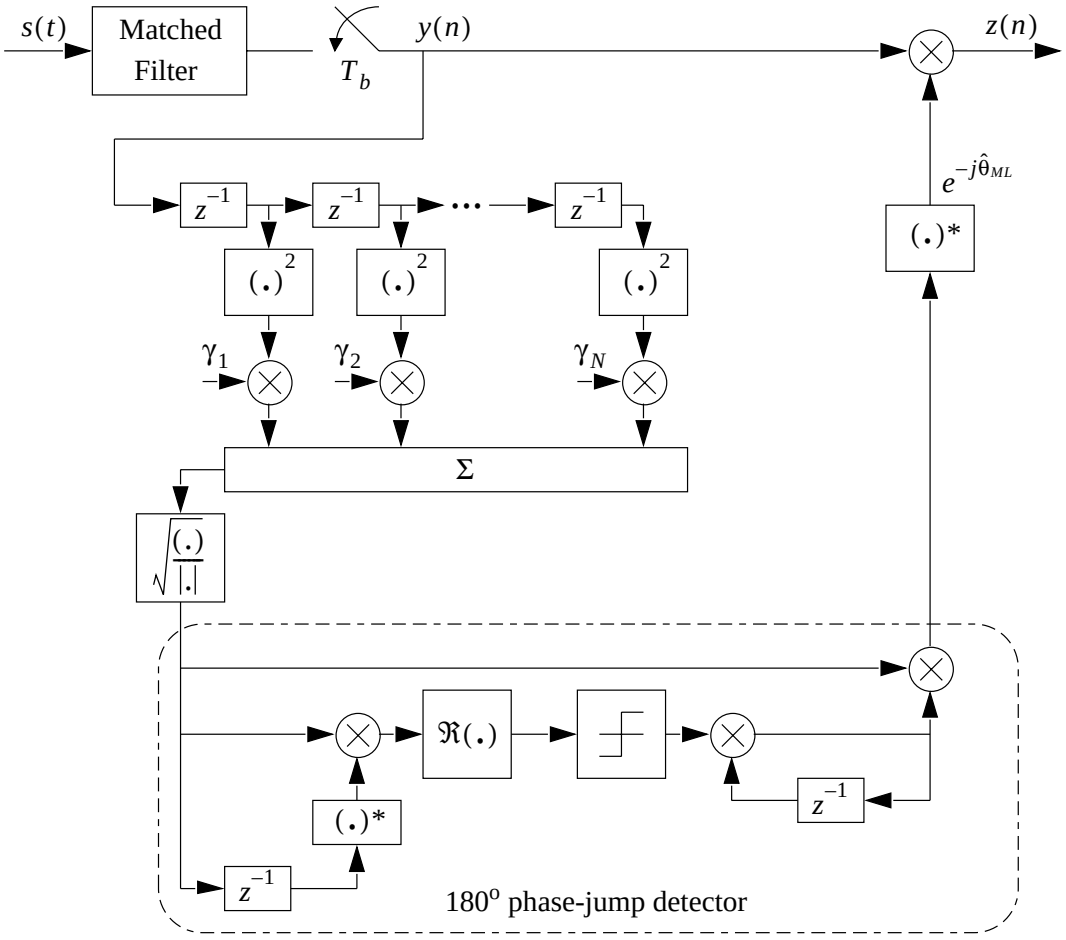

Figure 8.4: Modified First-Order ML Phase Estimation Scheme for Compensation of Small Residual Frequency Offsets.

successive received signal vectors $\mathbf{r}(n)$ and $\mathbf{r}(n+1)$ are N samples apart in the received signal $r(m)$, where N is the spreading code length. Thus, for the mth element in the nth signal vector, we have

$$\begin{aligned} r(m+nN) &= \sum_{k=1}^{K} a_k\, e^{j\left(2\pi\frac{f_k}{f_s}(m+nN)+\psi_k\right)}\, d_k(m-m_k+nN)\, c_k(m-m_k) \\ &\quad + \nu(m+nN) \\ &= \sum_{k=1}^{K} a_k\, e^{j\left(2\pi\frac{f_k}{f_s}m+\psi_k\right)}\, e^{j\left(2\pi\frac{f_k}{f_s}nN\right)}\, d_k(m-m_k+nN)\, c_k(m-m_k) \\ &\quad + \nu(m+nN). \end{aligned} \tag{8.2}$$

In this equation, the total instantaneous phase offset on the mth element of the nth input signal vector has been broken up into a component that varies over time and another component that is time-invariant for that element. The received signal vector may be expressed as

$$\mathbf{r}(n) = \sum_{k=1}^{K} a_k \, e^{j\psi_k} \, e^{j\left(2\pi \frac{f_k}{f_s} nN\right)} \, \mathbf{s}_k(n) + \boldsymbol{\nu}(n) \tag{8.3}$$

where the mth element of $\mathbf{s}_k(n)$ is given by

$$s_{km}(n) = d_k(m - m_k + nN) \left[e^{j\left(2\pi \frac{f_k}{f_s} m\right)} \, c_k(m - m_k) \right]. \tag{8.4}$$

This means that the kth user's data signal is spread by a new time-invariant spreading code $\bar{\mathbf{c}}_k$ whose mth element is $e^{j2\pi f_k (m+m_k)/f_s} \, c_k(m)$. Note that the time-invariant phase is incorporated into the spreading code while the time-varying phase offset is retained as a frequency offset. Furthermore, the contribution from the kth user's signal to any element in subsequent received signal vectors has a constant phase shift of $e^{j2\pi f_k N/f_s}$. It may be seen that the time-invariant correlation matrix $\mathbf{R} = E[\mathbf{r}(n)\,\mathbf{r}^H(n)]$ is independent of this phase shift. The cross-correlation vector, however, is time-varying:

$$\begin{aligned} \mathbf{p}(n) &= E[d_1(n)\,\mathbf{r}(n)] \\ &= a_1 \, e^{j\psi_1} \, e^{j\left(2\pi \frac{f_1}{f_s} nN\right)} \, \bar{\mathbf{c}}_1. \end{aligned} \tag{8.5}$$

As a result, the time-dependent MMSE solution is

$$\begin{aligned} \mathbf{w}_{\text{opt}}(n) &= \mathbf{R}^{-1} \, \mathbf{p}(n) \\ &= a_1 \, e^{j\psi_1} \, e^{j\left(2\pi \frac{f_1}{f_s} nN\right)} \, \mathbf{R}^{-1} \, \bar{\mathbf{c}}_1 \\ &= e^{j\left(2\pi \frac{f_1}{f_s} nN\right)} \, \tilde{\mathbf{w}}_{\text{opt}} \end{aligned} \tag{8.6}$$

where

$$\tilde{\mathbf{w}}_{\text{opt}} \stackrel{\triangle}{=} a_1 \, e^{j\psi_1} \, \mathbf{R}^{-1} \, \bar{\mathbf{c}}_1 \tag{8.7}$$

is a time-invariant vector. We note that the fixed vector of Equation (8.7) depends on the new code vector $\bar{\mathbf{c}}_1$. We may also write Equation (8.6) as

$$\mathbf{w}_{\text{opt}}(n) = e^{j\left(2\pi \frac{f_1}{f_s} N\right)} \, \mathbf{w}_{\text{opt}}(n-1). \tag{8.8}$$

Equation (8.6) shows that the MMSE solution is a rotating vector in the presence of frequency offsets on the signals. The frequency of rotation depends on the offset f_1 on the desired user's signal and the length N of the spreading code. As Equation (8.8) shows, this may be interpreted as a constant phase shift between the optimal vectors for successive symbols.

8.4 MSE of the Adaptive Receiver with the LMS Algorithm in the Presence of Frequency Offsets

The MSE of the adaptive filter at time instant n is given by

$$J(n) = E[|[d(n) - \mathbf{w}^H(n)\,\mathbf{r}(n)]|^2] \tag{8.9}$$

where the weight vector may be written in terms of the optimal vector $\mathbf{w}_{\text{opt}}$ and the weight error vector $\mathbf{v}(n)$ as

$$\mathbf{w}(n) = \mathbf{w}_{\text{opt}} + \mathbf{v}(n). \tag{8.10}$$

Using Equation (8.10) in Equation (8.9) and further simplifying [39], we get

$$J(n) = J_{\min} + E[\mathbf{v}^H(n)\mathbf{R}\,\mathbf{v}(n)]. \tag{8.11}$$

The independence assumption has been used in deriving the above equation.

From Equation (8.11) it is clear that the MSE is composed of the MMSE and a second additive term that is dependent on the weight-error vector. Since the latter term is positive (the correlation matrix $\mathbf{R}$ is positive definite, so $E[\mathbf{v}^H(n)\mathbf{R}\mathbf{v}(n)]$ is positive for all k), the MSE with the LMS algorithm is always greater than the MMSE by an amount known as the *excess mean-squared error* (EMSE):

$$\begin{aligned} J_{\text{ex}}(n) &\triangleq J(n) - J_{\min} && (8.12)\\ &= E[\mathbf{v}^H(n)\mathbf{R}\mathbf{v}(n)]. && (8.13) \end{aligned}$$

At any k, the weight error vector is the sum of the error vectors due to gradient noise and weight error lag [108]. Thus, it may be expressed as

$$\begin{aligned} \mathbf{v}(n) &= \mathbf{w}(n) - \mathbf{w}_{\text{opt}}(n) \\ &= \underbrace{\mathbf{w}(n) - E[\mathbf{w}(n)]}_{\text{weight vector noise}} + \underbrace{E[\mathbf{w}(n)] - \mathbf{w}_{\text{opt}}(n)}_{\text{weight vector lag}} \end{aligned} \tag{8.14}$$

where the expectations are ensemble averages [108]. Any difference between $E[\mathbf{w}(n)]$ and the actual optimal vector $\mathbf{w}_{\text{opt}}(n)$ is attributed to the lag in the adaptation process, i.e., due to the adaptive weight vectors failing to keep up with the rotating optimal vector. The difference between the weight vector and its expected value is due to the gradient noise in the adaptation.

Using Equation (8.14) in Equation (8.13) for the EMSE yields [108]

$$\begin{aligned} J_{\text{ex}}(n) &= E\left[(\mathbf{w}(n) - E[\mathbf{w}(n)])^H \mathbf{R} (\mathbf{w}(n) - E[\mathbf{w}(n)])\right] \\ &\quad + E\left[(E[\mathbf{w}(n)] - \mathbf{w}_{\text{opt}}(n))^H \mathbf{R} (E[\mathbf{w}(n)] - \mathbf{w}_{\text{opt}}(n))\right]. \end{aligned} \tag{8.15}$$

where the property $E[\mathbf{w}_{\text{opt}}(n)] = \mathbf{w}_{\text{opt}}(n)$ has been used. The total EMSE is thus composed of the EMSE due to gradient noise,

$$J_{\text{ex(noise)}}(n) = E\left[(\mathbf{w}(n) - E[\mathbf{w}(n)])^H \mathbf{R} (\mathbf{w}(n) - E[\mathbf{w}(n)])\right], \tag{8.16}$$

and the EMSE due to lag,

$$J_{\text{ex(lag)}}(n) = E\left[(E[\mathbf{w}(n)] - \mathbf{w}_{\text{opt}}(n))^H \mathbf{R} (E[\mathbf{w}(n)] - \mathbf{w}_{\text{opt}}(n))\right]. \tag{8.17}$$

To compute the EMSE due to gradient noise, we note that the gradient noise is independent of the optimal weight vector $\mathbf{w}_{\text{opt}}(n)$. Therefore, gradient noise effects are not affected by the variability of $\mathbf{w}_{\text{opt}}(n)$ and, hence, lag effects may be ignored [108]. Defining

$$\hat{\mathbf{v}}(n) \triangleq \mathbf{w}(n) - E[\mathbf{w}(n)], \tag{8.18}$$

we get

$$J_{\text{ex(noise)}}(n) = E\left[\hat{\mathbf{v}}^H(n) \mathbf{R} \hat{\mathbf{v}}(n)\right] \tag{8.19}$$

Using the independence assumption, it can be shown that Equation (8.19) becomes [108]

$$J_{\text{ex(noise)}}(n) \approx \mu J_{\min} \operatorname{tr}[\mathbf{R}]. \tag{8.20}$$

Substitution of Equation (6.35) yields

$$\begin{aligned} \operatorname{tr}[\mathbf{R}] &= \operatorname{tr}[\sigma_\nu^2 \mathbf{I}_N + N\sigma_1^2 \mathbf{Q} \mathbf{L} \mathbf{Q}^H] \\ &= N\sigma_\nu^2 + N\sigma_1^2 \operatorname{tr}[\mathbf{L} \mathbf{Q} \mathbf{Q}^H] \\ &= N\sigma_\nu^2 + N\sigma_1^2 \operatorname{tr}[\mathbf{L} \mathbf{X}] \\ &= N\sigma_\nu^2 + N\sigma_1^2 \operatorname{tr}[\mathbf{L}] \\ &= N(\sigma_\nu^2 + \sum_{i=1}^{K_1} \sigma_i^2), \end{aligned} \tag{8.21}$$

resulting in

$$J_{\text{ex(noise)}}(n) \approx \mu\, J_{\min}\, N(\sigma_\nu^2 + \sum_{i=1}^{K_1} \sigma_i^2). \tag{8.22}$$

In the derivation of the EMSE due to lag, statistical knowledge of $E[\mathbf{w}(n)] - \mathbf{w}_{\text{opt}}(n)$ is required. Gradient noise effects may be neglected in determining lag effects so that we may assume $E[\mathbf{w}(n)] = \mathbf{w}(n)$ [108]. Therefore, we evaluate $\mathbf{v}^H(n)\,\mathbf{R}\,\mathbf{v}(n)$.

In the absence of gradient noise,

$$\mathbf{w}(n+1) = \mathbf{w}(n) - \mu[-\boldsymbol{\nabla}(J(n))] \tag{8.23}$$

and

$$J(n) = J_{\min} + \mathbf{v}^H(n)\,\mathbf{R}\,\mathbf{v}(n) \tag{8.24}$$

so that

$$\boldsymbol{\nabla}(J(n)) = 2\,\mathbf{R}\,\mathbf{v}(n), \tag{8.25}$$

yielding

$$\mathbf{w}(n+1) = \mathbf{w}(n) - 2\mu\,\mathbf{R}\,\mathbf{v}(n). \tag{8.26}$$

This may be rewritten as

$$\begin{aligned} \mathbf{w}(n+1) - \mathbf{w}_{\text{opt}}(n+1) &= \mathbf{w}(n) - \mathbf{w}_{\text{opt}}(n) - 2\mu\,\mathbf{R}\,\mathbf{v}(n) \\ &\quad + \mathbf{w}_{\text{opt}}(n) - \mathbf{w}_{\text{opt}}(n+1), \end{aligned} \tag{8.27}$$

that is,

$$\mathbf{v}(n+1) = \mathbf{v}(n) - 2\mu\,\mathbf{R}\,\mathbf{v}(n) + \mathbf{w}_{\text{opt}}(n) - \mathbf{w}_{\text{opt}}(n+1). \tag{8.28}$$

We assume that the weight vector $\mathbf{w}(n)$ lags behind the optimum vector $\mathbf{w}_{\text{opt}}(n)$ by a constant phase under steady-state conditions[3]. This phase lag depends on the tracking ability of the algorithm, i.e., the step-size and the SNR. Thus, the weight error vector

[3]Since gradient noise is assumed to be absent, this assumption is reasonable. If the phase lag monotonically decreases, then it will eventually converge to zero and this analysis becomes meaningless. If the phase lag monotonically increases, then the algorithm will diverge.

rotates at the same rate as the optimum weight vector at steady-state. Then, using Equation (8.8), we may write

$$\mathbf{v}(n+1) = e^{j\left(2\pi\frac{f_1}{f_s}N\right)}\,\mathbf{v}(n). \tag{8.29}$$

Using Equations (8.29) and (8.8) in Equation (8.28), we obtain

$$e^{j\left(2\pi\frac{f_1}{f_s}N\right)}\,\mathbf{v}(n) = \mathbf{v}(n) - 2\mu\,\mathbf{R}\,\mathbf{v}(n) + \mathbf{w}_{\text{opt}}(n) - e^{j\left(2\pi\frac{f_1}{f_s}N\right)}\,\mathbf{w}_{\text{opt}}(n), \tag{8.30}$$

which may be rewritten as

$$\left(2\mu\,\mathbf{R} - \left(1 - e^{j\left(2\pi\frac{f_1}{f_s}N\right)}\right)\mathbf{I}\right)\mathbf{v}(n) = \left(1 - e^{j\left(2\pi\frac{f_1}{f_s}N\right)}\right)\mathbf{w}_{\text{opt}}(n). \tag{8.31}$$

Assuming that the frequency offset is not zero, $e^{j\left(2\pi\frac{f_1}{f_s}N\right)} \neq 1$, i.e., $1 - e^{j\left(2\pi\frac{f_1}{f_s}N\right)} \neq 0$. Then, Equation (8.31) may be rearranged into

$$\left(\frac{2\mu}{1 - e^{j\left(2\pi\frac{f_1}{f_s}N\right)}}\,\mathbf{R} - \mathbf{I}\right)\,\mathbf{v}(n) = \mathbf{w}_{\text{opt}}(n) \tag{8.32}$$

or equivalently,

$$\mathbf{v}(n) = \left[\frac{2\mu}{1 - e^{j\left(2\pi\frac{f_1}{f_s}N\right)}}\,\mathbf{R} - \mathbf{I}\right]^{-1}\,\mathbf{w}_{\text{opt}}(n). \tag{8.33}$$

Therefore,

$$\begin{aligned}
&\mathbf{v}^H(n)\,\mathbf{R}\,\mathbf{v}(n) \\
&\quad= \left[\left(\frac{2\mu}{1 - e^{j\left(2\pi\frac{f_1}{f_s}N\right)}}\,\mathbf{R} - \mathbf{I}\right)^{-1}\mathbf{w}_{\text{opt}}(n)\right]^H \mathbf{R} \\
&\qquad\qquad \cdot \left[\left(\frac{2\mu}{1 - e^{j\left(2\pi\frac{f_1}{f_s}N\right)}}\,\mathbf{R} - \mathbf{I}\right)^{-1}\mathbf{w}_{\text{opt}}(n)\right] \\
&\quad= \mathbf{w}_{\text{opt}}^H(n)\,\left(\frac{2\mu}{1 - e^{-j\left(2\pi\frac{f_1}{f_s}N\right)}}\,\mathbf{R} - \mathbf{I}\right)^{-1}\,\left(\mathbf{R}^{-1}\right)^{-1} \\
&\qquad\qquad \cdot \left(\frac{2\mu}{1 - e^{j\left(2\pi\frac{f_1}{f_s}N\right)}}\,\mathbf{R} - \mathbf{I}\right)^{-1}\mathbf{w}_{\text{opt}}(n) \\
&\quad= \mathbf{w}_{\text{opt}}^H(n)\,\left[\left(\frac{2\mu}{1 - e^{j\left(2\pi\frac{f_1}{f_s}N\right)}}\,\mathbf{R} - \mathbf{I}\right)\,\mathbf{R}^{-1}\left(\frac{2\mu}{1 - e^{-j\left(2\pi\frac{f_1}{f_s}N\right)}}\,\mathbf{R} - \mathbf{I}\right)\right]^{-1}\mathbf{w}_{\text{opt}}(n) \\
&\quad= \mathbf{w}_{\text{opt}}^H(n)\,\left(\frac{4\mu^2}{2\left(1 - \cos\left(2\pi\frac{f_1}{f_s}N\right)\right)}\,\mathbf{R} - 2\mu\,\mathbf{I} + \mathbf{R}^{-1}\right)^{-1}\mathbf{w}_{\text{opt}}(n).
\end{aligned} \tag{8.34}$$

Substituting Equation (8.6), the EMSE due to lag is

$$\begin{aligned} J_{\text{ex(lag)}} &= \sigma_1^2\, \mathbf{c}_1^H\, \mathbf{R}^{-1} \left(\frac{4\mu^2}{2\left(1-\cos\left(2\pi\frac{f_1}{f_s}N\right)\right)}\, \mathbf{R} - 2\mu\, \mathbf{I} + \mathbf{R}^{-1} \right)^{-1} \mathbf{R}^{-1}\, \mathbf{c}_1 \\ &= \sigma_1^2\, \mathbf{c}_1^H \left(\frac{2\mu^2}{1-\cos\left(2\pi\frac{f_1}{f_s}N\right)}\, \mathbf{R}^3 - 2\mu\, \mathbf{R}^2 + \mathbf{R} \right)^{-1} \mathbf{c}_1. \end{aligned} \tag{8.35}$$

Using the eigenvalue decomposition of $\mathbf{R}$,

$$\mathbf{R} = \mathbf{M}\, \mathbf{\Lambda}\, \mathbf{M}^H, \tag{8.36}$$

Equation (8.35) may be re-expressed as

$$J_{\text{ex(lag)}} = \sigma_1^2\, \bar{\mathbf{c}}_1^H\, \mathbf{M} \left(\frac{2\mu^2}{1-\cos\left(2\pi\frac{f_1}{f_s}N\right)}\, \mathbf{\Lambda}^3 - 2\mu\, \mathbf{\Lambda}^2 + \mathbf{\Lambda} \right)^{-1} \mathbf{M}^H\, \bar{\mathbf{c}}_1. \tag{8.37}$$

Thus, the total EMSE is given by

$$J_{\text{ex}}(n) = J_{\text{ex(noise)}}(n) + J_{\text{ex(lag)}}(n) \tag{8.38}$$

where $J_{\text{ex(noise)}}(n)$ is given by Equation (8.22) and $J_{\text{ex(lag)}}(n)$ is given by Equation (8.35) or Equation (8.37). The EMSE due to gradient noise is independent of the frequency offset but depends on the step-size, the MMSE, the individual signal powers, and the noise variance. The EMSE due to the lag caused by frequency offset depends on the offset, the step-size and the input correlation matrix.

Figure 8.5 plots the MMSE $J_{\min}$, the EMSE due to gradient noise $J_{\text{ex(noise)}}(n)$, the EMSE due to lag $J_{\text{ex(lag)}}(n)$, and the total MSE $J(n)$ versus the frequency offset f_1 on the desired-user's signal when the step-size $\mu = 0.001$. For obtaining this figure, seven synchronous users are assumed to be present with AWGN. The curves are obtained by averaging over 900 trials where spreading codes for the seven users are randomly selected from a set of Gold codes of length 15. The sampling frequency is 3.84 Msamples/s. The figure shows that $J_{\text{ex(lag)}}(n)$ and, hence, $J(n)$ are very sensitive to a change in the frequency offset f_1. When the frequency offset is approximately 300 Hz, $J_{\text{ex(lag)}}(n)$ begins to exceed $J_{\min}$. On the other hand, the curve for $J_{\text{ex(noise)}}(n)$ shows that gradient noise has a very subdued effect. The graphs demonstrate that the excessive lag due to a low step-size can have devastating effects on the MSE of the adaptive filter.

Figure 8.6 depicts similar curves for a step-size $\mu = 0.004$. In this case, the higher step-size reduces the lag error and yields low values of $J_{\text{ex(lag)}}(n)$. However, gradient noise is

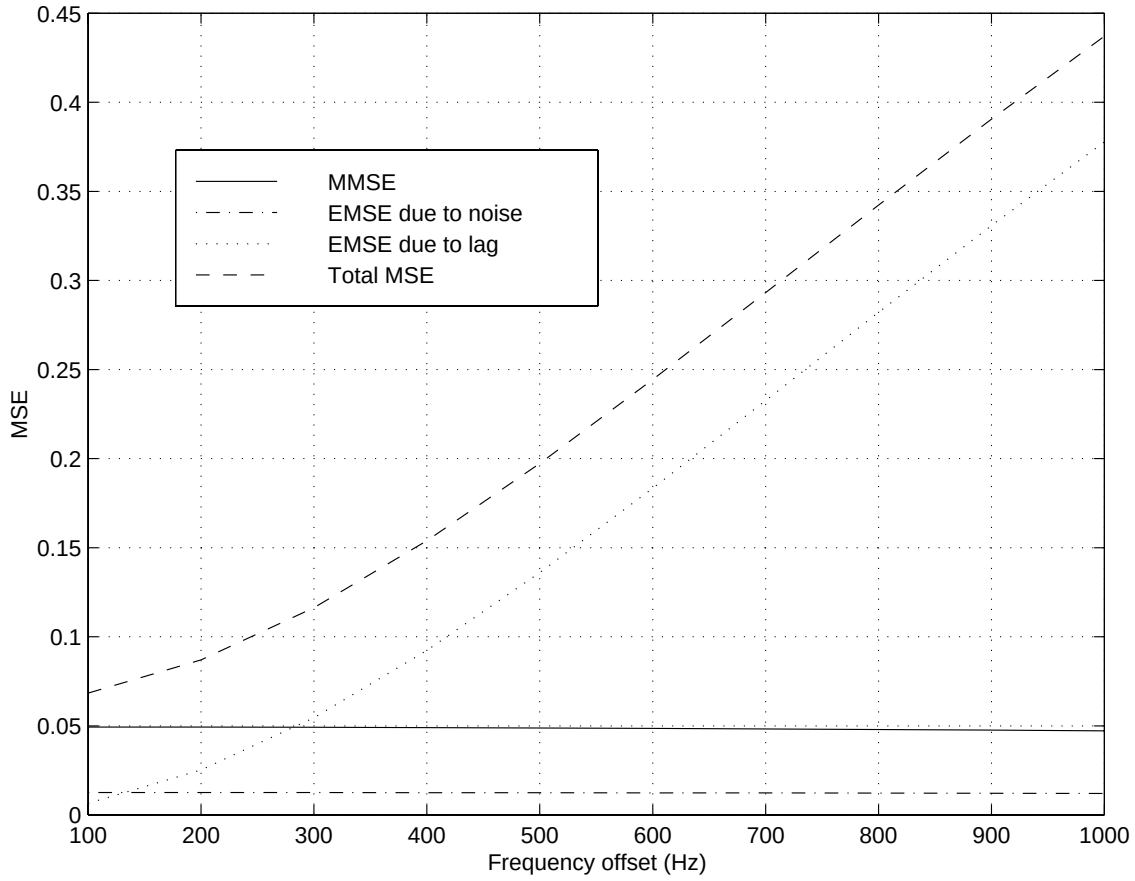

Figure 8.5: Variation of MSEs with Frequency Offset for a Step-Size $\mu = 0.001$.

dominant here and results in significant values for $J_{\text{ex(noise)}}(n)$ that are nearly equal to the $J_{\min}$. Comparing Figures 8.5 and 8.6, we see that a step-size of 0.001 is preferable for frequency offsets less than about 250 Hz whereas the step-size of 0.004 is desirable for higher frequency offsets. However, the large EMSE due to gradient noise may preclude the use of such high step-sizes.

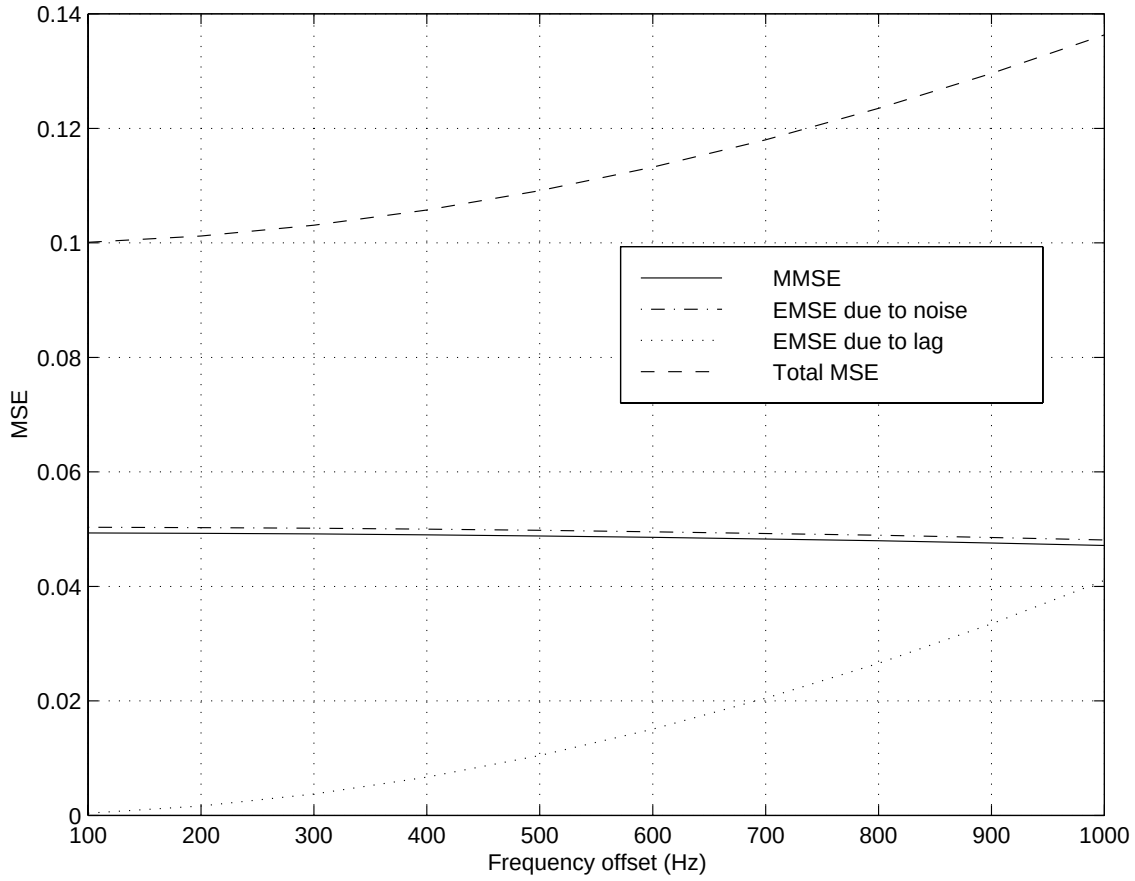

Figure 8.6: Variation of MSEs with Frequency Offset for a Step-Size $\mu = 0.004$.

8.5 Using an Adaptive Receiver in the Presence of Frequency Offsets: The Differentially Coherent Adaptive Receiver

Carrier frequency offset results in a rotating constellation for the detected symbols. The rate of this rotation depends on the magnitude of the frequency offset and its direction is determined by the sign of the offset. For a fixed frequency offset, the additional phase shift imparted to each symbol is fixed as well. Thus, the phase shift imparted to every symbol is small for "small" frequency offsets.

When it is not possible to track the carrier phase in a receiver, differentially coherent detection [14, 106], also termed differential detection, may be used along with corresponding differential encoding of information symbols at the transmitter (for PSK). In

differentially encoded PSK, the modulating symbols are formed by taking the phase difference between successive information symbols. Thus, the information is encoded in the *phase difference* of the transmitted symbols rather than being present in the transmitted symbols themselves. At the receiver, the information is recovered by measuring the phase difference between successive detected symbols. However, using differential detection instead of coherent detection can result in degraded BER since a noisy detected symbol may force errors in the two successive estimated symbols it influences.

Differential detection may also be used when small carrier frequency offsets are not tracked. The differentially detected symbol constellation is now spread in phase, this spread being dependent on the frequency offset. As long as the frequency offset (and hence, the phase spread) is small compared with the phase separation between neighboring constellation points, differential detection may be used with some degradation in performance.

An adaptive filter is capable of tracking channel variations over time if the step-size is large enough to accomplish this. As Section 8.4 demonstrated, however, the MSE of the adaptive receiver has another component, the EMSE due to the weight vector lag. The higher the frequency offset, the greater the EMSE due to lag. Furthermore, as seen in Section 8.4, a higher step-size improves the ability of the adaptive receiver to track the rotating phase and reduces the lag error but increases the EMSE due to gradient noise. Thus, there is a tradeoff between tracking ability and the EMSE due to gradient noise. Moreover, since there is a limit to the step-size, there is also a limit to the rate of variations in the channel that the adaptive filter can tolerate. Due to the lag in the adaptive filter vector, the detected symbol constellation is rotated. The degree of this phase rotation depends on channel parameters, the step-size, and the frequency offset on the desired signal. Thus, for large frequency offsets, the phase rotation can be large and differential detection must be used to rotate the detected symbol constellation back, thereby improving the receiver performance. Figure 8.7 shows the receiver structure for adaptive filtering in conjunction with differential detection. This structure is a natural derivative of the previous structure. In this receiver, the adaptation of the filter $\mathbf{w}$ is based on the difference between the detected symbols $y(n)$ at its output, i.e., *prior* to differential detection, and the encoded symbols $b(n)$ or their estimates $\hat{b}(n)$. Differential detection is simply implemented by multiplying the output of the adaptive filter by the conjugate of the previous output, which precedes the current output by the symbol period, T.

However, the differentially detected symbol $z(n)$ forms the decision statistic. Therefore, it is desirable to minimize the error in $z(n)$ rather than $y(n)$. Yoshida et al. [109] first exploited this when coming up with a modification to the receiver structure for fading channel applications. This modified receiver is depicted in Figure 8.8.

In the new structure, the adaptation of the filter $\mathbf{w}$ is based on the difference between the differentially detected symbols $z(n)$ and the pre-encoded symbols $d(n)$ or their estimates

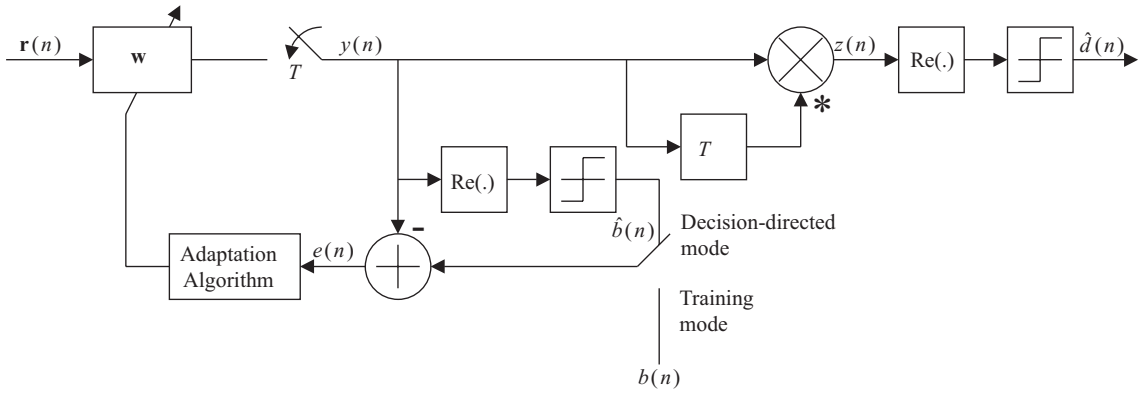

Figure 8.7: Receiver with Adaptive Filtering and Differential Detection.

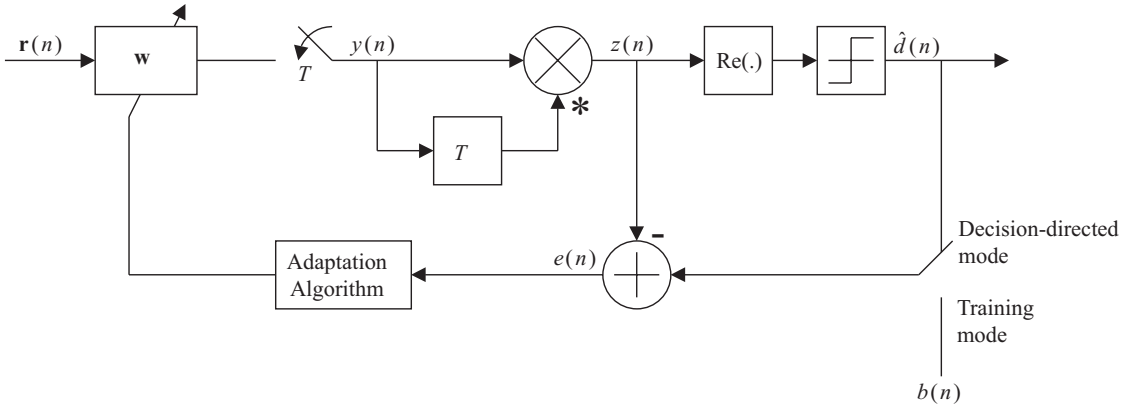

Figure 8.8: Adaptive Receiver Incorporating Differential Detection.

$\hat{d}(n)$. With a carrier frequency offset, there is a fixed phase shift between successive symbols. When the differentially coherent receiver can perfectly track this time-varying phase but the current weight vector lags behind the optimum vector by a constant phase, the weight vector lag does not affect the MSE at the receiver output since successive symbols in the differential detection are affected by the same phase lag. This is assuming that the effects of gradient noise and lag can be separated, as was done for the coherent receiver in Section 8.4. However, this assumption may not be valid for the differentially coherent receiver.

The weight vector adaptation equation must be modified to account for the differential detection before symbol estimation, which results from the modification of the cost

function . The new MSE cost function is

$$J(n) = E[|e(n)|^2] \tag{8.39}$$

where

$$\begin{aligned} e(n) &= d(n) - z(n), & (8.40)\\ z(n) &= y(n)\, y^*(n-1), & (8.41)\\ y(n) &= \mathbf{w}^H(n)\, \mathbf{r}(n). & (8.42) \end{aligned}$$

Equation (8.39) may be expanded as

$$J(n) = E\left[e^*(n)\, \left(d(n) - \mathbf{w}^H(n)\, \mathbf{r}(n)\, \mathbf{r}^H(n-1)\, \mathbf{w}(n-1)\right)\right]. \tag{8.43}$$

The instantaneous estimate of the gradient with respect to $\mathbf{w}^*(n)$ is given by

$$\begin{aligned} \hat{\boldsymbol{\nabla}}(J(n)) &= e^*(n)\, \left[-\mathbf{r}^H(n-1)\, \mathbf{w}(n-1)\, \mathbf{r}(n)\right]\\ &= -e^*(n)\, y^*(n-1)\, \mathbf{r}(n), & (8.44) \end{aligned}$$

where we have used the fact that $\boldsymbol{\nabla}(e^*(n)) = \mathbf{0}$. Therefore, the new adaptation equation for the LMS algorithm is

$$\mathbf{w}(n+1) = \mathbf{w}(n) + \mu\, e^*(n)\, y^*(n-1)\, \mathbf{r}(n) \tag{8.45}$$

where μ is the step-size. The weight update equation involves memory due to the presence of $y^*(n-1)$. This makes the algorithm extremely difficult to analyze for convergence. Analysis of the algorithm assuming the presence of frequency offsets on the signals, as was done for the conventional LMS algorithm in Section 8.4, will demonstrate the impact of frequency offsets on the MSE at the receiver output.

8.6 Stationary Points of the Modified MMSE Cost Function

The stationary point of a cost function was defined in Section 5.2. The stationary points of the modified MMSE cost function are derived in this section. To derive the stationary

points of the cost function of Equation (8.39), we rewrite it using Equations (8.40), (8.41), and (8.42) and replacing $\mathbf{w}(n)$ with $\mathbf{w}$:

$$\begin{aligned} J(n) &= E\left\{\left[d(n) - \mathbf{w}^H(n)\,\mathbf{r}(n)\,\mathbf{r}^H(n-1)\,\mathbf{w}(n-1)\right]^* \right. \\ &\quad \cdot \left. \left[d(n) - \mathbf{w}^H(n)\,\mathbf{r}(n)\,\mathbf{r}^H(n-1)\,\mathbf{w}(n-1)\right]\right\} \\ &= E\left[|d(n)|^2\right] - E\left[d^*(n)\,\mathbf{w}^H(n)\,\mathbf{r}(n)\,\mathbf{r}^H(n-1)\,\mathbf{w}(n-1)\right] \\ &\quad - E\left[d(n)\,\mathbf{w}^H(n-1)\,\mathbf{r}(n-1)\,\mathbf{r}^H(n)\,\mathbf{w}(n)\right] \\ &\quad + E\left[\mathbf{w}^H(n-1)\,\mathbf{r}(n-1)\,\mathbf{r}^H(n)\,\mathbf{w}(n)\right. \\ &\qquad \left. \cdot\, \mathbf{w}^H(n)\,\mathbf{r}(n)\,\mathbf{r}^H(n-1)\,\mathbf{w}(n-1)\right]. \end{aligned} \tag{8.46}$$

Each term of Equation (8.46) is considered separately.

We first note that

$$E\left[|d(n)|^2\right] = 1. \tag{8.47}$$

The encoded symbol $d(n)$ may be written as

$$d(n) = b(n)\,b^*(n-1) \tag{8.48}$$

where $b(n)$ is the pre-encoded symbol. Furthermore, $\mathbf{r}(n-1)$ and $\mathbf{r}(n)$ are independent, as are $b(n-1)$ and $b(n)$. The second term of Equation (8.46) may then be written as

$$\begin{aligned} &E\left[d^*(n)\,\mathbf{w}^H(n)\,\mathbf{r}(n)\,\mathbf{r}^H(n-1)\,\mathbf{w}(n-1)\right] \\ &\quad = \mathbf{w}^H(n) E\left[b^*(n)\,\mathbf{r}(n)\right]\, E\left[b(n-1)\,\mathbf{r}^H(n-1)\right]\mathbf{w}(n-1) \\ &\quad = \mathbf{w}^H(n)\mathbf{p}(n)\,\mathbf{p}^H(n-1)\,\mathbf{w}(n-1) \end{aligned} \tag{8.49}$$

where

$$\mathbf{p}(n) \triangleq E\left[b^*(n)\,\mathbf{r}(n)\right] \tag{8.50}$$

is the cross-correlation vector at time instant n. It can be similarly shown that

$$E\left[d(n)\,\mathbf{w}^H(n-1)\mathbf{r}(n-1)\,\mathbf{r}^H(n)\,\mathbf{w}(n)\right] = \mathbf{w}^H(n-1)\,\mathbf{p}(n-1)\,\mathbf{p}^H(n)\,\mathbf{w}(n). \tag{8.51}$$

The last term of Equation (8.46) may be simplified as

$$\begin{aligned} & E\left[\mathbf{w}^H(n-1)\,\mathbf{r}(n-1)\,\mathbf{r}^H(n)\,\mathbf{w}(n)\,\mathbf{w}^H(n)\,\mathbf{r}(n)\,\mathbf{r}^H(n-1)\,\mathbf{w}(n-1)\right] \\ &= E\left[\mathbf{w}^H(n-1)\,\mathbf{r}(n-1)\,\mathbf{r}^H(n-1)\,\mathbf{w}(n-1)\right]\, E\left[\mathbf{w}^H(n)\,\mathbf{r}(n)\,\mathbf{r}^H(n)\,\mathbf{w}(n)\right] \\ &= \mathbf{w}^H(n-1)E\left[\mathbf{r}(n-1)\,\mathbf{r}^H(n-1)\right]\mathbf{w}(n-1)\,\mathbf{w}^H(n)E\left[\mathbf{r}(n)\,\mathbf{r}^H(n)\right]\mathbf{w}(n) \\ &= \mathbf{w}^H(n-1)\,\mathbf{R}\,\mathbf{w}(n-1)\,\mathbf{w}^H(n)\,\mathbf{R}\,\mathbf{w}(n). \end{aligned} \tag{8.52}$$

Using Equations (8.49), (8.51), and (8.52) in Equation (8.46), we have

$$\begin{aligned} J(n) &= 1 - \mathbf{w}^H(n)\mathbf{p}(n)\,\mathbf{p}^H(n-1)\,\mathbf{w}(n-1) - \mathbf{w}^H(n-1)\,\mathbf{p}(n-1)\,\mathbf{p}^H(n)\,\mathbf{w}(n) \\ &\quad + \mathbf{w}^H(n-1)\,\mathbf{R}\,\mathbf{w}(n-1)\,\mathbf{w}^H(n)\,\mathbf{R}\,\mathbf{w}(n). \end{aligned} \tag{8.53}$$

When it assumed that frequency offsets are absent, i.e., the received signal is stationary, Equation (8.53) reduces to

$$J(n) = 1 - 2\,\mathbf{w}^H\mathbf{p}\,\mathbf{p}^H\,\mathbf{w} + \left(\mathbf{w}^H\,\mathbf{R}\,\mathbf{w}\right)^2. \tag{8.54}$$

Clearly, this is a multi-modal cost function, which is to be expected because of the memory in the filter.

Figure 8.9 illustrates the cost function for a two-weight adaptive filter. For the generation of the performance surface, it has been assumed that there are two synchronous signals with no frequency offsets and spreading codes $[1, -1]$ and $[1, 1]$ with powers of 1 and 0.25, respectively. The AWGN variance is taken to be 0.25. These parameters yield

$$\mathbf{R} = \begin{bmatrix} 1.50 & -0.75 \\ -0.75 & 1.50 \end{bmatrix}$$

and

$$\mathbf{p} = \begin{bmatrix} 1 \\ -1 \end{bmatrix}.$$

The cost function has been clipped at the value 1.2. There are two minima for the real-weights case, with one optimal solution being the negative of the other.

The gradient of the cost function with respect to $\mathbf{w}^*(n)$ is given by

$$\boldsymbol{\nabla}(J(n)) = -\mathbf{p}(n)\,\mathbf{p}^H(n-1)\,\mathbf{w}(n-1) + \mathbf{w}^H(n-1)\,\mathbf{R}\,\mathbf{w}(n-1)\,\mathbf{R}\,\mathbf{w}(n). \tag{8.55}$$

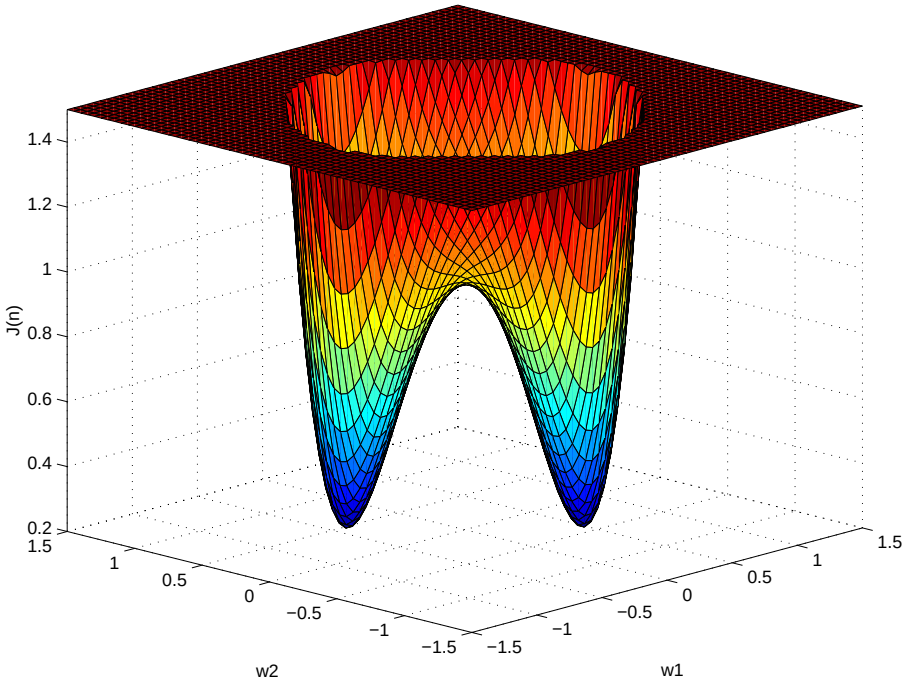

Figure 8.9: Cost Function for a Two-Weight Adaptive Filter.

The stationary points of the cost function are obtained by equating the gradient to the null vector. Thus, the stationary points are defined by

$$\mathbf{w}_{\text{opt}}^{H}(n-1)\,\mathbf{R}\,\mathbf{w}_{\text{opt}}(n-1)\,\mathbf{R}\,\mathbf{w}_{\text{opt}}(n) - \mathbf{p}(n)\,\mathbf{p}^{H}(n-1)\,\mathbf{w}_{\text{opt}}(n-1) = \mathbf{0} \tag{8.56}$$

where $\mathbf{w}_{\text{opt}}(n)$ is the optimum weight vector at time instant n. Premultiplying throughout by $\mathbf{R}^{-1}$ and rearranging, we get

$$\mathbf{w}_{\text{opt}}^{H}(n-1)\,\mathbf{R}\,\mathbf{w}_{\text{opt}}(n-1)\,\mathbf{w}_{\text{opt}}(n) = \mathbf{R}^{-1}\,\mathbf{p}(n)\,\mathbf{p}^{H}(n-1)\,\mathbf{w}_{\text{opt}}(n-1). \tag{8.57}$$

Disregarding the trivial solution $\mathbf{w}_{\text{opt}}(n-1) = \mathbf{w}_{\text{opt}}(n) = \mathbf{0}$, it may be inferred that if the received signals are stationary, the optimum weight vector is the eigenvector of the rank-one matrix $\mathbf{R}^{-1}\,\mathbf{p}\,\mathbf{p}^{H}$ associated with the only non-zero eigenvalue. It is scaled such that the eigenvalue is equal to the filter output power $\mathbf{w}_{\text{opt}}^{H}\,\mathbf{R}\,\mathbf{w}_{\text{opt}}$. It is observed that the weight vector

$$\mathbf{w}_{\text{opt}}(n) = e^{j\phi}\,\mathbf{R}^{-1}\,\mathbf{p}(n) \tag{8.58}$$

for any arbitrary phase ϕ is a solution to Equation (8.57) because

$$\begin{aligned}
&\mathbf{w}_{\text{opt}}^H(n-1)\,\mathbf{R}\,\mathbf{w}_{\text{opt}}(n-1)\,\mathbf{w}_{\text{opt}}(n)\Big|_{\mathbf{w}_{\text{opt}}(n)=e^{j\phi}\,\mathbf{R}^{-1}\,\mathbf{p}(n)} \\
&= \left(e^{-j\phi}\,\mathbf{p}^H(n-1)\,\mathbf{R}^{-1}\right)\,\mathbf{R}\,\left(e^{j\phi}\,\mathbf{R}^{-1}\,\mathbf{p}(n-1)\right)\left(e^{j\phi}\,\mathbf{R}^{-1}\,\mathbf{p}(n)\right) \\
&= e^{j\phi}\,\mathbf{p}^H(n-1)\,\mathbf{R}^{-1}\,\mathbf{p}(n-1)\,\mathbf{R}^{-1}\,\mathbf{p}(n) \qquad (8.59)
\end{aligned}$$

and

$$\begin{aligned}
&\mathbf{R}^{-1}\,\mathbf{p}(n)\,\mathbf{p}^H(n-1)\,\mathbf{w}_{\text{opt}}(n-1)\Big|_{\mathbf{w}_{\text{opt}}(n)=e^{j\phi}\,\mathbf{R}^{-1}\,\mathbf{p}(n)} \\
&= \mathbf{R}^{-1}\,\mathbf{p}(n)\,\mathbf{p}^H(n-1)\,\left(e^{j\phi}\,\mathbf{R}^{-1}\,\mathbf{p}(n-1)\right) \\
&= e^{j\phi}\,\mathbf{p}^H(n-1)\,\mathbf{R}^{-1}\,\mathbf{p}(n-1)\,\mathbf{R}^{-1}\,\mathbf{p}(n). \qquad (8.60)
\end{aligned}$$

Thus, any phase shifted version of the MMSE solution defines a stationary point of the modified cost function of Equation (8.39), implying an infinite number of solutions. This is an intuitively satisfying result, since the modified receiver is expected to have interference rejection properties similar to the original receiver while being insensitive to any constant phase shift, which is handled by the differential detection, on the filter solution. It is important to note that the optimum solution of Equation (8.58) is a rotating vector, similar to the MMSE solution for the coherent receiver.

The MMSE is obtained by using the optimal solution $\mathbf{w}(n) = e^{j\phi}\,\mathbf{R}^{-1}\,\mathbf{p}(n)$ in Equation (8.53).

$$\begin{aligned}
\varepsilon_{\min} &= 1 - \left(e^{-j\phi}\,\mathbf{p}^H(n)\,\mathbf{R}^{-1}\right)\,\mathbf{p}(n)\,\mathbf{p}^H(n-1)\,\left(e^{j\phi}\,\mathbf{R}^{-1}\,\mathbf{p}(n-1)\right) \\
&\quad - \left(e^{-j\phi}\,\mathbf{p}^H(n-1)\,\mathbf{R}^{-1}\right)\,\mathbf{p}(n-1)\,\mathbf{p}^H(n)\,\left(e^{j\phi}\,\mathbf{R}^{-1}\,\mathbf{p}(n)\right) \\
&\quad + \left(e^{-j\phi}\,\mathbf{p}^H(n-1)\,\mathbf{R}^{-1}\right)\,\mathbf{R}\,\left(e^{j\phi}\,\mathbf{R}^{-1}\,\mathbf{p}(n-1)\right) \\
&\qquad \cdot \left(e^{-j\phi}\,\mathbf{p}^H(n)\,\mathbf{R}^{-1}\right)\,\mathbf{R}\,\left(e^{j\phi}\,\mathbf{R}^{-1}\,\mathbf{p}(n)\right) \\
&= 1 - \mathbf{p}^H(n-1)\,\mathbf{R}^{-1}\,\mathbf{p}(n-1)\,\mathbf{p}^H(n)\,\mathbf{R}^{-1}\,\mathbf{p}(n). \qquad (8.61)
\end{aligned}$$

It is evident from this expression that the MMSE of the adaptive filter with differential detection is higher than the MMSE without differential detection.

8.7 Receiver Structures Investigated

Several receiver structures that incorporate carrier recovery were considered for performance study. Preliminary simulations were run to determine the structures worth investigating further. The simulation parameters that were varied included loop bandwidth

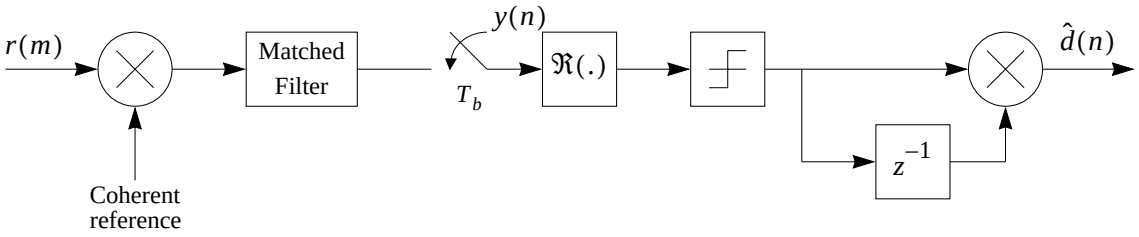

Figure 8.10: Ideal Coherent Matched Filter Receiver.

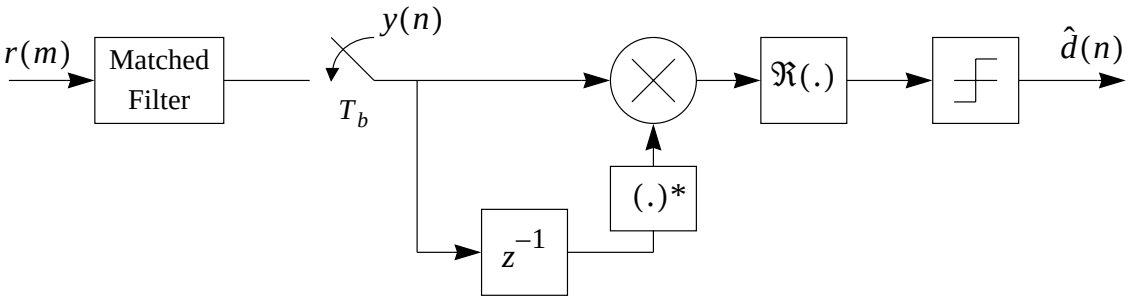

Figure 8.11: Differentially Coherent Matched Filter Receiver.

for the Costas loop and the length N of the averager for the open-loop estimators. Low to modest SNRs were used to test the performance of various receivers, i.e., matched filter receiver, Rake receiver, and adaptive receiver, incorporating these offset compensation schemes in a single user AWGN environment. The performance metrics employed to evaluate the feasibility of the receiver structures were BER, acquisition time (when applicable), and complexity. The final candidate receiver structures are briefly described in the following paragraphs. Bi-phase PSK modulation is used for the entire study.

Four different matched filter receiver structures were found worthy of an extended study. The matched filter is a FIR filter matched to the desired user's spreading code. The first of these is the ideal coherent matched filter receiver for differentially encoded BPSK (DEBPSK) modulation and is pictured in Figure 8.10. In the figure, $\Re(\cdot)$ denotes extraction of the real part. The input signal has a complex representation. A coherent (complex exponential) carrier reference is assumed to be available to the receiver. In this receiver, a bit decision is made before differential decoding. $\hat{d}(n)$ is the differentially decoded information bit. The second structure is the differentially coherent matched filter receiver depicted in Figure 8.11. No carrier reference is available to this receiver, which performs differential detection ahead of bit estimation. Next is the matched filter receiver with a Costas loop reference, illustrated in Figure 8.12. The notation $\Im(\cdot)$ in the

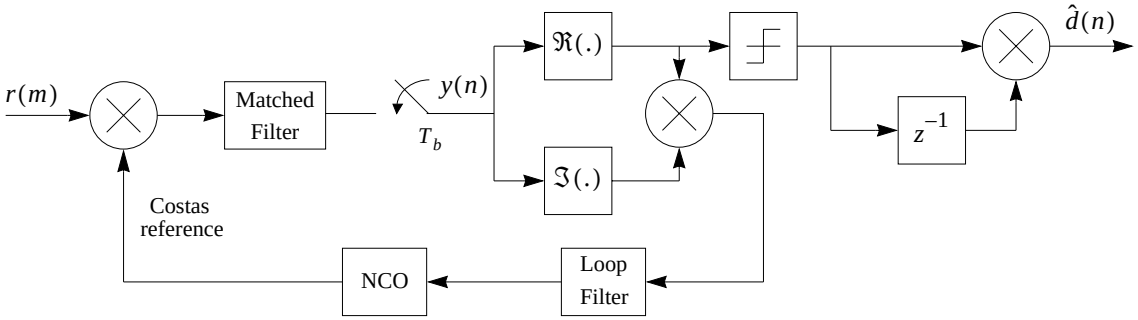

Figure 8.12: Matched Filter Receiver with Costas Loop Carrier Recovery.

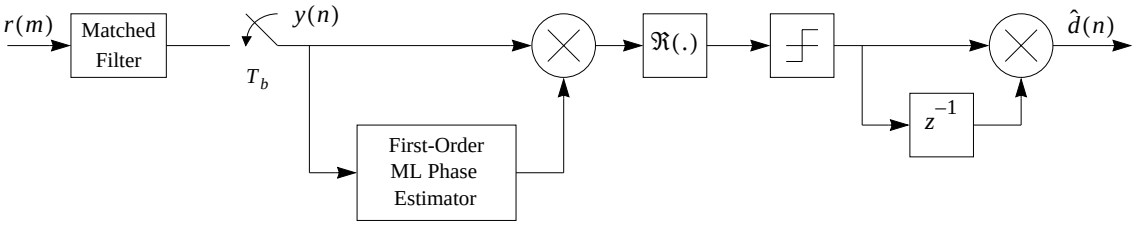

Figure 8.13: Matched Filter Receiver with Modified First-Order ML Phase Estimation.

figure represents extraction of the imaginary part. The Costas reference generated by the NCO is a complex exponential. The error control signal is generated by mixing the real and the imaginary parts of the sampled matched filter output and filtering the mixed signal with the loop filter. Hardlimiting of the real part before mixing, as illustrated in Figure 8.2, is *not* performed since the receiver is intended for use in environments with significant MAI, where the signal-to-noise-plus-interference-ratio is expected to be low. Differential decoding again follows bit estimation. The final matched filter receiver is given in Figure 8.13 and makes use of the modified first-order open-loop phase estimation scheme for offset compensation. Thus, this structure differs from the previous ones in that the estimated phase is used for compensation at the matched filter output rather than its input.

The Rake receiver structure used for the simulation study is a three-finger Rake and is depicted in Figure 8.14. Differential detection is performed in each finger separately. The real part of the estimate in each finger is weighted by its power, represented as a cubing operation in Figure 8.14, before the outputs of the three fingers are summed. The combined statistic is used to make the final bit decision.

Four adaptive receiver structures merited investigation. The ideal coherent adaptive receiver, illustrated in Figure 8.15, is the first of these and is similar to the ideal coherent

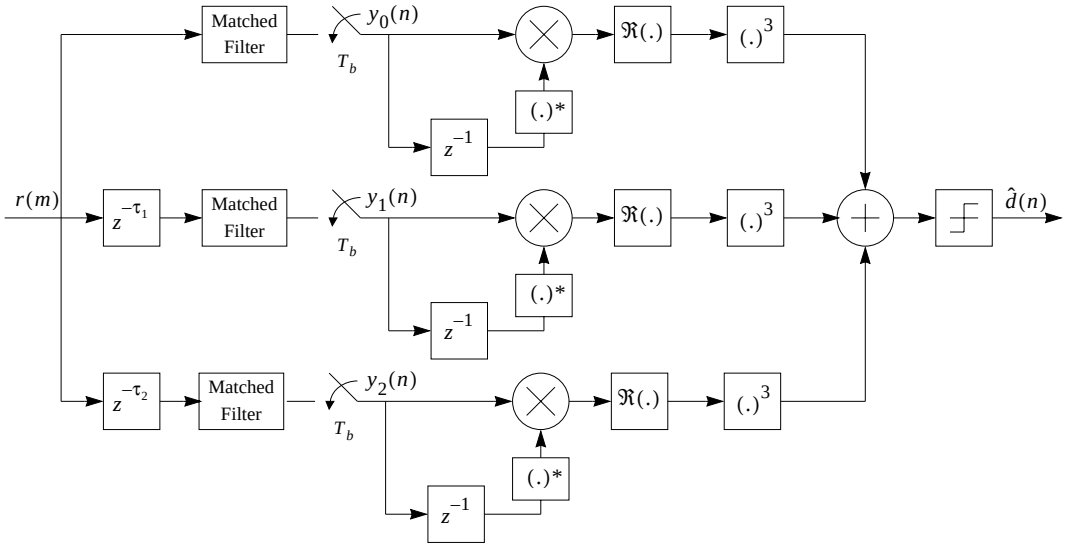

Figure 8.14: Rake Receiver with Differentially Coherent Detection.

matched filter receiver. Hardlimiting is done prior to differential decoding as in the case of the matched filter. The filter output is the estimate used to adapt the filter weights. The next structure is the adaptive filter structure incorporating differential detection that was discussed in Section 8.5 and pictured in Figure 8.8. Figure 8.16 shows the adaptive receiver with Costas loop carrier recovery and is similar to its matched filter counterpart. Here again, the real part of the matched filter output is not hardlimited when being mixed with the imaginary part to generate the error control signal, since the receiver is intended for use in low signal-to-noise-plus-interference-ratio environments. The adaptive receiver with the ML open-loop phase estimation scheme is the last of the structures and is shown in Figure 8.17. Like its matched filter counterpart, the phase compensation in this receiver is performed at the filter output. The adaptation algorithm is suitably modified to incorporate the phase compensation of the symbol estimate, much like that in the differentially coherent receiver.

The list of receivers and their parameters are summarized in Table 8.1. $B_{L,c}$ is the loop bandwidth[4] of the Costas loop and R_b is the bit rate of the information signal. N is the length of the averager in the ML phase estimation scheme.

[4]The loop bandwidth is defined as the noise bandwidth for the loop. If $H(\omega)$ is the loop transfer function, then the loop bandwidth is given by

$$B_L = \int_{-\infty}^{\infty} |H(\omega)|^2 \, d\omega \quad \text{rad/s}.$$

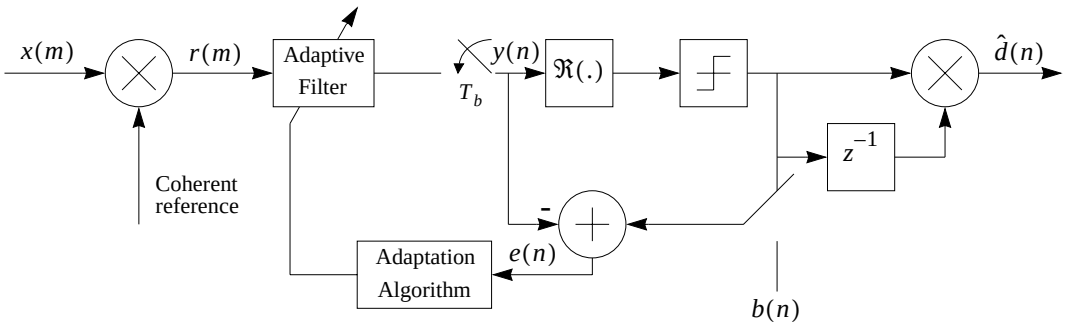

Figure 8.15: Ideal Coherent Adaptive Receiver.

8.8 Simulation Results

8.8.1 Simulation Model

For the entire simulation study, Gold codes of length 15 are used. Each simulation point is obtained by averaging the results of one hundred Monte Carlo trials. For each trial, code assignment to users is random. COP bi-phase modulation with differential encoding is used. The main system parameters are summarized in Table 8.2. The frequency offsets on the signals are Gaussian random variables with mean zero and standard deviation of $\sigma_f = (1/80)R_b = 1600$ Hz for the desired signal and $(1/40)R_b = 3200$ Hz for the MAI signals. The latter is applicable in the asynchronous case with the assumption that the frequency uncertainty is greater for the MAI signals than for the desired signal; in the synchronous case, all signals have the same offset. These values are reasonable for modest priced oscillators available in the market. The NLMS algorithm is used for update of the adaptive filter weights with a step-size of 0.5 during training and 0.1 in the decision-directed mode. The length of the training period is fixed at one hundred bits for all cases, and this is also the synchronization time alloted for the offset compensation loops. Perfect code synchronization is assumed. In the case of multipath channels, perfect knowledge of the delays of the first three components is assumed for the Rake receiver. A form of automatic gain control (AGC) is implemented to avoid observed catastrophic failure of the adaptive receiver for large differences between the powers of the received signal of interest and the reference signal. The AGC normalizes the received signal by the square root of the sum of the squares of the individual user amplitudes.

Several channel models are used for the simulations. Results are provided here for AWGN channels and for one multipath fading channel model. The features of this channel model are listed in Table 8.3. The "Typical Urban" channel model is obtained from the COST-207 final report [97]. The fading envelopes described as "Gauss 1" and "Gauss 2" are obtained by using Gaussian functions for the Doppler spectra.

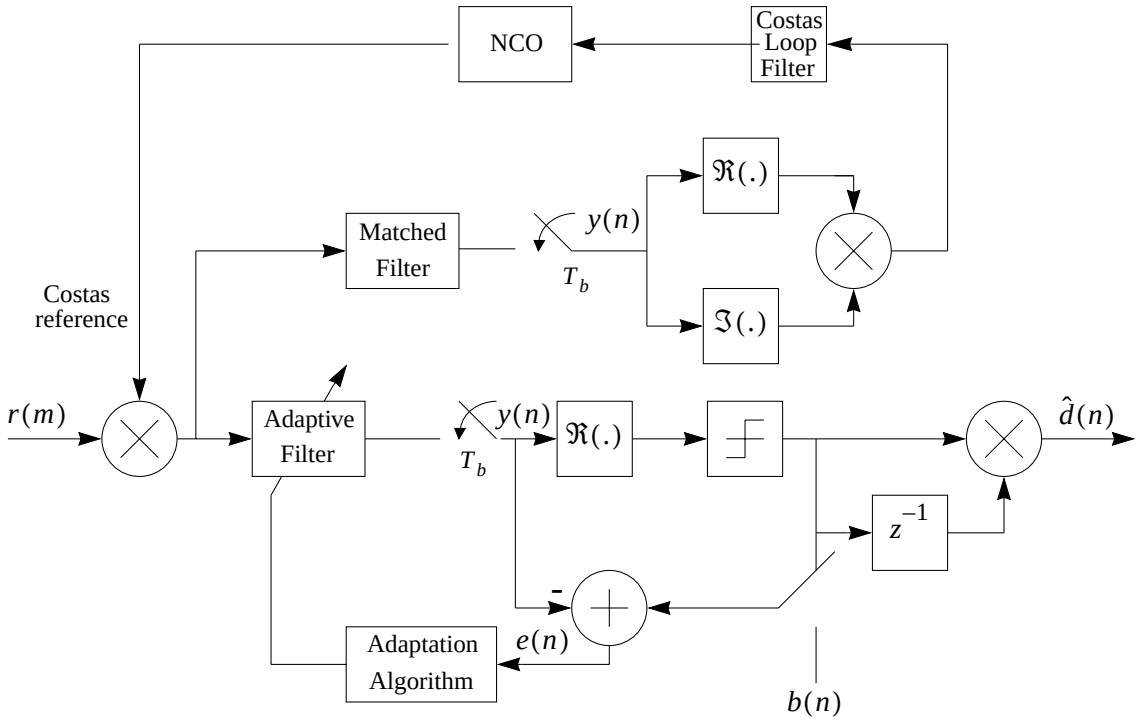

Figure 8.16: Adaptive Receiver with Costas Loop Carrier Recovery.

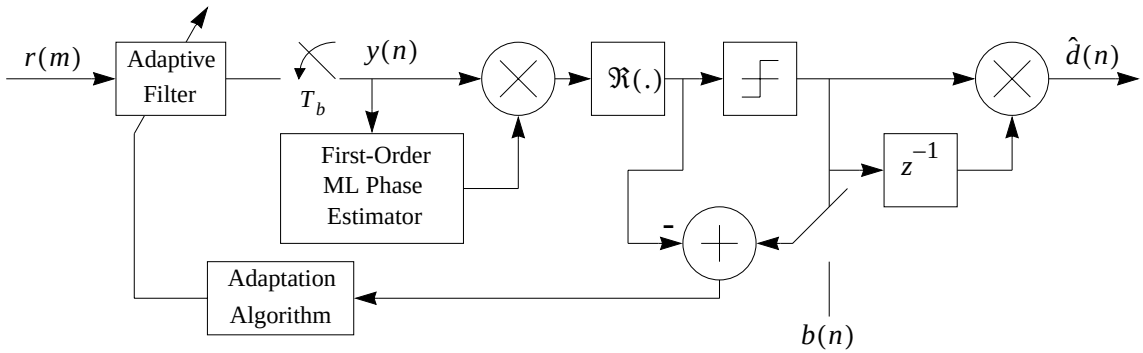

Figure 8.17: Adaptive Receiver with Modified First-Order ML Phase Estimation.

Table 8.1: Receiver Structures and Their Parameters Used for Simulation Study.

Description	**Parameters**
Matched Filter Receivers:	
Ideal coh. DEBPSK	
Diff. coh. DBPSK	
Costas loop alone	$B_{L,c} = 10^{-1.5} R_b$ $B_{L,c} = 10^{-1} R_b$
Modified 1st-order open-loop est.	$N = 50$ $N = 16$ $N = 5$
Rake Receiver:	
3-Finger diff. coherent	
Adaptive Filter Receivers:	
Ideal coherent	
Diff. coherent	
Costas loop	$B_{L,c} = 10^{-1.5} R_b$ $B_{L,c} = 10^{-1} R_b$
Modified 1st-order open-loop est.	$N = 50$ $N = 16$ $N = 5$

Both forward and reverse links of a cellular CDMA system are simulated. For the forward link simulations, all the signals are assumed to be synchronous with equal powers. The carrier phase, uniformly distributed over $(-\pi, \pi]$, and frequency offset, randomly generated for each simulation trial, are identical for all users. Gold codes are used with the optimal time offsets yielding the minimum cross-correlation of $-1/15$ between any two codes. For the fading channel simulations, the same channel is used for the signals of all the users. For the reverse link simulations, the signals are asynchronous, each with a different randomly generated (for each trial) carrier phase and frequency offset. Log-normal distribution of powers is assumed, with a mean of zero and standard deviations of 2 and 20 for the cases of tight and loose power control, respectively. The delays of the users are randomly generated for each trial. Furthermore, the signal from each user fades independently assuming that the signals pass through different channels. The complex weight fractionally spaced linear adaptive receiver (CWFSLAR), which is referred to as the CLFSR in Chapter 2, is the adaptive receiver used. The matched filter (MF) receiver is simply the fractionally spaced filter matched to the spreading signal of the desired user.

Table 8.2: System Parameters.

Description	**Value**
Carrier frequency	2.050 GHz
Bit rate	128 kbps
Processing gain	15
Chip rate	1.92 Mcps
Sample rate	3.84 Msps

Table 8.3: Multipath Channel Models.

Channel Model	**Multipath delay**	**Multipath amplitude**	**Fading envelope**
COST-207	0.0 μs	0.7071	Rayleigh
Typical Urban	0.2 μs	1.0	Rayleigh
	0.6 μs	0.7937	Gauss 1
	1.6 μs	0.5	Gauss 1
	2.4 μs	0.4	Gauss 2
	5.0 μs	0.3162	Gauss 2

8.8.2 Simulation Results for AWGN

By way of preface to the simulation results, we demonstrate the performance degradation that results from using a a differentially coherent receiver instead of an ideal coherent receiver. Simulation results for both matched filter receiver and adaptive receiver in the forward link of a CDMA are plotted in Figure 8.18, showing the variation of the BERs of the receivers with increasing number of users in the system. This figure ably illustrates the dependence of the performance of the adaptive receiver on the carrier reference. The apparently huge increase in the system capacity facilitated by using the CWFSLAR instead of the MF is diminished when coherent detection is replaced with differential detection. The performance degradation of the MF (A) is small compared with that of the CWFSLAR (B) in which the BER reduces by almost an order of magnitude. In the single user case, the ideal coherent adaptive receiver performs slightly worse than the matched filter receiver because of the excess MSE resulting from gradient noise. (Recall that the step-size is 0.5 during training and 0.1 in the decision-directed mode. The excess MSE is smaller for smaller step-sizes.) The difference in BER, however, is magnified in the case of differential detection. The differentially coherent adaptive receiver starts performing better than its matched filter counterpart only when there are four or more users in the system, i.e., for modest and large system loads. But

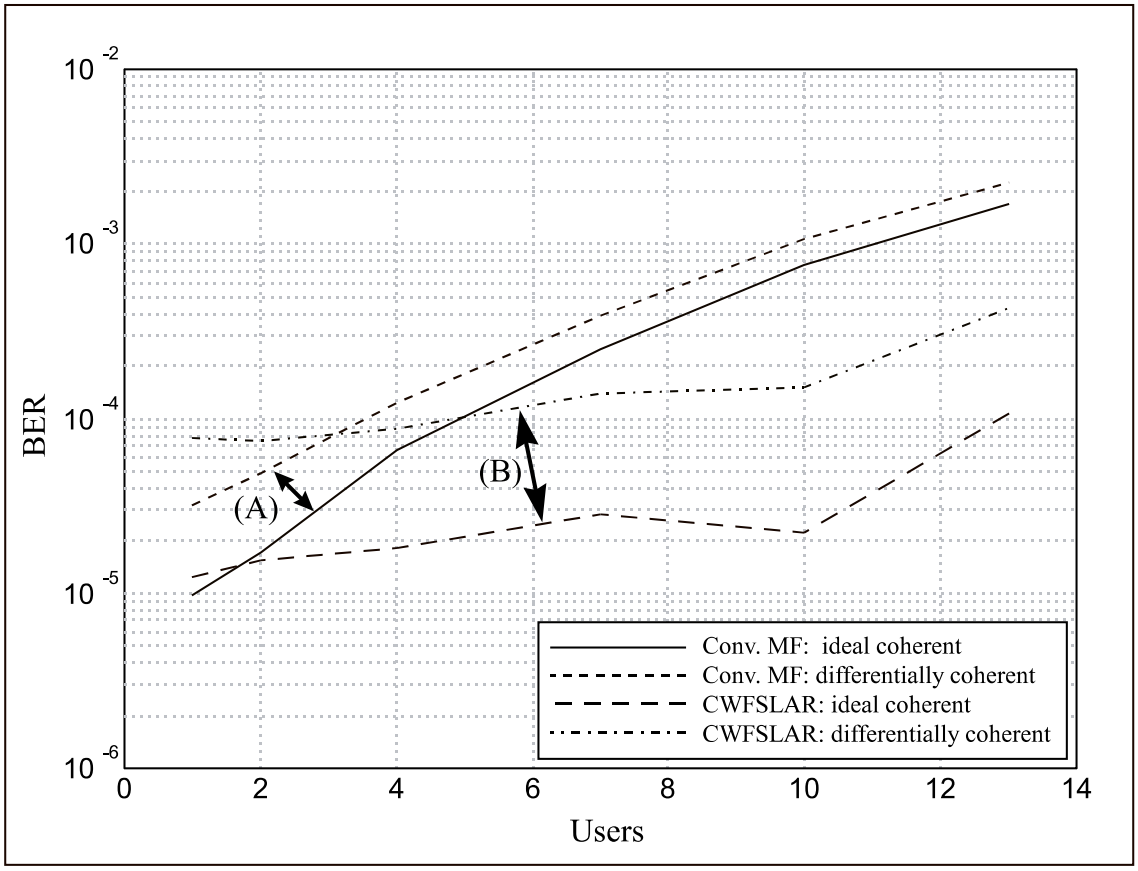

Figure 8.18: Comparison of Performances of Ideal Coherent and Differential Receivers with $E_b/N_0 = 10$ dB.

the low crosscorrelations of the spreading codes aid the MF, which deteriorates rather gently. These results clearly underline the importance of having a coherent reference when possible. The results suggest a favorable tradeoff between the cost of a pilot channel, which affords this reference, and the system capacity.

Case 1: Forward Link

Figures 8.19 and 8.20 graph the BER versus the number of users for the CWFSLAR and MF, respectively, using a coherent reference, Costas loop offset compensation, and differential detection. Given the short synchronization time of one hundred bits, it is important that the Costas loop settles fast to minimize its interaction with the converging adaptive filter, so only wide loop bandwidths are considered for the adaptive receiver. The Costas loop receiver performs remarkably well in both figures when there is a single user and the loop bandwidth, $B_{L,c} = 10^{-1}R_b$. We note however, that it performs very poorly when $B_{L,c} = 10^{-1.5}R_b$, which can be attributed to the relatively high frequency uncertainty ($2\sigma_f = (1/40)R_b \approx 10^{-1.6}R_b$). The most outstanding feature of these figures, however, is the degradation of the Costas loop receivers with increasing MAI, much more so for the adaptive receiver. The MF with the Costas loop quickly becomes worse than the differentially coherent receiver and degrades relatively slowly. On the other hand, the adaptive receiver with the Costas loop is dramatically poor compared with the other two offset compensation schemes in the presence of MAI. Thus, the interaction between the adaptive receiver and the Costas loop appears to have a severely debilitating effect on both subsystems, with each simultaneously trying to compensate for the offset in its own way. It should be noted here that hardlimiting in the I-arm of the Costas loop was not employed to avoid problems in high MAI situations. The highlight of these results is that the adaptive receiver with differential detection is vastly superior to other receivers with offset compensation, especially in the presence of strong MAI.

The performance with the modified ML first-order open-loop phase estimation schemes is shown in Figures 8.21 and 8.22. Results are plotted for different averaging lengths N. The performance results of the ideal coherent and differential receivers are also provided for comparison. In obtaining the γ_i parameter for the ML estimators, $f_{\max} = 2\sigma_f$ was used. In the MF case, the estimators with $N = 16$ and $N = 50$ are much worse than the other schemes when the number of users is low. All the estimators yield similar performance results for large system loads. It is noteworthy that the receiver with $N = 5$ *consistently* performs slightly better than the differentially coherent receiver. When the number of users is low, similar observations may be made for the CWFSLAR. One notable difference is that the receiver employing ML estimation with $N = 5$ performs distinctly better than the adaptive receiver using differential detection. Furthermore, this trend is reversed for large system loads. Using $f_{\max} = 2\sigma_f$, rather than the actual frequency offset, for the open-loop estimators may explain the superior performance of the implementation with $N = 5$ compared with the other two implementations. The suboptimality of the

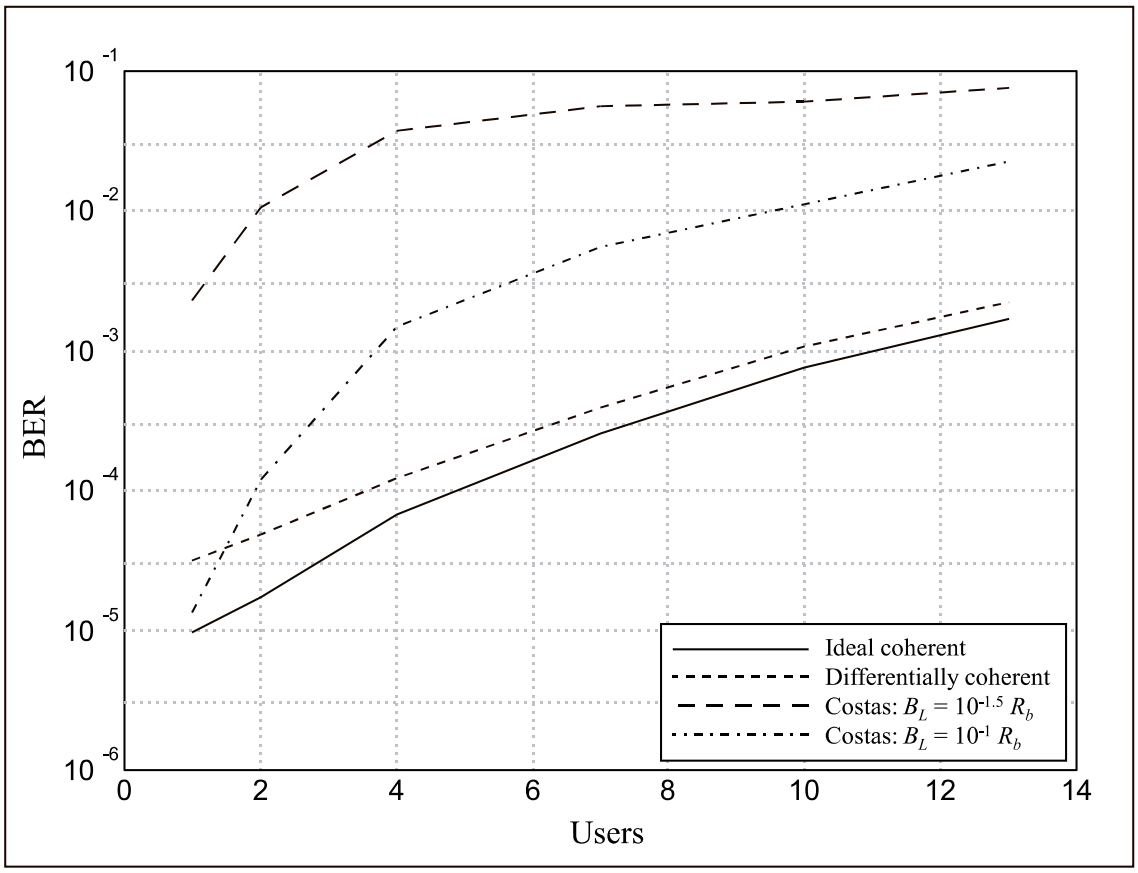

Figure 8.19: Comparison of Performances of Matched Filter Receiver with Ideal Coherent Reference, Differential Detection, and Costas Loop Compensation on the Forward Link of an AWGN Channel; $E_b/N_0 = 10$ dB.

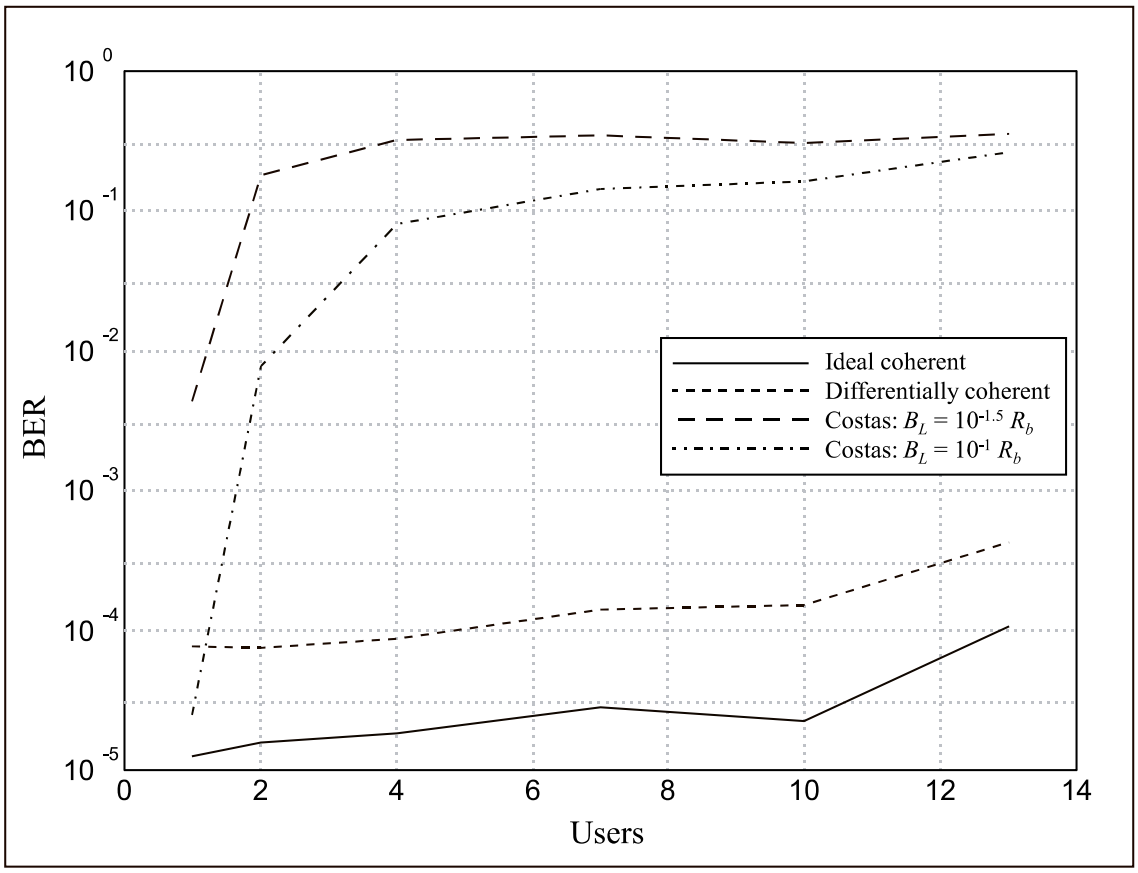

Figure 8.20: Comparison of Performances of Adaptive Receiver with Ideal Coherent Reference, Differential Detection, and Costas Loop Compensation on the Forward Link of an AWGN Channel; $E_b/N_0 = 10$ dB.

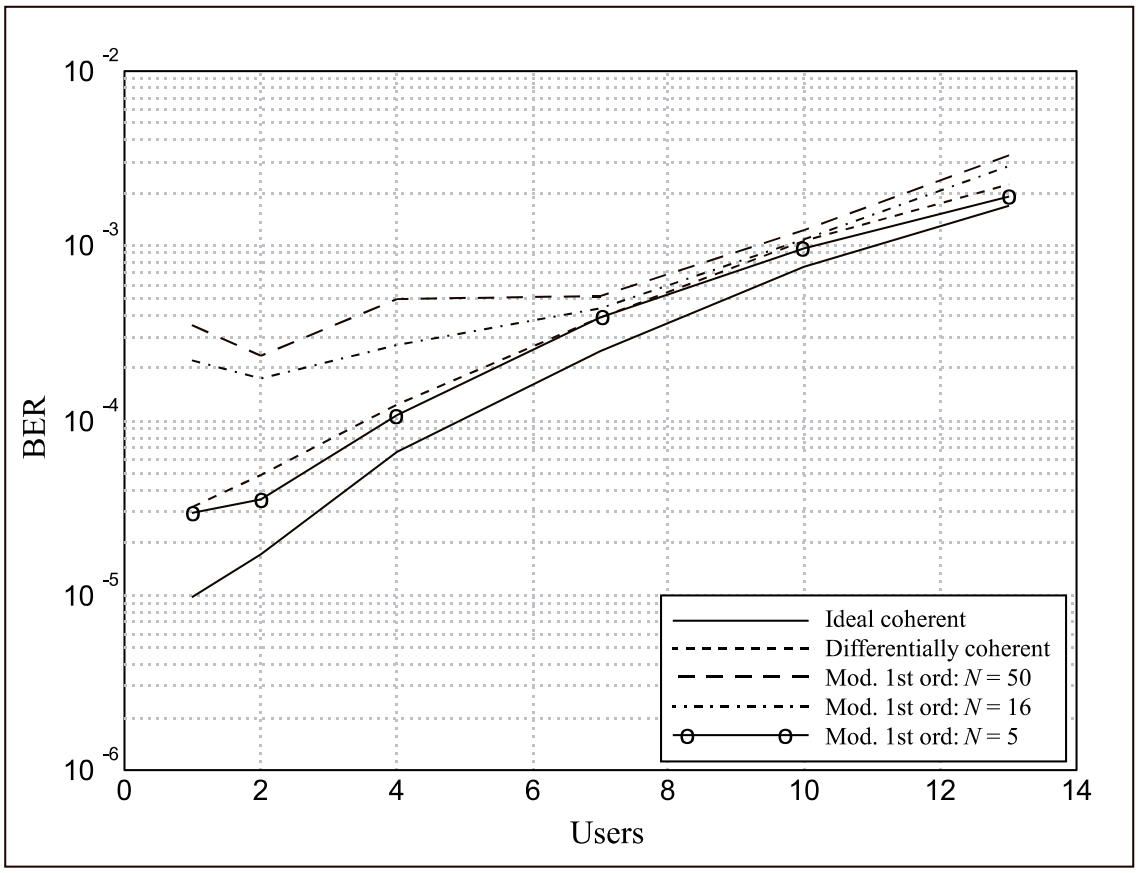

Figure 8.21: Comparison of Performances of Matched Filter Receiver with Ideal Coherent Reference, Differential Detection, and Modified First-Order ML Phase Estimation on the Forward Link of an AWGN Channel; $E_b/N_0 = 10$ dB.

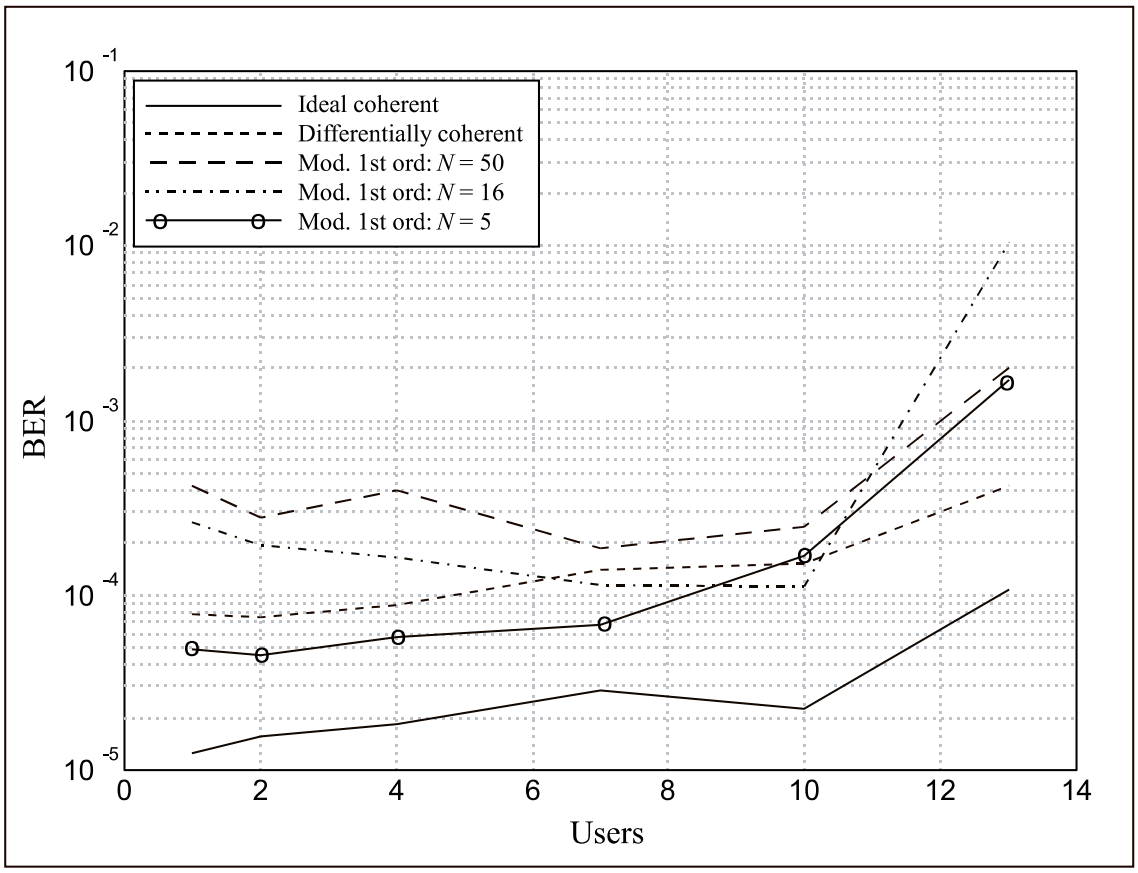

Figure 8.22: Comparison of Performances of Adaptive Receiver with Ideal Coherent Reference, Differential Detection, and Modified First-Order ML Phase Estimation; on the Forward Link of an AWGN Channel $E_b/N_0 = 10$ dB.

estimators due to the use of a fixed value of $f_{\max}$ is amplified when N is large. The salient point is, the adaptive receiver with the first-order ML phase estimation ($N = 5$) is best, closely followed by the adaptive receiver with differential detection. The latter, however, does not have the additional complexity of phase estimation and is a good choice for implementation.

Case 2: Reverse Link

The next set of results demonstrate the performance of the various receivers previously considered on the reverse link of a CDMA channel under "strict" power control assumptions. Figures 8.23 and 8.24 show the results for the MF and CWFSLAR, respectively, with the Costas loop used for offset compensation. Clearly, all the receivers perform poorly. The differentially coherent MF and the MF with the Costas loop ($B_{L,c} = 10^{-1}R_b$) fare similarly, only slightly worse than the ideal coherent MF. The Costas loop receiver with $B_{L,c} = 10^{-1.5}R_b$ experiences almost catastrophic failure. The results for the adaptive receiver are more interesting. The differentially coherent receiver, while performing worse than the coherent receiver, is nevertheless greatly superior to all the MF receivers. The adaptive receiver with Costas loop offset compensation, however, is not better than its matched filter counterpart. Again, the interaction between the two closed-loop subsystems is the contributing factor to the lack of adequate performance. The Costas loop receiver was found to perform worse on the forward link than on the reverse link, where the asynchronous MAI is relatively benign. This is worth noting since the loop has to lock on to the lone carrier received on the forward link as opposed to having to capture and lock on to one, that of the desired user, of the many received carriers on the reverse link.

The results for the modified first order open-loop estimation schemes are plotted in Figures 8.25 and 8.26. Again, as in the case of the forward link, the MF receivers using ML phase estimation with $N = 16$ and $N = 50$ are worse than the coherent and the differentially coherent receiver. The performance with $N = 5$, however, is similar to that of the differentially coherent receiver. The better performance obtained with $N = 5$ may again be explained as in the synchronous case. The observations for the adaptive receiver are similar to the forward link case with two exceptions. First, the BERs of all the receivers degrade more rapidly here because the adaptive receiver is generally superior in synchronous channels than in asynchronous channels. Secondly, a sharp decline with increasing MAI is observed in the performance of the receiver with the ML phase estimator using $N = 5$. This does not match the trend of the other receivers. The distinctly high values of the BER are a result of the catastrophic failure of the adaptive receiver in the decision-directed mode. The adaptive receiver fails when it adapts on wrong decisions over an extended period, causing it to lose convergence. The BER then soars to 0.5. Ignoring these limitations for the moment, the adaptive receiver with differential detection is the best of the realizable receivers considered.

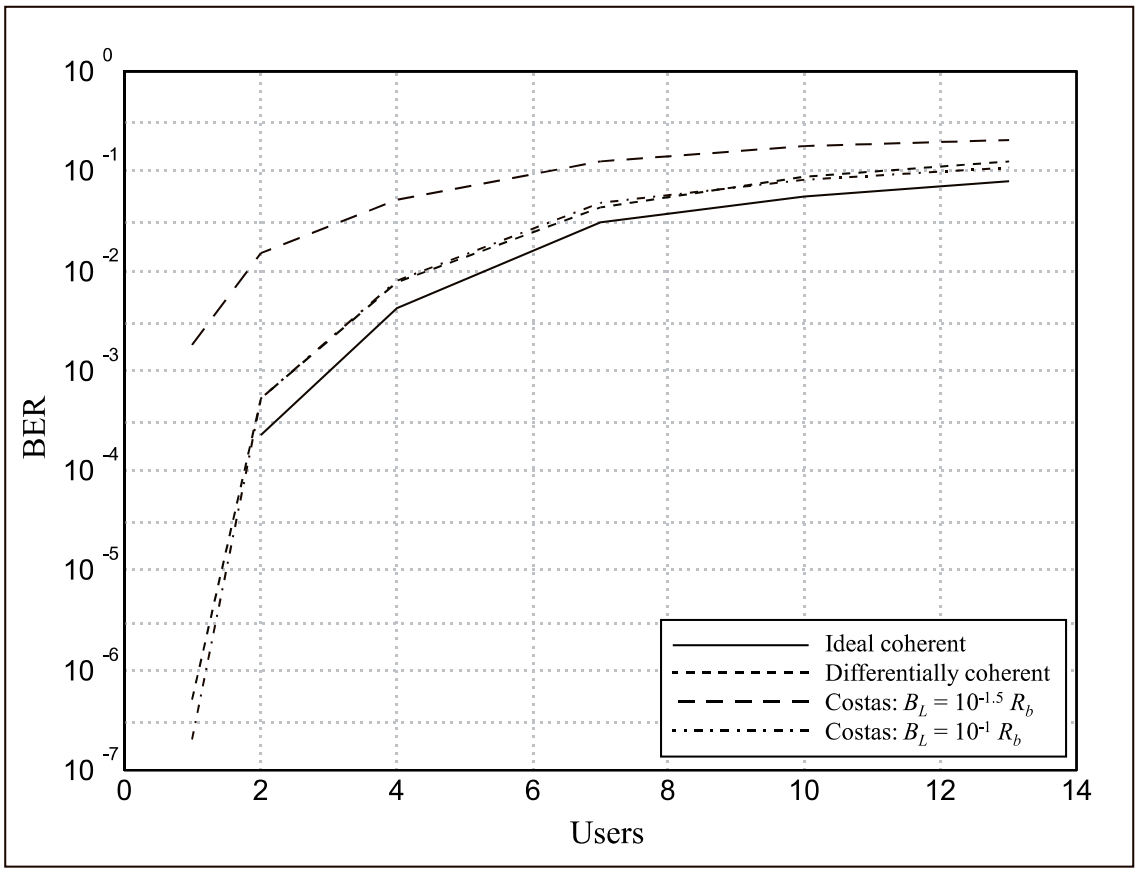

Figure 8.23: Comparison of Performances of Matched Filter Receiver with Ideal Coherent Reference, Differential Detection, and Costas Loop Compensation on the Reverse Link of an AWGN Channel with "Strict" Power Control; $E_b/N_0 = 12$ dB.

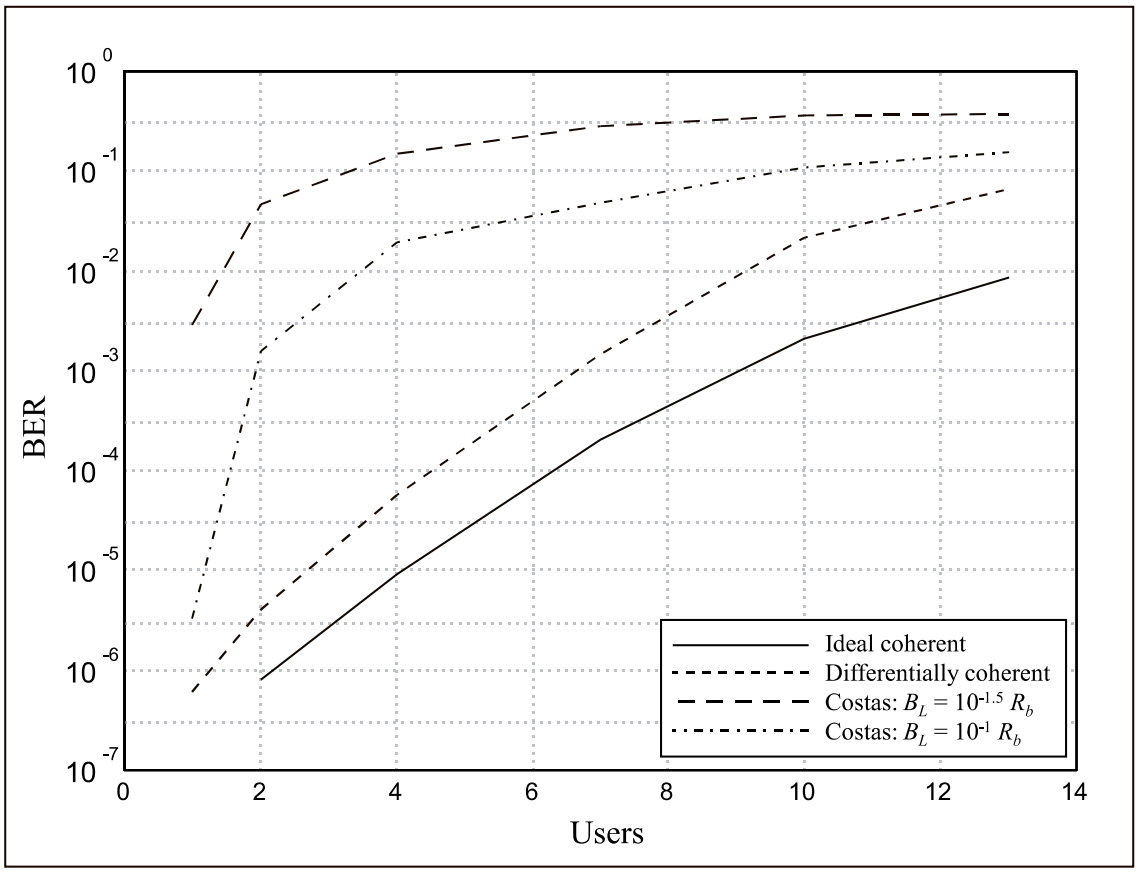

Figure 8.24: Comparison of Performances of Adaptive Receiver with Ideal Coherent Reference, Differential Detection, and Costas Loop Compensation on the Reverse Link of an AWGN Channel with "Strict" Power Control; $E_b/N_0 = 12$ dB.

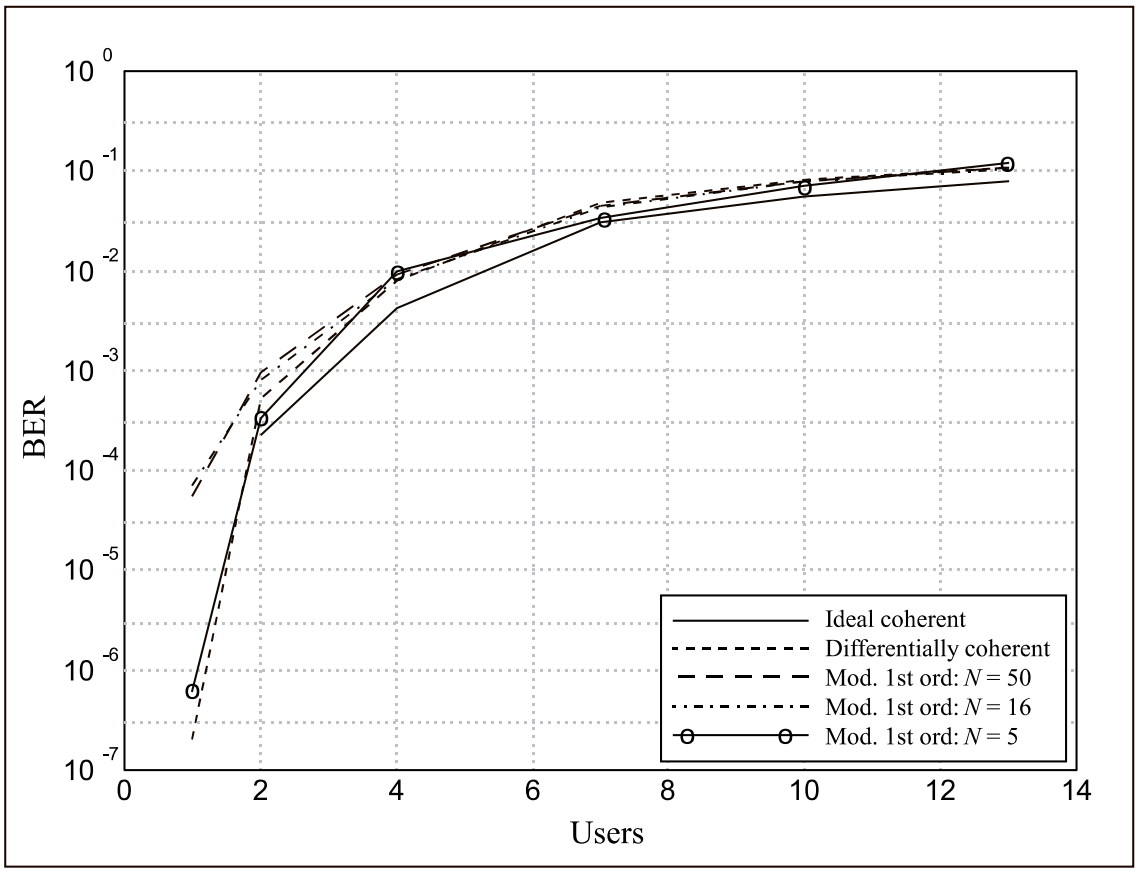

Figure 8.25: Comparison of Performances of Matched Filter Receiver with Ideal Coherent Reference, Differential Detection, and Modified First-Order ML Phase Estimation on the Reverse Link of an AWGN Channel with "Strict" Power Control; $E_b/N_0 = 12$ dB.

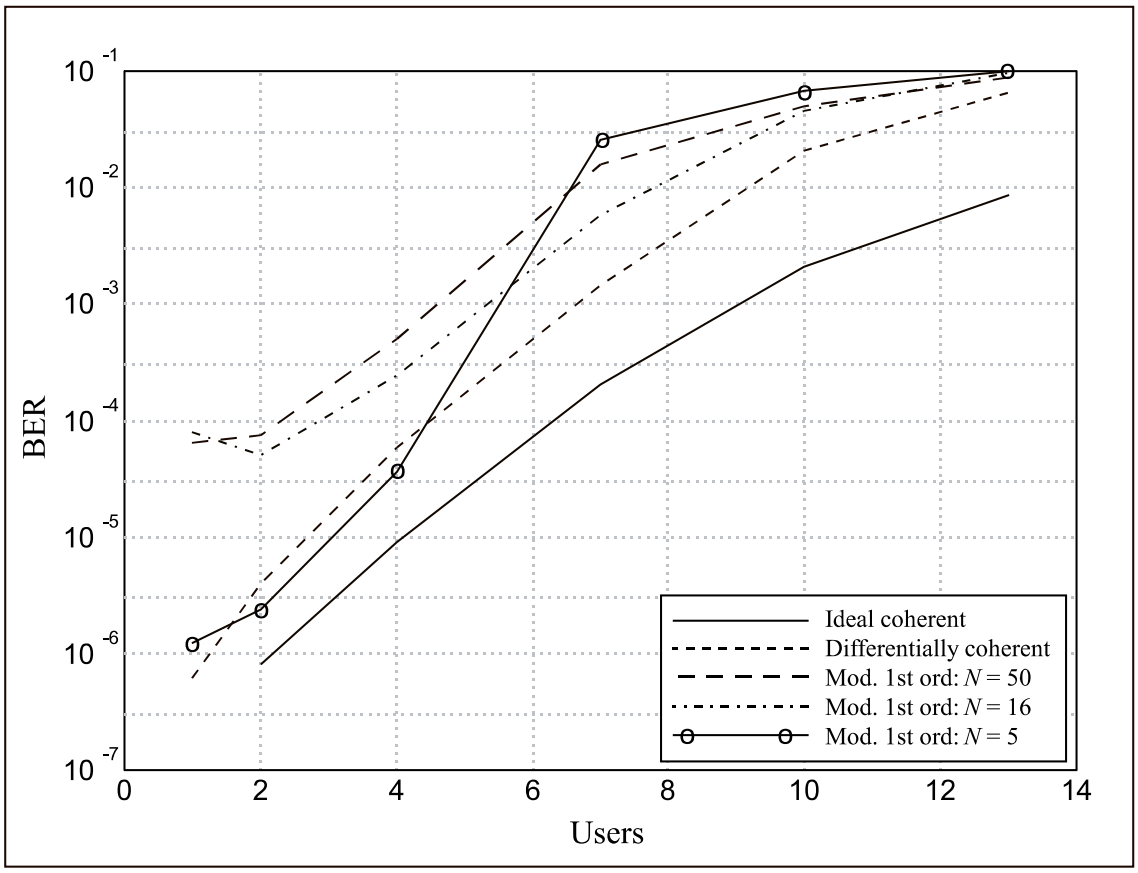

Figure 8.26: Comparison of Performances of Adaptive Receiver with Ideal Coherent Reference, Differential Detection, and Modified First-Order ML Phase Estimation on the Reverse Link of an AWGN Channel with "Strict" Power Control; $E_b/N_0 = 12$ dB.

Next we consider the case of "loose" power control. Figures 8.27 through 8.30 demonstrate the performance of the previously considered receivers for this case. It is observed that the performance of matched filter receiver is uniformly poor regardless of the offset compensation scheme used with it. The well known handicap of the MF, i.e., its inability to counter the near-far problem, shows up here yet again. Thus, even a coherent carrier reference does not help the receiver, which is not capable of overcoming the interference. The results for the CWFSLAR are, however, noteworthy. The immediately striking aspect of the adaptive receiver graphs is the receiver's performance with an ideal coherent reference. This receiver clearly demonstrates its resilience to the near-far effect. Both the Costas loop receivers perform badly, and the differentially coherent adaptive receiver performs marginally better. The performance of the adaptive receivers with ML phase estimation approaches that of the receiver with differential detection. The poor performance of the adaptive receiver can be attributed to the adaptive receiver failing more often than with strict power control. As pointed out earlier, catastrophic failures cause BERs close to 0.5 and these bias the final results. Even the coherent receiver failed on occasion but not as much as the other adaptive receivers. A large number of incorrect decisions in quick succession can cause the adaptive filter to lose convergence and ultimately diverge, leading to catastrophic failure. Until a proper formula is established to correct the results when the receiver fails, unbiased results are impossible. Such a formula should specify how the receiver may be penalized when it detects catastrophic failure and re-trains the adaptive filter. It was observed that increasing the initial training to one thousand bits did not impact the performance of the adaptive receiver significantly and, therefore, failure of the adaptive receiver cannot be attributed to insufficient training.

8.8.3 Simulation Results for Fading Channels

Results are now presented for the "Typical Urban" channel model described in Table 8.3. We note the proximity of the first two arriving multipath components, with the separation being less than half a chip period. The second component is stronger than the first creating a hard to equalize non-minimum phase channel.

Case 1: Forward Link

Figure 8.31 depicts the performance of the three-finger Rake receiver and the adaptive receiver with ideal coherent detection, differential detection, Costas loop reference, and ML phase estimation. A wideband Costas loop ($B_{L,c} = 10^{-1}R_b$) was employed, and $N = 16$ was used for the ML phase estimation scheme. The Costas loop receiver is consistently worse than the other receivers for all system loads. The coherent receiver is better than only the Costas loop receiver. It should be emphasized here that, for the "ideal coherent" receiver, the reference used was that of the *first* arriving multipath component. Thus, while there is a zero frequency shift on the first component, every other multipath

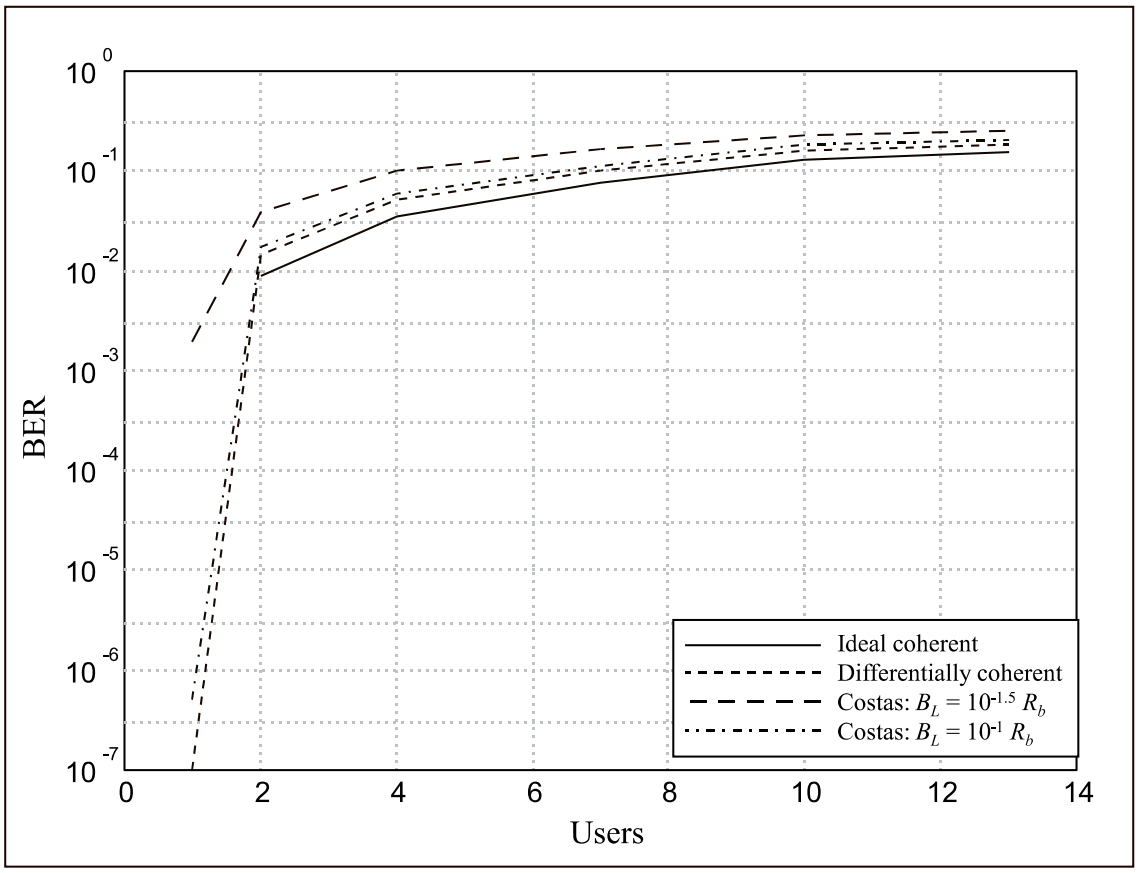

Figure 8.27: Comparison of Performances of Matched Filter Receiver with Ideal Coherent Reference, Differential Detection, and Costas Loop Compensation on the Reverse Link of an AWGN Channel with "Loose" Power Control; $E_b/N_0 = 12$ dB.

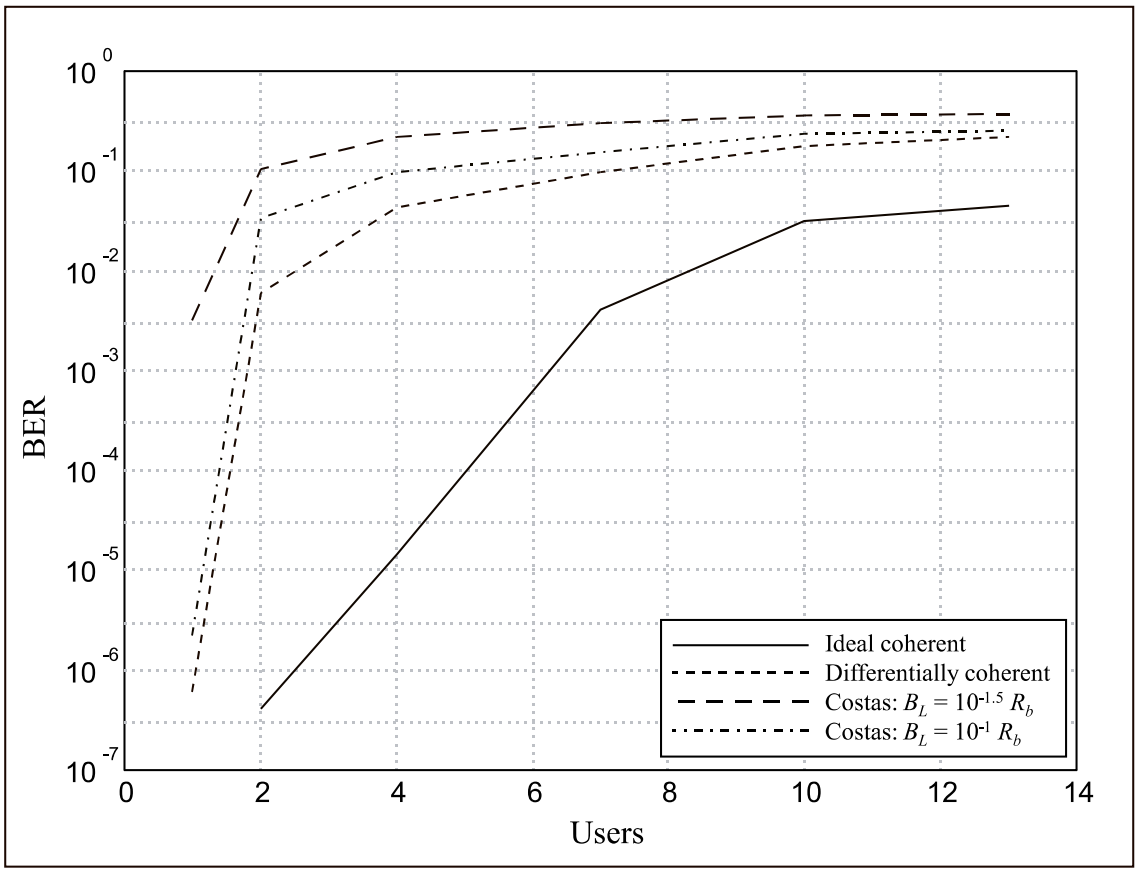

Figure 8.28: Comparison of Performances of Adaptive Receiver with Ideal Coherent Reference, Differential Detection, and Costas Loop Compensation on the Reverse Link of an AWGN Channel with "Loose" Power Control; $E_b/N_0 = 12$ dB.

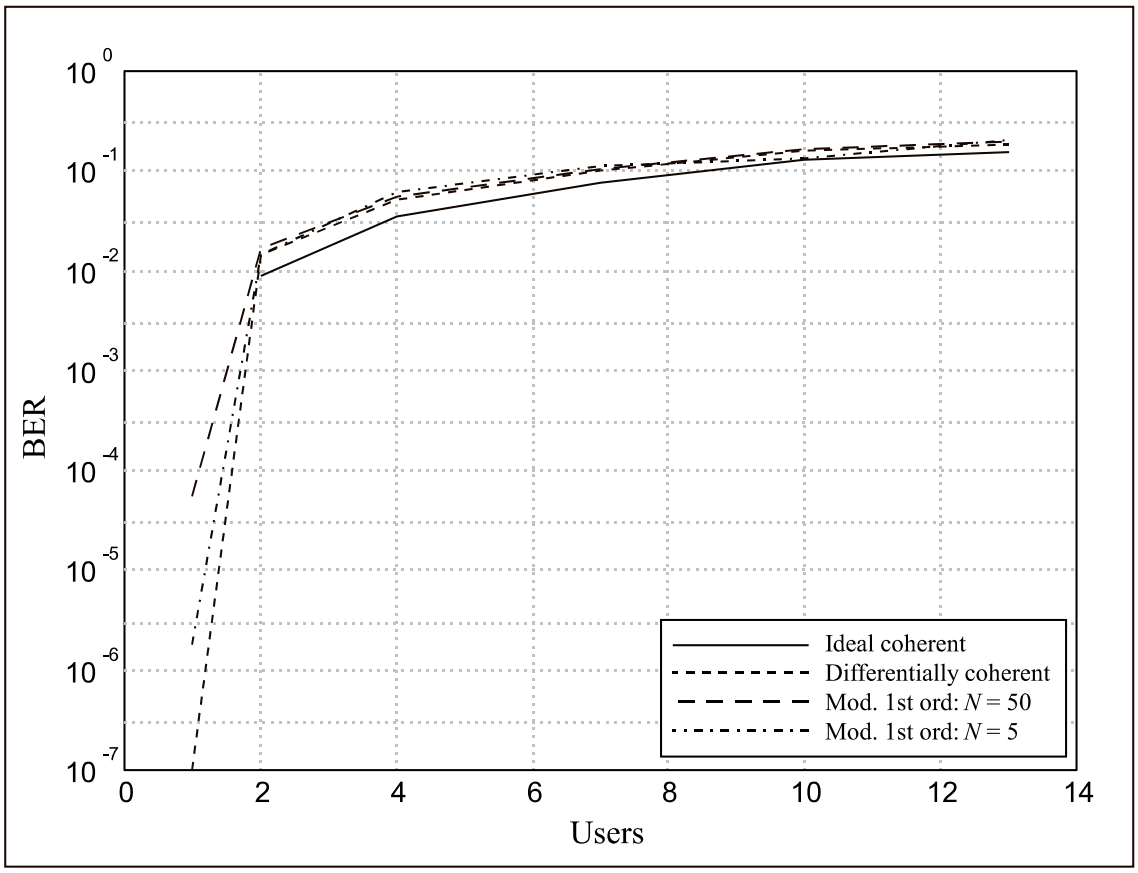

Figure 8.29: Comparison of Performances of Matched Filter Receiver with Ideal Coherent Reference, Differential Detection, and Modified First-Order ML Phase Estimation on the Reverse Link of an AWGN Channel with "Loose" Power Control; $E_b/N_0 = 12$ dB.

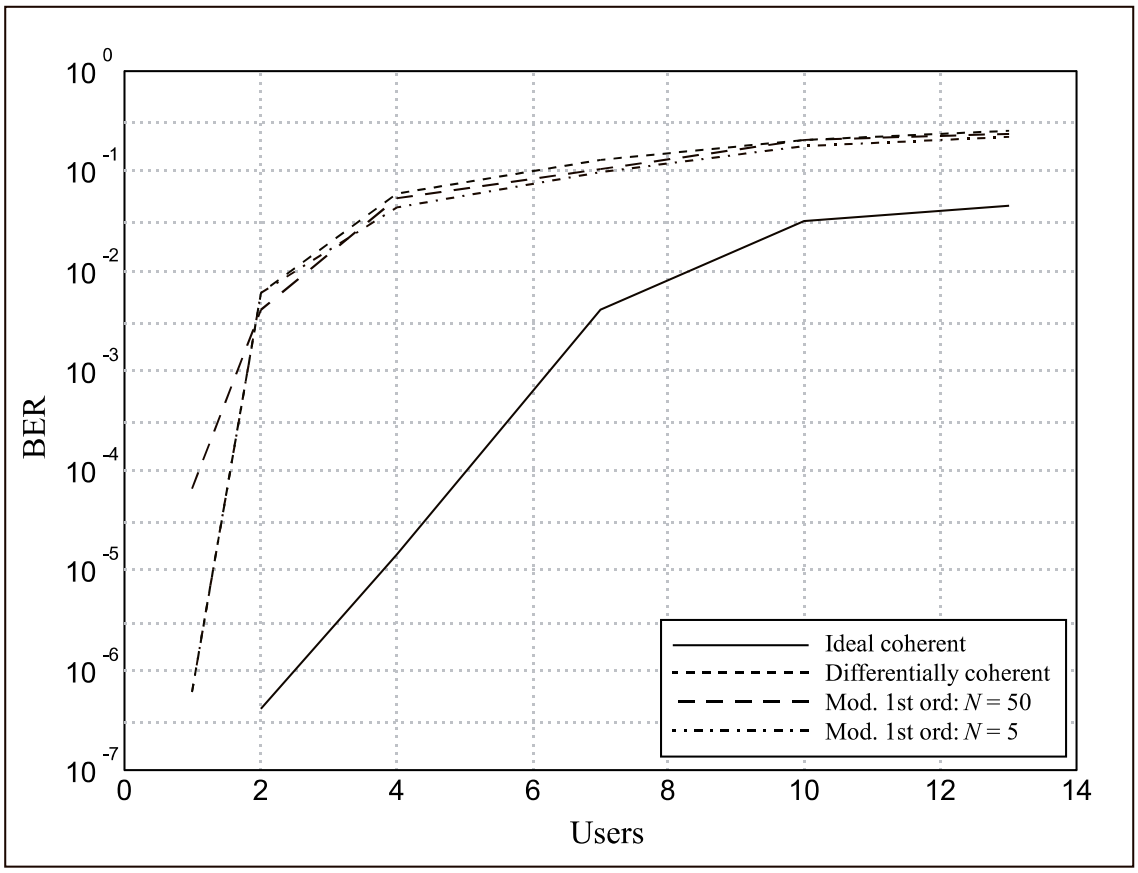

Figure 8.30: Comparison of Performances of Adaptive Receiver with Ideal Coherent Reference, Differential Detection, and Modified First-Order ML Phase Estimation on the Reverse Link of an AWGN Channel with "Loose" Power Control; $E_b/N_0 = 12$ dB.

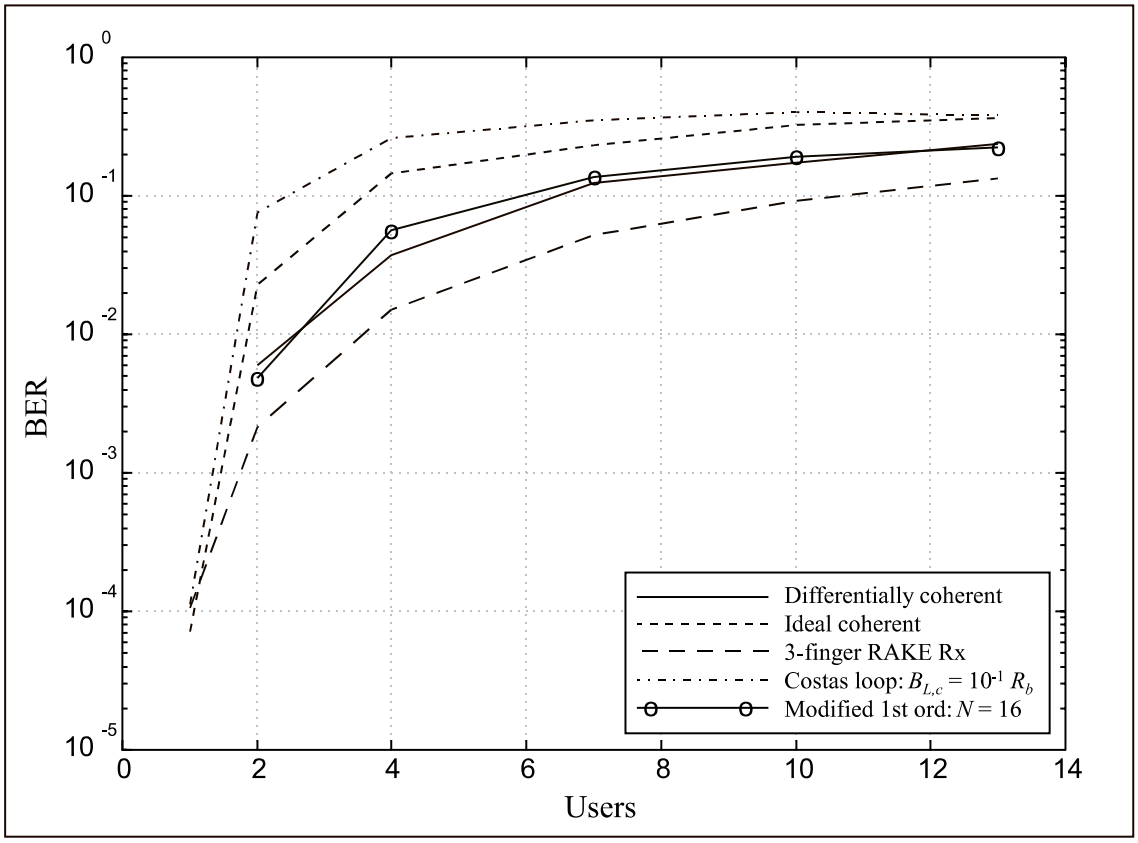

Figure 8.31: Comparison of Performances of Differentially Coherent Three-Finger Rake and Adaptive Receiver with "Ideal Coherent" Reference, Differential Detection, Costas Loop Compensation, and Modified First-Order ML Phase Estimation on the Forward Link of the "Typical Urban" Channel; $E_b/N_0 = 24$ dB; Vehicle Speed is 45 km/h.

component is offset in frequency, and the results demonstrate the adaptive receiver's inability to resolve this unusual problem. In contrast, the input signal to the adaptive receiver employing differential detection has all components with identical frequency shifts but different phases owing to fading, and this receiver performs better. The receiver with the modified first-order ML phase estimation also performs reasonably well, closely approaching the differentially coherent receiver. The three-finger Rake receiver, however, is the best among the lot, well surpassing the other receivers. While surprising at first instance, this apparent anomaly can be explained. Since the channel is synchronous, MAI is not a significant source of impairment to the MF. While a single MF may not yield remarkable results, the combination of the outputs of three matched filters in the form of a Rake receiver does. Simply stated, the Rake receiver is a more effective (multipath) diversity combiner for these channels. Deep fades, which induce errors during decision-direction, also influence the performance of the adaptive receivers. While the Costas loop is able recover from errors caused during these fades, the adaptive filter may not be able to do so, leading to suboptimal solutions and, in extreme cases, even failure of the adaptive filter. These help, albeit in part, in explaining the observed results. Simulation results, not exhibited here, have shown that the adaptive differentially coherent receiver does outperform the Rake receiver at lower vehicular speeds, thus proving to be the best of the realizable receivers.

Case 2: Reverse Link

The corresponding results for the reverse link with "strict" power control are provided in Figure 8.32. Here again, the adaptive receiver with the Costas loop is worst. The Rake receiver is only marginally better. The receiver with ML phase estimation and the differentially coherent receiver exhibit a similar performance under these conditions, except in the low interference case when the differential receiver is better. Surprisingly, the "ideal coherent" receiver is best for modest to large levels of MAI. The degradation of the performance of the Rake receiver compared with the synchronous case may be explained as due to the impact of the pernicious MAI on the asynchronous reverse link. This degradation far outweighs the gains from diversity combining. Although the adaptive receiver with ML estimation matches the performance of the receiver with differential detection, the latter is a better candidate with its reduced complexity.

8.9 Summary

Practical receivers are faced with the problem of overcoming frequency offsets resulting from Doppler as well as imperfect oscillators. Some conventional techniques for offset compensation were discussed. The Costas loop, commonly used for phase tracking, can also be used for frequency offset compensation provided its loop bandwidth is large

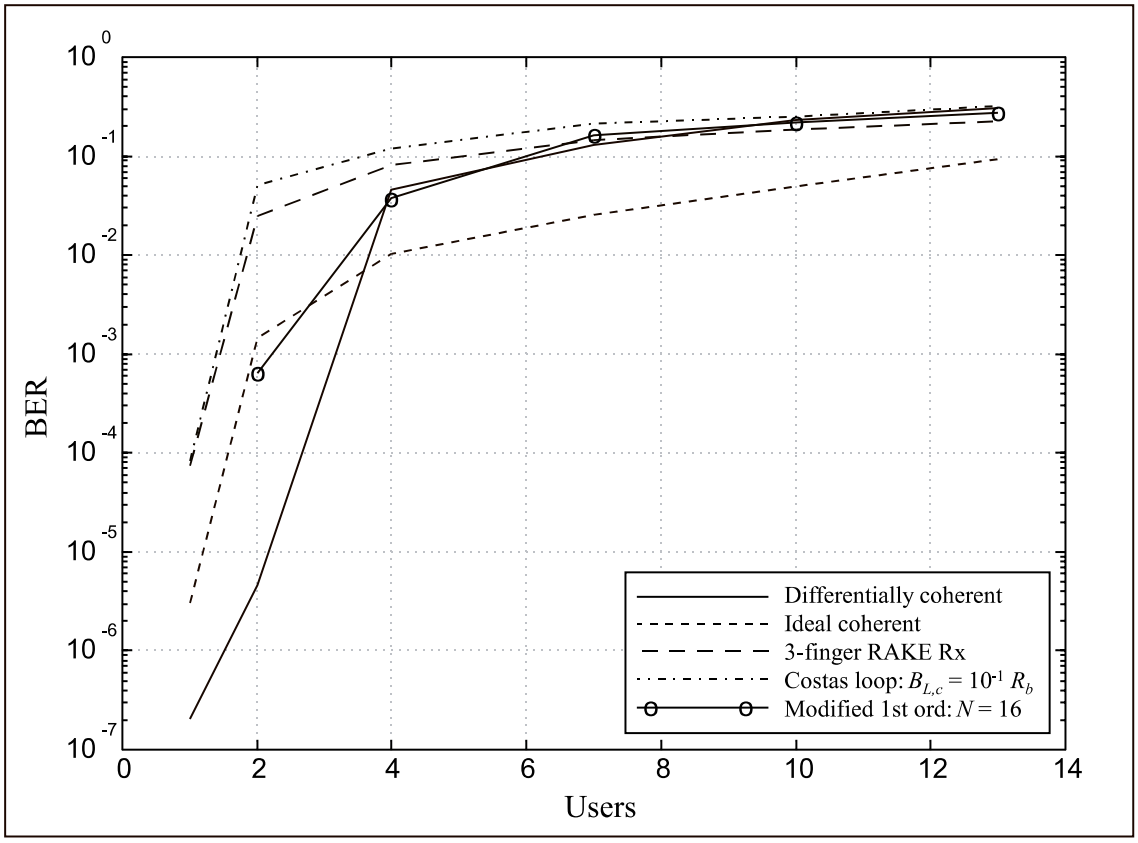

Figure 8.32: Comparison of Performances of Differentially Coherent Three-Finger Rake and Adaptive Receiver with "Ideal Coherent" Reference, Differential Detection, Costas Loop Compensation, and Modified First-Order ML Phase Estimation on the Reverse Link of the "Typical Urban" Channel with "Strict" Power Control; $E_b/N_0 = 24$ dB; Vehicle Speed is 45 km/h.

enough. The first-order maximum likelihood (ML) phase estimators can be used for phase offset compensation. The modified first-order ML phase estimation scheme allows for the compensation of small frequency offsets. The adaptive receiver alone can be used to compensate for frequency offsets when it is implemented as a differentially coherent receiver, in which, differential detection is integrated with filtering and the differentially detected signal becomes the estimated signal. The cost function of this modified adaptive receiver is correspondingly changed as is the filter weight update equation. This adaptive receiver compensates for frequency offsets on the desired signal by subsuming the compensating frequency offset in its filter solution, which was reflected in the study of the stationary points of the modified minimum mean-squared error (MMSE) cost function. The MMSE of the differential receiver is higher than that of the conventional adaptive receiver, a penalty paid for differential detection. Simulation results of various receiver structures were exhibited for additive white Gaussian noise and fading multipath channels. Results were presented for the synchronous forward link as well as the asynchronous reverse link. Among the realizable receivers (without a coherent reference) the differential adaptive receiver generally performed on par with the adaptive receiver using modified ML phase estimation and better than the matched filter receivers and the adaptive receiver with Costas loop compensation. The only situation in which the Rake receiver was superior was a synchronous multipath channel. The simulations revealed that the differential adaptive receiver is effective for frequency offset compensation in most instances. The use of the adaptive receiver with phase estimation is justified only when the gains it offers offers outweigh the increase in receiver complexity.

Chapter 9

Performance of Reduced Complexity Algorithms in Adaptive CDMA Receivers

9.1 Introduction

A serious consideration in the implementation of a novel radio function in a receiver is the function's computational complexity. Complex adaptive FIR filtering can be a significant load on the power resources of the receiver; this is not only due the actual *filtering* operation, consisting of a complex multiply-and-accumulate (MAC) operation, but also the complex *adaptation algorithm* itself. Algorithms that reduce the complexity of the LMS algorithm have been proposed in the literature. However, these algorithms are real versions and their application for CDMA interference rejection has not been tested. In this chapter, we propose complex differentially coherent versions of the algorithms that are derived from the differentially coherent version of the LMS algorithm, studied in Chapter 8. The convergence behavior of the reduced complexity algorithms and the LMS algorithm in CDMA environments are compared through simulations. BER performances of the three algorithms are evaluated through simulations.

Only the real part of the filter output in a coherent adaptive receiver affects the BER. This can be exploited to minimize a real error function as opposed to a complex error function [69]. Table 9.1 compares the computational complexities of an adaptive filter that minimizes the complex error and a filter that minimizes only the real part of the error with the LMS algorithm. The table demonstrates that when only the real part of the error is used, the number of real multiplication operations is reduced by 50% and the number of real addition operations is reduced by 33%. Thus, halving the number of real multiplication operations results in a significant reduction in the computational

Table 9.1: Computational Complexity of an N-Tap Adaptive Filter Employing the LMS Algorithm.

Filter Computing	**Mathematical Equation**	**Comp. Complexity/Symbol**	
		Real Multiplies	Real Adds
Complex output	$y(k) = \mathbf{w}^H(k)\,\mathbf{x}(k)$	$4N$	$4N-2$
	$e(k) = d(k) - y(k)$	0	2
	$\mu_1(k) = \mu\, e^*(k)$	2	0
	$\mathbf{u}(k) = \mu_1(k)\,\mathbf{x}(k)$	$4N$	0
	$\mathbf{w}(k+1) = \mathbf{w}(k) + \mathbf{u}(k)$	0	$2N$
	Total	$8N+2$	$6N$
Real output	$y(k) = \Re\{\mathbf{w}^H(k)\,\mathbf{x}(k)\}$	$2N$	$2N-1$
	$\tilde{e}(k) = d(k) - y(k)$	0	1
	$\mu_1(k) = \mu\,\tilde{e}(k)$	1	0
	$\mathbf{u}(k) = \mu_1(k)\,\mathbf{x}(k)$	$2N$	0
	$\mathbf{w}(k+1) = \mathbf{w}(k) + \mathbf{u}(k)$	0	$2N$
	Total	$4N+1$	$4N$

complexity. As demonstrated by Majmundar [55], the performance of the receiver is not compromised in most cases by this modified implementation.

As seen from Table 9.1, the update equation, which includes the last five equations, accounts for a majority of the computational complexity. Therefore, simplifying the adaptation algorithm aids in making the implementation of adaptive filters practicable in CDMA receivers. The objective of this chapter is to study two adaptation algorithms that are computationally less complex than the conventional LMS algorithm and to compare their performances with that of the LMS algorithm when used in CDMA receivers for MAI rejection.

The weight update equation of the simplified LMS algorithm is

$$\mathbf{w}(k+1) = \mathbf{w}(k) + \mu\, e(k)\,\mathbf{x}(k) \tag{9.1}$$

where

$$\begin{aligned} \tilde{e}(k) &= d(k) - y(k), & (9.2)\\ y(k) &= \Re\{\mathbf{w}^H(k)\,\mathbf{x}(k)\}, & (9.3) \end{aligned}$$

$\mathbf{w}(k)$ is the weight vector, $\mathbf{x}(k)$ is the input signal vector, and $d(k)$ is the reference information signal. Clearly, the computational load is primarily due to the product $e(k)\,\mathbf{x}(k)$, which requires $2N$ multiplication operations. In the equation, μ can be of the

Table 9.2: Computational Complexity of an N-Tap Differentially Coherent Adaptive Filter Employing the LMS Algorithm.

Filter Computing	**Mathematical Equation**	**Comp. Complexity/Symbol**	
		Real Multiplies	Real Adds
Complex output	$y(k) = \mathbf{w}^H(k)\,\mathbf{x}(k)$	$4N$	$4N-2$
	$z(k) = y(k)\,y^*(k-1)$	4	2
	$e(k) = d(k) - z(k)$	0	2
	$e_1(k) = e^*(k)\,y^*(k-1)$	4	2
	$\mu_1(k) = \mu\,e_1(k)$	2	0
	$\mathbf{u}(k) = \mu_1(k)\,\mathbf{x}(k)$	$4N$	0
	$\mathbf{w}(k+1) = \mathbf{w}(k) + \mathbf{u}(k)$	0	$2N$
	Total	$8N+10$	$6N+4$
Real output	$y(k) = \mathbf{w}^H(k)\,\mathbf{x}(k)$	$4N$	$4N-2$
	$z(k) = \Re\{y(k)\,y^*(k-1)\}$	2	1
	$\tilde{e}(k) = d(k) - z(k)$	0	1
	$e_1(k) = \tilde{e}(k)\,y^*(k-1)$	2	0
	$\mu_1(k) = \mu\,e_1(k)$	2	0
	$\mathbf{u}(k) = \mu_1(k)\,\mathbf{x}(k)$	$4N$	0
	$\mathbf{w}(k+1) = \mathbf{w}(k) + \mathbf{u}(k)$	0	$2N$
	Total	$8N+6$	$4N$

form 2^{-n} where n is an integer, so the multiplication by μ can be implemented as a shift by n bits.

The computational complexity of the adaptation algorithm is increased in the differentially coherent implementation, as is evident from Table 9.2. The weight update equation in the case of complex outputs is discussed in Chapter 8. The weight update equation for the real output case is

$$\mathbf{w}(k+1) = \mathbf{w}(k) + \mu\,\tilde{e}(k)\,y^*(k-1)\,\mathbf{x}(k) \tag{9.4}$$

where

$$\tilde{e}(k) = d(k) - z(k), \tag{9.5}$$
$$z(k) = \Re\{y(k)\,y^*(k-1)\}, \tag{9.6}$$

and $y(k)$ is as defined in Equation (9.3). In this receiver, the number of multiplication operations remains essentially the same for both cases because the complex filter output is computed, although only the real part of the differentially detected symbol is necessary

for making a bit decision. The modified complex error term $e_1(k) = \tilde{e}(k)\, y^*(k-1)$ is multiplied with each of the input vector elements in the update vector computation. The update equation again accounts for nearly 50% of all multiplication operations.

9.2 The Sign Algorithm

Using the sign of the error instead of the actual error completely eliminates the need for any multiplication in Equation (9.1). This is seen from the weight update equation, which now reduces to

$$\mathbf{w}(k+1) = \mathbf{w}(k) + \mu\, \mathrm{sgn}\{e(k)\}\, \mathbf{x}(k) \tag{9.7}$$

where the sign function $\mathrm{sgn}\{\cdot\}$ is defined as

$$\mathrm{sgn}\{x\} = \begin{cases} -1 & x < 0 \\ 0 & x = 0 \\ +1 & x > 0 \end{cases} \tag{9.8}$$

and the error term

$$e(k) = d(k) - y(k), \tag{9.9}$$

$$y(k) = \mathbf{w}^T(k)\, \mathbf{x}(k). \tag{9.10}$$

If μ is chosen to be in the form 2^{-n}, the only arithmetic operation involved in the weight update is addition, thereby avoiding the costly multiplication operations. The above algorithm is commonly referred to as the *sign algorithm* [110, 111, 112, 113]. The sign algorithm has been extensively investigated for digital echo cancellation applications. Earlier studies have focused on real (as opposed to complex) adaptive filters. In this study, however, a complex version of the algorithm will be proposed and applied.

9.3 The Signed Regressor Algorithm

Another method of simplifying the LMS algorithm is through the use of clipped data. The resulting algorithm is termed the *signed regressor (SR) algorithm* in modern literature and takes the form

$$\mathbf{w}(k+1) = \mathbf{w}(k) + \mu\, e(k)\, \mathrm{sgn}\{\mathbf{x}(k)\} \tag{9.11}$$

for real filtering where $e(k)$ is as previously defined and the sgn$\{\cdot\}$ function operating on a vector is defined as the function operating on each element of the vector. Here again, multiplication is eliminated in the weight update. Even if μ is not constrained to be a negative power of two, only one multiplication operation is necessary for computing the product $\mu\, e(k)$. The SR algorithm has also been studied for digital echo cancellation and other adaptive filtering applications [111, 112, 114, 115, 116]. A complex version of the algorithm will be proposed and applied here.

9.4 Geometric Interpretation of Convergence of the Algorithms

Simplification of the LMS algorithm by using clipped data or a clipped error has an immediate impact on the convergence properties of the algorithm because each simplification yields a further approximation to the gradient estimate of the LMS algorithm. We will draw from the geometric interpretation of [111] for an intuitive understanding.

Figure 9.1 illustrates the change in the weight error vector during weight update with the LMS algorithm for the two-dimensional case. The weight error vector $\mathbf{v}(k)$ at the kth iteration is defined by

$$\mathbf{v}(k) \triangleq \mathbf{w}(k) - \mathbf{w}_{\text{opt}} \tag{9.12}$$

where $\mathbf{w}_{\text{opt}}$ is the optimum weight vector in the stationary channel. Then, subtracting $\mathbf{w}_{\text{opt}}$ from both sides of the LMS weight update equation, we get

$$\mathbf{v}(k+1) = \mathbf{v}(k) + \mu\, e(k)\, \mathbf{x}(k). \tag{9.13}$$

The weight error vector $\mathbf{v}(k)$ is modified by the update vector, which is a scaled version of the input vector $\mathbf{x}(k)$. The direction of the update vector is determined by $\mathbf{x}(k)$ and the sign of the error $e(k)$, which also controls the weight error vector's magnitude. The step-size μ scales the instantaneous gradient estimate $-2e(k)\,\mathbf{x}(k)$ and determines the rate of convergence. The new weight error vector $\mathbf{v}(k+1)$ is thus obtained as the sum of the two previously discussed vectors. The LMS algorithm works so that the magnitude of the weight error vector is diminished at every iteration due to an appropriate update vector. Eventually, when the algorithm converges, the magnitude reduces to almost zero and the residual update vector is due to the imperfect gradient estimate. This *gradient noise* prevents the error vector from completely vanishing and causes it to have a small random magnitude (due to the random error) and a direction determined by the input vector. The residual error vector is responsible for the *excess MSE*.

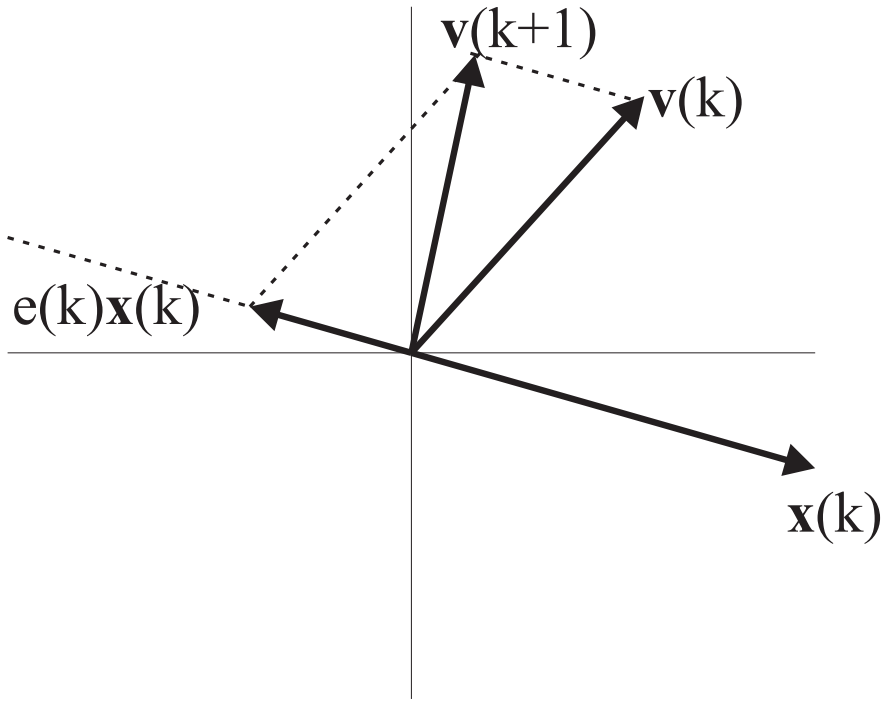

Figure 9.1: Geometric Interpretation of the Weight Vector Update in the LMS Algorithm.

The preceding interpretation is useful in studying the two reduced complexity algorithms as well. Figure 9.2 shows a similar illustration for the sign algorithm. The update equation for the weight error vector for this algorithm is

$$\mathbf{v}(k+1) = \mathbf{v}(k) + \mu \operatorname{sgn}\{e(k)\}\, \mathbf{x}(k). \tag{9.14}$$

The update vector in this case is $\mu \operatorname{sgn}\{e(k)\}\, \mathbf{x}(k)$. Thus, the direction of the update vector is still controlled by $\mathbf{x}(k)$ and the sign of $e(k)$. However, the error $e(k)$ plays no role in determining the magnitude of the update vector, which is solely controlled by the step-size μ. Thus, during the initial stages of convergence when the error can potentially be large, the changes to the weight error vector may be smaller than in the case of the LMS algorithm and will result in slower convergence. Increasing the step-size can hasten convergence but has an adverse effect on the residual error. The residual error vector after convergence is the update vector $\mu \operatorname{sgn}\{e(k)\}\, \mathbf{x}(k)$ whose magnitude is independent of the actual error. Therefore, the residual error vector's magnitude is determined by the magnitude of $\mathbf{x}(k)$ as well as the step-size μ. If we assume the magnitude of $\mathbf{x}(k)$ remains approximately constant, then the magnitude of the residual error vector is $\mu\, ||\mathbf{x}(k)||$, which is indicated by the circle in Figure 9.2. The danger of using a large step size is now clear. The step-size is the sole factor that controls the residual MSE. A large μ

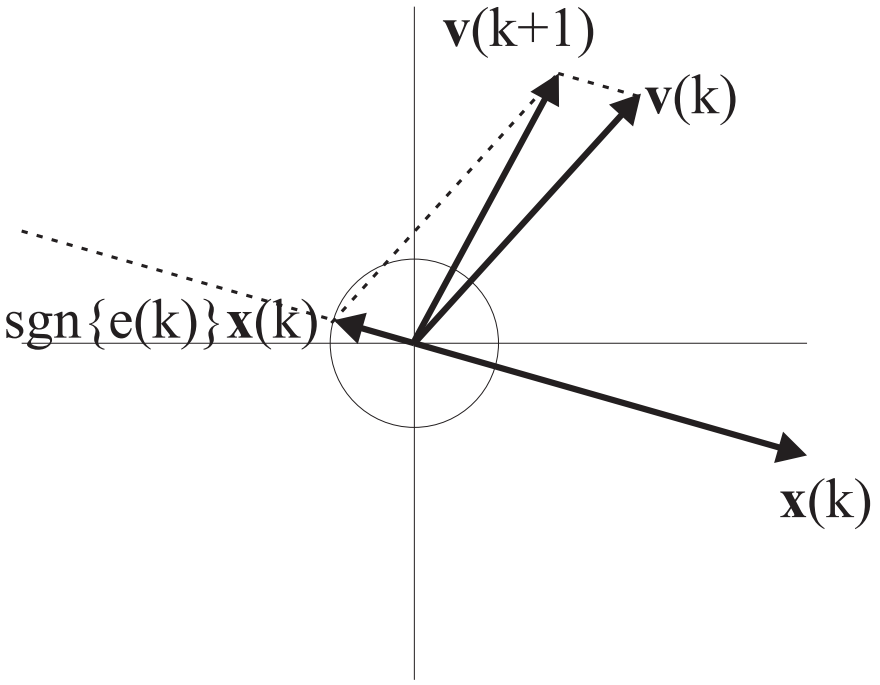

Figure 9.2: Geometric Interpretation of the Weight Vector Update in the Sign Algorithm.

can improve convergence speed but will also contribute to a large excess MSE. Time varying step-size techniques are useful here but they do increase the complexity of the implementation.

We finally consider the geometric interpretation of weight update for the SR algorithm in Figure 9.3. The corresponding weight error vector update equation is

$$\mathbf{v}(k+1) = \mathbf{v}(k) + \mu\, e(k)\, \mathrm{sgn}\{\mathbf{x}(k)\}. \tag{9.15}$$

As illustrated in the figure, the clipped vector $\mathrm{sgn}\{\mathbf{x}(k)\}$ is generally not aligned with the input vector $\mathbf{x}(k)$. In the two-dimensional case being considered, the clipped input vector can have one of only four, or 2^N in the N-dimensional case, possible directions. This leads to incorrect adaptation on an *instantaneous* basis. The degradation of the performance of this algorithm compared with the LMS algorithm arises from the deviation of the equivalent "gradient vector" $-2e(k)\,\mathrm{sgn}\{\mathbf{x}(k)\}$ from the true instantaneous estimate $-2e(k)\,\mathbf{x}(k)$. This deviation of the gradient vector estimate causes incorrect instantaneous adjustments to the weight vector. The gradient vector can have only the four different directions of the clipped input vector. Therefore, the algorithm has to work within this constraint and a monotonic decrease of the weight error vector is not guaranteed, as Figure 9.3 illustrates. However, as noted in [114], this can lead to correct average

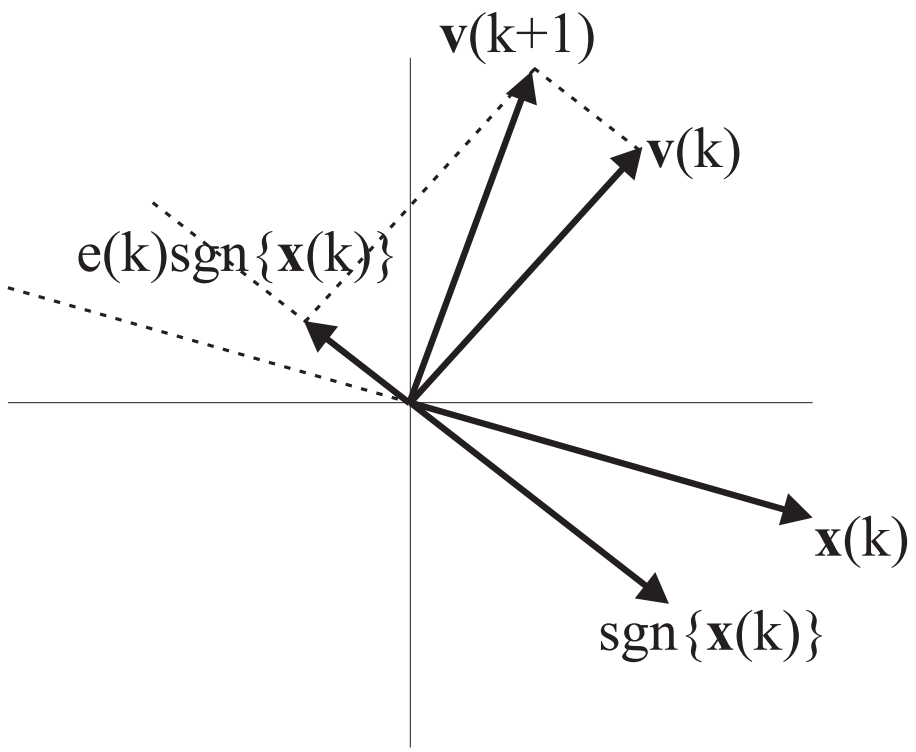

Figure 9.3: Geometric Interpretation of the Weight Vector Update in the SR Algorithm.

convergence of the algorithm. Furthermore, the authors of [114] note that the average convergence cannot be expected when the input data is not Gaussian. The authors point out that this drawback coupled with the lower hardware complexity of the sign algorithm supports the use of the latter algorithm in spite of its slower convergence.

9.5 Comparison of Convergence of LMS Algorithm with Reduced Complexity Algorithms

Appendix A describes the convergence behavior of the sign algorithm and the SR algorithm and provides a comparison with the LMS algorithm. However, the analysis assumes that the signals are jointly Gaussian. While this assumption is not true for CDMA systems in practice, it nevertheless provides a common platform for comparison. Furthermore, it enables the prediction of the general trend the algorithms follow. Deviation of practical conditions from assumed conditions means that the actual results deviate as well. However, this deviation of results is not significant in practice.

In this section, we compare the convergence performance of the LMS algorithm, the sign algorithm, and the SR algorithm through simulations under similar conditions in a CDMA system. We assume that the channel is stationary and that the desired signal is corrupted by MAI and AWGN. Employing the results of Appendix A, we use step-sizes that yield the same excess MSE for all three algorithms.

We consider the case of seven users. Gold codes of length 15 are used for the spreading codes of all the users. The synchronous case is considered here, so the crosscorrelation between any two users is $-1/15$. To evaluate the MMSE, we make use of Equation (6.55). The crosscorrelation matrix $\mathbf{X}$ is of order 7 and has diagonal elements equal to unity and non-diagonal elements equal to $-1/15$ regardless of the actual codes used, since Gold codes always yield this minimum crosscorrelation value in the synchronous case. The crosscorrelation vector $\mathbf{x}$ is simply the first column of the matrix $\mathbf{X}$. Equal powers are assumed for all users, so the order-7 matrix $\mathbf{L}$ is a diagonal matrix with all the diagonal elements equal to unity. We use a SNR $E_b/N_0 = 10$ dB, so that $\gamma = 20$. Equation (6.55) now yields the MMSE

$$\epsilon_{\min} = 0.0494. \tag{9.16}$$

The filter weight vector is initialized to $\mathbf{0}$ for all three algorithms. The MSE is obtained by averaging over 900 trials. For each trial, a different set of spreading codes is randomly chosen from the set of Gold codes. The step-size for the sign algorithm is $\mu_S = 10^{-13}$. The noise variance is calculated to be $\sigma_n^2 = 1.5$. The variance of the input signal is the sum of the noise variance and the variances of the seven independent signals. This means that $\sigma_x = \sqrt{8.5} \approx 2.3262$. Equations (1.41) and (1.56) are used for determining the step-sizes for the LMS algorithm and the SR algorithm, respectively.

Figure 9.4 shows the convergence curves for the three algorithms. Clearly, the LMS algorithm converges the fastest in about 200 iterations. The sign algorithm takes roughly 400 iterations to converge. The SR algorithm converges after approximately 300 iterations. As the figure indicates, the steady-state MSE is nearly equal with all three algorithms. Thus, the theoretical results derived in Sections A.1 and A.2 for the sign algorithm and the SR algorithm, respectively, are justified. The SR algorithm converges only a little slower than the LMS algorithm, whereas the sign algorithm is considerably slower.

The convergence times may seem prohibitively long from the previous example, but this is because the weight vector for each algorithm is initialized to the $\mathbf{0}$ vector. Initializing the weight vector to the matched filter coefficients drastically reduces the convergence time. Figure 9.5 shows the convergence curves in this case. The convergence times are about 70–80 of iterations and are not significantly different for the three algorithms. However, when the convergence times are larger, the convergence curves can be expected to be clearly distinct for the three algorithms.

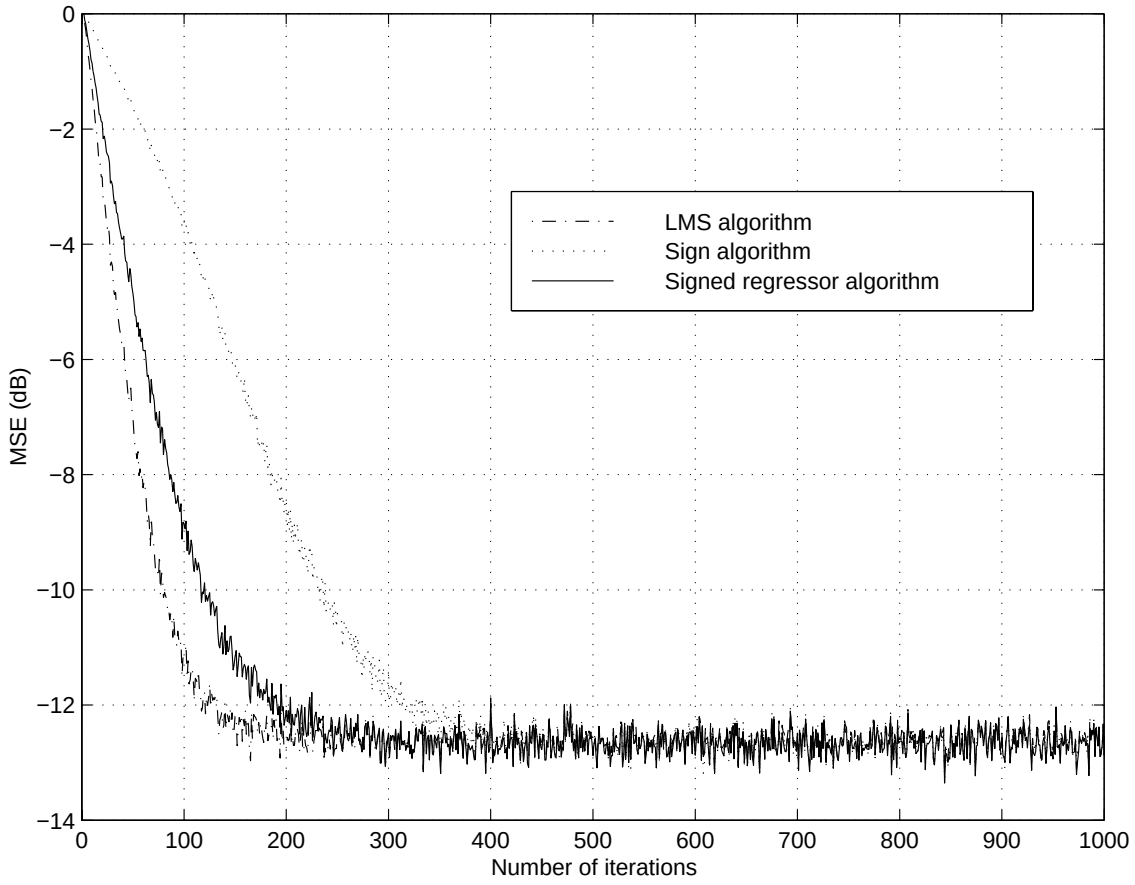

Figure 9.4: Comparison of Convergence of the LMS Algorithm, the Sign Algorithm, and the Signed Regressor Algorithm when the Weight Vector is Initialized to $\mathbf{0}$.

9.6 Complex Differentially Coherent Implementation of the Reduced Complexity Algorithms

The preceding discussions were restricted to real versions of the sign algorithm and the SR algorithm. These real versions, however, are useful when coherent recovery is performed where the receiver becomes coherent and the despreading filter is real. When coherent carrier recovery is not possible, a differentially coherent implementation becomes necessary. Chapter 8 described a differentially coherent adaptive receiver. The modified LMS algorithm was discussed in that context. It is necessary to present corresponding modifications to the sign algorithm and the SR algorithm, which will be in this section.

The differentially coherent version of the complex LMS algorithm was discussed in Chap-

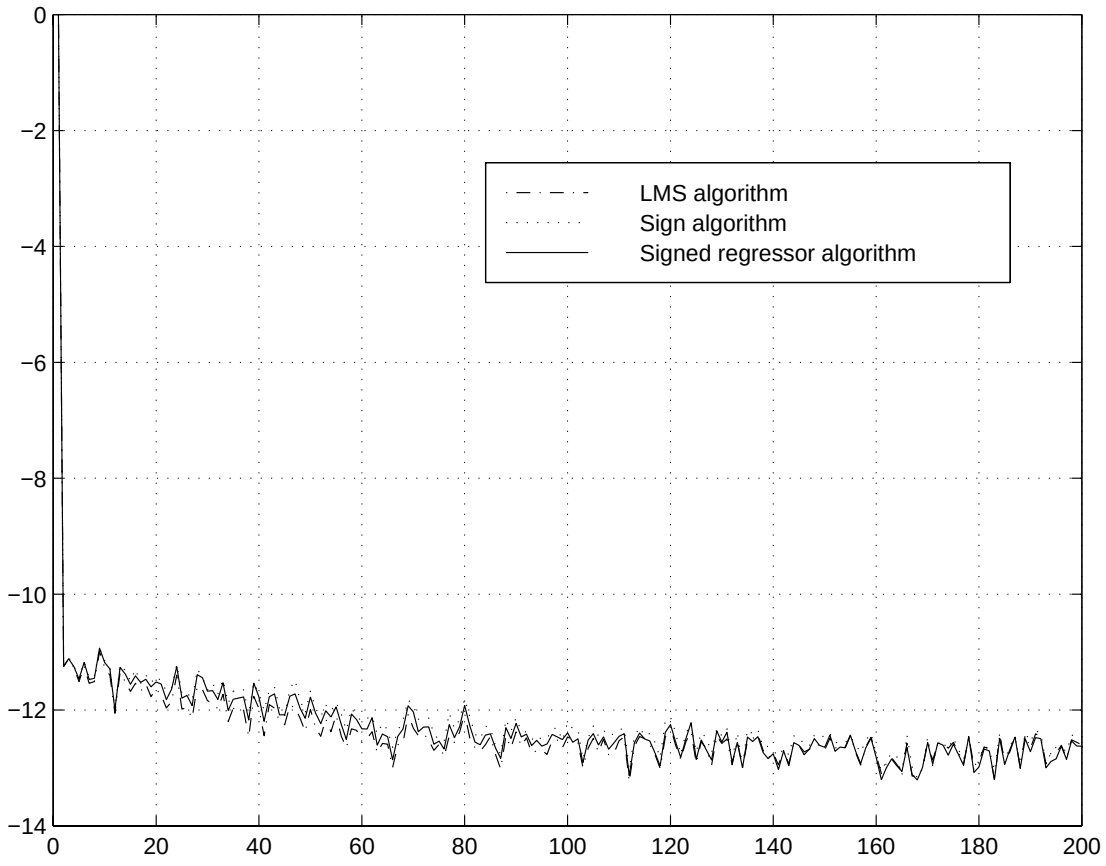

Figure 9.5: Comparison of Convergence of the LMS Algorithm, the Sign Algorithm, and the Signed Regressor Algorithm when the Weight Vector is Initialized to the Matched Filter Coefficient Vector.

ter 8, where the limitation of the conventional complex LMS algorithm in the presence of carrier frequency offsets was noted. To avoid the same difficulties, we directly propose complex differentially coherent versions of the reduced complexity algorithms. As will be seen in this section, the extension of a coherent complex version of the sign algorithm to a differentially coherent version is not direct. Therefore, even if a complex coherent version of the sign algorithm is analyzed, the analysis cannot be extended to the differentially coherent version. As seen in Chapter 8, it is difficult to analyze the differentially coherent version of the LMS algorithm because of the memory in the update equation. A similar difficulty can be expected in the analysis of the differentially coherent versions of the reduced complexity algorithms. Therefore, in this section, we merely propose complex differentially coherent versions of the reduced complexity algorithms and leave convergence analysis of these algorithms for future research, which may follow similar future analysis for the corresponding LMS algorithm.

We first note that the LMS algorithm with real error for the differentially coherent adaptive receiver is

$$\mathbf{w}(k+1) = \mathbf{w}(k) + \mu_L \, \Re\{e(k)\} \, y^*(k-1) \, \mathbf{x}(k) \tag{9.17}$$

where

$$\begin{aligned} e(k) &= d(k) - z(k), && (9.18)\\ z(k) &= y(k) \, y^*(k-1), && (9.19)\\ y(k) &= \mathbf{w}^H(k) \, \mathbf{x}(k), && (9.20) \end{aligned}$$

and $d(k)$ is the reference signal. Equation (9.17) shows that merely using $\text{sgn}[\Re\{e(k)\}]$ for the sign algorithm does not reduce the computational complexity, as in Section 9.2, because of the presence of the factor $y^*(k-1)$. Rather than perform a similar coarse quantization on $y^*(k-1)$, i.e., rather than use $\text{sgn}[\Re\{e(k)\}] \, \text{sgn}[y^*(k-1)]$, we propose the following modified weight update equation for the differentially coherent implementation of the sign algorithm:

$$\mathbf{w}(k+1) = \mathbf{w}(k) + \mu_S \, \left(\text{sgn}\left[\Re\left\{\tilde{e}(k)\right\}\right] + j \, \text{sgn}\left[\Im\left\{\tilde{e}(k)\right\}\right]\right) \, \mathbf{x}(k) \tag{9.21}$$

where

$$\tilde{e}(k) = \Re\{e(k)\} \, y^*(k-1) \tag{9.22}$$

is a modified complex error function. Thus, each of the real and imaginary parts of the modified complex error $\tilde{e}(k)$ is quantized to one bit since $\tilde{e}(k)$ contains information

in both these parts[1]. Using $(\text{sgn}\,[\Re\{\tilde{e}(k)\}] + j\,\text{sgn}\,[\Im\{\tilde{e}(k)\}])$ can be expected to yield better results than using $\text{sgn}[\Re\{e(k)\}]\,\text{sgn}[y^*(k-1)]$. Multiplication operations are not required for the implementation of Equation (9.21). A comparison of the computational complexity of the three algorithms for the differentially coherent implementation will be presented later in this section.

For the complex differentially coherent implementation of the SR algorithm, we propose the update equation

$$\begin{aligned}\mathbf{w}(k+1) &= \mathbf{w}(k) + \mu_R\,\Re\{e(k)\}\,y^*(k-1)\;(\text{sgn}\,[\Re\{\mathbf{x}(k)\}] \\ &\quad + j\,\text{sgn}\,[\Im\{\mathbf{x}(k)\}])\end{aligned} \tag{9.23}$$

where a complex (one-bit) quantization is performed on the input vector. The complex quantization is necessary since both real and imaginary parts of $\mathbf{x}(k)$ contain information. The effective power of the quantized input vector is greater than that of the real case by a factor $\sqrt{2}$. The step-size μ_R is divided by $\sqrt{2}$ to provide an equivalent step-size to μ_L.

Figure 9.6 shows the convergence curves for the differentially coherent implementations of the three algorithms. It is necessary to initialize the weight vector to a non-null vector since a null vector will yield a zero filter output, which will make the update vector $\mathbf{0}$. Therefore, each of the coefficients is initialized to a small value, 10^{-5}. The figure illustrates that the sign algorithm and the SR algorithms exhibit almost the same convergence behavior. The SR algorithm, however, converges more slowly than before. The convergence time for the SR algorithm is now slightly more than that for the sign algorithm, about 500 iterations. Thus, clipping the complex input signal vector has a more serious impact in this case. The steady-state MSE is the same for the three algorithms. Comparing Figure 9.6 with 9.4 indicates that the steady-state MSE is slightly higher in this case, which is expected due to the higher MMSE of the differentially coherent receiver (cf. Chapter 8) and (possibly) a higher excess MSE.

The convergence behavior when the filter weights are initialized to the matched filter coefficients is illustrated in Figure 9.7. Again, convergence is rapid for all three algorithms, making it difficult to distinguish between the convergence times. For the BER simulation study performed in this chapter, the filter weights are initialized to the matched filter coefficients to save convergence time.

Table 9.3 shows a comparison of the computational complexities of the three algorithms. The table clearly demonstrates how the computational complexities of the signed algorithm and the SR algorithm are much lower than that of the LMS algorithm. The SR

[1] A complex coherent version of the algorithm could take the form

$$\mathbf{w}(k+1) = \mathbf{w}(k) + \mu_S\,\text{sgn}\,[\Re\{e(k)\}]\;\mathbf{x}(k).$$

Clearly, Equation (9.21) is not a simple extension of this update equation because of the nature of the nonlinear function $\text{sgn}(\cdot)$.

Table 9.3: Computational Complexity of an N-Tap Differentially Coherent Adaptive Filter Employing the LMS Algorithm, Sign Algorithm, and Signed Regressor Algorithm.

Adaptation Algorithm	**Mathematical Equation**	**Comp. Complexity/Symbol**	
		Real Multiplies	Real Adds
LMS	$y(k) = \mathbf{w}^H(k)\,\mathbf{x}(k)$	$4N$	$4N-2$
	$z(k) = \Re\{y(k)\,y^*(k-1)\}$	2	1
	$\tilde{e}(k) = d(k) - z(k)$	0	1
	$e_1(k) = \tilde{e}(k)\,y^*(k-1)$	2	0
	$\mu_1(k) = \mu_L\,e_1(k)$	2	0
	$\mathbf{u}(k) = \mu_1(k)\,\mathbf{x}(k)$	$4N$	0
	$\mathbf{w}(k+1) = \mathbf{w}(k) + \mathbf{u}(k)$	0	$2N$
	Total	$8N+6$	$6N$
Sign	$y(k) = \mathbf{w}^H(k)\,\mathbf{x}(k)$	$4N$	$4N-2$
	$z(k) = \Re\{y(k)\,y^*(k-1)\}$	2	1
	$\tilde{e}(k) = d(k) - z(k)$	0	1
	$e_1(k) = \tilde{e}(k)\,y^*(k-1)$	2	0
	$\mu_1(k) = \operatorname{sgn}\left[\Re\left\{\tilde{e}(k)\right\}\right]\,\mu_S + j\operatorname{sgn}\left[\Im\left\{\tilde{e}(k)\right\}\right]\,\mu_S$	0	0
	$\mathbf{u}(k) = \mu_1(k)\,\mathbf{x}(k)$	0	0
	$\mathbf{w}(k+1) = \mathbf{w}(k) + \mathbf{u}(k)$	0	$2N$
	Total	$4N+4$	$6N$
SR	$y(k) = \mathbf{w}^H(k)\,\mathbf{x}(k)$	$4N$	$4N-2$
	$z(k) = \Re\{y(k)\,y^*(k-1)\}$	2	1
	$\tilde{e}(k) = d(k) - z(k)$	0	1
	$e_1(k) = \tilde{e}(k)\,y^*(k-1)$	2	0
	$\mu_1(k) = \mu_R\,e_1(k)$	2	0
	$\mathbf{u}(k) = \mu_1(k)\operatorname{sgn}\left[\Re\left\{\mathbf{x}(k)\right\}\right] + j\,\mu_1(k)\operatorname{sgn}\left[\Im\left\{\mathbf{x}(k)\right\}\right]$	0	0
	$\mathbf{w}(k+1) = \mathbf{w}(k) + \mathbf{u}(k)$	0	$2N$
	Total	$4N+6$	$6N$

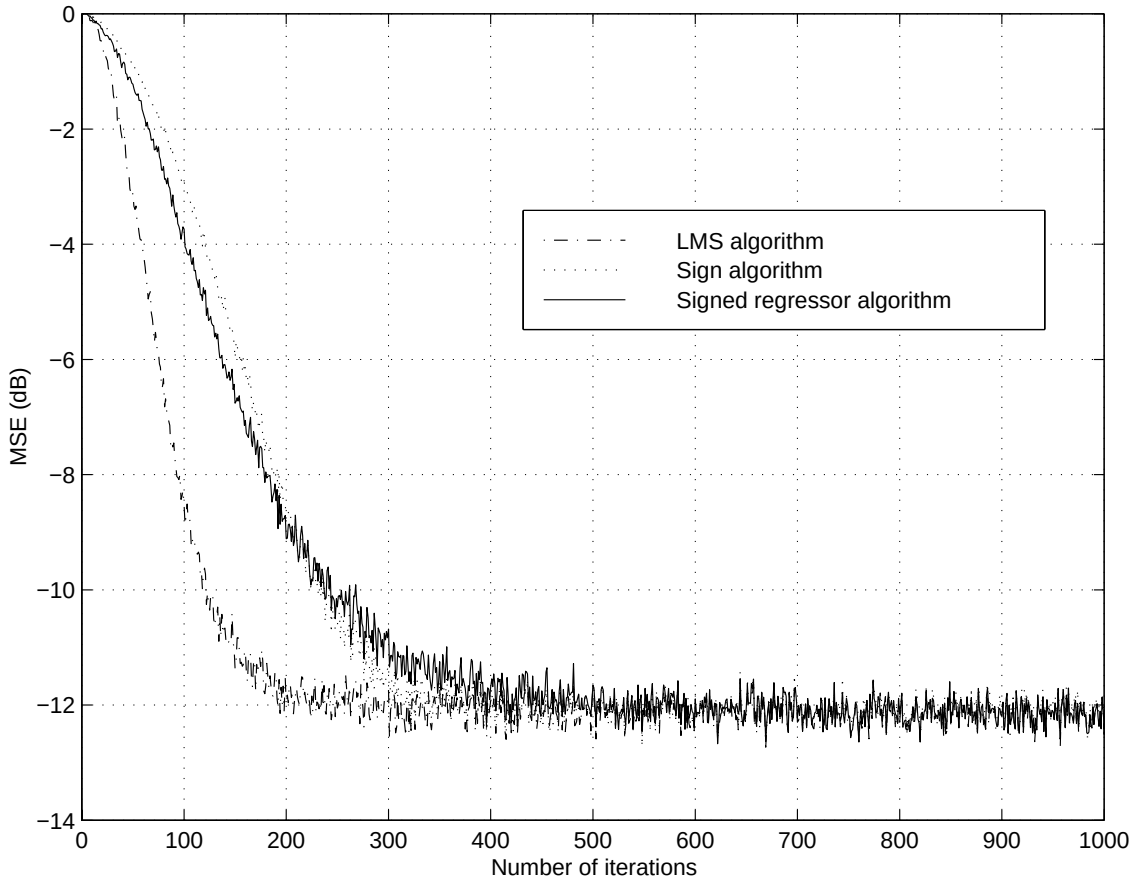

Figure 9.6: Comparison of Convergence of the LMS Algorithm, the Sign Algorithm, and the Signed Regressor Algorithm for the Differentially Coherent Receiver when the Weight Vector Coefficients are Initialized to 10^{-5}.

algorithm has two more multiplication operations than the sign algorithm, but this is negligible compared with the additional computations. Eliminating half of the multiplication operations results in a dramatic reduction of the complexity, which is why the two reduced complexity algorithms are attractive alternatives to the LMS algorithm.

9.7 Simulation Results for BER Performance

Similar MSE performance can be extracted from the three adaptation algorithms discussed in this chapter, the LMS algorithm, the sign algorithm, and the SR algorithm, by selecting appropriate values for their step-sizes. However, the step-size is a function of

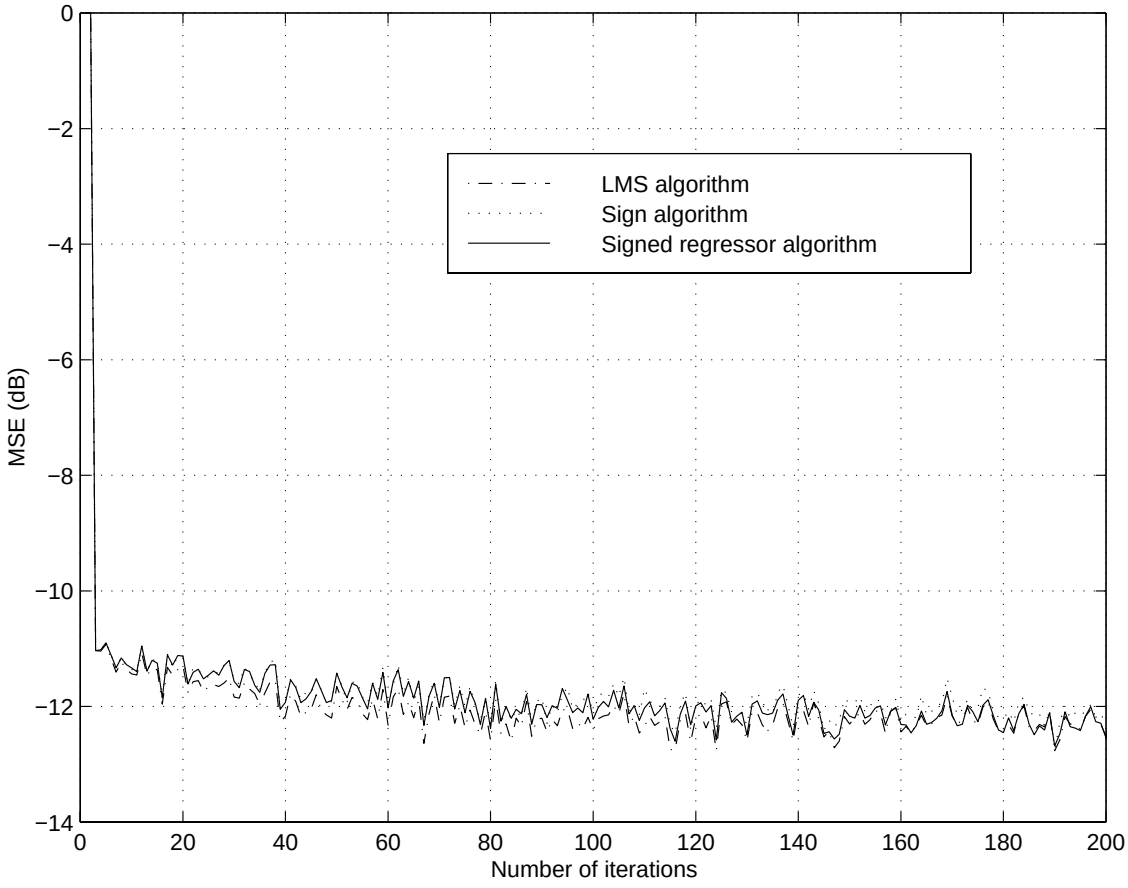

Figure 9.7: Comparison of Convergence of the LMS Algorithm, the Sign Algorithm, and the Signed Regressor Algorithm for the Differentially Coherent Receiver when the Weight Vector is Initialized to the Matched Filter Coefficient Vector.

the channel characteristics, including the SNR, signal-to-interference power ratios, and multipath characteristics. In a practical realization, channel characteristics are unknown and it would be more realistic to choose one step-size for the adaptation algorithm and to use the same step-size under all conditions. A normalized implementation, such as the NLMS algorithm discussed in Chapter 4, decreases the dependence of the algorithm's performance on the environment. However, such an implementation cannot be considered here because it would add complexity to the algorithm and reduction of complexity is the primary objective of this study. The approach of fixing the step-size helps illustrate the change in relative performances of the three algorithms when some channel characteristic is altered. The choice of step-sizes for the simulations is explained in Section 9.7.1. Since the step-sizes chosen yield reasonable convergence times, BER results presented here can be expected to be typical. In this section, BER performance of the three algorithms is evaluated as a function of the number of users in the system.

Gold codes of length 15 are used for all of the simulations. BER estimates are obtained by averaging over multiple trials (see next paragraph). For each trial, spreading codes for the users are randomly chosen from the set of Gold codes while ensuring that no two users are assigned the same code. All applicable random parameters, such as phase and delay, are randomly generated in every trial. Perfect synchronization with the desired spreading code is assumed. Although no carrier offset is assumed, the results are not expected to vary much in the presence of moderate frequency offsets on the signals.

The algorithms operate in the decision-directed mode after they are allowed to converge. The decision-directed algorithm performs poorly in closed-eye situations, such as when the signal undergoes a deep fade or when there is extremely strong interference, which sometimes leads to a loss of convergence of the algorithm resulting in divergence, i.e., the algorithm fails catastrophically, or captures another signal. The latter happens when the algorithm converges to one of the many undesirable local minima of the cost function. In such situations, the BER rises to 0.5. While it is important to penalize the receiver for this failure of the algorithm in some way, there is no simple method to achieve this. Simply counting all the errors does not seem fair because loss of convergence is unpredictable and can happen anytime during a simulation run unless a method is developed to detect loss of convergence so retraining can be requested. The average BER is obtained over 90 trials in AWGN channel simulations and 900 trials in multipath fading channel simulations. To overcome the shortcoming of the decision-directed algorithm, only 1000 bits are used in each simulation trial, i.e., the filter is re-trained every 1000 bits. If the BER of the receiver exceeds 0.25 during the trial, the algorithm is regarded to have "failed" and the errors accumulated during the simulation trial are discarded. More bits are not used in each trial to reduce the probability of failure of the algorithms since the algorithms can be expected to "fail" more often with longer simulation trials.

9.7.1 Performance in an AWGN Channel

Case 1: Synchronous Forward Link

The forward link of CDMA system is considered first. The signals emanate from a common base station and are, therefore, chip and bit synchronous. Furthermore, all signals have equal power. However, differential detection is used at the receiver due to the absence of carrier recovery. The step-size for the sign algorithm is chosen to be $\mu_S = 10^{-13}$. The step-sizes for the LMS and the SR algorithms are experimentally chosen so that all three algorithms yield almost the same BER with seven users at $E_b/N_0 = 9$ dB. Simulations are carried out to determine the variation of the BER with increasing number of users in the system for SNRs of 9 and 10 dB.

The simulation results are depicted in Figure 9.8. The performances of the three algorithms are very similar but not exactly the same. At lower MAI levels, the SR algorithm performs slightly worse than the other two algorithms. It can be expected that the steady-state MSEs exhibit a similar relationship. At lower interference levels, the input signal standard deviation σ_x is lower than with seven users. Equation (1.56) suggests that a lower step-size has to be used for the SR algorithm to obtain the same steady-state MSE as with the LMS algorithm. On the other hand, the performance of the sign algorithm is not significantly different from that of the LMS algorithm. This can be attributed to the small adjustment to the step-size μ_S of the sign algorithm required to obtain the same MSE as with the LMS algorithm. We note that at $E_b/N_0 = 9$ dB, $\sqrt{\epsilon_{\min}} = 0.2294$ with a single user, $\sqrt{\epsilon_{\min}} = 0.2335$ with seven users, and $\sqrt{\epsilon_{\min}} = 0.2766$ with fifteen users ($\sqrt{\epsilon_{\min}}$ is the only factor in Equation (1.41) that changes with number of users). In contrast, the corresponding values of σ_x are 1.6995, 2.9813, and 4.1095, respectively, which are significantly different from each other. Therefore, the actual step-sizes differ from those required to obtain the same MSE performance with the LMS and the SR algorithms and this is reflected in the BER performance as well. Another interpretation of these results is that among the three algorithms, the LMS algorithm is most sensitive to an increase in MAI in terms of BER performance while the sign algorithm is least sensitive. This is perhaps because the excess MSE of the sign algorithm depends on $\sqrt{\epsilon_{\min}}$ whereas the excess MSE of each of the other two algorithms depends on $\epsilon_{\min}$.

Case 2: Asynchronous Reverse Link

For the reverse link of the CDMA system, the signals are assumed to be transmitted asynchronously, with each user having a randomly generated phase and delay. However, power control is assumed. The same step-sizes as in Case 1 are used here since computation of step-sizes for identical steady-state MSEs is difficult in this case. Furthermore, it is interesting to evaluate the impact of an asynchronous link on the algorithms optimized for the forward link.

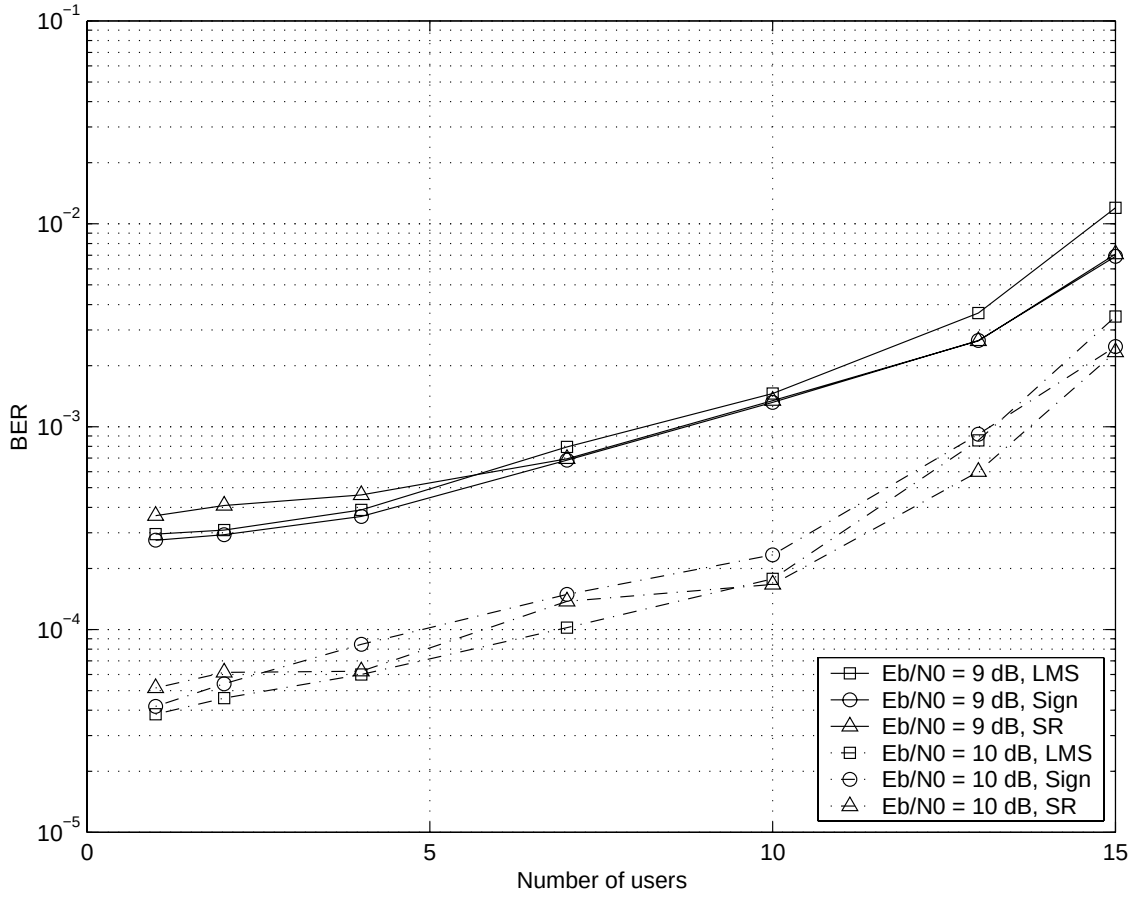

Figure 9.8: BER performance of the LMS Algorithm, Sign Algorithm, and SR Algorithm on the Forward Link of an AWGN Channel.

Figure 9.9 illustrates the simulation results for the case of perfect power control, where all users have equal power. One observation of the reverse link is that the convergence times for the algorithms are higher because of the increase in effective number of users increases the eigenvalue spread[2]. This also affects the BER performance, as the plots indicate. However, it is evident from the figure that the performance of all the algorithms is interference limited with ten or more users. The BERs are indistinguishable for small to moderate user loads. For large user loads, however, the LMS algorithm tends to perform poorly. The step-size (and consequently, the gradient noise) turns out to be very large in these situations and the algorithm often fails in the decision-directed mode. Some normalization of the input signal would help. The SR algorithm performs better because the input signal vector is clipped, so its power is constrained. Differences in the excess MSEs of the sign and SR algorithms, while expected even at such high loads, are small compared with the MMSE achievable with an optimum filter and hence do not cause significant differences in performance. A notable result is that the algorithms perform very similarly over most of the range of system loads.

Figure 9.10 shows the performance of the three algorithms under the conditions of "tight" power control. Here we assume that the (time-invariant) powers of the users are lognormally distributed with a mean of zero and a standard deviation of $\sqrt{2}$ dB. The performance in this case is almost identical to the case of perfect power control. The performance of the algorithms under the conditions of "loose" power control, where the standard deviation of the powers of the users is $\sqrt{20}$ dB, is depicted in Figure 9.11. The plots show that there is very little degradation due to loose power control. Due to the use of fixed step-sizes and the lack of any normalization, the algorithms tend to experience catastrophic failure sometimes in the decision-directed mode, with the failure rate being higher for larger user loads. The results of such "failed" trials are discarded. Thus, the sign algorithm and the SR algorithm also preserve the near-far resistant property of the MMSE receiver.

9.7.2 Performance in Multipath Fading Channels

Section 9.7.1 demonstrated the performance of the reduced complexity algorithms in stationary AWGN channels. We now consider their performance in time-varying multipath fading channels. In stationary channels, initial convergence time of the algorithms is the only concern. As seen in Section 9.6, there is not a significant difference between the convergence times of the reduced complexity algorithms and the LMS algorithm when the filter weights are initialized to the matched filter coefficients. The convergence time is on the order of a several tens of iterations for moderate system loads. However, the tracking ability of algorithms, another attribute, is important when the algorithms are

[2]Each asynchronous MAI signal appears on an average as two synchronous MAI signals with half the power.

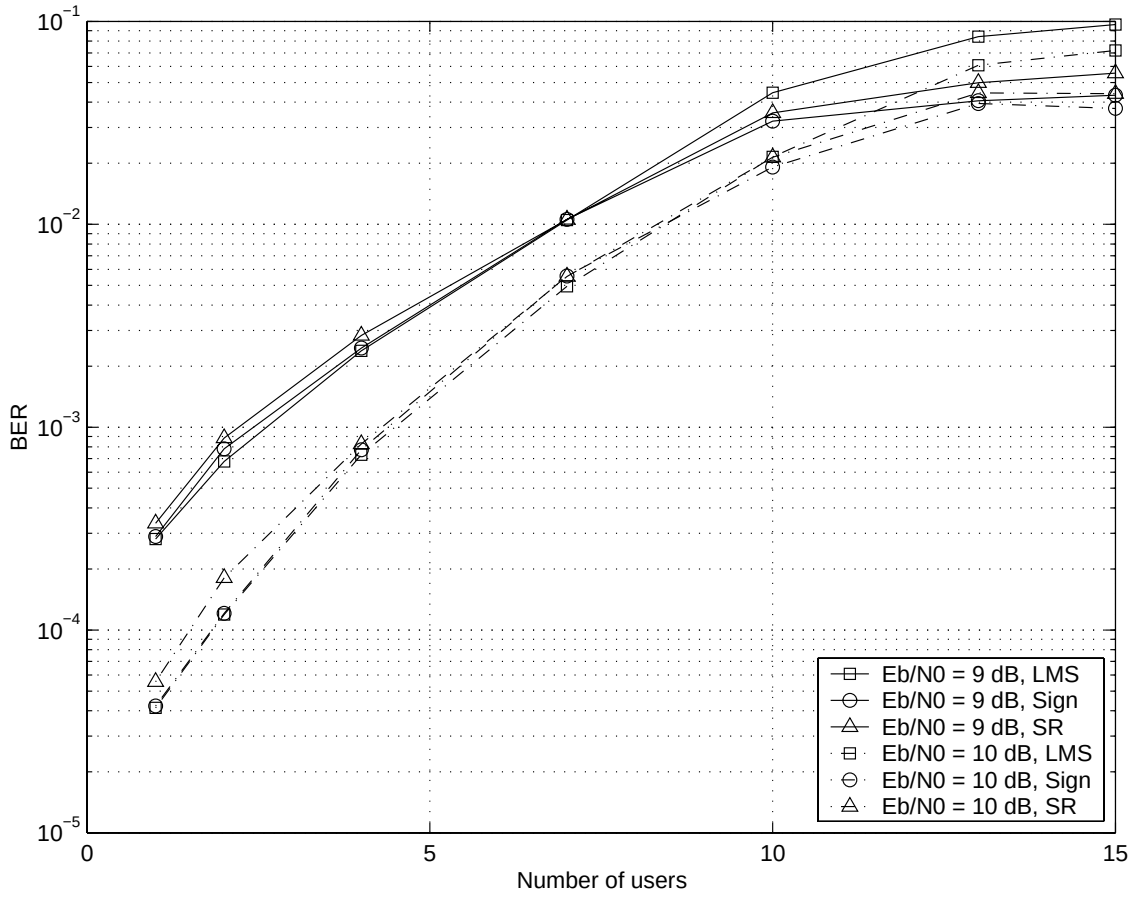

Figure 9.9: BER performance of the LMS Algorithm, Sign Algorithm, and SR Algorithm on the Reverse Link (with Perfect Power Control) of an AWGN Channel.

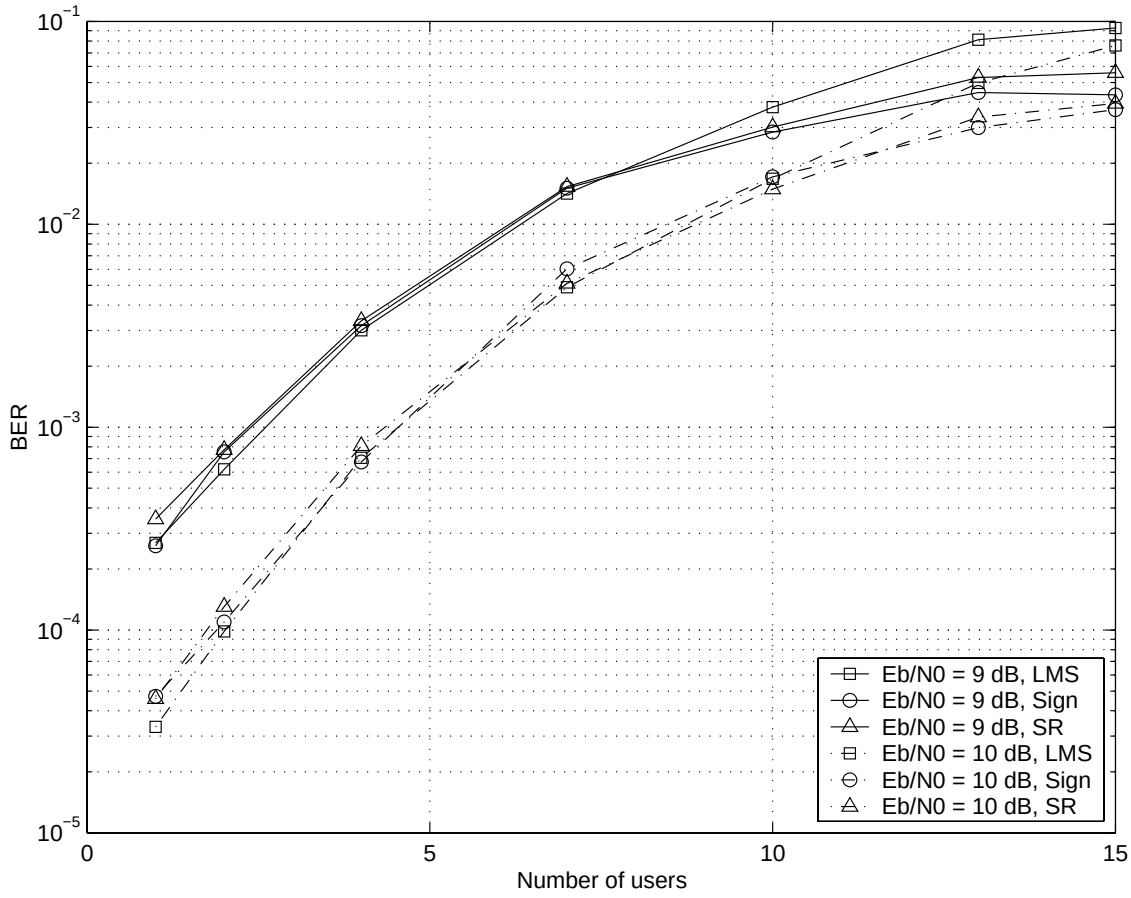

Figure 9.10: BER performance of the LMS Algorithm, Sign Algorithm, and SR Algorithm on the Reverse Link (with "Tight" Power Control) of an AWGN Channel.

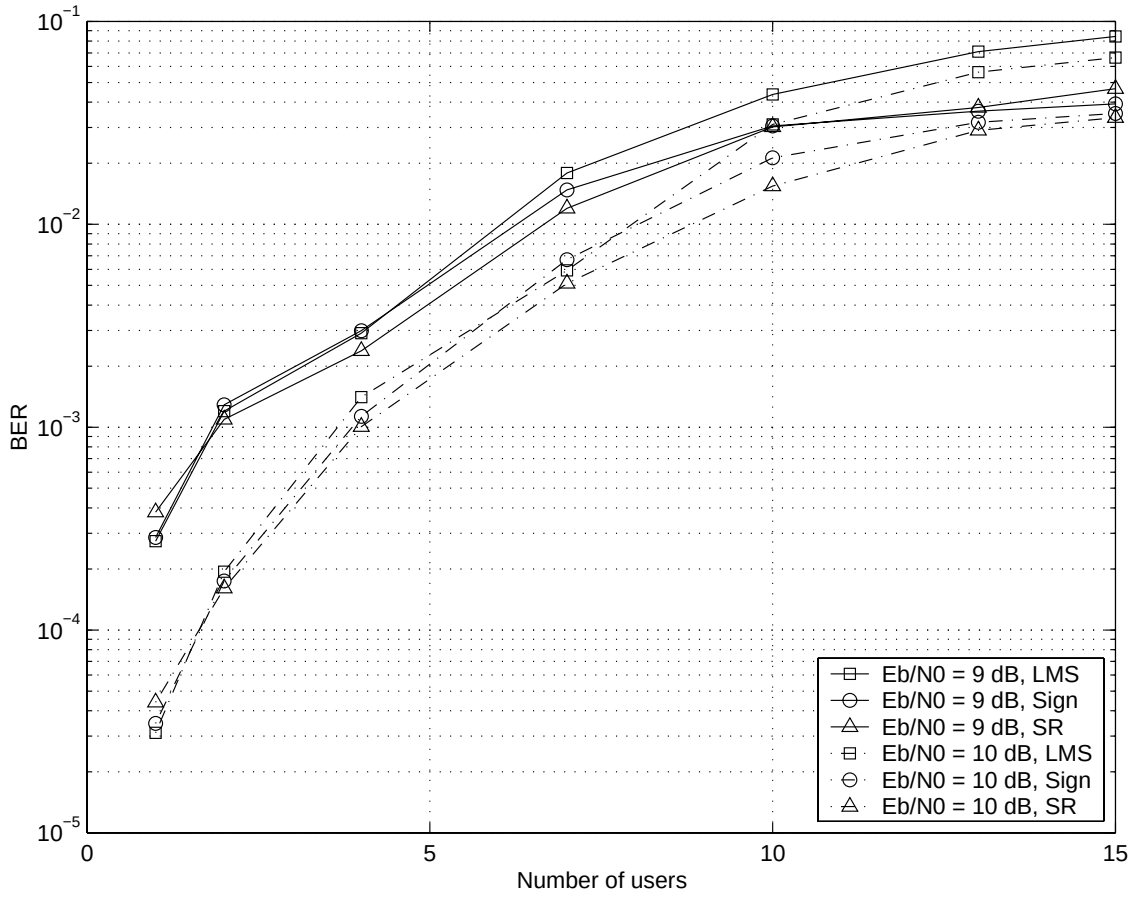

Figure 9.11: BER performance of the LMS Algorithm, Sign Algorithm, and SR Algorithm on the Reverse Link (with "Loose" Power Control) of an AWGN Channel.

Table 9.4: Simulations Parameters.

Carrier frequency	2.050 GHz
Data rate	128 kbps
Chip rate	1.92 Mcps
Sample rate	3.84 Mcps
Vehicular speed	45 km/h
E_b/N_0	25 dB

Table 9.5: Multipath Channel Models Used for Simulations.

Channel Model	**Multipath Delay** (μs)	**Multipath Amplitude**	**Type of Fading**
Two-Ray Rayleigh	0.0	1	Rayleigh
	5.0	0.5	Rayleigh
COST-207 Rural	0.0	1.0	Ricean
	0.2	0.7937	Rayleigh
	0.4	0.3162	Rayleigh
	0.6	0.1	Rayleigh

used in time-varying channels. The tracking ability of the reduced complexity algorithms is reflected in their BER performances in fading channels. The simulation parameters are summarized in Table 9.4.

Performance of the algorithms is considered for the two multipath channel models shown in Table 9.5. A two-ray Rayleigh fading model and the COST-207 Rural channel model [97] are used. Simulation results show that the algorithms fail at a very high rate in the COST-207 Urban channel, so it is not presented here. The channel models selected represent two different scenarios. In the first model, the two multipath components have a large separation, about 10 chip periods. In the second model, the four multipath components are spread over a single chip period. It is interesting to evaluate the extent to which multipath affects the performance of the algorithms in these diverse situations. In each case, the SNR (E_b/N_0) is measured with respect to the first multipath component. Therefore, superior performance is expected at low interference levels when the improvement in SNR due to greater multipath offsets the decrease in the signal-to-interference ratio due to the associated interference (cf. Chapter 6). For the reverse link simulations, it is assumed that the vehicle speeds of all mobile units are 45 km/h. Apart from using the same average power for all signals, no other form of power control is used and each signal propagates through an independently fading channel.

Case 1: Performance in a Synchronous, Two-Ray Rayleigh Fading Channel

The variation of the BER with an increasing number of interferers is plotted in Figure 9.12. The performances of the three algorithms differ slightly in this channel. The sign algorithm exhibits the poorest performance among the three algorithms throughout the range of system loads. The inferior performance stems from the poor tradeoff between tracking ability and gradient noise when the step-size is altered. As seen in Section 9.4, the residual weight error vector after convergence is strongly dependent on the step-size because of the quantization of the error. Therefore, increasing the step-size to improve the tracking ability can have a detrimental effect on the excess MSE, especially during deep fades when the SNR falls to small magnitudes. On the other hand, decreasing the step-size to reduce the gradient noise during fades (gradient noise is not significant otherwise) degrades the algorithm's ability to track the time-varying channel. Other algorithms are better able to tradeoff tracking ability with steady-state MSE. The LMS algorithm and the SR algorithm are thus able to perform better than the sign algorithm, as the BER curves of Figure 9.12 demonstrate. However, the slightly better performance of the SR algorithm compared with the LMS algorithm at low MAI levels is a result of not using the optimum step-size for the LMS algorithm. That is, the performance of the LMS algorithm can be expected to match the performance of the SR algorithm with a more appropriate step-size that would provide a better tradeoff between tracking ability and excess MSE, yielding a better BER performance. Experiments show that the performance of the sign algorithm cannot be improved much more by choosing a more "optimum" step-size, whereas the performance of the LMS and the SR algorithms can be improved slightly in low interference situations.

The impact of employing decision-direction in closed-eye situations, i.e., when the decisions are not correct with a high probability, is important in assessing the performance of the reduced complexity algorithms. While the behavior of the LMS algorithm has been characterized, the behavior of the other two algorithms is not well known. Whether the performance of the reduced complexity algorithms is degraded more or less than that of the LMS algorithm, it is clear that the overall BER is strongly influenced by the algorithms' reaction to a closed eye, since most of the bit errors occur during this time.

Case 2: Performance in a Synchronous Rural Channel

Figure 9.13 shows the plot of BER versus number of users for this case. Recall that multipath is more severe in this scenario, which helps improve the available SNR. All the multipath components arrive within a delay of one chip period so self-interference from adjacent symbols is much less. However, there is increased interference due to multipath signals of other users. The powers of the three delayed components are -2 dB, -10 dB, and -20 dB down, respectively, from the first component. The overall effect on the performance is seen in the figure. All three algorithms yield lower BERs than in Case 1,

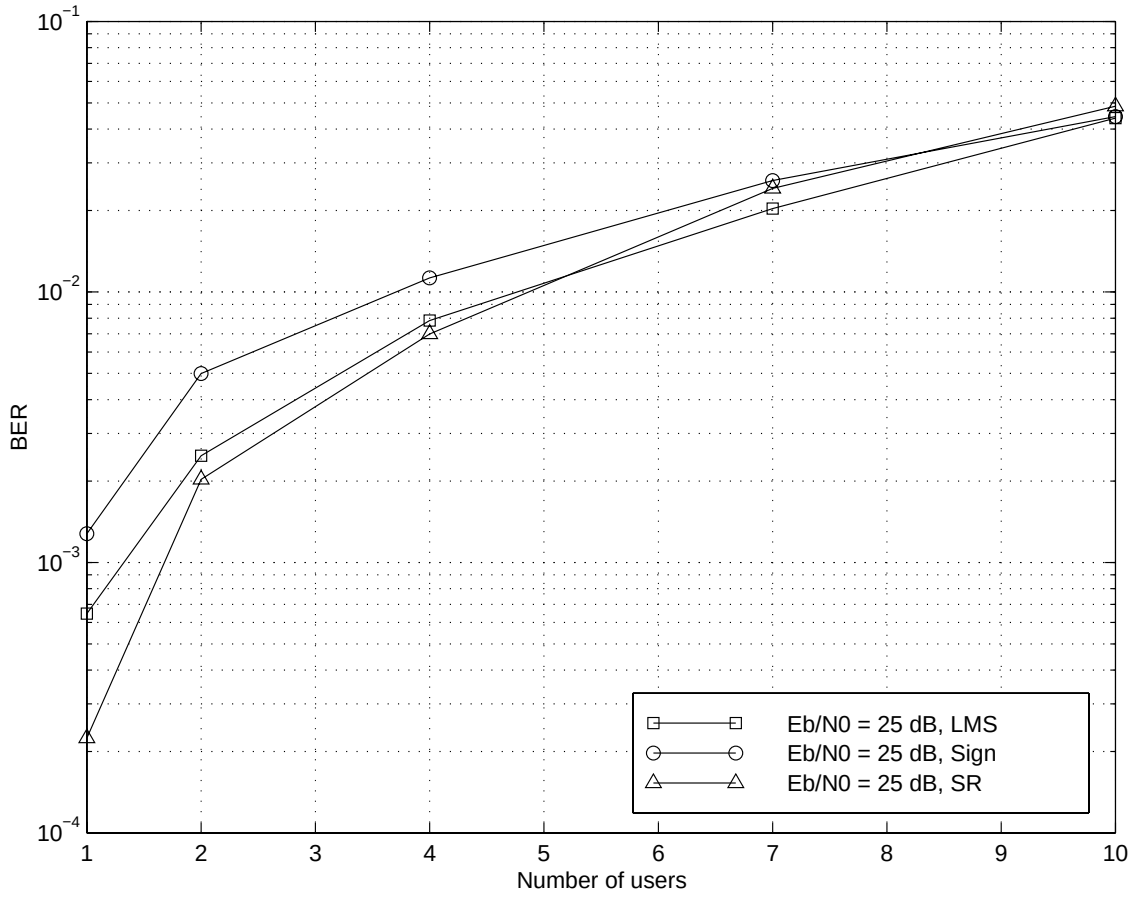

Figure 9.12: BER performance of the LMS Algorithm, Sign Algorithm, and SR Algorithm on the Forward Link of a Two-Ray Rayleigh Fading Channel.

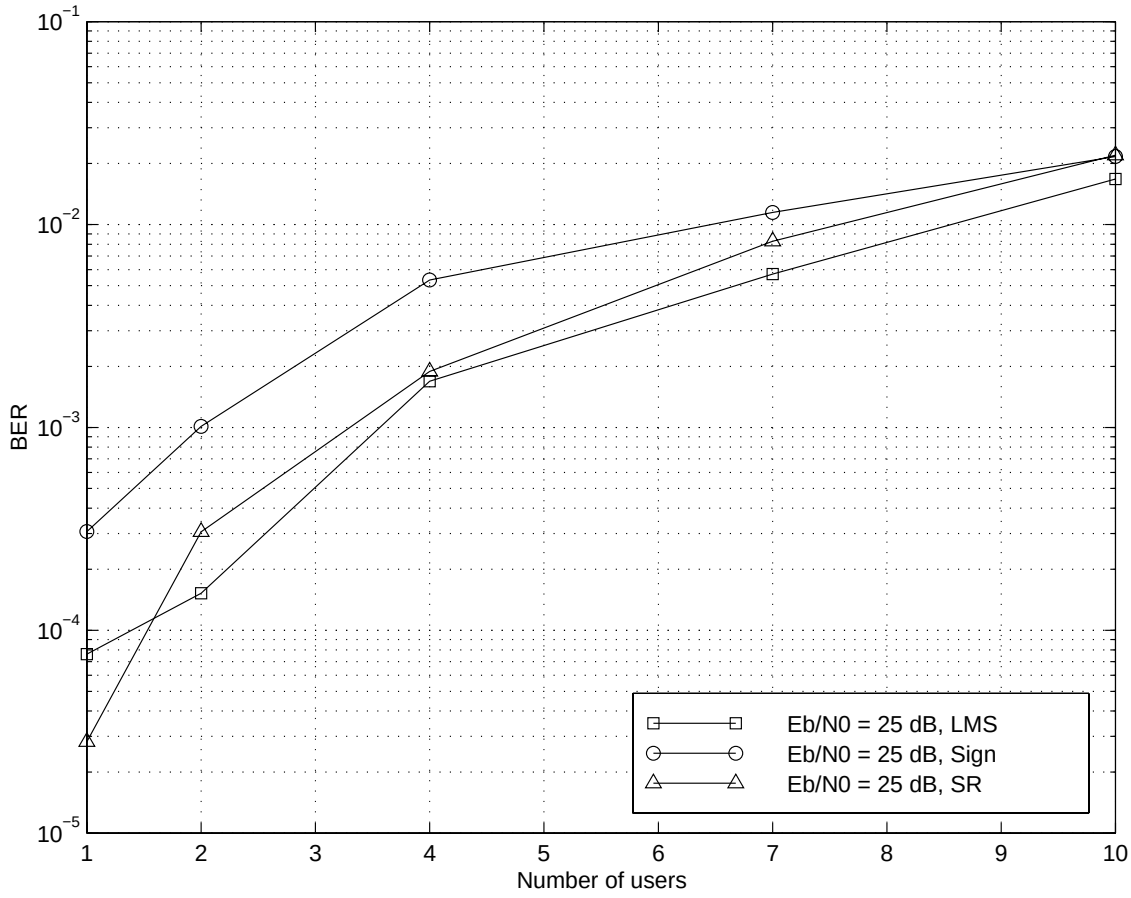

Figure 9.13: BER performance of the LMS Algorithm, Sign Algorithm, and SR Algorithm on the Forward Link of a COST-207 Rural Channel.

with the improvement being higher at lower MAI levels. The performance improvement of the sign algorithm, however, is less than that of the other two algorithms, which may again be attributed to a poor tradeoff between tracking ability and gradient noise. Except for the single-user case, the LMS algorithm outdoes the SR algorithm. When there is no MAI, the gradient noise is greater for the LMS algorithm than for the SR algorithm, resulting in better BER performance for the SR algorithm. Interference is higher for all other cases, making the chosen step-size more optimum. As reported in Case 1, the sign algorithm cannot perform much better, whereas the other two algorithms can yield slightly lower BERs when more "optimum" step-sizes are used in obtaining each point on the curves.

Case 3: Performance in an Asynchronous, Two-Ray Rayleigh Fading Channel

The simulation results in this case are illustrated in Figure 9.14. Both the sign algorithm and the SR algorithm perform slightly worse than the LMS algorithm. Except for the single-user case, both reduced complexity algorithms yield similar BERs over the entire range. The more dynamic nature of the reverse link compared with the forward link degrades the performance of all three algorithms. Despite the near-far resistance of the receiver, the algorithms are not sufficiently able to track the time-varying channel. Since signal powers vary over time, the SNR and the signal-to-interference ratios change, which changes the optimum solution. This is further aggravated by poor performance with decision-direction in closed-eye situations. The LMS algorithm is best able to track the channel while limiting the steady-state MSE, thus exhibiting a superior performance. Due to the lack of much multipath diversity in this channel, the time-varying nature of the channel has a significant negative impact on all three algorithms.

Case 4: Performance in an Asynchronous Rural Channel

The plots of Figure 9.15 demonstrate the performance of the three algorithms in this environment. Again, there is not a significant difference between the performances of the three algorithms. The LMS algorithm is slightly better than the SR algorithm, which in turn yields a small improvement over the sign algorithm. All three algorithms exploit multipath diversity to give lower BERs compared with the two-ray Rayleigh fading channel. The BER curves also demonstrate how the algorithms compare with regard to trading excess MSE with tracking ability in a very dynamic radio channel. Observations have shown that the other step-sizes do not alter the BER results significantly and the relative positions of the curves indicate what is achievable with the three algorithms.

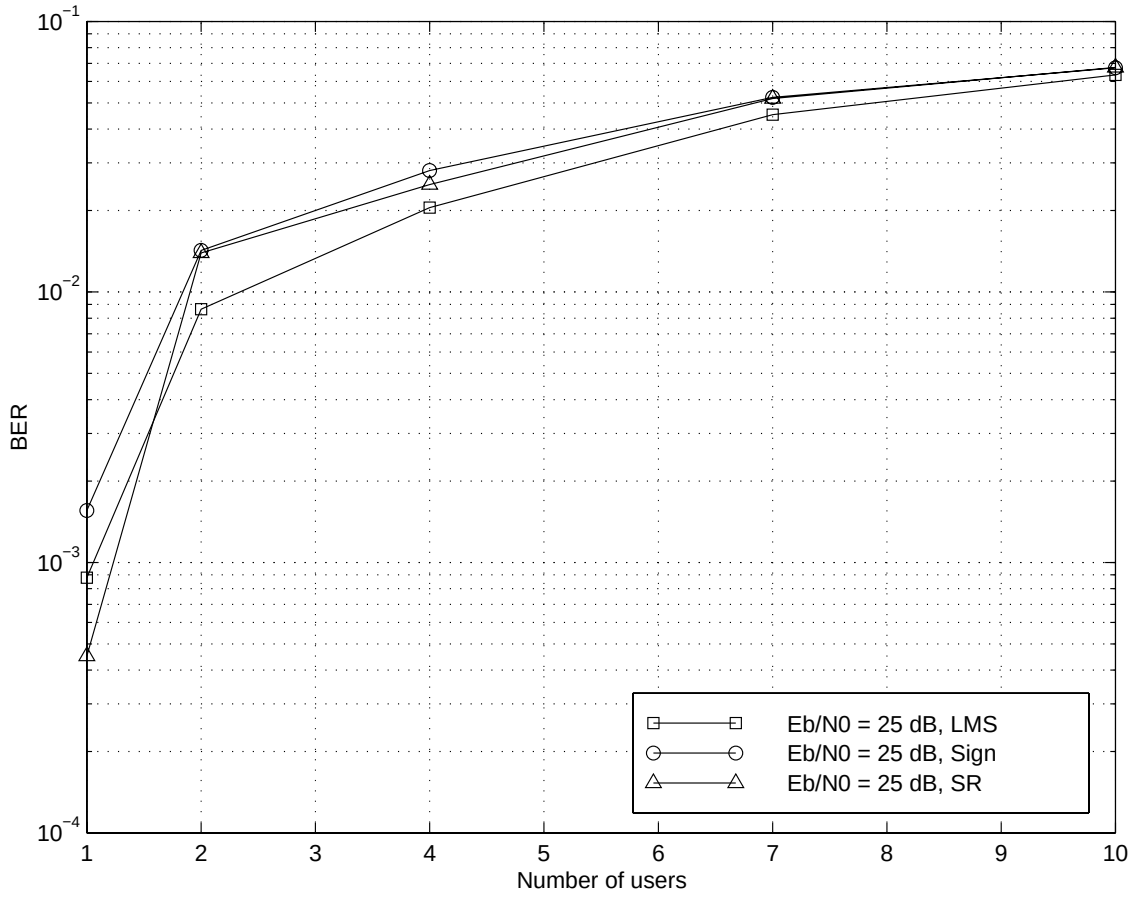

Figure 9.14: BER performance of the LMS Algorithm, Sign Algorithm, and SR Algorithm on the Reverse Link of a Two-Ray Rayleigh Fading Channel.

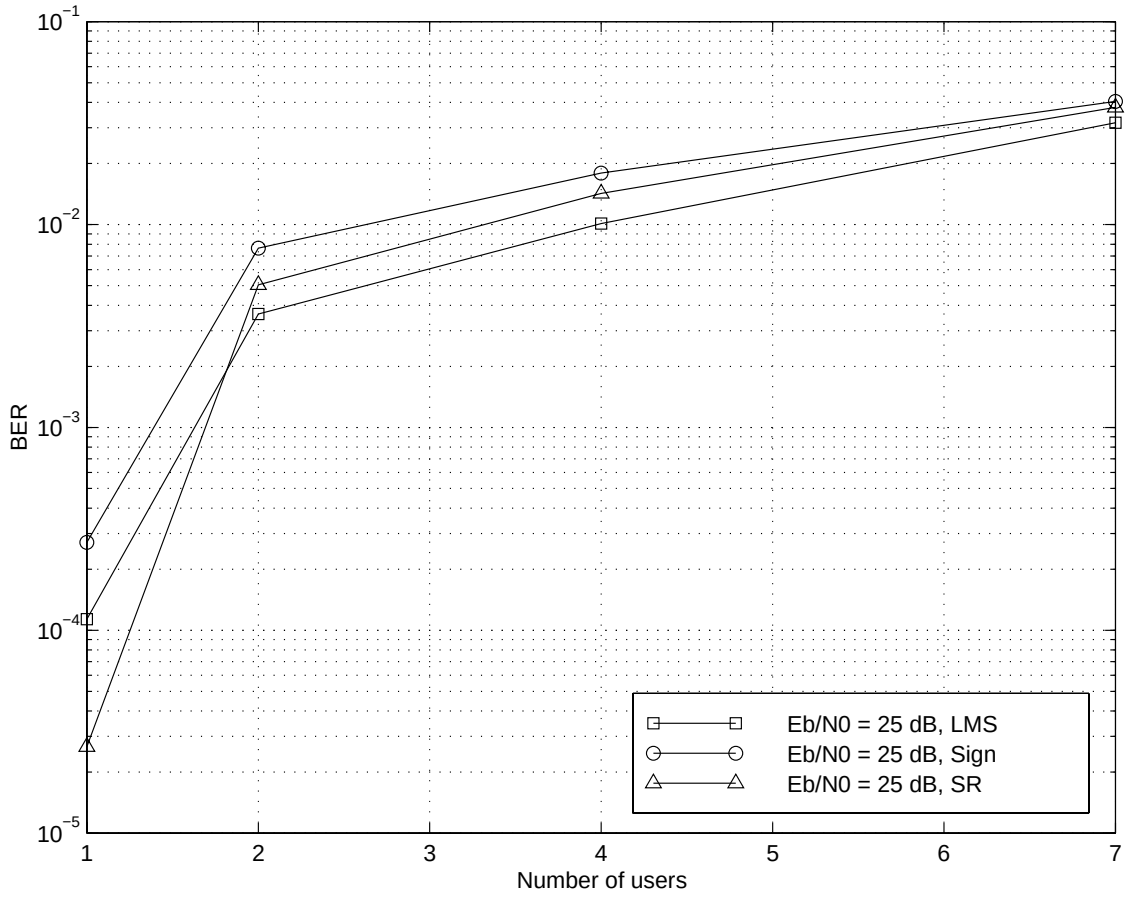

Figure 9.15: BER performance of the LMS Algorithm, Sign Algorithm, and SR Algorithm on the Reverse Link of a COST-207 Rural Channel.

9.8 Summary

The complex LMS algorithm is simple and effective in adaptively implementing the MMSE criterion. However, the weight update equation accounts for approximately as much computational complexity as the linear FIR filtering operation. Exploiting the need for only the real part of the filter output for BPSK modulation reduces the computational complexity. This complexity reduction disappears, however, in the differentially coherent implementation. As alternatives, the sign algorithm and the signed regressor algorithm can eliminate the need for multiplication in the real versions of the adaptation algorithms. Convergence of the two reduced complexity algorithms are discussed in Appendix A using Gaussian assumptions on the input and reference signals. A geometric interpretation of the convergence of the weight error vector was described. The relationship between the step-sizes of each of the reduced complexity algorithms and the LMS algorithm for achieving the same steady-state MSE under these assumptions was presented. Complex versions of the reduced complexity algorithms for a differentially coherent receiver were proposed. Convergence curves were presented to show that these reduced complexity algorithms converge more slowly than the LMS algorithm. Simulation results were presented to demonstrate the BER performances of the two reduced complexity algorithms and the LMS algorithm when the step-sizes are fixed. In AWGN channels, the reduced complexity algorithms are able to match the performance of the LMS algorithm. The LMS algorithm is slightly more susceptible to gradient noise at higher levels of interference. In fading channels, the sign algorithm experiences degradation due to its poor tradeoff between tracking ability and steady-state MSE. The signed regressor algorithm is superior to the sign algorithm and is often only slightly worse than the LMS algorithm. The investigation in this chapter reveals that when reduction of computational complexity is necessary, the reduced complexity algorithms, especially the promising signed regressor algorithm, can be employed at the cost of a small degradation in receiver performance, which is especially important for field-programmable gate array (FPGA) implementation.

Chapter 10

Conclusions and Future Work

10.1 Conclusions

The work reported herein was undertaken in an effort to move from current knowledge of adaptive CDMA receivers towards making them applicable in practical wireless systems. The objectives were to develop novel techniques and analyze existing techniques in the area of adaptive CDMA receivers. While the new techniques presented serve to overcome some of the drawbacks in the current application of adaptive receivers, the theoretical analyses assist in better understanding the influence of the radio environment on the performance of adaptive receivers. Third-generation systems are making provisions for the incorporation of interference cancellation schemes in future CDMA receivers. As this advanced technology becomes feasible, it is important to minimize its weaknesses before being implemented. The research reported here aids in moving adaptive receivers closer to implementation. Furthermore, third-generation systems call for the improvisation of receiver technology to make it suitable for the wide range of services being proposed for these systems. Some of the work presented here is a step in that direction. The following paragraphs outline the major conclusions drawn from this research.

The conventional matched filter or correlation receiver suffers severe degradation in the presence of strong multiple access interference. The matched filter is optimum when the additive noise is Gaussian but fails to exploit the structure in the MAI that causes the interference to be non-Gaussian. Over the past several years, a number of receivers have been studied for use in a CDMA system. Some of them are useful only when all signals are demodulated. Termed multi-user receivers, they are highly complex and sensitive to estimation of certain system parameters. Single user receivers, on the other hand, are characterized by lower complexity and have fewer system requirements. Hence, they are widely applicable. The classification of single user CDMA receivers was detailed in Chapter 2. Adaptive receivers form a large class in this context. Adaptive receiver

structures proposed in the literature were briefly introduced and their attributes were noted. A limitation of adaptive receivers is that they are feasible only for short code systems, since the complexity of the adaptive receiver increases linearly with the number of adaptive filter weights and hence the length of the spreading code.

Cyclostationarity forms the basis of CDMA interference rejection. An adaptive receiver exploits the cyclostationary property of not only the signal of interest, but also that of the interference signals, effectively mitigating interference. To underline the importance of this property and to gain insight into the cyclostationary property of spread spectrum signals, Chapter 3 outlined the basic principles of cyclostationarity. The attributes of cyclostationarity were explained as were some applications that exploit this property of signals. Spectral correlation of DS/SS signals was addressed. The well known result that the optimum receiver is a single filter when all of the users have the same code lengths was demonstrated.

The adaptation algorithm forms the key computational aspect of the adaptive filter. An enormous body of literature exists on this topic. A small subset of these algorithms have been popular in CDMA receiver applications due to their relative simplicity and proven attributes. The LMS algorithm has long been used in adaptive equalization and continues to be common among adaptive CDMA receiver proponents. This, and other other blind adaptation algorithms were outlined in Chapter 4.

The LCCMA is a blind algorithm, originally purported for adaptive arrays, that was proposed for CDMA systems when the analogy between the two applications was recognized. It attempts to restore the constant modulus property of the desired signal that has been destroyed by interference, and, in doing so, mitigates the interference. A linear constraint is used to ensure that the desired signal is captured rather than one of the MAI signals, which have constant moduli as well. As the analysis of the stationary points of the LCCM cost function in Chapter 5 revealed, the algorithm treats multipath of the signal of interest as interference and, hence, tries to suppress it rather than exploit it as a form of diversity. This has detrimental results in fading channels. The MLCCMA proposed in the chapter was designed to overcome this weakness of LCCMA by using multiple constraints that help to capture the energy in the multipath components, whose delay is assumed to be known and whose effective combination boosts the performance of the receiver. Simulation results for different frequency-selective fading channels were provided to demonstrate the merits of the algorithm.

The use of a complex fractionally spaced FIR filter for CDMA interference rejection has been thoroughly investigated in the literature. The analytical results presented in Chapter 6 complement existing knowledge of the performance of an adaptive receiver. The MMSE obtained with the optimum solution was expressed as a function of cross-correlation between the spreading codes of the various users in the system, their interference-to-signal power ratios, and the SNR of the signal of interest. The analysis for static multipath channels further revealed the impact of multipath on the MMSE.

The near-far resilience of MMSE receivers was demonstrated analytically through a new approach after making some simple assumptions. An equivalent analysis was provided for the matched filter receiver to demonstrate its poor near-far resilience.

When the spreading codes of different users in a CDMA system are of unequal length, the single filter receiver ceases to be the optimum receiver structure. Chapter 7 derived the optimum receiver structure consisting of a bank of filters for this case. The decision statistic for a sequence of symbols is obtained by cycling through the outputs of these filters. It was shown that the number of filters in the filter bank is equal to the ratio of the least common multiple of the code lengths to the code length of the signal of interest. Expressions for the MSE of a filter bank receiver and the MSE of a single filter receiver were derived and compared. A numerical example was provided to illustrate the superiority of the filter bank receiver in a multi-rate system. Simulation results were furnished to demonstrate the superior BER performance of the filter bank receiver when compared with a matched filter receiver and a single filter receiver. Application of the filter bank receiver was demonstrated when MAI signals have different code lengths as well as when they have different chip rates. Gains of about 2 to 3 dB were demonstrated. The adaptive filter bank receiver is susceptible to channel variations in multipath fading channels. Although not very effective in rapidly time-varying channels, it maintains a strong superiority over the single adaptive filter receiver in slowly varying channels.

When a coherent carrier reference is unavailable to a receiver through a pilot channel, the receiver must either generate its own reference or compensate for frequency offsets resulting from imperfect local oscillators. Chapter 8 reviewed some of the offset compensation techniques used in practice. The application of these techniques in matched filter receivers and adaptive receivers used in CDMA systems was discussed. It was shown that the optimum solution in the presence of frequency offsets is a rotating vector with the rate depending on the frequency offset on the desired signal. Mean-square error analysis of the coherent adaptive receiver employing the LMS algorithm provided a measure of the degradation of the adaptive receiver due to a frequency offset. It was explained that incorporation of differential detection into adaptive filtering permits the elimination of a separate carrier offset compensation scheme. This is distinct from implementing differential detection independent of the adaptive filtering, in which case the adaptive filter performance can be severely degraded. It was demonstrated that adaptive differentially coherent receiver yields good results, questioning the use of separate offset compensation schemes in adaptive receivers whose complexity cannot be justified.

Reduced complexity adaptation algorithms used for echo-cancellation generate interest because of their simplicity. In Chapter 9, the application of the sign algorithm and the signed regressor algorithm for adaptive CDMA receivers was investigated. Complex versions of the algorithms were proposed for a differentially coherent adaptive receiver. Multiplication operations during weight update are almost completely eliminated with the reduced complexity algorithms. It was seen that when the filter weights are initialized to the matched filter coefficients, the slower convergence of the reduced complexity

algorithms is not a serious issue. BER results showed that the reduced complexity algorithms match the performance of the LMS algorithm in AWGN channels. In multipath fading channels, however, the sign algorithm is not as effective as the LMS algorithm because of the poor tradeoff between the algorithm's tracking ability and gradient noise when the step-size is changed. On the other hand, the BER performance of the signed regressor algorithm is only slightly inferior to that of the LMS algorithm. Therefore, the signed regressor algorithm should be considered for implementation in adaptive CDMA receivers.

10.2 Recommendations for Future Work

Chapter 7 discussed the applicability of adaptive filter bank receivers in third-generation multi-rate CDMA systems. However, the true worth of these receivers can be evaluated by simulating the performance with a complete model of the personal communications system. Capacity gains yielded by the proposed receiver can then be better estimated. Furthermore, given the great diversity of third-generation systems, a large number of cases must be investigated. The limitations of the approach must be identified and explored.

The MLCCMA proposed in Chapter 5 is effective in exploiting multipath diversity. However, its relatively high computational complexity precludes the use of the algorithm in filter bank receivers. As Chapter 7 revealed, there is a need for a robust but simple algorithm that can overcome the drawbacks of the decision-directed algorithm. Future research can explore this topic.

The drawback of using the adaptive filter bank receiver in dynamically varying channels was discussed in Chapter 7. The limitation arises from adapting only the currently used weight vector every symbol, i.e., once every L symbols in an L-filter receiver. An interesting problem is to develop a new technique for reducing the lag in the weight vectors not being updated. Rapidly converging algorithms can be explored in this regard. It is also challenging to develop a technique that can separate the channel tracking from the interference rejection. Such a technique may be able to overcome the limitations of filter bank receivers.

Since FPGAs and fixed-point DSPs are likely to be used for future implementations of adaptive receivers, it is necessary to evaluate the performance of fixed-point implementations of adaptation algorithms for CDMA interference rejection. The investigation will reveal any limitations of such implementations.

In Chapter 9 of [117], a parallel interference cancellation receiver combined with an adaptive receiver was suggested for reducing the complexity of a multi-stage Rake receiver. The adaptive receiver following a single stage of interference cancellation is expected to suppress the interference that was not cancelled, while combining multipath like a Rake

receiver. The proposed receiver architecture requires extensive analysis and evaluation.

Advanced technologies, such as adaptive arrays, interference cancellation with multi-stage receivers, and adaptive single user receivers have been separately investigated in the past for evaluating their ability to enhance system capacity. Analogies between systems must be recognized to broaden the scope of newly developed techniques. Furthermore, there is a need for developing synergetic approaches that exploit the strengths of each technology.

Appendix A

Convergence of Sign and SR Algorithms

A.1 Convergence of the Sign Algorithm

References [111] and [118] provide detailed convergence analyses for the sign algorithm. In the following analysis, which we draw from [118], it is assumed that the input and reference signals are zero-mean Gaussian signals. Although this is generally not true for the signals considered in this research, this assumption simplifies the analysis. To study the convergence of the weight error vector, we take the expected value of both sides of Equation (9.14), as seen below.

$$E\left[\mathbf{v}(k+1)\right] = E\left[\mathbf{v}(k)\right] + \mu\, E\left[\mathrm{sgn}\{e(k)\}\,\mathbf{x}(k)\right]. \tag{1.1}$$

We note that

$$\begin{aligned} E\left[\mathrm{sgn}\{e(k)\}\,\mathbf{x}(k)\right] &= P(e(k)>0)\,E\left[\mathbf{x}(k)\,|\,e(k)>0\right] \\ &\quad - P(e(k)<0)\,E\left[\mathbf{x}(k)\,|\,e(k)<0\right] \end{aligned} \tag{1.2}$$

where $P(\cdot)$ denotes probability. The second expectation on the right hand side of Equation (1.2) may be expressed as

$$E\left[\mathbf{x}(k)\,|\,e(k)<0\right] = \int_{-\infty}^{\infty} \mathbf{x}(k)\, f_{\mathbf{x}}(\mathbf{x}(k)\,|\,e(k)<0)\, d\mathbf{x}(k) \tag{1.3}$$

where $f_{\mathbf{x}}(\mathbf{x} \,|\, e(k) < 0)$ is a conditional probability density function, which is related to the joint density function $f_{\mathbf{x}}(\mathbf{x}, e(k) < 0)$ by

$$\begin{aligned} f_{\mathbf{x}}(\mathbf{x}(k) \,|\, e(k) < 0) &= \frac{f_{\mathbf{x}}(\mathbf{x}(k)p, e(k) < 0)}{P(e(k) < 0)} \\ &= \frac{1}{P(e(k) < 0)} \int_{-\infty}^{0} f_{\mathbf{x}}(\mathbf{x}(k), e(k))\, de(k) \\ &= \frac{1}{P(e(k) < 0)} \int_{-\infty}^{0} f_{\mathbf{x}}(\mathbf{x}(k) \,|\, e(k))\, f_e(e(k))\, de(k). \end{aligned} \tag{1.4}$$

Substituting Equation (1.4) in Equation (1.3) we get

$$\begin{aligned} E\left[\mathbf{x}(k) \,|\, e(k) < 0\right] &= \int_{-\infty}^{\infty} \mathbf{x}(k)\, \frac{1}{P(e(k) < 0)} \\ &\qquad \cdot \int_{-\infty}^{0} f_{\mathbf{x}}(\mathbf{x}(k) \,|\, e(k))\, f_e(e(k))\, de(k)\, d\mathbf{x}(k) \\ &= \frac{1}{P(e(k) < 0)} \int_{-\infty}^{0} \int_{-\infty}^{\infty} \mathbf{x}(k)\, f_{\mathbf{x}}(\mathbf{x}(k) \,|\, e(k))\, d\mathbf{x}(k) \\ &\qquad \cdot f_e(e(k))\, de(k) \\ &= \frac{1}{P(e(k) < 0)} \int_{-\infty}^{0} E\left[\mathbf{x}(k) \,|\, e(k)\right]\, f_e(e(k))\, de(k). \end{aligned} \tag{1.5}$$

To evaluate the conditional expectation inside the integral, we use the Gauss-Markov theorem [98] given below.

Gauss-Markov Theorem Let $\mathbf{z}$ and $\mathbf{y}$ be random vectors that are distributed according to the multivariate distribution

$$\begin{bmatrix} \mathbf{z} \\ \mathbf{y} \end{bmatrix} = N \left[\begin{bmatrix} \mathbf{m}_z \\ \mathbf{m}_y \end{bmatrix}, \begin{bmatrix} \mathbf{R}_{zz} & \mathbf{R}_{zy} \\ \mathbf{R}_{yz} & \mathbf{R}_{yy} \end{bmatrix} \right]. \tag{1.6}$$

Then, the conditional distribution of $\mathbf{z}$, given $\mathbf{y}$, is multivariate normal with conditional mean $\hat{\mathbf{z}} = \mathbf{m}_z + \mathbf{R}_{zy}\, \mathbf{R}_{yy}^{-1}(\mathbf{y} - \mathbf{m}_y)$ and conditional covariance $\mathbf{P} = \mathbf{R}_{zz} - \mathbf{R}_{zy}\, \mathbf{R}_{yy}^{-1}\, \mathbf{R}_{yz}$:

$$\begin{aligned} \mathbf{z}|\mathbf{y} &: N[\hat{\mathbf{z}}, \mathbf{P}] \\ \hat{\mathbf{z}} &= \mathbf{m}_z + \mathbf{R}_{zy}\, \mathbf{R}_{yy}^{-1}(\mathbf{y} - \mathbf{m}_y) \\ \mathbf{P} &= \mathbf{R}_{zz} - \mathbf{R}_{zy}\, \mathbf{R}_{yy}^{-1}\, \mathbf{R}_{yz}. \end{aligned} \tag{1.7}$$

Then, from Equation (1.7), we get

$$E\left[\mathbf{x}(k)\,|\,e(k)\right] = \mathbf{m}_x(k) + \mathbf{r}_{xe}(k)\,r_{ee}^{-1}(k)\,(e(k) - m_e) \tag{1.8}$$

where

$$\begin{aligned}
\mathbf{m}_x(k) &\triangleq E\left[\mathbf{x}(k)\right], &(1.9)\\
\mathbf{r}_{xe}(k) &\triangleq E\left[(\mathbf{x}(k) - \mathbf{m}_x(k))\;(e(k) - m_e(k))\right], &(1.10)\\
m_e(k) &\triangleq E\left[e(k)\right], &(1.11)\\
r_{ee} &\triangleq E\left[(e(k) - m_e(k))\;(e(k) - m_e(k))\right]. &(1.12)
\end{aligned}$$

Based on the assumptions at the beginning of this section, we note that

$$\begin{aligned}
\mathbf{m}_x(k) &= \mathbf{0}, &(1.13)\\
m_e(k) &= 0, &(1.14)
\end{aligned}$$

and

$$\begin{aligned}
r_{ee} &= E\left[\Big(d(k) - \mathbf{w}^T(k)\,\mathbf{x}(k)\Big)\;\Big(d(k) - \mathbf{w}^T(k)\,\mathbf{x}(k)\Big)\right]\\
&\triangleq \sigma^2_{e|\mathbf{w}}(k) \approx \sigma^2_e(k). &(1.15)
\end{aligned}$$

The approximation is valid for small values of the step-size μ [118]. Furthermore,

$$\mathbf{r}_{xe}(k) = E\left[\mathbf{x}(k)\,(d(k) - \mathbf{w}^T(k)\,\mathbf{x}(k))\right] = \mathbf{p} - \mathbf{R}_{xx}\,E[\mathbf{w}(k)] \tag{1.16}$$

where

$$\mathbf{R}_{xx} \triangleq E\left[\mathbf{x}(k)\,\mathbf{x}^T(k)\right] \tag{1.17}$$

is the input correlation matrix and

$$\mathbf{p} \triangleq E\left[d(k)\,\mathbf{x}(k)\right] \tag{1.18}$$

is the crosscorrelation vector. Then Equation (1.8) becomes

$$E\left[\mathbf{x}(k)\,|\,e(k)\right] = \frac{\mathbf{p} - \mathbf{R}_{xx}\,E[\mathbf{w}(k)]}{\sigma^2_e(k)}\,e(k). \tag{1.19}$$

Substituting this expression in Equation (1.5), we get

$$E\left[\mathbf{x}(k)\,|\,e(k)<0\right] = \frac{\mathbf{p}-\mathbf{R}_{xx}\,E[\mathbf{w}(k)]}{\sigma_e^2(k)\,P(e(k)<0)}\int\limits_{-\infty}^{0} e(k)\,f_e(e(k))\,de(k) \tag{1.20}$$

where

$$f_e(e) = \frac{1}{\sqrt{2\,\pi}\,\sigma_e}\exp\left(-\frac{e^2}{2\,\sigma_e^2}\right). \tag{1.21}$$

Noting that

$$\begin{aligned}\int\limits_{-\infty}^{0} e\,\exp\left(-\frac{e^2}{2\,\sigma_e^2}\right)\,de &= \frac{1}{2}\int\limits_{-\infty}^{0}\exp\left(-\frac{e^2}{2\,\sigma_e^2}\right)\,2e\,de\\ &= -\frac{1}{2}\int\limits_{0}^{\infty}\exp\left(-\frac{z}{2\,\sigma_e^2}\right)\,dz\\ &= -\sigma_e^2,\end{aligned} \tag{1.22}$$

we get

$$\begin{aligned}E\left[\mathbf{x}(k)\,|\,e(k)<0\right] &= \frac{\mathbf{p}-\mathbf{R}_{xx}\,E[\mathbf{w}(k)]}{\sigma_e^2(k)\,P(e(k)<0)}\,\frac{1}{\sqrt{2\,\pi}\,\sigma_e(k)}\,\left(-\sigma_e^2(k)\right)\\ &= -\frac{\mathbf{p}-\mathbf{R}_{xx}\,E[\mathbf{w}(k)]}{P(e(k)<0)}\,\frac{1}{\sqrt{2\,\pi}\,\sigma_e(k)}\end{aligned} \tag{1.23}$$

so that

$$P(e(k)<0)\,E\left[\mathbf{x}(k)\,|\,e(k)<0\right] = -\frac{1}{\sqrt{2\,\pi}\,\sigma_e(k)}\,\left(\mathbf{p}-\mathbf{R}_{xx}\,E[\mathbf{w}(k)]\right). \tag{1.24}$$

In a similar manner, we can show that

$$P(e(k)>0)\,E\left[\mathbf{x}(k)\,|\,e(k)>0\right] = \frac{1}{\sqrt{2\,\pi}\,\sigma_e(k)}\,\left(\mathbf{p}-\mathbf{R}_{xx}\,E[\mathbf{w}(k)]\right). \tag{1.25}$$

Substituting these expressions in Equation (1.2), we get

$$\begin{aligned}E\left[\mathrm{sgn}\{e(k)\}\,\mathbf{x}(k)\right] &= \frac{1}{\sqrt{2\,\pi}\,\sigma_e(k)}\,\left(\mathbf{p}-\mathbf{R}_{xx}\,E[\mathbf{w}(k)]+\mathbf{p}-\mathbf{R}_{xx}\,E[\mathbf{w}(k)]\right)\\ &= \sqrt{\frac{2}{\pi}}\,\frac{1}{\sigma_e(k)}\left(\mathbf{p}-\mathbf{R}_{xx}\,E[\mathbf{w}(k)]\right).\end{aligned} \tag{1.26}$$

Gersho [113] points out that the sign algorithm is the SGD algorithm that uses the mean absolute error (MAE) as the cost function. The MAE cost function is defined by

$$J(k) = E\left[|e(k)|\right] = E\left[\left|d(k) - \mathbf{w}^H\,\mathbf{x}(k)\right|\right]. \tag{1.27}$$

The gradient of this cost function is

$$\boldsymbol{\nabla}(J(k)) = -E\left[\mathrm{sgn}\{e(k)\}\,\mathbf{x}(k)\right] \tag{1.28}$$

and the minimum of the cost function is obtained by setting the gradient to zero. Using Equation (1.26) for the gradient, we get

$$\sqrt{\frac{2}{\pi}}\,\frac{1}{\sigma_e(k)}\left(\mathbf{p} - \mathbf{R}_{xx}\,\mathbf{w}_{\mathrm{opt}}\right) = 0, \tag{1.29}$$

so that

$$\mathbf{w}_{\mathrm{opt}} = \mathbf{R}_{xx}^{-1}\,\mathbf{p}, \tag{1.30}$$

which is also the MMSE solution. Using

$$\mathbf{p} = \mathbf{R}_{xx}\,\mathbf{w}_{\mathrm{opt}} \tag{1.31}$$

in Equation (1.26) results in

$$\begin{aligned} E\left[\mathrm{sgn}\{e(k)\}\,\mathbf{x}(k)\right] &= \sqrt{\frac{2}{\pi}}\,\frac{1}{\sigma_e(k)}\left(\mathbf{R}_{xx}^{-1}\,\mathbf{w}_{\mathrm{opt}} - \mathbf{R}_{xx}\,E[\mathbf{w}(k)]\right) \\ &= -\sqrt{\frac{2}{\pi}}\,\frac{1}{\sigma_e(k)}\,\mathbf{R}_{xx}^{-1}\,E[\mathbf{v}(k)]. \end{aligned} \tag{1.32}$$

Equation (1.1) now reduces to

$$\begin{aligned} E\left[\mathbf{v}(k+1)\right] &= E\left[\mathbf{v}(k)\right] - \frac{\mu}{\sigma_e(k)}\sqrt{\frac{2}{\pi}}\,\mathbf{R}_{xx}\,E[\mathbf{v}(k)] \\ &= \left(\mathbf{I} - \frac{\mu}{\sigma_e(k)}\sqrt{\frac{2}{\pi}}\,\mathbf{R}_{xx}\right)E[\mathbf{v}(k)]. \end{aligned} \tag{1.33}$$

Using the notation of Chapter 4, Equation (1.33) may be equivalently expressed as

$$\tilde{\mathbf{v}}(k+1) = \left(\mathbf{I} - \frac{\mu}{\sigma_e(k)}\sqrt{\frac{2}{\pi}}\,\boldsymbol{\Lambda}\right)\,\tilde{\mathbf{v}}(k) \tag{1.34}$$

and it follows that

$$\tilde{v}_i(k+1) = \left(1 - \frac{\mu}{\sigma_e(k)}\sqrt{\frac{2}{\pi}}\,\lambda_i\right)^k \tilde{v}_i(0) \tag{1.35}$$

where λ_i is the ith diagonal element of matrix Λ and an eigenvalue of the correlation matrix $\mathbf{R}_{xx}$. Then, the condition for convergence in the mean of the algorithm is

$$0 < \mu < \sqrt{2\,\pi}\,\frac{\sigma_e(k)}{\lambda_{\max}} \tag{1.36}$$

where $\lambda_{\max}$ is the largest eigenvalue of $\mathbf{R}_{xx}$. If $\epsilon_{\min}$ is the minimum value of $\sigma_e^2(k)$ attained (i.e., the MMSE), then, since $\lambda_{\max} < \mathrm{tr}\{\mathbf{R}_{xx}\}$, a sufficient condition for convergence is

$$0 < \mu < \sqrt{2\,\pi}\,\frac{\sqrt{\epsilon_{\min}}}{\mathrm{tr}\{\mathbf{R}_{xx}\}} \tag{1.37}$$

where

$$\epsilon_{\min} = \sigma_d^2 - \mathbf{p}^T\,\mathbf{R}_{xx}^{-1}\,\mathbf{p}. \tag{1.38}$$

Mathews and Cho [118] show that the steady state error for the sign algorithm is given by the approximate expression

$$\sigma_e^2(\infty) = \epsilon_{\min} + \frac{\mu}{2}\sqrt{\frac{\pi}{2}}\,\sqrt{\epsilon_{\min}}\,\left(\sum_{i=1}^{N}\lambda_i\right) \tag{1.39}$$

where N is the order of the matrix $\mathbf{R}_{xx}$. For the LMS algorithm, the steady state error is given by

$$\sigma_e^2(\infty) = \epsilon_{\min} + \frac{\mu}{2}\,\epsilon_{\min}\,\left(\sum_{i=1}^{N}\lambda_i\right). \tag{1.40}$$

To obtain the same steady state error with both algorithms, the step-size μ_S for the sign algorithm is related to the step-size μ_L for the LMS algorithm by

$$\mu_S = \sqrt{\frac{2\,\epsilon_{\min}}{\pi}}\,\mu_L. \tag{1.41}$$

If μ is set to the above value in Equation (1.35), then we get

$$\tilde{v}_i(k+1) = \left(1 - \frac{2}{\pi}\frac{\sqrt{\epsilon_{\min}}}{\sigma_e(k)}\mu_L\,\lambda_i\right)^k \tilde{v}_i(0). \tag{1.42}$$

Since $2 < \pi$ and $\sqrt{\epsilon_{\min}} \leq \sigma_e(k)$, we have $2\sqrt{\epsilon_{\min}}/\pi\,\sigma_e(k) < 1$, so that the decay rate of the transformed weight error in the above equation is lower for the sign algorithm than for the LMS algorithm. In other words, with a similar steady-state MSE performance, the sign algorithm always converges slower than the LMS algorithm.

A.2 Convergence of the Signed Regressor Algorithm

Convergence of the SR algorithm is analyzed in [111, 115, 116] and the discussion here will be based on [115, 116]. Making the same assumptions about the data as in Section A.1, we consider the expectations of both sides of Equation (9.15):

$$\begin{aligned} E[\mathbf{v}(k+1)] &= E[\mathbf{v}(k)] + \mu\,E[e(k)\,\mathrm{sgn}\{\mathbf{x}(k)\}] \\ &= E[\mathbf{v}(k)] + \mu\,E\left[\{d(k) - (\mathbf{w}_{\mathrm{opt}} + \mathbf{v}(k))^T\,\mathbf{x}(k)\}\,\mathrm{sgn}\{\mathbf{x}(k)\}\right] \end{aligned} \tag{1.43}$$

where $\mathbf{w}_{\mathrm{opt}}$ is the optimum vector, which is the Wiener solution of Equation (1.30) [116]. Expanding the right-hand side yields

$$\begin{aligned} E[\mathbf{v}(k+1)] &= E[\mathbf{v}(k)] + \mu\,E\left[\{d(k) - \mathbf{w}_{\mathrm{opt}}^T\,\mathbf{x}(k)\}\,\mathrm{sgn}\{\mathbf{x}(k)\}\right] \\ &\quad - \mu\,E\left[\mathrm{sgn}\{\mathbf{x}(k)\}\,\mathbf{x}^T(k)\right]\,E\left[\mathbf{v}(k)\right] \\ &= E[\mathbf{v}(k)] + \mu\,E[e_{\mathrm{opt}}(k)\,\mathrm{sgn}\{\mathbf{x}(k)\}] \\ &\quad - \mu\,E\left[\mathrm{sgn}\{\mathbf{x}(k)\}\,\mathbf{x}^T(k)\right]\,E\left[\mathbf{v}(k)\right] \end{aligned} \tag{1.44}$$

where $e_{\mathrm{opt}}(k)$ is the error obtained with the optimum weight vector. By the principle of orthogonality discussed in Chapter 4 for the LMS algorithm,

$$E[e_{\mathrm{opt}}(k)\,\mathbf{x}(k)] = \mathbf{0}, \tag{1.45}$$

implying that $e_{\mathrm{opt}}(k)$ and $\mathbf{x}(k)$ are uncorrelated. Due to the Gaussian assumption on the two signals, this translates into statistical independence of $e_{\mathrm{opt}}(k)$ and $\mathbf{x}(k)$. Thus,

$$E[e_{\mathrm{opt}}(k)\,\mathrm{sgn}\{\mathbf{x}(k)\}] = \mathbf{0}. \tag{1.46}$$

Eweda [116] notes that Price's theorem [119] may be applied on the individual elements of $E\left[\text{sgn}\{\mathbf{x}(k)\}\,\mathbf{x}^T(k)\right]$ to obtain

$$E\left[\text{sgn}\{\mathbf{x}(k)\}\,\mathbf{x}^T(k)\right] = \frac{1}{\sigma_x}\sqrt{\frac{2}{\pi}}\mathbf{R}_{xx} \tag{1.47}$$

where

$$\sigma_x \triangleq \sqrt{E\left[x_i^2(k)\right]}, \quad i = 1, 2, \ldots, N, \tag{1.48}$$

$x_i(k)$ being the ith element of the input vector $\mathbf{x}(k)$. Using Equations (1.46) and (1.47) in Equation (1.44), we get

$$\begin{aligned} E[\mathbf{v}(k+1)] &= E[\mathbf{v}(k)] - \frac{\mu}{\sigma_x}\sqrt{\frac{2}{\pi}}\mathbf{R}_{xx}\,E[\mathbf{v}(k)] \\ &= \left(\mathbf{I} - \frac{\mu}{\sigma_x}\sqrt{\frac{2}{\pi}}\mathbf{R}_{xx}\right)\,E[\mathbf{v}](k). \end{aligned} \tag{1.49}$$

Following previous notation, we then get

$$\tilde{\mathbf{v}}(k+1) = \left(\mathbf{I} - \frac{\mu}{\sigma_x}\sqrt{\frac{2}{\pi}}\mathbf{\Lambda}\right)\,\tilde{\mathbf{v}}(k). \tag{1.50}$$

The corresponding update equation for the ith element of the transformed error vector is

$$\tilde{v}_i(k+1) = \left(1 - \frac{\mu}{\sigma_x}\sqrt{\frac{2}{\pi}}\,\lambda_i\right)^k\,\tilde{v}_i(0), \tag{1.51}$$

from which we get the following condition for convergence (in the mean) of the SR algorithm:

$$0 < \mu < \sqrt{2\,\pi}\,\frac{\sigma_x}{\lambda_{\max}} \tag{1.52}$$

where $\lambda_{\max}$ is again the largest eigenvalue of $\mathbf{R}_{xx}$. Since

$$N\,\sigma_x^2 = \text{tr}\{\mathbf{R}_{xx}\} = \sum_{i=1}^{N}\lambda_i \tag{1.53}$$

and $\lambda_{\max} < \mathrm{tr}\{\mathbf{R}_{xx}\}$, a sufficient condition for convergence is

$$0 < \mu < \sqrt{\frac{2\,\pi}{N\,\mathrm{tr}\{\mathbf{R}_{xx}\}}}. \tag{1.54}$$

From [116] we get the following approximate expression for steady-state MSE with the SR algorithm:

$$\sigma_e^2(\infty) \approx \epsilon_{\min} + \sqrt{\frac{2}{\pi}}\,\frac{\mu}{2}\,N\,\sigma_x\,\epsilon_{\min}. \tag{1.55}$$

Comparing Equation (1.55) with Equation (1.40), to obtain the same steady-state MSE with the LMS algorithm and the SR algorithm, we find the step-size μ_R for the SR algorithm to be related to μ_L by

$$\begin{aligned} \mu_R &= \sqrt{\frac{2}{\pi}}\,\frac{\sum_{i=1}^{N}\lambda_i}{N\,\sigma_x}\,\mu_L \\ &= \sqrt{\frac{2}{\pi}}\,\frac{N\,\sigma_x^2}{N\,\sigma_x}\,\mu_L \\ &= \sqrt{\frac{2}{\pi}}\,\sigma_x\,\mu_L. \end{aligned} \tag{1.56}$$

Letting $\mu = \mu_R$ in Equation (1.51), where the expression of Equation (1.56) is used for μ_R, we arrive at

$$\tilde{v}_i(k+1) = \left(1 - \sqrt{\frac{2}{\pi}}\,\mu_L\,\lambda_i\right)^k \tilde{v}_i(0). \tag{1.57}$$

Since $\sqrt{2/\pi} < 1$, Equation (1.57) shows that the SR algorithm converges slower than the LMS algorithm. The lower convergence rate is due to an equivalent step-size that is smaller by a factor $\sqrt{2/\pi}$. The same result is reported in [115].

Bibliography

[1] European Telecommunications Standards Institute, "Universal Mobile Telecommuniations System (UMTS); UMTS Terrestrial Radio Access (UTRA); Concept Evaluation (UMTS 30.06 version 3.0.0): Technical Report," ETSI Secretariat, Valbonne, France, 1997, TR 101 146 V3.0.0 (1997-12).

[2] K. Buchanan *et al.*, "IMT-2000: Service Provider's Perspective," *IEEE Personal Communications*, pp. 8–13, Aug. 1997.

[3] E. Nikula, A. Toskala, E. Dahlman, L. Girard, and A. Klein, "FRAMES Multiple Access for UMTS and IMT-2000," *IEEE Personal Communications*, pp. 16–24, Apr. 1998.

[4] T. Ojanperä and Ramjee Prasad, "An Overview of Third-Generation Wireless Personal Communications: A European Pespective," *IEEE Personal Communications*, pp. 59–65, Dec. 1998.

[5] T. S. Rappaport, *Wireless Communications, Principles and Practice*, IEEE Press, New York, 1996.

[6] V. K. Garg and J. E. Wilkes, *Wireless and Personal Communications Systems*, Prentice Hall, Upper Saddle River, New Jersey, 1993.

[7] N. Abramson, Ed., *Multiple Access Communications—Foundations for Emerging Technologies*, IEEE Press, New York, 1993.

[8] S. Vembu and A. J. Viterbi, "Two Different Philosophies in CDMA — a Comparison," *Proc. 46th IEEE VTC*, 1996, pp. 869–873.

[9] P. Jung, P. W. Baier, and A. Steil, "Advantages of CDMA and Spread Spectrum Techniques over FDMA and TDMA in Cellular Mobile Radio Applications," *IEEE Trans. Veh. Technol.*, vol. 42, no. 3, pp. 357–364, Aug. 1993.

[10] S. Glisic and B. Vucetic, *Spread Spectrum CDMA Systems for Wireless Communications*, Artech House, Inc., Boston, 1997.

[11] A. J. Viterbi, "The Orthogonal-Random Waveform Dichotomy for Digital Mobile Personal Communication," *IEEE Personal Communications*, pp. 18–24, First Quarter 1994.

[12] K. S. Gilhousen, I. M. Jacobs, R. Padovani, and Jr. L. A. Weaver, "Increased Capacity Using CDMA for Mobile Satellite Communication," *IEEE J. Sel. Areas Commun.*, vol. 8, no. 4, pp. 503–514, May 1990.

[13] K. S. Gilhousen, I. M. Jacobs, R. Padovani, A. J. Viterbi, Jr. L. A. Weaver, and C. E. Wheatley III, "On the Capacity of a Cellular CDMA System," *IEEE Trans. Veh. Technol.*, vol. 40, no. 2, pp. 303–312, May 1991.

[14] J. G. Proakis, *Digital Communications*, McGraw-Hill, New York, second edition, 1989.

[15] W. C. Y. Lee, *Mobile Cellular Telecomunications*, McGraw-Hill, New York, second edition, 1995.

[16] A. J. Viterbi, A. M. Viterbi, K. S. Gilhousen, and E. Zehavi, "Soft Handoff Extends CDMA Cell Coverage and Increases Reverse Link Capacity," *IEEE J. Sel. Areas Commun.*, vol. 12, no. 8, pp. 1281–1288, Oct. 1994.

[17] S. P. Nicoloso, "An Investigation of Carrier Recovery Techniques for PSK Modulated Signals in CDMA and Multipath Mobile Environments," M.S. Thesis, Virginia Polytechnic Institute and State University, June 1997.

[18] R. E. Ziemer and R. L. Peterson, *Introduction to Digital Communication*, Macmillan Publishing Company, New York, 1992.

[19] R. E. Ziemer and R. L. Peterson, *Digital Communications and Spread Spectrum Systems*, Macmillan Publishing Company, New York, 1985.

[20] M. K. Simon, J. K. Omura, R. A. Scholtz, and B. K. Levitt, *Spread Spectrum Communication Handbook*, McGraw-Hill, New York, 1994.

[21] J. D. Parsons, *The Mobile Radio Propagation Channel*, Halsted Press, New York, 1992.

[22] S. Verdú, "Minimum Probability of Error for Asynchronous Gaussian Multiple-Access Channels," *IEEE Trans. Info. Theory*, vol. IT-32, pp. 85–96, Jan. 1986.

[23] S. Verdú and H. V. Poor, "Abstract Dynamic Programming Models under Commutativity," *SIAM J. Control and Optimization*, vol. 24, pp. 990–1006, July 1987.

[24] S. Verdú, "Recent Progress in Multiuser Detection," in *Advances in Communication and Signal Processing*. Springer-Verlag, Berlin-Heidelberg, 1989.

[25] R. Lupas and S. Verdú, "Linear Multiuser Detectors for Synchronous Code-Division Multiple Access Channels," *IEEE Trans. Info. Theory*, vol. 35, no. 1, pp. 123–136, Jan. 1989.

[26] R. Lupas and S. Verdú, "Near-Far Resistance of Multiuser Detectors in Asynchronous Channels," *IEEE Trans. Commun.*, vol. 38, no. 14, pp. 496–508, Apr. 1990.

[27] P. Patel and J. Holtzman, "Analysis of a Simple Succesive Interference Cancellation Scheme in a DS/CDMA System," *IEEE J. Sel. Areas Commun.*, vol. 12, no. 5, pp. 796–807, June 1994.

[28] M. K. Varanasi and B. Aazhang, "Multistage Detection in Asynchronous Code-Division Multiple-Access Communications," *IEEE Trans. Commun.*, vol. 38, no. 4, pp. 509–519, Apr. 1990.

[29] D. Divsilar and M. K. Simon, "Improved CDMA Performance Using Parallel Interference Cancellation," *Proc. IEEE MILCOM*, Oct. 1994, pp. 911–917.

[30] A. Kaul and B. D. Woerner, "Analytic Limits on the Performace of Adaptive Multistage Interference Cancellation for CDMA," *IEE Electronics Letters*, vol. 30, no. 25, pp. 2093–2095, Dec. 1994.

[31] S. Striglis, A. Kaul, N. Yang, and B. D. Woerner, "A Multistage RAKE Receiver for Improved Capacity of CDMA Systems," *Proc. 44th IEEE VTC*, 1994, pp. 789–793.

[32] R. M. Buehrer, N. S. Correal, and B. D. Woerner, "A Comparison of Multiuser Receivers for Cellular CDMA," *Proc. IEEE GLOBECOM*, 1996, pp. 1571–1577.

[33] R. M. Buehrer, *The Application of Multiuer Detection to Cellular CDMA*, Ph.D. Dissertation, Virginia Polytechnic Institute and State University, June 1996.

[34] A. Duel-Hallen, J. Holtzman, and Z. Zvonar, "Multiuser Detection for CDMA Systems," *IEEE Personal Communications*, pp. 46–58, Apr. 1995.

[35] F.-C. Cheng and J. M. Holtzman, "Effect of Tracking Error on DS/CDMA Successive Interference Cancellation," *Proc. IEEE GLOBECOM — Communications Theory Mini-Conference*, 1994, pp. 166–170.

[36] R. M. Buehrer, A. Kaul, S. Striglis, and B. D. Woerner, "Analysis of DS-CDMA Parallel Interference Cancellation with Phase and Timimg Errors," *IEEE J. Sel. Areas Commun.*, pp. 1522–1535, Oct. 1996.

[37] P. B. Rapajic and B. S. Vucetic, "Adaptive Receiver Structures for Asynchronous CDMA Systems," *IEEE J. Sel. Areas Commun.*, vol. 12, no. 4, pp. 685–697, May 1994.

[38] S. Haykin, *Adaptive Filter Theory*, Prentice Hall, Englewood Cliffs, NJ, second edition, 1991.

[39] B. Widrow and S. D. Stearns, *Adaptive Signal Processing*, Prentice Hall, Englewood Cliffs, NJ, 1985.

[40] M. Abdulrahman, A. U. H. Sheikh, and D. D. Falconer, "Decision Feedback Equalization for CDMA in Indoor Wireless Communications," *IEEE J. Sel. Areas Commun.*, vol. 12, no. 4, pp. 698–706, May 1994.

[41] I. Howitt, J. H. Reed, V. Vemuri, and T. C. Hsia, "Recent Developments in Applying Neural Networks to Equalization and Interference Rejection," *Proc. Virginia Tech's Third Symposium on Wireless Personal Communcations*, 1993, pp. 1–1–1–12.

[42] B. Mulgrew, "Applying Radial Basis Functions," *IEEE Signal Processing Magazine*, pp. 50–64, Mar. 1996.

[43] V. Aue and J. H. Reed, "An Interference Robust CDMA Demodulator that Uses Spectral Correlation Properties," *Proc. 44th IEEE VTC*, 1994, pp. 563–567.

[44] J. H. Reed and T. C. Hsia, "The Performance of Time-Dependent Adaptive Filters for Interference Rejection," *IEEE Trans. Signal Processing*, vol. 38, no. 8, pp. 1373–1385, Aug. 1990.

[45] U. Madhow and M. L. Honig, "Error Probability and Near-Far Resistance of Minimum Mean Squared Error Interference Suppression Schemes for CDMA," *Proc. IEEE GLOBECOM*, 1992, pp. 1339–1343.

[46] U. Madhow and M. L. Honig, "MMSE Interference Suppression for Direct-Sequence Spread-Spectrum CDMA," *IEEE Trans. Commun.*, vol. 42, no. 12, pp. 3178–3188, Dec. 1994.

[47] U. Madhow and M. L. Honig, "Minimum Mean Squared Error Interference Suppression Schemes for Direct-Sequence Spread-Spectrum Code-Division Multiple-Access," *Proc. 1st ICUPC*, 1992, pp. 273–277.

[48] C. N. Pateros and G. J. Saulnier, "Interference Suppression and Multipath Mitigation Using an Adaptive Correlator Direct Sequence Spread Spectrum Receiver," *Proc. IEEE ICC*, 1992, pp. 662–666.

[49] M. Abdulrahman, D. D. Falconer, and A. U. H. Sheikh, "Equalization for Interference Cancellation in Spread Spectrum Multiple Access Systems," *Proc. 42nd IEEE VTC*, 1992, pp. 71–74.

[50] P. N. Monogioudis, R. Tafazolli, and B. G. Evans, "Linear Adaptive Fractionally Spaced Equalization of CDMA Multiple-Access Interference," *IEE Electronics Letters*, vol. 29, no. 21, pp. 1823–1825, Oct. 1993.

[51] S. L. Miller, "An Adaptive Direct-Sequence Code-Division Multiple-Access Receiver for Multiuser Interference Rejection," *IEEE Trans. Commun.*, vol. 43, no. 2/3/4, pp. 1746–1755, Feb./Mar./Apr. 1995.

[52] S. L. Miller, "Training Analysis of Adaptive Interference Suppression for Direct-Sequence Code-Division Multiple-Access Systems," *IEEE Trans. Commun.*, vol. 44, no. 4, pp. 488–495, Apr. 1996.

[53] H. V. Poor and S. Verdú, "Probability of Error in MMSE Multiuser Detection," *IEEE Trans. Info. Th.*, vol. 43, no. 3, pp. 858–871, May 1997.

[54] R. S.-K. Cheng, "Coded CDMA Systems with and without MMSE Multiuser Equalizer," *Proc. Proc. IEEE ICUPC*, 1996, pp. 174–178.

[55] M. V. Majmundar, "Adaptive Single User Receivers for Direct Sequence CDMA Systems," M.S. Thesis, Virginia Polytechnic Institute and State University, 1996.

[56] S. U. H. Qureshi, "Adaptive Equalization," *Proc. of the IEEE*, vol. 73, no. 9, pp. 1349–1387, Sept. 1985.

[57] M. Abdulrahman, A. U. H. Sheikh, and D. D. Falconer, "DFE Convergence for Interference Cancellation in Spread Spectrum Multiple Access Systems," *Proc. 43rd IEEE VTC*, 1993, pp. 807–810.

[58] E. G. Ström and S. L. Miller, "Optimum Complexity Reduction of Minimum Mean Square Error DS-CDMA Receivers," *Proc. 44th IEEE VTC*, 1994, pp. 568–572.

[59] W. A. Gardner, *Introduction to Random Processes With Applications to Signals and Systems*, Macmillan Publishing Company, New York, 1986.

[60] W. A. Gardner, *Statistical Spectral Analysis: A Nonprobabilistic Theory*, Prentice Hall, Englewood Cliffs, NJ, 1988.

[61] W. A. Gardner, Ed., *Cyclostationarity in Communications and Signal Processing*, IEEE Press, New York, 1994.

[62] N. R. Mangalvedhe, "An Eigenstructure Technique for Direct Sequence Spread Spectrum Synchronization," M.S. Thesis, Virginia Polytechnic Institute and State University, 1995.

[63] N. R. Mangalvedhe and J. H. Reed, "Evaluation of a Soft Synchronization Technique for DSSS Signals," *IEEE J. Sel. Areas in Commun.*, vol. 14, no. 8, pp. 1643–1652, Oct. 1996.

[64] W. A. Gardner, "Cyclic Wiener Filtering: Theory and Method," *IEEE Trans. Commun.*, vol. 41, no. 1, pp. 151–163, Jan. 1993.

[65] W. S. Brown and R. B. Crane, "Conjugate Linear Filtering," *IEEE Trans. Info. Theory*, vol. IT-15, no. 4, pp. 462–465, July 1969.

[66] C.-K. Chen, *Spectral Correlation Characterization of Modulated Signals with Applications to Signal Detection and Source Location*, Ph.D. Dissertation, University of California, Davis, 1988.

[67] J. H. Reed, C. D. Greene, and T. C. Hsia, "Demodulation of a Direct Sequence Spread-Spectrum Signal Using an Optimal Time-Dependent Filter," *Proc. IEEE MILCOM*, 1989, pp. 657–662.

[68] R. D. Holley, "Time Dependent Adaptive Filters for Interference Cancellation in CDMA Systems," M.S. Thesis, Virginia Polytechnic Institute and State University, 1993.

[69] V. Aue, "Optimum Linear Single User Detection in Direct-Sequence Spread-Spectrum Multiple Access Systems," M.S. Thesis, Virginia Polytechnic Institute and State University, 1994.

[70] M. L. Honig and D. G. Messerschmitt, *Adaptive Filters: Structures, Algorithms and Applications*, Kluwer Academic Publishers, Boston, 1984.

[71] P. M. Clarkson, *Optimal and Adaptive Signal Processing*, CRC Press, Boca Raton, FL, 1993.

[72] S. V. Vaseghi, *Advanced Signal Processing and Digital Noise Reduction*, John Wiley & Sons, New York, 1996.

[73] M. J. Panik, *Classical Optimization: Foundations and Extensions*, North-Holland Publishing Company, Amsterdam, 1976.

[74] J. E. Mazo, "Analysis of Decision-Directed Equalizer Convergence," *The Bell Sys. Tech. J.*, pp. 1857–1876, Dec. 1980.

[75] O. Macchi and E. Ewada, "Convergergence Analysis of Self-Adaptive Equalizers," *IEEE Trans. Info. Th.*, vol. IT-30, no. 2, pp. 161–176, Mar. 1984.

[76] S. J. Nowlan and G. E. Hinton, "A Soft Decision-Directed LMS Algorithm for Blind Equalization," *IEEE Trans. Commun.*, vol. 41, no. 2, pp. 275–279, Feb. 1993.

[77] M. L. Honig, U. Madhow, and S. Verdú, "Blind Adaptive Interference Suppression Schemes for Near-Far Resistant CDMA," *Proc. IEEE GLOBECOM*, 1994, pp. 379–384.

[78] M. L. Honig, U. Madhow, and S. Verdu, "Blind Adaptive Multiuser Detection," *IEEE Trans. Info. Th.*, vol. 41, no. 4, pp. 944–960, July 1995.

[79] J. R. Treichler, Jr. C. R. Johnson, and M. G. Larimore, *Theory and Design of Adaptive Filters*, John Wiley & Sons, New York, 1987.

[80] N. Zečević, "Blind Algorithms for CDMA Interference Rejection," M.S. Thesis, Virginia Polytechnic Institute and State University, 1996.

[81] N. Zečević and J. H. Reed, "Blind Adaptation Algorithms for Direct-Sequence Spread-Spectrum CDMA Single-User Detection," *Proc. IEEE 47th VTC*, 1997, pp. 2133–2137.

[82] J. R. Treichler and B. G. Agee, "A New Approach to Multipath Correction of Constant Modulus Signals," *IEEE Trans. Acous. Speech Sig. Proc.*, vol. ASSP-31, no. 2, pp. 459–472, Apr. 1983.

[83] D. N. Godard, "Self-Recovering Equalization and Carrier Tracking in Two-Dimensional Data Communication Systems," *IEEE Trans. Commun.*, vol. COM-28, no. 11, pp. 1867–1875, Nov. 1980.

[84] R. Gooch and J. Lundell, "The CM Array: An Adaptive Beamformer for Constant Modulus Signals," *Proc. IEEE ICASSP*, 1986, pp. 2523–2526.

[85] R. Mendonza, J. H. Reed, T. C. Hsia, and B. G. Agee, "Interference Rejection Using the Time-Dependent Constant Modulus Algorithm (CMA) and the Hybrid CMA/Spectral Correlation Discriminator," *IEEE Trans. Signal Processing*, vol. 39, no. 9, pp. 2108–2111, Sept. 1991.

[86] W. Lee, B. Vojcic, and R. L. Pickholtz, "Constant Modulus Algorithm for Blind Multiuser Detection," *Proc. IEEE ISSSTA*, 1996, pp. 1262–1266.

[87] M. J. Rude and L. J. Griffiths, "Incorporation of Linear Constraints into the Constant Modulus Algorithm," *Proc. IEEE ICASSP*, 1989, pp. 968–971.

[88] M. J. Rude and L. J. Griffiths, "A Linearly Constrained Adaptive Algorithm for Constant Modulus Signal Processing," *Proc. EUSIPCO-90*, 1990, pp. 237–240.

[89] L. J. Griffiths and C. W. Jim, "An Alternative Approach to Linearly Constrained Adaptive Beamforming," *IEEE Trans. Antennas and Propagation*, vol. AP-30, no. 1, pp. 27–34, Jan. 1982.

[90] B. D. Van Veen and K. M .Buckley, "Beamforming: A Versatile Approach to Spatial Filtering," *IEEE ASSP Magazine*, pp. 4–24, Apr. 1988.

[91] J. Litva and T. K.-Y. Lo, *Digital Beamforming in Wireless Communications*, Artech House Publishers, Boston, 1996.

[92] D. H. Johnson and D. E. Dudgeon, *Array Signal Processing: Concepts and Techniques*, Prentice Hall, Englewood Cliffs, NJ, 1993.

[93] B. G. Agee, "Solving the Near-Far Problem: Exploitation of Spatial and Spectral Diversity in Wireless Personal Communication Networks," *Proc. Virginia Tech's Third Symposium on Wireless Personal Communications*, 1993, pp. 15–1–15–12.

[94] G. L. Turin, "Introduction to Spread Spectrum Antimultipath Techniques and their Application to Urban Digital Radio," *Proceedings of the IEEE*, vol. 68, no. 3, pp. 328–353, Mar. 1980.

[95] R. Cameron and B. D. Woerner, "Measurement-Based Performance Evaluation of CDMA Sytems in Multipath Fading," *Proc. 43rd IEEE VTC*, 1993, pp. 368–371.

[96] D. H. Brandwood, "A Complex Gradient Operator and its Application to Adaptive Array Theory," *IEE Proc., Pts. F and H*, vol. 130, no. 1, pp. 11–16, Feb. 1983.

[97] Commission of the European Communities, "Digital Land Mobile Radio Communications: COST-207 Final Report," Office for Official Publications of the European Communities, Brussels, 1989, ISBN 92-825-9946-9.

[98] L. L. Scharf, *Statistical Signal Processing: Detection, Estimation, and Time Series Analysis*, Addison-Wesley Publishing Company, Reading, MA, 1991.

[99] G. H. Golub and C. F. Van Loan, *Matrix Computations*, The Johns Hopkins University Press, Baltimore, 1989.

[100] B. Noble and J. W. Daniel, *Applied Linear Algebra*, Prentice Hall, Englewood Cliffs, NJ, 1977.

[101] R. Carsello *et al.*, "IMT-2000 Standards: Radio Aspects," *IEEE Personal Communications*, pp. 30–40, Aug. 1997.

[102] T. Ottosson and A. Svensson, "On Schemes for Multirate Support in DS-CDMA Systems," *Wireless Personal Communications*, vol. 6, no. 3, pp. 265–287, Feb. 1998.

[103] E. R. Ferrara, Jr., "Frequency-Domain Implementations of Periodically Time-Varying Filters," *IEEE Trans. Acoustics, Speech and Sig. Proc.*, vol. ASSP-33, no. 4, pp. 883–892, Aug. 1985.

[104] R. C. Dixon, *Spread Spectrum Systems*, John Wiley & Sons, New York, second edition, 1984.

[105] R. Pandya *et al.*, "IMT-2000 Standards: Network Aspects," *IEEE Personal Communications*, pp. 20–29, Aug. 1997.

[106] W. K. Lindsey and M. K. Simon, *Telecommunication Systems Engineering*, Dover Publications, New York, 1973.

[107] D. Divsalar and M. K. Simon, "Pseudocoherent Demodulation of DPSK Radio Signals," JPL New Technology Report, NPO-19205, June 1995.

[108] B. Widrow, J. M. McCool, M. G. Larimore, and Jr. C. R. Johnson, "Stationary and Nonstationary Learning Characteristics of the LMS Adaptive Filter," *Proc. of the IEEE*, vol. 64, no. 8, pp. 1151–1162, Aug. 1976.

[109] S. Yoshida, A. Ushirokawa, S. Yanagi, and Y. Furuya, "DS/CDMA Adaptive Interference Canceller on Differential Detection in Fast Fading Channel," *Proc. 44th IEEE VTC*, 1994, pp. 780–784.

[110] N. A. M. Verhoeckx, H. C. van den Elzen, F. A. M. Snijders, and P. J. van Gerwen, "Digital Echo Cancellation for Baseband Data Transmission," *IEEE Trans. Acous. Speech Sig. Proc.*, vol. ASSP-27, no. 6, pp. 768–781, Dec. 1979.

[111] T. A. C. M Claasen and W. F. G. Mecklenbräuker, "Comparison of the Convergence of Two Algorithms for Adaptive FIR Digital Filters," *IEEE Trans. Acous. Speech Sig. Proc.*, vol. ASSP-29, no. 3, pp. 670–678, June 1981.

[112] H. Sari, "Performance Evalutation of Three Equalization Algorithms," *Proc. IEEE ICASSP*, 1982, pp. 1385–1389.

[113] A. Gersho, "Adaptive Filtering with Binary Reinforcement," *IEEE Trans. Info. Theory*, vol. IT-30, no. 2, pp. 191–199, Mar. 1984.

[114] T. A. C. M Claasen and W. F. G. Mecklenbräuker, "Authors' Reply to "Comments on 'Comparison of the Convergence of Two Algorithms for Adaptive FIR Digital Filters"'," *IEEE Trans. Acous. Speech Sig. Proc.*, vol. ASSP-34, no. 1, pp. 202–203, Feb. 1986.

[115] N. J. Bershad, "Comments on "Comparison of the Convergence of Two Algorithms for Adaptive FIR Digital Filters," *IEEE Trans. Acous. Speech Sig. Proc.*, vol. ASSP-33, no. 6, pp. 1604–1606, Dec. 1985.

[116] E. Eweda, "Analysis and Design of a Signed Regressor LMS Algorithm for Stationary and Nonstationary Adaptive Filtering with Correlated Gaussian Data," *IEEE Trans. Circuits and Systems*, vol. ASSP-37, no. 11, pp. 1367–1374, Nov. 1990.

[117] N. R. Mangalvedhe and J. H. Reed, "Development and Analysis of Adaptive Interference Rejection Techniques for Direct Sequence Code Division Multiple access Systems," MPRG Technical Report MPRG-TR-98-13, MPRG, Virginia Tech, December 1998.

[118] V. J. Mathews and S. H. Cho, "Improved Convergence Analysis of Stochastic Gradient Adaptive Filters Using the Sign Algorithm," *IEEE Trans. Acous. Speech Sig. Proc.*, vol. ASSP-35, no. 4, pp. 450–454, Apr. 1987.

[119] R. Price, "A Useful Theorem for Nonlinear Devices Having Gaussian Inputs," *IRE Transactions on Info. Theory*, vol. IT-4, pp. 69–72, June 1958.

Vita

Nitin Mangalvedhe was born on June 19, 1970 in Bangalore, India. He obtained his B.E. in Electronics Engineering from Bangalore University, India in 1992 and started his graduate study at Virginia Tech in Spring 1993. He completed his M.S. in Electrical Engineering in 1995. Nitin's Master's research was in the area of DS/SS synchronization.

Nitin commenced his Ph.D. in 1995, at which time he started working on the GloMo project, involving the development of spectrally efficient receivers for CDMA systems. Between 1995 and 1997, he worked on algorithm development and hardware development for the GloMo project. From 1997 to 1999, Nitin was the Lead Engineer for first GloMo I and then GloMo II, and supervised the hardware implementation of several advanced CDMA receivers. His Ph.D. research focused on adaptive receivers for DS-CDMA systems. Nitin's areas of interest include DS-CDMA systems, adaptive interference rejection, and adaptive antenna arrays.